

Synthesis of the spiroketal moiety of didemnaketal A

by

Jason Alan Davy
MSc, University of Guelph, 2007
BSc, University of Guelph, 2005

A Dissertation Submitted in Partial Fulfillment
of the Requirements for the Degree of

DOCTORATE OF PHILOSOPHY

in the Department of Chemistry

© Jason Alan Davy, 2014
University of Victoria

All rights reserved. This dissertation may not be reproduced in whole or in part, by
photocopy or other means, without the permission of the author.

Supervisory Committee

Synthesis of the spiroketal moiety of didemnaketol A

by

Jason Alan Davy
MSc, University of Guelph, 2007
BSc, University of Guelph, 2005

Supervisory Committee

Dr. Jeremy Wulff, Department of Chemistry
Supervisor

Dr. Peter Wan, Department of Chemistry
Departmental Member

Dr. Robin Hicks, Department of Chemistry
Departmental Member

Dr. Martin Boulanger, Department of Biochemistry and Microbiology
Outside Member

Abstract

Supervisory Committee

Dr. Jeremy Wulff, Department of Chemistry

Supervisor

Dr. Peter Wan, Department of Chemistry

Departmental Member

Dr. Robin Hicks, Department of Chemistry

Departmental Member

Dr. Martin Boulanger, Department of Biochemistry and Microbiology

Outside Member

The ascidian isolation artifact didemnaketol A is a highly oxygenated polyisoprenoid capable of inhibiting HIV-1 protease through an unusual dissociative mechanism. However, recent synthetic efforts have cast doubt on stereochemical assignments in the originally published structure. In the interest of elucidating the true structure of didemnaketol A through total synthesis, we present a strategy for rapidly accessing the putative spiroketal fragment by exploiting its latent symmetry. In a single step, double Sharpless asymmetric dihydroxylation reactions (SAD) allowed us to simultaneously set all seven stereogenic centers and assemble this complex fragment from non-chiral material. The precursor was obtainable through a racemic synthesis in which the geometric isomers of a nine-membered cyclic enone converged in a ring-opening cross metathesis reaction (ROCM).

Table of Contents

Supervisory Committee	ii
Abstract	iii
Table of Contents	iv
List of Schemes	vi
List of Tables	x
List of Figures	xi
List of Abbreviations	xiv
Acknowledgments	xix
Dedication	xxi
Chapter 1 — Introduction	1
1.1 HIV and AIDS	1
1.2 HIV-PR Inhibitors	7
1.3 Dissociative Inhibitors	10
1.4 Natural Dissociative Inhibitors	16
1.5 Investigating the Didemnaketals	19
1.6 Total Syntheses of Didemnaketals	22
1.7 Reevaluating of the Structural Hypothesis	44
1.8 Our Proposed Synthesis	53
Chapter 2 — Photochemical Approaches	59
2.1 Outlook and Goals	59
2.2 Synthesizing 9-Membered Rings	60
2.3 Application of Snapper's Model	69
2.4 Photochemical Cycloaddition Approach	72
2.5 Electrocyclic Ring Closure Approach	74
2.6 Attempted Decarboxylations	80
2.7 Unexpected Radical Cascades	82
Chapter 3 — Radical Lactonizations	86
3.1 Lactonization Strategies	86
3.2 Trialkylborane and Water	95
3.3 Potential Natural Product Targets	96
3.4 Synthesis of Xanthate Precursors	97
3.5 Radical Cyclizations	100
3.6 Attempted Lactonization Cascades	107
Chapter 4 — Nonenone Synthesis	110
4.1 Reevaluation of Tactics	110
4.2 Silyl Enol Synthesis	112
4.3 Anionic Oxy-Cope	120
4.4 Enigmatic Decarboxylation	124
4.5 Decarboxylation Resolved	126
Chapter 5 — Spiroketal	134

5.1 Outlook and Goals	134
5.2 Ring Opening Cross Metathesis.....	135
5.3 Asymmetric Dihydroxylations.....	137
5.4 Singly Anomeric Spiroketal.....	140
5.5 Doubly Anomeric Spiroketal	153
5.6 Comparison with Didemnaketol A.....	156
Chapter 6 — Final Coupling.....	162
6.1 Overview and Analysis of Tactics	162
6.2 Model Spiroketal.....	168
6.3 Preliminary Coupling Attempts	170
6.4 Transformation-based Assignment of Stereochemistry.....	174
6.5 Recent Developments	177
6.6 Future Outlook	180
Chapter 7 — Experimental	183
7.1 General Remarks.....	183
7.2 Experiments pertaining to Chapter 2	185
7.3 Experiments pertaining to Chapter 3	204
7.4 Experiments pertaining to Chapter 4	225
7.5 Experiments pertaining to Chapter 5	239
7.6 Experiments pertaining to Chapter 6	249
Bibliography	261
Appendix 1 — X-Ray Crystallography	275
Appendix 2 — List of Numbered Compounds	299

List of Schemes

Scheme 1. The synthesis of the polyisoprenoid chain used by both Ito (49) and Fuwa (50).....	26
Scheme 2. The respective syntheses by Ito and Fuwa for the C9-C15 fragment (55 by Ito, 60 by Fuwa) of didemnaketal B from (S)-3-hydroxyisobutyrate (39).....	27
Scheme 3. Ito's synthesis of the C16-C21 fragment (64) from (S)-glutamic acid (44) ..	28
Scheme 4. Ito's completion of the spiroketal moiety of didemnaketal B (69).....	29
Scheme 5. Fuwa's synthesis of the C16-C21 (43) fragment from (R)-glycidol (70).....	31
Scheme 6. Fuwa's completion of the spiroketal moiety of didemnaketal B (77)	32
Scheme 7. Fuwa's construction of the C7-C15 building block (82) for the total synthesis of didemnaketal B.....	33
Scheme 8. Fuwa's completion of the total synthesis of the posited structure for didemnaketal B (33).....	34
Scheme 9. Tu's convergent assembly of the spiroketal moiety of didemnaketal A starting from (R)-pulegone (40).....	36
Scheme 10. Tu's synthesis of the linear chain (108) of didemnaketal A starting from (S)-carvone (99).....	39
Scheme 11. Tu's assembly of the C1-C8 fragment (112) for the synthesis of didemnaketal A	40
Scheme 12. Tu's assembly of the C9-C16 fragment (117) of didemnaketal A from (S)-citronelle (113).....	41
Scheme 13. Tu's assembly of the C17-C22 fragment for the synthesis of the posited structure of didemnaketal A.....	42
Scheme 14. Tu's final assembly of the posited structure for didemnaketal A (32).	43
Scheme 15. The mechanism of the Corey–Nicolaou macrolactonization.....	62
Scheme 16. Koikowski's fragmentation approach to the synthesis of the core of jatrophatrione (154)	63
Scheme 17. Paquette's fragmentation approach in first total synthesis of jatrophatrione (154).....	63
Scheme 18. Krieter based approached to the construction of nine-membered rings using a Mn-facilitated [4+5] cycloaddition	64
Scheme 19. Kato's two-step synthesis of nine-membered rings through an oxy-Cope ring expansion.....	65
Scheme 20. Janardhanam's preparation of <i>syn</i> -1,5-diene oxy-Cope precursors.....	66
Scheme 21. von Zezschwitz's preparation of <i>anti</i> -1,5-diene oxy-Cope precursors.....	67
Scheme 22. Snapper's preparation of <i>syn</i> -1,5-diene oxy-Cope precursors.....	67
Scheme 23. Snapper's anionic oxy-Cope leading to a mixture of <i>cis</i> and <i>trans</i> nine-membered cyclic enones	68
Scheme 24. Snapper's investigation of the transition state distribution for the anionic oxy-Cope ring expansion of cyclopentanes	68

Scheme 25. Application of Snapper's transition state predictions for the synthesis of a keystone intermediate in our didemnaketal A synthesis.....	70
Scheme 26. The attempted photochemical [2+2] cycloaddition and the resulting unexpected rearrangement	73
Scheme 27. The key step in Griengl's synthesis of sarkomycin A (197).....	73
Scheme 28. Bartlett's mechanism for the formation of tropolone (200).....	74
Scheme 29. Day's photochemical electrocyclization of tropolone	75
Scheme 30. A high yielding practicable photochemical electrocyclization of tropolone (204).....	76
Scheme 31. Silylation, conjugate reduction, and alkylation of the [3.0.2] bicyclic core	78
Scheme 32. Ring opening ring closing metathesis providing a 5/6 spirocyclic system..	79
Scheme 33. Attempted Wolff–Kishner reduction	80
Scheme 34. Attempted Mozingo reduction	81
Scheme 35. Ketone (206) reduction and xanthate (219) formation	82
Scheme 36. Radical cascade observed in [3.0.2] bicycle during attempted Barton-McCombie deoxygenation.....	83
Scheme 37. Selective and non-diastereoselective access to 222 through RORCM and NaBH ₄ reduction respectively for the purpose of making the Barton–McCombie substrates, 223	84
Scheme 38. Radical cascade observed in 5 / 6 fused spirocyclic system during attempted Barton-McCombie deoxygenation. TOCSY spin systems (green, blue) and NOESY correlations (red) were used to solve the structure of 225	85
Scheme 39. Corey's use of the halolactonization for the synthesis of prostaglandin F _{2α} (230).....	87
Scheme 40. Lactonization involving acyloxy radical intermediates are low yielding due to competing decarboxylation pathways.....	88
Scheme 41. Barton and Beckwith photolysis of <i>N</i> -iodoamides (239) and Corey's oxidative method are examples of C–O bond forming radical lactonization that avoid forming acyloxy radicals.....	89
Scheme 42. Lactones formed through the intramolecular addition of a radical to an α,β-unsaturated ester	90
Scheme 43. The Stork–Ueno radical lactonization method	91
Scheme 44. Bachi's oxyacyl radical cyclization using selenocarbonate precursors	91
Scheme 45. Xanthate-based lactonizations onto alkenes (Bachi) and alkynes (Nozaki)	93
Scheme 46. Yamamoto's xanthate mediated cascade cyclization.....	94
Scheme 47. Wood's tin-free conditions for the Barton–McCombie reaction	96
Scheme 48. Synthesis of a lactonization precursor from 5-norbornen-2-ol.....	98
Scheme 49. Synthesis of a bicyclo[3.3.0]octane lactonization precursor (276).....	98
Scheme 50. Synthesis of a bicyclo[3.2.0]heptane lactonization precursor (281).....	99
Scheme 51. The proposed mechanism for the Bachi-type oxygen-directed radical lactonization.....	100
Scheme 52. The proposed mechanism for the tin-free oxygen-directed radical lactonization.....	102
Scheme 53. Synthesis and xanthate-mediated radical lactonization of a silyl-protected precursor (298).....	105

Scheme 54. Synthesis and attempted xanthate-mediated radical lactonization of a strained precursor.	106
Scheme 55. Lewis acid-mediated [2+2] cycloadditions.....	112
Scheme 56. Tandem Friedel–Crafts acylation / Nazarov cyclization followed by an activated Zn reduction of the resulting α -chloroketone.....	115
Scheme 57. The catalytic cycle for the 1,4-hydrosilylation of an enone, producing a silyl enol ether (<i>eg.</i> 310).....	116
Scheme 58. The synthesis of our anionic oxy-Cope precursor (246).....	121
Scheme 59. Ring expanding anionic oxy-Cope reaction to make a mixture of <i>cis</i> - and <i>trans</i> - 247 , key intermediates in our didemnaketal synthesis.....	123
Scheme 60. Mechanism for a standard decarboxylation of an β -keto ester.....	124
Scheme 61. Attempted hydrolysis of <i>cis</i> -(2,7- <i>syn</i>)- 337 under acidic and basic conditions.....	125
Scheme 62. A low yielding Krapcho decarboxylation of the <i>cis</i> -(2,7- <i>syn</i>)- 337 , giving the key intermediate <i>meso cis</i> - 143	126
Scheme 63. DBU mediated conditions for the anionic oxy-Cope reaction producing <i>trans</i> -(2,7- <i>syn</i>)- 337 as a mixture of atropisomers and diastereomers.....	127
Scheme 64. The proposed conformation of <i>cis</i> -(2,7- <i>syn</i>)- 337 , accounting for the slow hydrolysis of the methyl ester.....	129
Scheme 65. The proposed conformation of <i>trans</i> -(2,7- <i>syn</i>)- 247 , accounting for the slow decarboxylation of the β -keto acid.....	130
Scheme 66. Tomooka’s enolization of <i>trans</i> - 163 , giving the less strained product, 1-(E)-5(E)- 339 exclusively.....	131
Scheme 67. Three step sequence transforming anionic oxy-Cope precursor 336 into the key intermediate 143 , isolated as an inconsequential mixture of <i>cis</i> and <i>trans</i> isomers.....	133
Scheme 68. The metathesis equilibrium appears to disfavour 9-membered rings.....	135
Scheme 69. Attempted dual asymmetric dihydroxylations leading to an unexpected non-anomeric spiroketal 259 as evidenced by TOCSY spin systems (blue, green, purple and cyan) and nOe correlations (red).....	140
Scheme 70. Use of thermodynamic control in accessing the non-anomeric spiroketal domain of spongistatin.....	145
Scheme 71. Crimmons uses a catalytic hydrogenation to kinetically trap a non-anomeric spiroketal.....	146
Scheme 72. Fuwa uses an iodo-spiroketalization to kinetically trap a non-anomeric spiroketal.....	147
Scheme 73. Observed non-anomeric spiroketal 350 arises through a cascading asymmetric dihydroxylation / hemiketalization / hetero-Michael addition sequence	148
Scheme 74. Hashimoto’s hemiketalization / hetero-Michael addition cascade used in the synthesis of (+)-pinnatoxin A.....	149
Scheme 75. The catalytic cycle for the Sharpless dihydroxylation with speculative mechanistic considerations to account for the observed non-hydroxy spiroketal 350	150
Scheme 76. Curtin–Hammett equilibrium kinetically trapping the non-anomeric spiroketal 350	151
Scheme 77. Catalytic cycle for biphasic Sharpless dihydroxylation and the monophasic Upjohn dihydroxylation.....	154

Scheme 78. Dual asymmetric dihydroxylations performed under Upjohn conditions leading to doubly anomeric spiroketal 341 as evidenced by TOCSY spin systems (blue, green, purple, and cyan) nOe correlations (red).	155
Scheme 79. A poorly selective esterification of our spiroketal fragment 341	156
Scheme 80. <i>Bis</i> -olefination of 378 followed by reductive removal of the protecting esters to give the crystalline diol 382 and the restoration of 341 by ozonolysis.....	158
Scheme 81. The oxidative cleavage of 289 to form aldehyde 291 , a suitable NHK coupling partner for late-stage assembly of didemnaketol A.....	160
Scheme 82. An expedient synthesis of the non-methylated analogue of the spiroketal domain of didemnaketol A.....	169
Scheme 83. ¹ H NMR spectral overlay comparing the initial spiroketal starting material (395 in red) with the diastereomeric mixture obtained after oxidative cleavage, NHK coupling using methyl vinyl bromide, then ozonolysis (in blue).....	174
Scheme 84. Three methods for inverting hindered alcohols that failed to accomplish the desired epimerization of the C11 alcohol	176

List of Tables

Table 1. Trends in ring strain for cycloalkanes, (CH ₂) _n	61
Table 2. Xanthate-mediated radical lactonizations producing an assortment of compounds resembling natural product cores.....	102
Table 3. Solvent optimization of the Xanthate-mediated radical lactonization	104
Table 4. Synthesis and xanthate-mediated radical lactonization trained precursors with potential cascade pathways	108
Table 5. Attempted enolization of 3-methylcyclopentanone (311) using increasingly bulky bases.....	113
Table 6. The optimization of hydrosilylation conditions aimed at eliminating enol isomerization.....	119
Table 7. Heats of formation for <i>cis</i> - and <i>trans</i> - 143 , along with their E and Z enol tautomers (340) calculated <i>ab initio</i> using the B3LYP 6-31 G(d) basis set.	132
Table 8. Synthesis of <i>meso</i> - 142 through the ring opening / cross metathesis of <i>cis</i> and <i>trans</i> - 143	136
Table 9. Sharpless asymmetric dihydroxylations using AD-mix- α and modified conditions consistently produce the singly anomeric spiroketal 350	142
Table 10. A comparison between the Felkin–Ahn and Cram Chelate models for predicting the stereochemical outcome on the C11 alcohol of 140 following an NHK coupling.....	168
Table 11. Attempted Wittig-type olfinations aimed at probing the final assembly of didemnaketel A	171
Table 12. An evaluation of NHK coupling conditions aimed at probing the final assembly of didemnaketel A.....	172

List of Figures

Figure 1. The prevalence of HIV/AIDS in developing countries compared to the percent of the population with access to treatment as of 2007 ¹	1
Figure 2. An HIV viron fusing with the cell membrane of a healthy T-4 cell, depositing RNA (green) and the three viral proteins. The interaction is obstructed with Selzentry (1) and Fuzeon (2)	3
Figure 3. Pro-viral RNA (green) is processed into DNA (red) by HIV-RT and incorporated into the host cell's genome by HIV-IN, both of which are druggable targets (eg. 3-7). The compromised DNA is then transcribed in to m-RNA (blue)	5
Figure 4. Immature polypeptides encoded in the m-RNA (blue) are synthesized then processed into viral enzymes by HIV-PR. These enzymes, along with pro-viral RNA (green), congregate under a viral bud and evacuate the cell in a new viron.....	6
Figure 5. HIV-PR is shown with expansions of the three important structural domains: the molecular flap (top), the catalytic site (middle), and the antiparallel β -sheet (bottom)	7
Figure 6. All current commercially available HIV-PR inhibitors.....	8
Figure 7. Hot spots (shown in red) in the protein-protein interaction between the subunits (blue and green) of HIV-PR. Leu-97 is an interior peptide and, therefore, not visible.....	11
Figure 8. Examples from the various classes of HIV-PR dimerization inhibitors.....	13
Figure 9. The potent dimerization inhibitor, N-palmitoyl-Try-Glu-Leu-OH (27) bound to HIV-PR monomer in the super-closed conformation	14
Figure 10. Recently discovered nonpeptidic dissociative inhibitors of HIV-PR.....	15
Figure 11. Ursolic acid (30) and schisanlactone A (31), naturally occurring dimerization inhibitors of HIV-PR.....	17
Figure 12. Natural HIV-PR inhibitors, didemnaketel A (32) and B (33)	19
Figure 13. The decomposition of the ascidian isolate, didemnaketel C (34), into HIV-PR inhibitors didemnaketel A (32) and B (33).....	20
Figure 14. Rich's analogues based on the linear (35) and spiroketal (36) domains of didemnaketel A	21
Figure 15. A retrosynthetic comparison of the spiroketal assembly performed by Tu, Fuwa, and Ito	24
Figure 16. Discrepancies in the chemical shift of the ¹ H and ¹³ C NMR spectra are plotted, comparing products discovered by Faulkner with the synthetic analogues prepared by Tu and Fuwa	45
Figure 17. Faulkner's degradation analysis of didemnaketel C for assigning the relative stereochemistry of the natural product.....	48
Figure 18. The Mosher method for determining the absolute stereochemistry of a chiral secondary alcohol predicts that $\Delta\delta_{(S-R)}$ is negative for the substituent L ₁ and positive for L ₂	49

Figure 19. Faulkner's Mosher analysis for elucidating the absolute stereochemistry of didemnaketal C at C5, C8, and C21. Chiral shifts are reported in blue while atom numbers are labeled in red	50
Figure 20. Faulkner's determination of the absolute stereochemistry of the spiroketal domain using the Mosher method and using PGME amide. The potential interference between the MTPA auxiliaries on C8 and C11 is indicated as well as the anomalous hydrogen bond	52
Figure 21. A retrosynthetic analysis for Dr. Caleb Bromba's assembly of the linear branch of didemnaketal A (135)	54
Figure 22. A retrosynthetic analysis for the late-stage coupling between the linear and spiroketal domains (135 and 141 , respectively) of didemnaketal A (32).....	55
Figure 23. A retrosynthetic analysis for the synthesis of the spiroketal moiety of didemnaketal A (139)	57
Figure 24. Use of symmetry for the expeditious assembly of the spiroketal moiety of didemnaketal A	59
Figure 25. Retrosynthetic analysis of the anionic oxy-Cope precursor	71
Figure 26. TOCSY spin systems (purple, green, blue) and NOESY correlations (red) used to solve the structure of 220	83
Figure 27. Some of the possible synthetic strategies for forming lactones.....	86
Figure 28. The oxyacyl radical compared with the xanthate derived radical intermediate in the oxygen-directed lactonization	93
Figure 29. Natural products with lactone cores accessible through an oxygen-directed radical cyclization	97
Figure 30. A retrosynthetic re-evaluation of our entry into the didemnaketal A synthesis	111
Figure 31. Commonly used hydrosilylation catalysts	117
Figure 32. Crystal structure of the <i>trans</i> nine-membered cyclic ketone 338	131
Figure 33. Our strategy for completing the synthesis of the spiroketal moiety of didemnaketal A	134
Figure 34. Chiral chinchona alkaloids used as ligands in the Sharpless asymmetric dihydroxylation	137
Figure 35. Sharpless' mnemonic for choosing AD-mix (top left) and the hyperconjugative resonance structures that contribute to the anomeric effect (top right). The predicted out-come for the AD-mix- α dihydroxylation of <i>meso</i> - 142 is shown along with the four hypothetical modes of spiroketalization. Favorable anomeric relationships are highlighted in blue while substituents with unfavorable 1,3-diaxial interactions are shown in red.....	138
Figure 36. The cytotoxic marine macrolide, spongistatin 1 (351) with an expansion of the non-anomeric C / D ring system	143
Figure 37. Discrepancies in the chemical shift of the ^1H and ^{13}C NMR spectra are plotted, comparing the spiroketal domain of the authentic sample with 380 and the synthetic version prepared by Tu	157
Figure 38. Crystal structure of the <i>bis</i> -allylic alcohol 382 , confirming a stereochemical arrangement that matches the spiroketal domain of nominal didemnaketal A.....	159
Figure 39. A retrosynthetic analysis for the final assembly of didemnaketal A featuring a Suzuki–Miyaura coupling.....	164

Figure 40. A retrosynthetic analysis for the final assembly of didemnaketral A, featuring a Wittig-type olefination	165
Figure 41. A retrosynthetic analysis for the final assembly of didemnaketral A, featuring an NHK coupling	167
Figure 42. Crystal structure of the model spiroketal 394	170
Figure 43. The original structural hypothesis proposed for didemnaketral A and a structural isomer prepared by Tu, neither of which matched the spectral data for the authentic sample.....	177
Figure 44. The original structural hypothesis proposed for didemnaketral B and the revised structure as verified by Fuwa in which the spiroketal moiety is inverted.....	179
Figure 45. A possible dissociative inhibitor derived from the symmetrical didemnaketral-like spiroketal 407 compared with an established molecular tong inhibitor of HIV-PR (23)	182

List of Abbreviations

9-BBN	9-borabicyclo(3.3.1)nonane
Ac	acetyl
AD	asymmetric dihydroxylation
AIBN	azobisisobutyronitrile
AIDS	acquired immunodeficiency syndrome
BDE	bond dissociation energy
BI	Boehringer Ingelheim
BMS	Bristol-Myers Squibb
Bn	benzyl
Bu	butyl
Bz	benzoyl
CBS	Corey-Bakshi-Shibata
CDA	chiral derivatizing agent
Cp	cyclopentadiene
cy	cyclohexane
DCM	dichloromethane
DDQ	2,3-Dichloro-5,6-Dicyanobenzoquinone
DEAD	diethyl azodicarboxylate
(DHQ) ₂ AQN	hydroquinine anthraquinone-1,4-diyl diether
(DHQ) ₂ PHAL	hydroquinine 1,4-phthalazinediyl diether

(DHQD) ₂ PHAL	hydroquinidine 1,4-phthalazinediyl diether
DIBAL	diisobutylaluminium hydride
DMAP	<i>N,N</i> -dimethyl-4-aminopyridine
DMF	<i>N,N</i> -dimethylformamide
DMP	Dess–Martin periodinane
DMS	dimethyl sulfide
DMSO	dimethyl sulfoxide
DNA	deoxyribonucleic acid
dppf	1,1'- <i>bis</i> (diphenylphosphino)ferrocene
EI	electron ionization
EKO	exploring key orientations
equiv	equivalents
ESI	electrospray ionization
Et	ethyl
FDA	United States Food and Drug Administration
FI	fusion inhibitor
GSK	GlaxoSmithKline
HAART	highly active antiretroviral therapy
H-G	Hoveyda–Grubbs
HIV	human immunodeficiency virus
HMPA	hexamethylphosphoramide
HRMS	high resolution mass spectrometry
HWE	Horner–Wadsworth–Emmons

IAA	isotope abundance analysis
Imid	imidazole
IN	integrase
<i>i</i> -Pr	isopropyl
IR	infrared
KHMDS	potassium <i>bis</i> (trimethylsilyl)amide
LA	Lewis acid
LAC	ligand accelerated catalysis
LAH	lithium aluminium hydride
LDA	lithium diisopropylamide
LHMDS	lithium <i>bis</i> (trimethylsilyl)amide
<i>m</i> -CPBA	<i>meta</i> -chloroperoxybenzoic acid
Me	methyl
MOM	methoxymethyl ether
<i>m</i> -RNA	messenger ribonucleic acid
Ms	mesyl
MTPA	α -methoxy- α -(trifluoromethyl)phenylacetic acid
NBS	<i>N</i> -bromosuccinimide
NHK	Nozaki–Hiyama–Kishi
NMM	<i>N</i> -methylmorpholine
NMO	<i>N</i> -methylmorpholine <i>N</i> -oxide
NMR	nuclear magnetic resonance
<i>n</i> Oe	nuclear Overhauser effect

PG	protecting group
PGME	phenylglycine methyl ester
Ph	phenyl
PI	protease inhibitor
PMB	<i>para</i> -methoxybenzyl
PMP	<i>para</i> -methoxyphenyl
ppm	parts per million
PPTS	pyridinium <i>para</i> -toluenesulfonate
PR	protease
PTSA	<i>para</i> -toluenesulfonic acid monohydrate
py	pyridine
ROCM	ring opening cross metathesis
RORCM	ring opening ring closing metathesis
RT	reverse transcriptase
rt	room temperature
SPS	solvent purification system
TBAF	tetra- <i>N</i> -butylammonium fluoride
TBDPS	<i>tert</i> -butyldiphenylsilyl
TBS	<i>tert</i> -butyldimethylsilyl
TEA	triethylamine
TES	triethylsilyl
THF	tetrahydrofuran
TIPS	triisopropylsilyl

TLC	thin layer chromatography
TMS	trimethylsilyl
Tr	trityl
Ts	<i>para</i> -toluenesulfonyl
UV	ultra violet
WHO	World Health Organization

Acknowledgments

Many people have helped me along the way, but I am the most deeply indebted to my supervisor, Jeremy Wulff. When I was struggling with my research, his deep understanding of chemistry and his untiring and enthusiasm always guided me to a resolution. I'm also tremendously grateful to Benoît Moreau, not just for his candid advice, but for exceeding the role of mentor and offer me his friendship as well. Thank you for making me to feel welcome in Montreal.

I gratefully acknowledge my supervisory committee—Dr. Peter Wan, Dr. Robin Hicks, Dr. Martin Boulanger, and Dr. Peter Wilson—for their thoughtful consideration of my research. Thank you also to Dr. Ori Granot, Dr. Tyler Trefz, Ms. Chris Greenwood and especially Mr. Chris Barr for sharing your analytical expertise. During my time here, I have grown as an instructor as well as a researcher, and for that I must thank Dr. Peter Marrs, Dr. Dave Berry, Ms. Kelli Fawkes, and Ms. Nichole Taylor. I thoroughly enjoyed the time I spent working for you.

Furthermore, it is a pleasure to acknowledge my lab mates. As undergraduate researchers, Jeremy Mason and Nadine Hewitt made significant contributions to this body of work. I appreciate your dedication and all your hard work. Special thanks are also due to Caleb Bromba, my partner on the didemnaketol project and a great friend—someone who was always available to commiserate the setbacks, puzzle over the

solutions, and celebrate the successes. Thanks also to Natasha O'Rourke for keeping me company during the late nights, to Mike Brant for keeping me laughing during the tense times, and to Katherine Davies for keeping me honest. Finally, a tip o' the hat to those Wulff group members with whom I've had less overlap, but no less admiration: Ronan Hanley, Jun Chen, Bobby Ryane, and Mark Fairchild. Best of luck to all of you!

I also wish to acknowledge Boehringer Ingelheim and the University of Victoria for their generous financial support.

Dedication

*For my parents who taught me to value education
And for Emma who supported me in that pursuit*

Chapter 1 — Introduction

1.1 HIV and AIDS

Acquired immune deficiency syndrome (AIDS) along with its antecedent condition, human immunodeficiency virus (HIV), poses an exigent threat to global health. In fact, the World Health Organization (WHO) estimates that as many as 33 million people are living with HIV, including 3.3 million children.¹ With 2.8 million new infections in 2010, the spread of the pandemic outpaces the annual increase in people receiving treatment; particularly in developing countries where the standard of care is low. Here, the effects of the virus are particularly devastating (see figure 1).

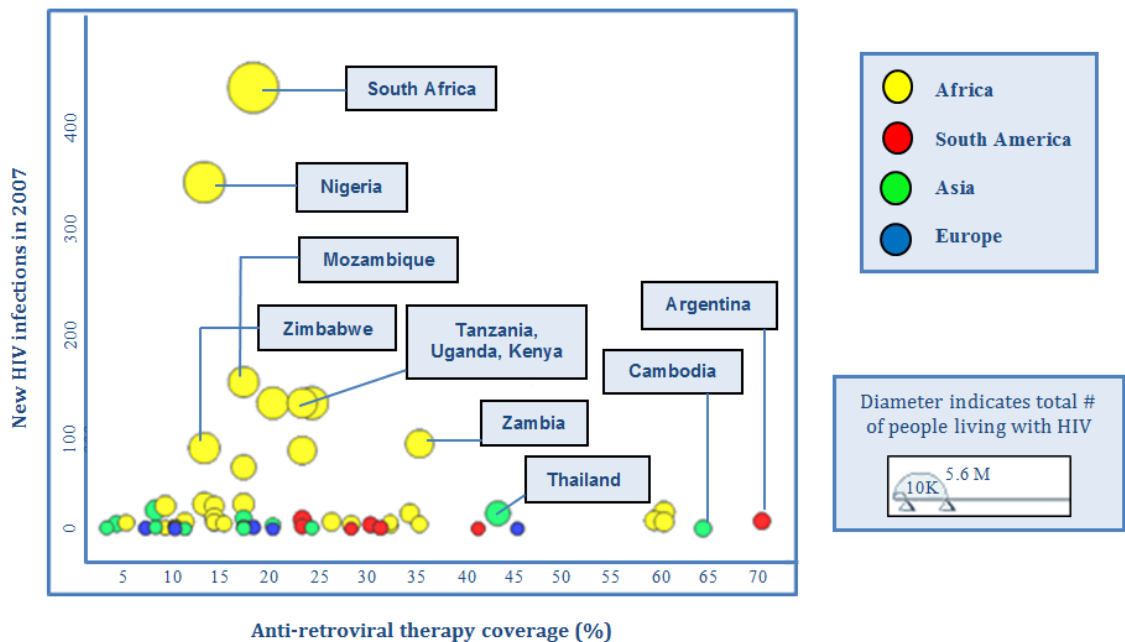


Figure 1. The prevalence of HIV/AIDS in developing countries compared to the percent of the population with access to treatment as of 2007¹

The AIDS virus cannot replicate or spread without first infecting a cellular host, usually a class of white blood cells known as the T-helper (or T-4 cell). Normally, when threatened with infection, T-4 cells constitute the vanguard of the body's resistance, initiating and coordinating the immunological response through various chemical signals. Thus, it is the insidious nature of HIV to prey on the very cells called upon to fight the infection.

After contracting HIV, however, it is often not immediately obvious that one's immunological defenses have been compromised. The infection is characterized by an initial latent period where the patient, though contagious, may experience symptoms that are no worse than those of a mild cold. During this period, which can sometimes last for years, the virus' genetic material becomes deeply entrenched in the patient's cells. At some critical point the virus dramatically accelerates its replication, up to a billion times per day, exhausting the infected cells, and destroying them as it spreads. The loss of white blood cells suppresses the immune system, making it increasingly easy for the virus to flourish. HIV is said to have progressed into AIDS when the number of T-4 cells drops below $200/\mu\text{l}$.² In this state the patient is highly vulnerable to cancer, tuberculosis, and other opportunistic infections.³ Eventually, these secondary diseases can no longer be treated effectively and they cause the patient's death.

Obviously, to be diagnosed as HIV positive is a terrifying prospect; however with access to state-of-the-art medicine, the progression of the disease can be held in check. Intensive research over the past three decades has revealed many therapeutic targets at

various stages in the HIV replication cycle, leading to a host of efficacious drugs. The virus' initial objective is to identify a suitable host cell and infiltrate the cellular membrane. Here is the first front at which it is possible to mount a pharmaceutical defense. The surface of an HIV viron is decorated with a protein complex (gp120 / gp41) that has evolved to recognize CD-4 glycoproteins, entities ubiquitous on the surface of healthy T-4 cells.⁴ The interaction between these two protein ensembles induces a cascade of conformational changes, drawing the viron toward the cell, docking it, then after unsheathing a harpoon-like protrusion (gp41), the viron punches a hole through the cellular membrane (as shown in figure 2).⁵ This fusion pore tears open until it is large enough for the viron to pour out its contents into the cytoplasm.

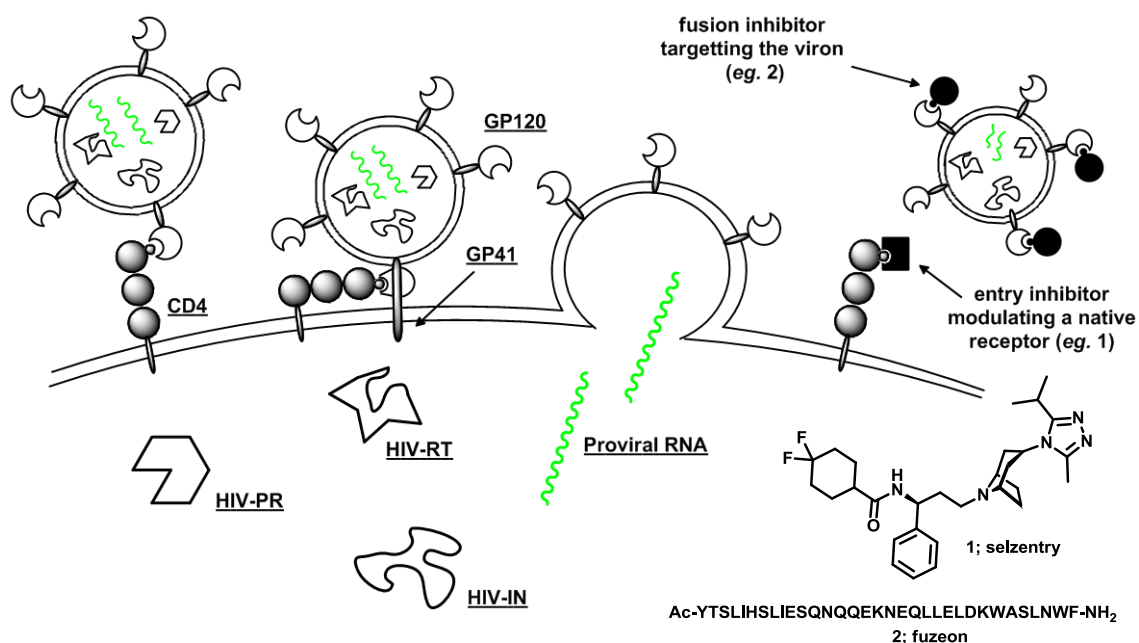


Figure 2. An HIV viron fusing with the cell membrane of a healthy T-4 cell, depositing RNA (green) and the three viral proteins. The interaction is obstructed with selzentry (1) and fuzeon (2)

However, the violation of the cell can be impeded through a class of anti-retroviral drugs, known as fusion inhibitors (FI). These agents are designed to obstruct contact between the two surface proteins either by preferentially binding the native CD-4 on healthy T-4 cells, as with selzentry (**1**, maraviroc, Pfizer), or by targeting the fusion proteins on the viral capsid, like fuzeon (**2**, enfuvirtide, Roche).⁶

If a viron successfully couples with a T-4 cell, then that cell receives into its cytoplasm two identical strands of pro-viral RNA and the three enzymes needed to process it: a reverse transcriptase (HIV-RT), an integrase (HIV-IN), and a protease (HIV-PR) (shown in figure 3). The reverse transcriptase binds the single-stranded RNA and converts it into double-stranded pro-viral DNA.⁷ Unfortunately, the absence of proof-reading enzymes ensures that this process is highly error-prone and the resulting mutations allow HIV to rapidly develop drug resistance.⁸ Currently, there are over a dozen drugs targeting this stage of the viral replication cycle. The majority of these, including the first FDA approved antiretroviral agent, retrovir (**3**, azidothymidine, GSK), are deoxynucleotide analogues. When HIV-RT mistakenly incorporates these fragments into the growing DNA chain, they terminate all further progress to the synthesis. There is also a growing class of non-nucleotide inhibitors that, upon binding non-competitively near the active site of HIV-RT, impede DNA synthesis by interfering with the movement of crucial protein domains. Notable examples of this class of drug include viramune (**4**, nevirapine, BI) and sustiva (**5**, efavirenz, BMS).

If HIV-RT operates uninhibited, then the pro-viral DNA will find an integrase enzyme (HIV-IN) to cleave dinucleotides from both ends of the strand, creating what are called “sticky ends”.⁹ The HIV-IN then ushers the DNA into the nucleus, finds a convenient loop of host’s DNA, and splices in the viral code. Fortunately, this enzyme is also a druggable target. Both stribild (6, elvitegravir, Gilead) and isentress (7, raltegravir, Merck) are examples of inhibitors that competitively bind the HIV-IN’s active site (as shown in figure 3).

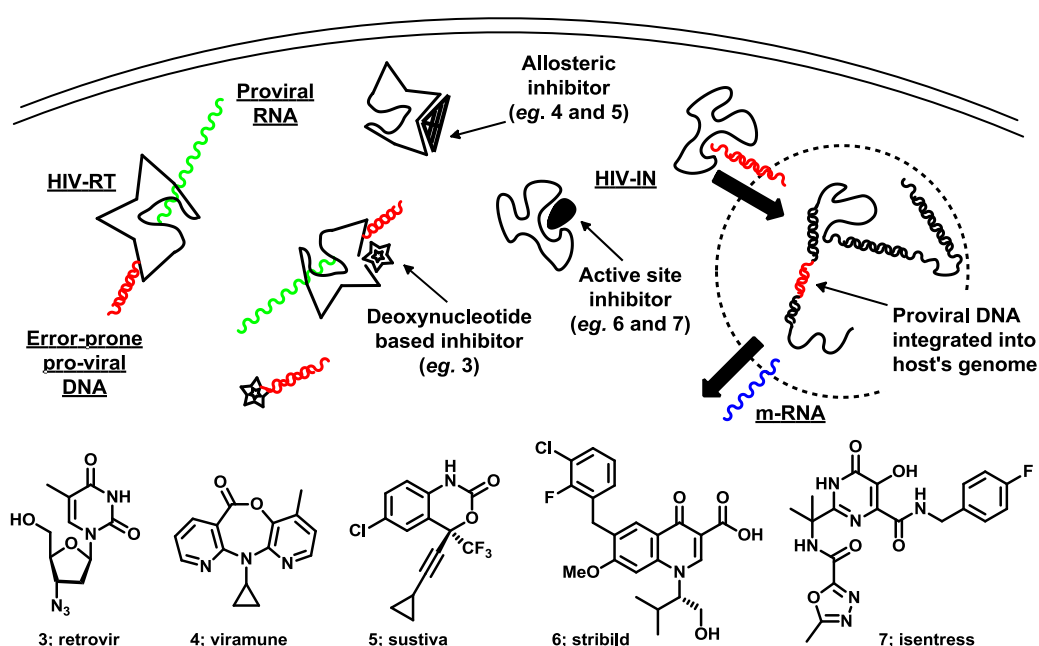


Figure 3. Pro-viral RNA (green) is processed into DNA (red) by HIV-RT and incorporated into the host cell’s genome by HIV-IN, both of which are druggable targets (eg. 3-7). The compromised DNA is then transcribed in to m-RNA (blue)

The integrated viral DNA can lie dormant for years, waiting until certain transcription factors signal the cell to process the malignant gene into m-RNA. After migrating from the nucleus out into the cytoplasm, the m-RNA is threaded through an array of ribosomes producing a long polypeptide, the raw material needed to re-construct the three viral

enzymes. Next, HIV-PR, acts as a pair of chemical scissors, cleaving the polypeptide into fragments which then self-assemble into mature enzymes.¹⁰ Along with the pieces of viral RNA, these enzymes migrate to staging zones under the cellular membrane. They are corralled into a viral bud and leave the cell acquiring a new envelope which is outfitted with host and viral surface proteins, primed to infect neighboring cells (as shown in figure 4). However, if proteolysis is blocked by inhibiting the retroviral aspartyl protease, the viral particles remain structurally immature, disorganized, and non-infectious.

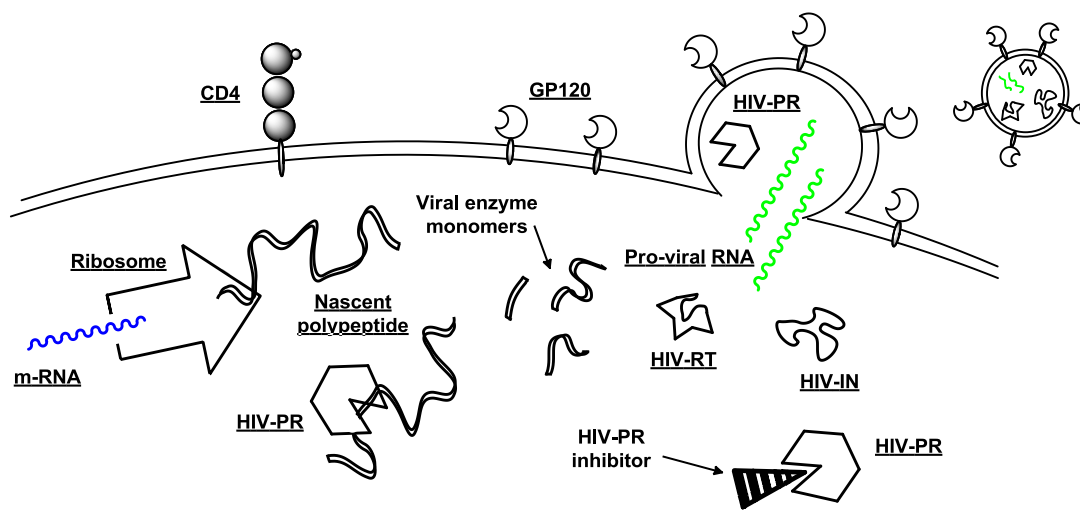


Figure 4. Immature polypeptides encoded in the m-RNA (blue) are synthesized then processed into viral enzymes by HIV-PR. These enzymes, along with pro-viral RNA (green), congregate under a viral bud and evacuate the cell in a new virion

HIV-PR is active only as a homodimer (shown in figure 5). A pair of identical 99 residue monomers self-assemble to form the C₂-symmetrical complex, each piece contributing mirroring halves to the catalyst's key structural features: the two molecular "flaps" which open to permit access to the binding pocket then, after closing, lock the substrate in a stabilizing network of hydrogen bonds; the interdigitating C- and N-termini

that form a 4-stranded antiparallel β -sheet, a clasp that holds the structure together; finally, the active site with its matching aspartic acids residues, one to activate the peptide, the other to direct the nucleophilic attack of water leading to proteolysis.¹¹

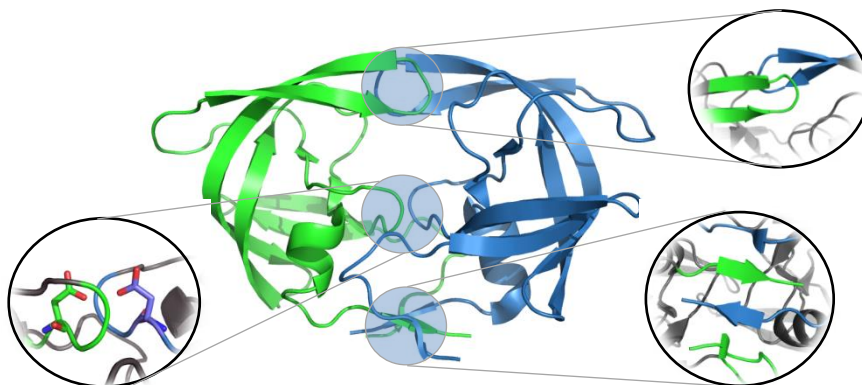


Figure 5. HIV-PR is shown with expansions of the three important structural domains: the molecular flap (top), the catalytic site (middle), and the antiparallel β -sheet (bottom)

1.2 HIV-PR Inhibitors

Peptide mimicry tailored to this active site has proven to be a fruitful approach to drug design. In 1995, Hoffman-La Roche released invirase (**10**, saquinavir, Roche), the first of the protease inhibitors (PI). Within ten years there were nine more similar drugs on the market: norvir (**8**, ritonavir, Abbott), aptivus (**9**, tipranavir, BI), reyataz (**11**, atazanavir, BMS), viracept (**12**, nelfinavir, Pfizer), prezista (**13**, darunavir, Tibotec), agrenerase (**14**, amprenavir, GSK), kaletra (**15**, lopinavir, Abbott), lexiva (**16**, fosamprenavir, ViiV), and crivivan (**17**, indinavir, Merck). All of these drugs (see figure 6) manifest the concept of transition state mimicry. The core scaffold is some non-cleavable dipeptide isostere, designed and optimized to have the same topology as the tetrahedral transition state of a

typical HIV-PR substrate. The common design origin of all PI's is revealed most conspicuously in one particular structural feature—the critical hydroxyl group which impersonates the attacking water molecule found hydrogen bonded to the carboxyl groups of the catalytically active aspartic acid residue (shown in figure 5).^{12,13}

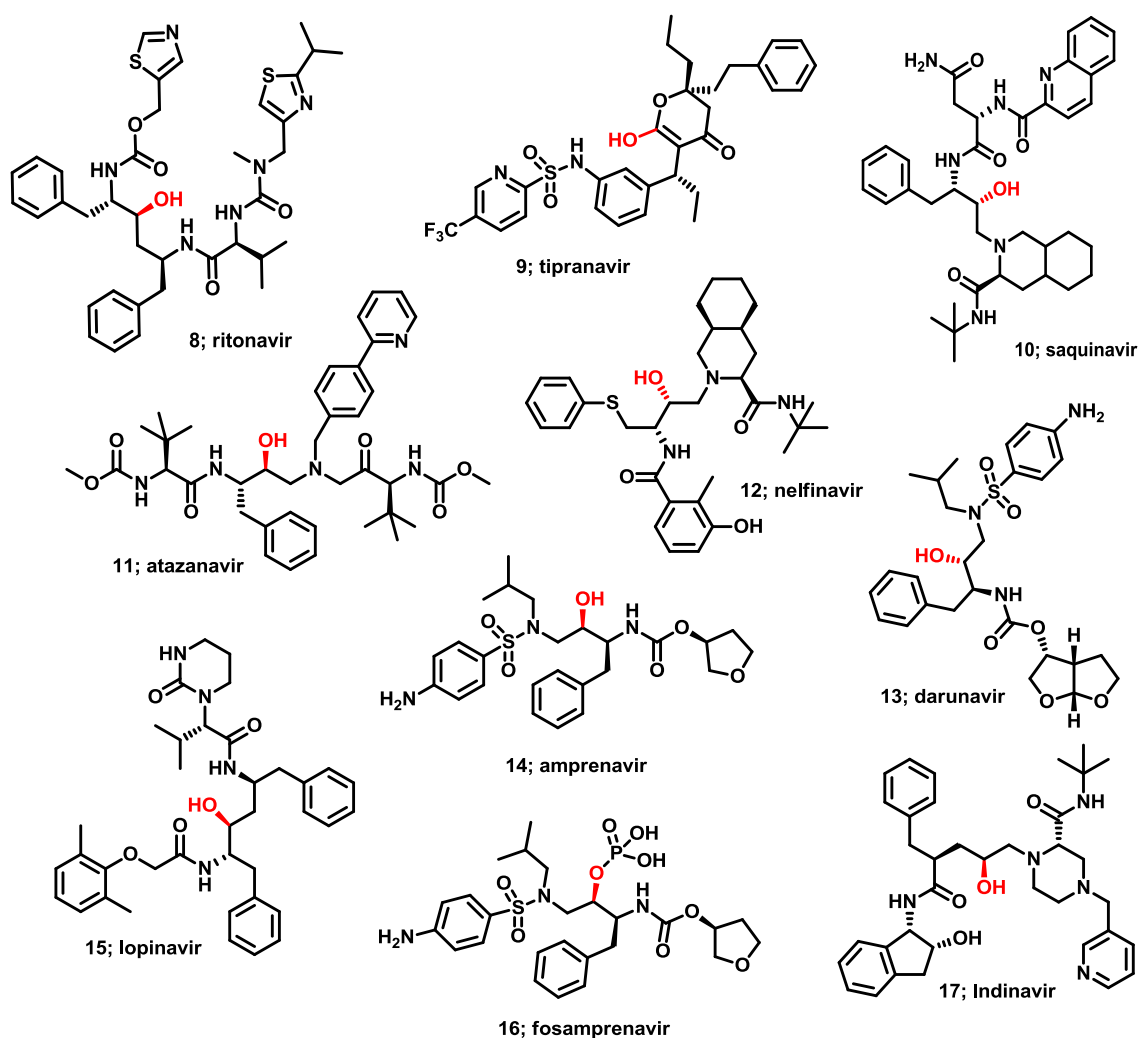


Figure 6. All current commercially available HIV-PR inhibitors

The advent of HIV-PR inhibitors heralded the development of "highly active antiretroviral therapy" (HAART), currently the first line of treatment in controlling the HIV infection.¹⁴ A patient receiving HAART is prescribed a combination of three or more drugs, at least two of which operate through distinct mechanisms. This redundancy is built into the treatment to help patients control their viral load, to delay the onset of symptoms and the progression of HIV into AIDS, but most importantly, it impedes the virus from evolving resistance. Whereas once an HIV diagnosis was considered a death sentence, with HAART it has become a chronic yet manageable disease.

Although both the length and the quality of patients' lives have dramatically improved, HIV/AIDS cannot yet be cured and HAART demands a complex, life-long regimen with a high pill burden and expensive treatment costs. Part of the problem is that many of the current protease inhibitors suffer from poor bioavailability or they are plagued with debilitating side effects and toxicity issue (*eg.* lipodystrophy, central adiposity, breast hypertrophy, hyperlipidemia, insulin resistance).¹⁴ Worse, the emergence of protease inhibitor resistant HIV-1 strains¹⁵ and the appearance of cross-resistance¹⁶ severely limit long term treatment options. It has been estimated that as many as a quarter of all newly infected patients are harboring at least one drug-resistant viral strain.¹⁷ Therefore, the development of novel drugs, particularly non-peptidic inhibitors which show broad-spectrum activity against multidrug-resistant HIV variants, remains a crucial therapeutic objective.

1.3 Dissociative Inhibitors

Even before the first crystal structure of HIV-PR had been solved,¹⁸ Meek and fellow researchers at GSK were already anticipating an alternative mode of inhibition—one that could prove virtually “drug-resistance-proof”.¹⁹ The dimeric HIV-PR exists in equilibrium with its monomeric subunit. However, as the catalytic site forms at the protein interface, only the dimeric structure is capable of maturing the virus. While there remains some contention over the dissociation constant (K_d) for this equilibrium,²⁰ under physiological conditions, it is believed to lie in the low μM range. HIV-PR is present in infected T-4 cells at a concentration of about 10 nM (although it is likely that localized concentrations may be much higher)²¹. Meeks and his coworkers theorized that, given such low concentrations along with such a high K_d , compounds that discourage protein dimerization should profoundly affect enzymatic activity by driving the equilibrium toward the monomer. Alternatively, the HIV-PR dimer may form through a templated association facilitated by the substrate and the inhibitor may disrupt this process. Either way, rather than inhibiting HIV-PR by blocking the active site, a dimerization inhibitor (also known as a dissociative inhibitor) would entirely preclude the formation of an active site.

In fact, the inactivation of HIV-PR through a dissociative mechanism is a highly feasible strategy. The stability of the dimeric complex rests on a small number so called “hot spots”, points of contact between subunits that are associated with high binding energy (colored red in figure 7). These vulnerabilities in the enzyme’s architecture have been revealed through virtual alanine scanning mutagenesis.²² Five sets of residues have

been identified as crucial for maintaining the structural integrity of HIV-PR: a key hydrogen bond associated with Arg-87; another interaction between the molecular “flaps” involving Ile-50; and a four-stranded antiparallel β -sheet with crucial contributions from Leu-5, Leu-97, and Phe-99. A dissociative inhibitor would likely target one or more of these three interactions.

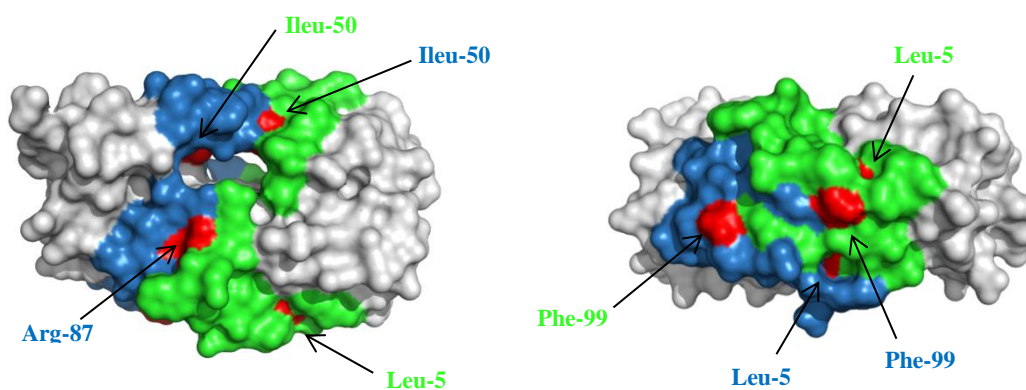


Figure 7. Hot spots (shown in **red**) in the protein-protein interaction between the subunits (**blue** and **green**) of HIV-PR. Leu-97 is an interior peptide and, therefore, not visible

It is fortunate, then, that all of these residues are remote from HIV-PR’s mutation-prone active site. Furthermore, these interfacial peptides are highly conserved among all known HIV-1 and HIV-2 isolates.^{23,24} If a mutation were to appear in one of the monomeric subunits it would almost certainly be deleterious to the dimerization affinity—that is, unless outrageous fortune happened to permit a concomitant mutation in the pairing subunit. As this event is highly improbable, dissociative inhibitors targeting the “hot spots” on HIV-PR should develop resistance much slower than drugs that bind in the active site.^{21,25}

In designing a dissociative inhibitor for HIV-PR, the most advantageous region to target is the β -sheet that forms between the interlocking C- and N-termini of the matched subunits. This region provides over half of the interfacial hydrogen bonds and contributes close to 75% of the total Gibbs free energy for HIV-PR dimerization.²⁶ Mutations and various other chemical manipulations in this region have been shown to disable the enzyme, confirming that this is indeed a vital interaction.

Proof that small molecules can actually disrupt the stability of the HIV-PR dimer was provided in 1991.²⁷ Zhang showed that the tetrapeptide, Ac-Thr-Leu-Asn-Phe-COOH (**18**), a sequence derived from the C-terminus of HIV-PR, did indeed inhibit HIV-PR through a dissociative mechanism. Later that year, Schramm showed that truncated peptides derived from the N-terminus (**19**) were also moderately active (shown in figure 8).^{28,29}

Following this discovery, various groups sought to improve binding by creating better β -sheet mimics. A pair of short peptide sequences derived from both the C- and N-terminus were synthesized and cross-linked with a flexible bridge. The optimal length for this linker was found to be 10 Å gap, approximately the length of three glycine residues (**19**)³⁰ or 14 methylene units^{31,36} (see **20** and **21** respectively in figure 8). The compounds were moderately active; however, some optimization through mutational and deletion analysis, as well as computer modeling, revealed peptide sequences with better hydrogen bonding interactions, thereby improving binding constants.³⁷

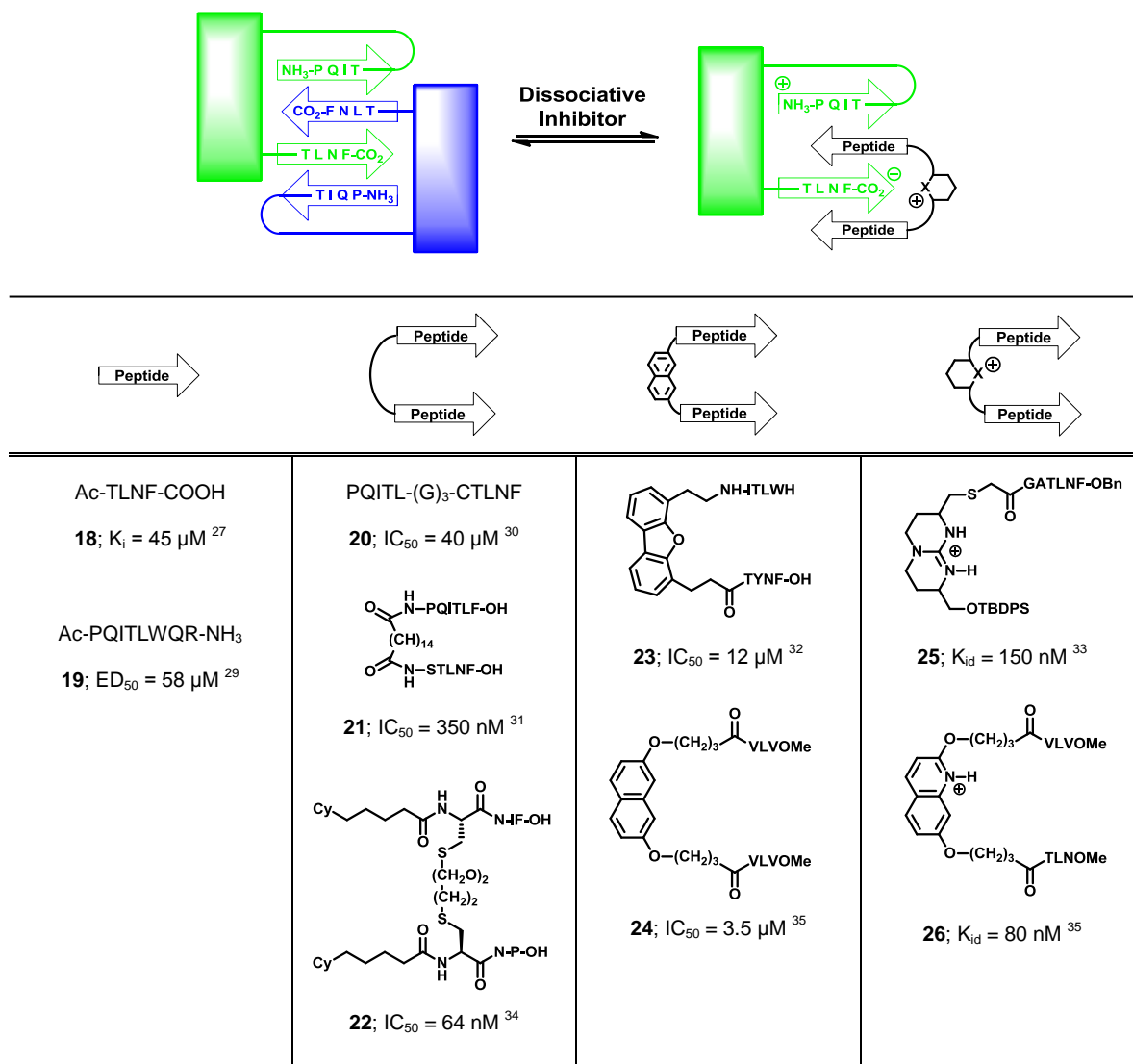


Figure 8. Examples from the various classes of HIV-PR dimerization inhibitors

It was theorized that, due to the conformational freedom in the flexible tether, these inhibitors were paying a severe entropic penalty binding the monomeric subunit. Accordingly, new inhibitors were designed around constrained scaffolds (*eg.* benzo, nafto^{35,38} (**24**), and dibenzofurano^{32,39} (**23**) in figure 8). In this motif, now known as “molecular tongs”, the two peptidic strands are pre-organized around the carbocycle to form the antiparallel beta sheets. These rigid tong scaffolds were further improved by

incorporating charged heterocycles; pyridines,⁴⁰ guanidiniums,³³ (25) and quinolines³⁵ (26), for example. The cationic heteroatoms are believed to form a salt bridge with the carboxylate anion on the C-terminus of the protease monomer.

Currently, the most potent dissociative inhibitors are short interface peptides with hydrophobic (*ie.* palmitoyl) moieties grafted onto the N-amino terminus (see compound 27 in figure 9).⁴¹ As before, the peptidic strand has been optimized to form a β -sheet between the C- and N- termini, disrupting enzyme dimerization. The inhibitor's lipophilic domain then binds to the hydrophobic pocket which is only exposed in the monomeric subunit. It has been theorized that the β -hairpin which forms one of the molecular flaps will fold over the lipophilic part of the inhibitor, gripping it in what has been termed a "super-closed" conformation. The compound N-palmitoyl-Try-Glu-Leu-OH (27) inhibits the dimerization of HIV-PR with K_{id} of 0.3 nM.

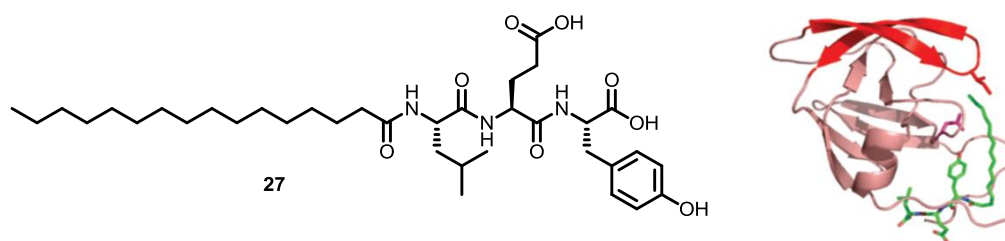


Figure 9. The potent dimerization inhibitor, N-palmitoyl-Try-Glu-Leu-OH (27) bound to HIV-PR monomer in the super-closed conformation

While enormous strides are being made toward increasing the potency of dissociative HIV-PR inhibitors, unfortunately, the peptidic nature of these compounds precludes them from ever being strong drug candidates. Generally, they suffer from poor bioavailability. If administered orally, they would only be metabolized in the gut. Otherwise, hydrolysis

by plasma and tissue peptidases would ensure that they have very short half-life *in vivo*. Therapeutic peptides also tend to elicit immunological responses. Finally, the monomer-inhibitor complexes are often poorly soluble in water. Consequently, there is an emerging trend to break away from peptide based inhibitors. Ongerer, for instance, has taken a conventional naphthalene based “molecular tong” and progressively diminished its peptidic character by introducing oligohydrazide bonds into the peptidomimetic arms.⁴² His best non-peptidic inhibitor (**28** in figure 10) had a K_{id} of 50 nM, not to mention reduced hydrophobicity and increased metabolic stability. Recently, Burgess reported a series of nanomolar inhibitors (*eg.* **29**) discovered through a method he calls “Exploring Key Orientations” (EKO).⁴³ EKO is an algorithm that analyzes protein-protein interaction interfaces then matches that data with appropriately decorated privileged scaffolds. It is anticipated that applications of this exciting new approach will soon extend far beyond HIV-PR inhibitors.

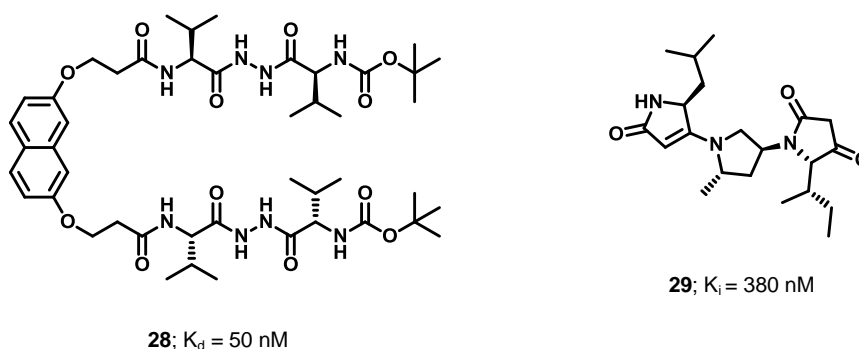


Figure 10. Recently discovered nonpeptidic dissociative inhibitors of HIV-PR

1.4 Natural Dissociative Inhibitors

Optimizing out vestiges of an inhibitor's peptidic origin for the sake of more drug-like attributes is a slow and tedious process. Furthermore, the peptidomimetic approach hems in the search for drug candidates to pitifully small region of an infinitely vast chemical space, a region with which investigators have already become thoroughly conversant.⁴⁴ An alternative to this restrictive paradigm is to use living organisms as a source of biologically active compounds. Natural products are built by protein-based machinery to interact with enzymes or receptors for the benefit of the host organism. Their size, stunning structural arrangements, and stereochemical complexity reflect continual evolutionary optimization for cell-permeability and protein recognition. Therefore, it's not surprising that many natural products already possess potency, selectivity, and various pharmacokinetic traits that are desirable in a therapeutic drug.

In 1987, the National Cancer Institute (NCI) spearheaded an extensive evaluation of natural sources, a search for compounds demonstrating promising antiretroviral activity. Within ten years, the program had screen over 60,000 aqueous and organic extracts derived from microorganisms, terrestrial plants and lichens, marine invertebrates, and algae. The effort was generously rewarded. Almost 15% of the species evaluated produced molecules that were active in the NCI's screen.⁴⁵ Academic and pharmaceutical research groups have continued the search thereafter and the catalogue of antiretroviral natural products grows every year.⁴⁶⁻⁴⁸ However, of these manifold non-peptidomimetic inhibitors, only three natural products have been demonstrated to inhibit HIV-PR through a dissociative mechanism.

Ursolic acid (**30** shown in figure 11) was the first of these rare inhibitors to be uncovered.⁴⁹ This pentacyclic triterpene is relatively abundant and can be found in many plants: peppermint, rosemary, lavender, oregano, thyme, hawthorn, prunes and especially apples. The waxy skin of a single apple may contain over 50 mg of ursolic acid. Shramm was led to the compound by querying the Cambridge Structural Database (CSD) for small molecules bearing a topographical resemblance to an ideal peptidic pharmacophore. The hits were then winnowed on the basis of commercial availability, structural rigidity, and through computer simulated docking to the HIV-PR monomer. Finally, the ideal compounds were evaluated in a HIV-PR inhibition assay. Ursolic acid emerged as one of the most potent of these predicted inhibitors, preventing HIV-PR dimerization at a K_i of 3.4 μM .

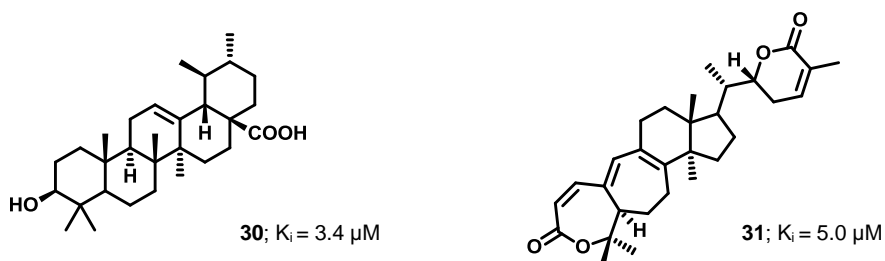


Figure 11. Ursolic acid (**30**) and schisanlactone A (**31**), naturally occurring dimerization inhibitors of HIV-PR

A structurally similar polycyclic triterpenoid known as schisanlactone A (**31** in figure 11) has also been identified as a dissociative inhibitor. The compound has two known sources in nature, both traditional ingredients in Chinese folk medicine: the magnolia vine called *Schisandra sp.*, which is taken as a sedative and used in tonics for boosting the immune system;⁵⁰ also, *Ganoderma colossum*, a Vietnamese mushroom thought to have anti-inflammatory and anti-microbial properties.⁵¹ Although schisanlactone A was first

discovered in 1983, its dissociative inhibition of HIV-PR at an IC_{50} of 5.0 μ M was not known until recently.⁵²

The final and the most potent of HIV-PR's natural dissociative inhibitors is didemnaketol A (**32**), a fascinating compound whose structure and synthesis will be the focus of the remainder of this thesis.⁵³ The compound is the namesake of the species in which it was discovered: *Didemnum* sp., a magenta colored ascidian, commonly known as a sea squirt. In the late 1970's, Faulkner harvested samples of the sea squirt from the shallows around Auluptagel, a tiny island in the Republic of Palau. Extracts from the species, containing variegated natural products, were taken up into a methanolic broth and placed in refrigerated (-20 °C) storage. Eleven years passed before interest in this sample was renewed when a screen for antiretroviral leads revealed that there were active compounds in these erstwhile extracts. Faulkner used a bioassay-guided fractionation to isolate a pair of sibling compounds: didemnaketol A, with an IC_{50} of 2 μ M, and the five-fold less potent didemnaketol B (**32** and **33**, respectively in figure 12).

Both molecules possess a long, highly oxygenated side-chain extending out of a spiroketal core with branching methyl groups at the two β -positions (*ie.* C14 and C18). Didemnaketol B has an additional polyisoprenoid chain (C45–C52) flanking the opposite side of the spiro rings. In didemnaketol A, this side-chain is truncated to a methyl ketone. The gross structures of both compounds were assigned using conventional 1-D NMR spectroscopy and 2-D correlation spectroscopy. At the time, however, much of the relative stereochemistry could not be assigned for lack of sample.

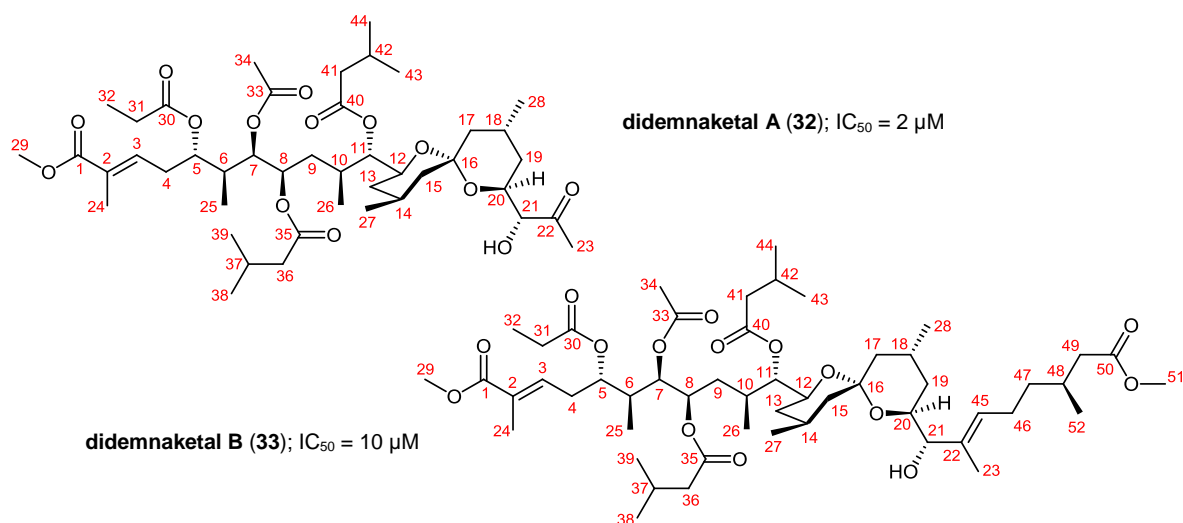


Figure 12. Natural HIV-PR inhibitors, didemnaketals A (**32**) and B (**33**)

1.5 Investigating the Didemnaketals

In order to complete the characterization of the natural product, Faulkner returned to Palau and retrieved more of the ascidian, hoping to replenish his supply of the natural products.⁵⁴ Unfortunately, he was not able to reproduce his former results. In fact, when testing the extracts of the fresh samples, Faulkner observed no activity whatsoever against HIV-PR. Both didemnaketals A and B were missing from the crude liquor and in their place a new compound was discovered—the HIV-PR invisible didemnaketals C (**34**). Likely, didemnaketals C is the true natural product and the progenitor of both inhibitors A and B. During the prolonged storage period, methanolysis of **34** resulted in a loss of the 2-hydroxyethanesulfonate, providing didemnaketals B (**33** shown in figure 13). Presumably, didemnaketals A (**32**) was produced through some serendipitous, though poorly understood, oxidative degradation at the C21 olefin.

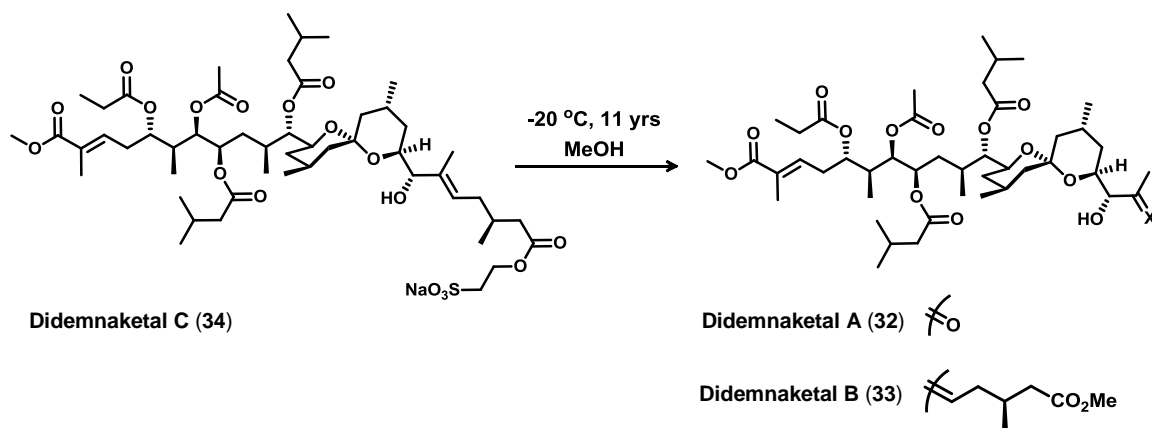


Figure 13. The decomposition of the ascidian isolate, didemnaketal C (34), into HIV-PR inhibitors didemnaketal A (32) and B (33)

What little is currently known about the nature of the interaction between didemnaketal A and HIV-PR comes from a study of synthetic analogues.⁵⁵ In attempting to ascertain which structural domain of didemnaketal A was responsible for enzyme recognition, Rich prepared series of spiroketals and a series of linear penta-ester chains and tested them in an activity assay.

At this time, neither the absolute stereochemistry nor the relative stereochemistry at nine of the twelve chiral centers had been assigned, meaning that didemnaketal A was one of 512 possible diastereomers. To simplify the synthesis and to reduce the number of diastereomeric analogues to a manageable sum, Rich opted to delete the branching methyl groups from both the linear chain and the spiroketal pendant. The analogues of the penta-ester side chain were truncated at C11, ablating the stereochemistry at that center, leaving only three chiral esters. Accordingly, the eight possible diastereomers

were synthesized in 16 steps. Likewise, non-methylated spiroketals were also synthesized as a mixture of four diastereomers in 14 step sequence starting from a known diol.

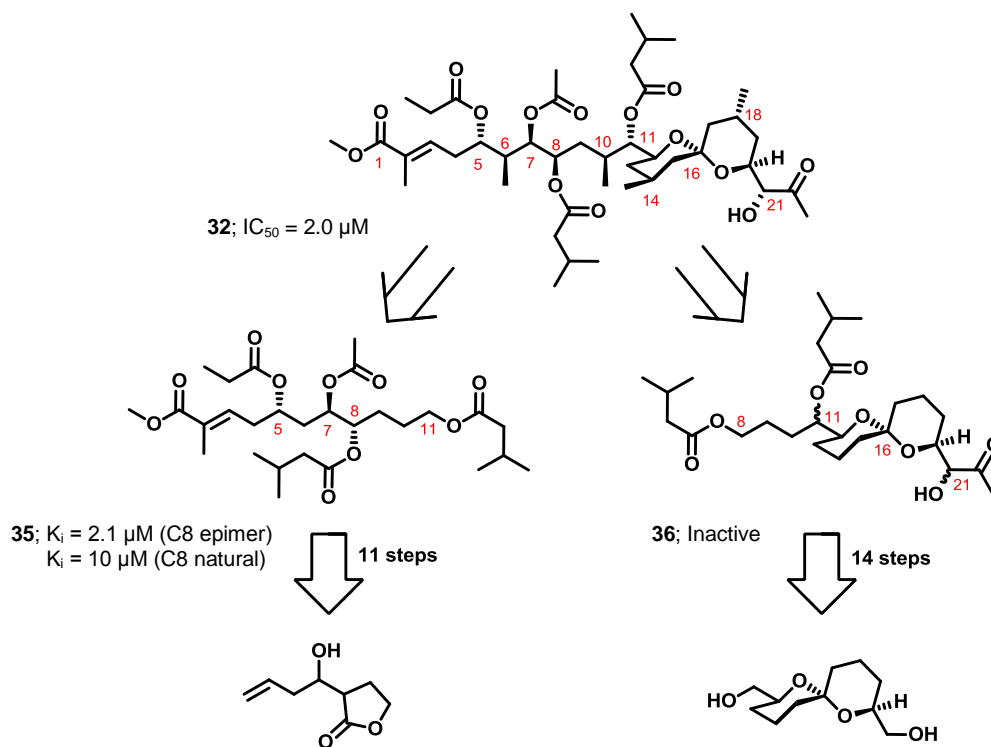


Figure 14. Rich's analogues based on the linear compound (**35**) and spiroketal (**36**) domains of didemnaketal A

Rich reports that none of the spiroketal analogues (**36**) showed any inhibition of HIV-PR; however, many of the linear penta-ester chains (**35**) were found to be active, the most potent of which was reported to have a K_i of $2.1 \mu\text{M}$. When a solution to the absolute stereochemistry of didemnaketal C was finally proposed by Faulkner,⁵⁶ the configuration was found to match Rich's best analog at two of the three stereocenters. The inversion at disparate center, C8, was found to contribute a five-fold increase in potency over the proposed natural configuration (as shown in figure 14).

Rich synthesized these compounds under the assumption that didemnaketol A behaved as a conventional inhibitor, somehow binding HIV-PR in the active site. He noticed, however, that his analogues defied maxims of rational drug design in several curious ways. In typical drug-like molecules, acyclic esters are not usually associated with structural features that contribute to protein recognition, though this sort of functional group is often used to improve bioavailability in the form of pro-drugs. This is because esters are highly labile under biological conditions, perhaps remaining intact long enough to improve absorption or distribution, but hydrolyzed long before the drug finds its target. Rich observed that when the esters were unmasked, revealing the free alcohols one at a time, the activity always diminished. This observation also contradicts the conventional wisdom of protease inhibitor design that a free alcohol is needed for binding.⁵⁷ The idiosyncrasy was reinforced by the fact that, though the spiroketal moiety bears an α -hydroxy group, Rich's analogues (*eg.* **35**) showed that this alcohol was irrelevant. These peculiarities prompted a more detailed analysis of the binding kinetics. A Zhang and Poorman plot—total enzyme concentration over the square root of the initial velocity ($E_0/V^{1/2}$) versus the square root of the initial velocity ($V^{1/2}$)—revealed parallel lines when the assay was performed with and without the inhibitor, an indication that the mechanism is dissociative and non-competitive.²⁷

1.6 Total Syntheses of Didemnaketol Targets

Why the magenta ascidians of Palau produce didemnaketol C is not known; likely, the natural product has some enzyme target, a target that perhaps resembles HIV-PR. However, the marine organism did not evolve alongside the virus; thus, the activity

observed for these secondary metabolites is merely coincidental. At best, the natural product is a starting place, a raw framework to which systematic modifications of the shape and structure will bring cumulative increases in potency and bioavailability. Ideally, a lead compound can be harvested from nature in abundance, modified to create a series of analogues, and the analogues used to probe the protein-protein interaction. In this case, unfortunately, adequate quantities are not easily obtained from Nature. In fact, didemnaketal A is the product of a poorly understood eleven year degradation process of an already scarce natural product obtained from a rare species with a remote habitat. Barriers such as these explain why the marriage between total synthesis and natural products has been so productive for drug discovery. Once an efficient route is established, the synthetic assembly of a natural product provides a reliable, plentiful, and ecologically non-disruptive supply. Total synthesis also offers both opportunity and incentive for the invention of new synthetic methodology.

Indeed, didemnaketal A presents an intriguing synthetic challenge which must be overcome before its biological potency can be understood and exploited. For instance, the irregular distribution of chiral methyl groups forestalls a rapid assembly. The variation in the esters decorating the side-chain demands a protecting group strategy with suitable orthogonality. Of the molecule's twelve stereogenic centers, more than half of them are embedded in the spiro architecture. However, despite the daunting complexity of the didemnaketal compounds, three other investigators (Tu,⁵⁸⁻⁶⁸ Ito,^{69,70} and Fuwa⁷¹⁻⁷³) have already published their progress towards the construction of didemnaketal structures.

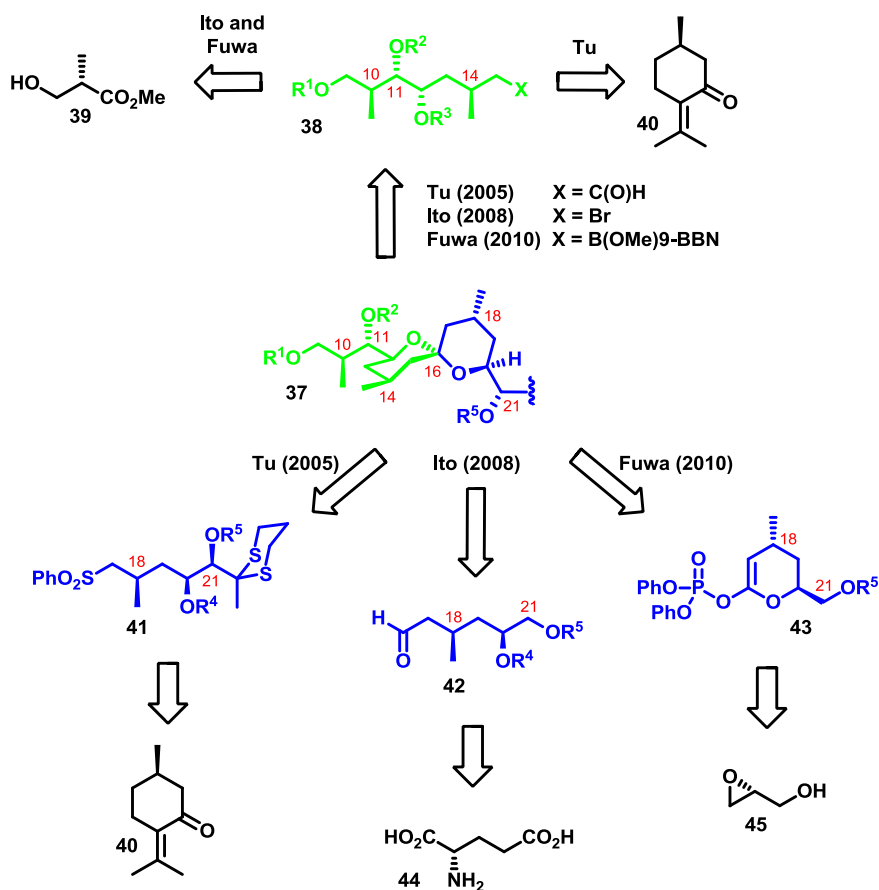


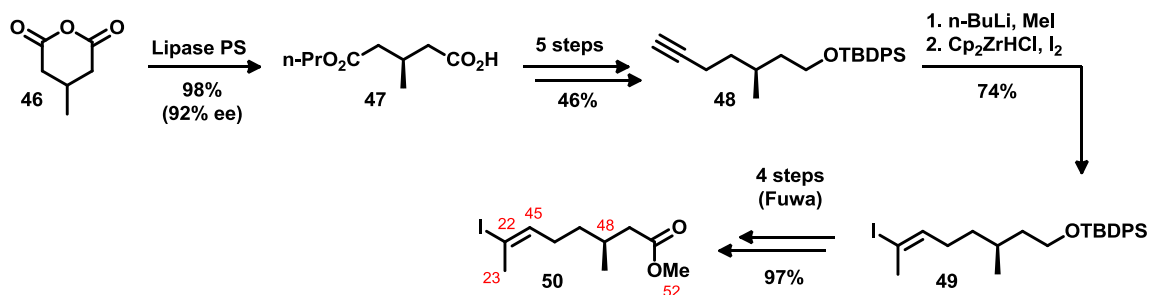
Figure 15. A retrosynthetic comparison of the spiroketal assembly performed by Tu, Fuwa, and Ito

All three approaches were conceptually similar, particularly with respect to the spiroketal moiety. The rings in the bicyclic architecture were assembled separately, using the chiral pool to derive key stereocenters, and then the fragments (coloured green and blue in figure 15) were fused at the ketal carbon. The use of this disconnection offers several tactical advantages. First, it roughly divides the spiroketal moiety in half, balancing the convergency of the synthesis. This central carbon is in an oxidation state that permits a variety of C-C bond forming options. Finally, though C16 is a chiral quaternary center in the final product, there is no burden to establish the stereochemistry

with the coupling. Instead, the anomeric effect should govern the subsequent spiroketalization, ensuring that there is thermodynamic preference for the desired orientation.

Beyond sharing these overarching themes, the works of Ito and Fuwa bear such striking similarities that it is convenient to discuss them together.^{69,72} Both groups published partial syntheses of didemnaketal B, appearing two years apart, using identical bond disconnections and similar fragments.

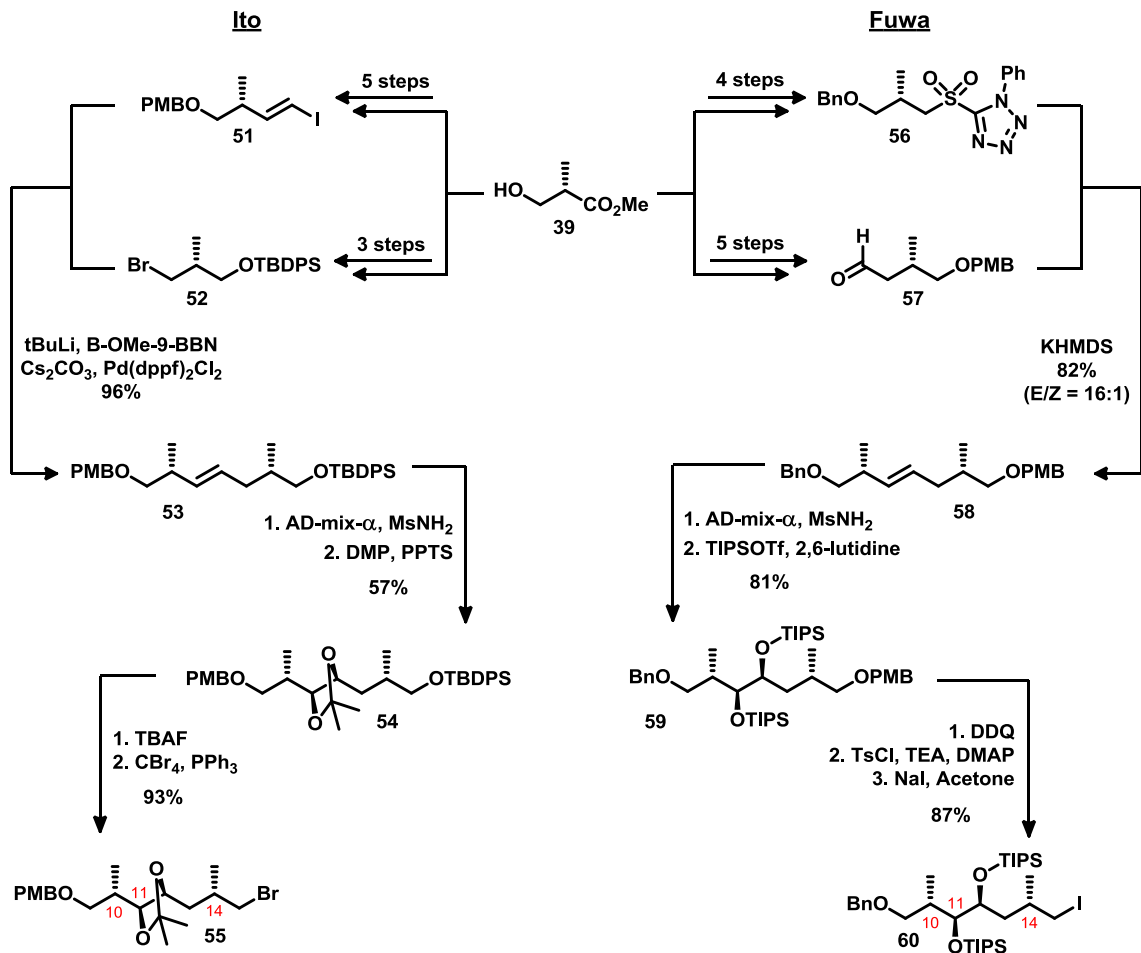
Ito published a method, later adopted by Fuwa, for making the polyisoprenoid chain C22-C28, the piece that distinguishes didemnaketals B and C from didemnaketal A. This five step sequence (shown in scheme 1) involved an initial enzymatic desymmetrization of 3-methylglutaric anhydride (**46**) using lipase-PS, giving **47** with a 92% enantiomeric excess. A series of selective reductions and protections allowed Ito to transform this *n*-propyl ester (**47**) into a tosylated alcohol, which was then displaced lithium acetylide. The resulting terminal alkyne (**48**) was deprotonated and methylated, after which a stereoselective iodination facilitated by Schwartz's reagent provided the vinyl iodide **49**. In the targeted product, didemnaketal B (**33**), this fragment would be terminated with a methyl ester; however, the harsh coupling conditions envisioned by Ito would not likely tolerate such reactive functional group. He was forced to carry forward the silyl protected alcohol (**49**). Fuwa, on the other hand, intending to use milder chemistry, proceeded to convert **49** to the methyl ester, taking an additional four steps to do so.



Scheme 1. The synthesis of the polyisoprenoid chain used by both Ito (**49**) and Fuwa (**50**)

Ito and Fuwa also adopted similar strategies for preparing the C9-C15 fragment, a piece that would ultimately form one of the spiroketal rings (green in figure 15). In both syntheses, the crucial stereogenic methyl groups at C10 and C14 were obtained from the same chiral pool material, methyl (*S*)-3-hydroxyisobutyrate (**39**). This starting material was rapidly elaborated into a pair of complementary sub-fragments (**51/52** by Ito and **56/57** by Fuwa in scheme 2) then coupled, assembling the larger C9-C15 building block. For instance, a lithium-halogen exchange of Ito's alkylbromide (**52**) provided the corresponding organoborate, the coupling partner to **53** in a high yielding β -alkyl Suzuki-Miyaura reaction. Similarly, using a comparable number of steps and by exploiting the same chiral starting material, Fuwa synthesized sulfone **56** and aldehyde **57**, matched partners for a Julia-Kozcienski olefination. In both cases, the coupling resulted in a C11-C12 olefin, flanked by alcohols with orthogonal protection and methyl groups possessing purchased chirality (**53** by Ito, **58** by Fuwa). In both cases, the olefin was asymmetrically dihydroxylated using Sharpless' conditions and the resulting diol was protected—Ito using an acetonide (**54**), whereas Fuwa opted for a pair of triisopropyl silyl ethers (**59**). Both groups then selectively deprotected one of the primary alcohols for

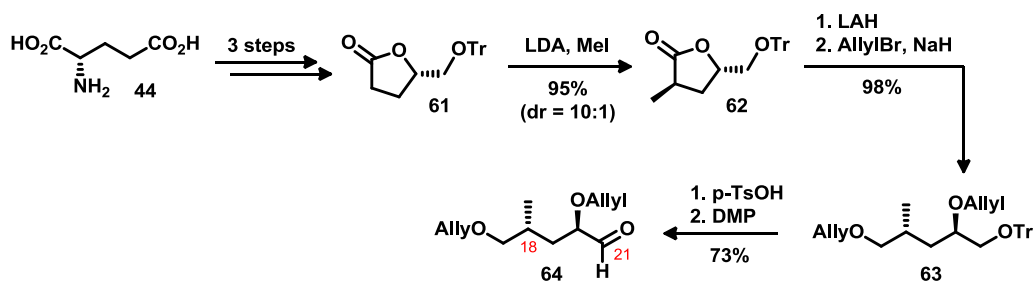
halogenation. Ito obtained the alkyl bromide **55** using Appel conditions, while Fuwa made an alkyl iodide (**60**) with the Finkelstein reaction.



Scheme 2. The respective syntheses by Ito and Fuwa for the C9-C15 fragment (**55** by Ito, **60** by Fuwa) of didemnaketol B from (S)-3-hydroxyisobutyrate (**39**)

The distinctions between the two syntheses become less superficial in their respective strategies for coupling the C9-C15 and the C16-C21 fragments. These differences are reflected in the construction of the latter piece. For instance, Ito's coupling involved lithiating **55**, then using the anion in a nucleophilic addition to the aldehyde bearing C16-C21 fragment (**64** in scheme 3). As before, the chirality of the aldehyde originates in

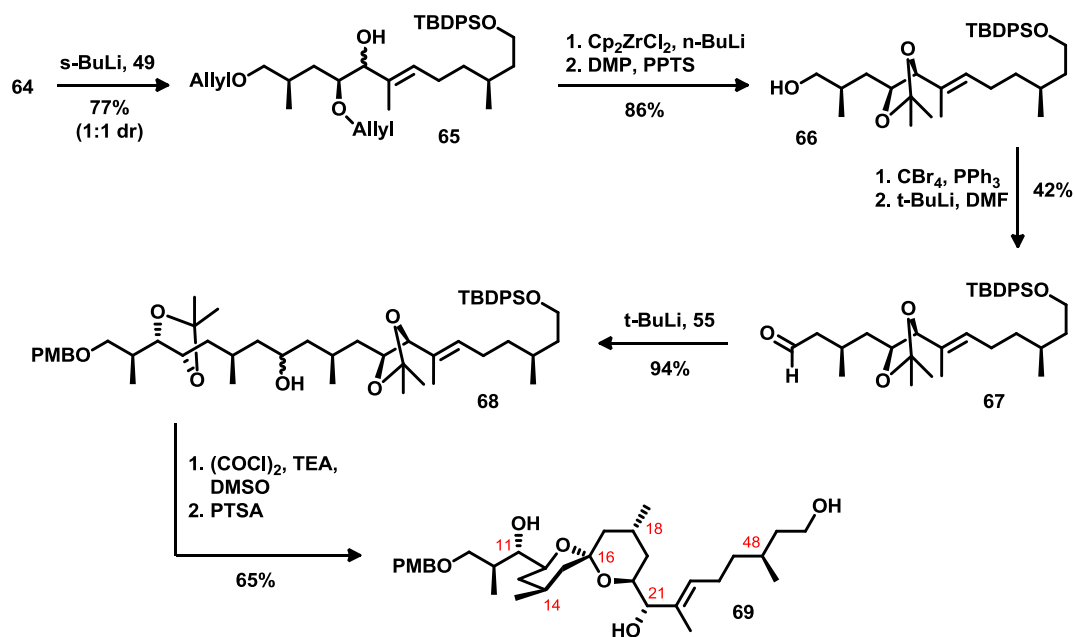
the chiral pool as glutamic acid. Ito converted this amino acid (**44**) into the enantiopure lactone **61** in 3 steps. The preexisting chirality was used to induce diastereoselectivity in the α -methylation of the lactone group. The lactone was then reductively opened, presenting a pair of free hydroxyl groups, amenable to allylation (**63**). Finally, the cleavage of the trityl group unmasked a primary alcohol which was oxidized with Dess-Martin periodane to aldehyde **64**.



Scheme 3. Ito's synthesis of the C16-C21 fragment (**64**) from (S)-glutamic acid (**44**)

With his three building blocks in hand, Ito tackled the final assembly of the spiroketal moiety (shown in scheme 4). First, the vinyl lithium derived from **49** was introduced to aldehyde **64**, accomplishing the coupling between C21 and C22, but not without producing inseparable diastereomers. The mixture (*ie.* compounds **65**) was carried forward through a deprotection of the two allyl ethers, facilitated by a zirconocene-like reagent. Upon reprotecting the 1,2-diol as an acetonide, it became possible to identify the desired diastereomer through nOe interactions and, ultimately, to separate it from the synthetically useless variant. The terminal alcohol (**66**) was brominated with an Appel reaction, lithiated with *t*-BuLi, and treated with DMF in a late-stage, low-yielding homologation. Using by now familiar conditions, Ito lithiated the C9-C15 bromide (**55** in scheme 2) and reacted the resulting anion with aldehyde **67**, giving compound **68** in

excellent yield but with poor diastereoselectivity. Fortunately, this time at least, the low diastereoselectivity was inconsequential as the resulting alcohol was immediately transformed to a ketone through a Swern oxidation. Treatment with PTSA accomplished the concomitant global deprotection of both acetonides as well as the desired spiroketalization, giving the **69** as a single diastereomer in 86% yield.

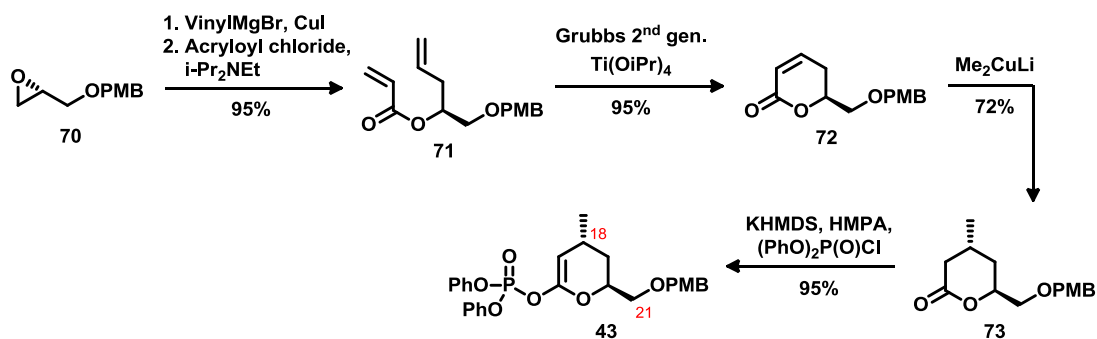


Scheme 4. Ito's completion of the spiroketal moiety of didemnaketals B (**69**)

When Ito published his partial synthesis in 2008, compound **69** represented to most advanced synthetic didemnaketals fragment; however, the approach had significant flaws that would make it difficult to complete the enterprise. Certain steps, for instance, bore significant losses of material. The non-diastereoselective coupling between C21 and C22 (scheme 4) eliminated half the reserve of an advanced intermediate **65**. There was also a stiff penalty for the late stage modification of compound **66**. This low yielding

homologation would have been easier to bear prior to the coupling. Ito concluded his synthesis at an intermediate with three free alcohols (**69**). To proceed would require developing chemistry that can distinguish between these alcohols. While it may be possible to selectively oxidize the terminal alcohol at C28, it is not obvious how the two secondary alcohols flanking the spiroketal would be differentiated, allowing for the selective installation of an isovaleric ester at C11 as per the structure of didemnaketal B.

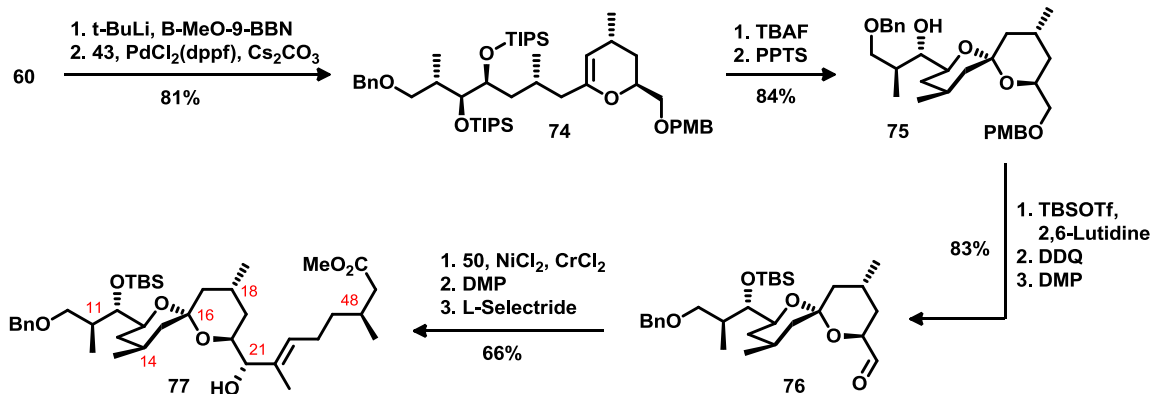
Though Fuwa's work was somewhat derivative of his predecessor, the modifications he introduced dramatically improved the efficiency and the elegance of the route. In preparing his version of the C16-C21 building block, Fuwa continued to follow Ito's lead. He found a starting material with a stereogenic heteroatom in the chiral pool, this time (*R*)-glycidol, and transformed it into a chiral lactone (**72** in scheme 5). First, a regioselective ring opening of the protected starting material (**70**) using vinyl Grignard and CuI gave a homo allylic alcohol which was esterified with acryloyl chloride, providing **71**. Grubbs' catalyst mediated a ring closing metathesis of the diene to produce an α,β -unsaturated lactone (**72**). Like Ito, Fuwa used the existing chirality of this rigidified scaffold to induce diastereoselectivity when introducing the C18 methyl group, a transformation accomplished through the conjugate addition of methyl cuprate. Whereas Ito, after installing the methyl group, cleaved his lactone to a linear precursor prior to coupling (shown in scheme 3), Fuwa cleverly avoided both the cleavage step and the subsequent protecting group chemistry by employing the cyclic precursor to accomplish the coupling. Doing so required treating the lactone with KHMDS and trapping the enolate with diphenylphosphoryl chloride to give the enol phosphate **43**.



Scheme 5. Fuwa's synthesis of the C16-C21 (**43**) fragment from (R)-glycidol (**70**)

Fuwa's method of joining the C9-C15 (**60** in scheme 2) and the C16-C21 (**43** in scheme 5) fragments is reminiscent of chemistry that appeared early in Ito's work (seen in scheme 2). The vinyl iodide (**60**) was converted to a boronate through a lithium halogen exchange and this sensitive boronate was used *in situ* to accomplish a β -alkyl Suzuki-Miyaura cross-coupling reaction with phosphonate **43**. The enocyclic enol ether **74** was obtained in 81% yield. Deprotection of the silyl groups allowed for spiroketalization under the influence of PPTS, giving **75** as the sole isolable product (shown in scheme 6). A reconfiguration of the protecting groups revealed the primary alcohol at C21 which then was oxidized with Des-Martin periodane to an aldehyde (**76**), a suitable coupling partner for a Nozaki-Hiyama-Kishi (NHK) reaction with vinyl iodide **50** (see scheme 1). The reaction proceeds in good yield and, unlike Ito's coupling method, it tolerates diemnaketal B's methyl ester, a functional group which Ito never managed to install. However, as is typical in NHK couplings, greater than a 2-fold excess of the **50** was used. Like Ito, Fuwa also faced the issue of poor selectivity at the C21 alcohol. However, Fuwa was able to salvage the diastereomeric integrity of the molecule

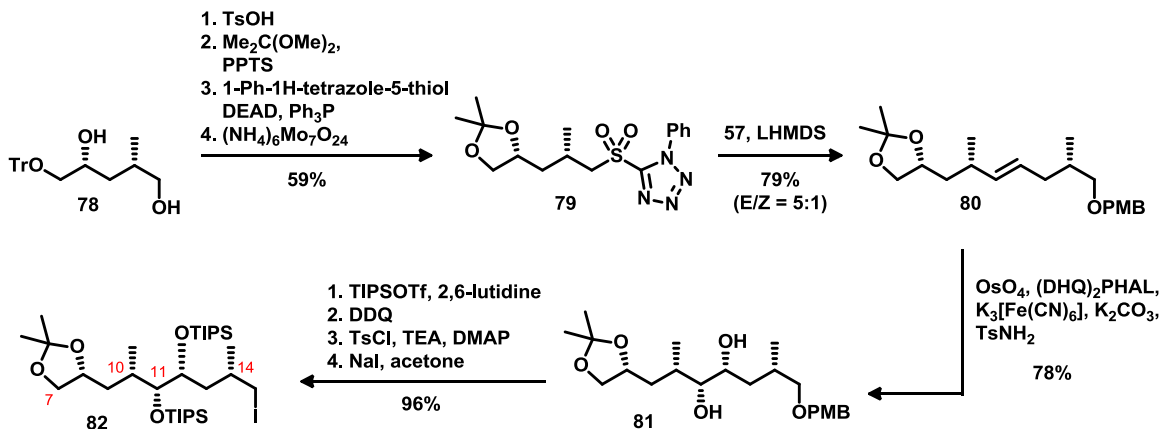
through a stereochemistry ablating oxidation followed by a restorative reduction with L-selectride. Thus, Fuwa produced **77**, a similar, albeit slightly more advanced, fragment of didemnaketol B, with the distinct advantage over his predecessor that the alcohols at C9, C11, and C21 are now orthogonally functionalized.



Scheme 6. Fuwa's completion of the spiroketal moiety of didemnaketol B (**77**)

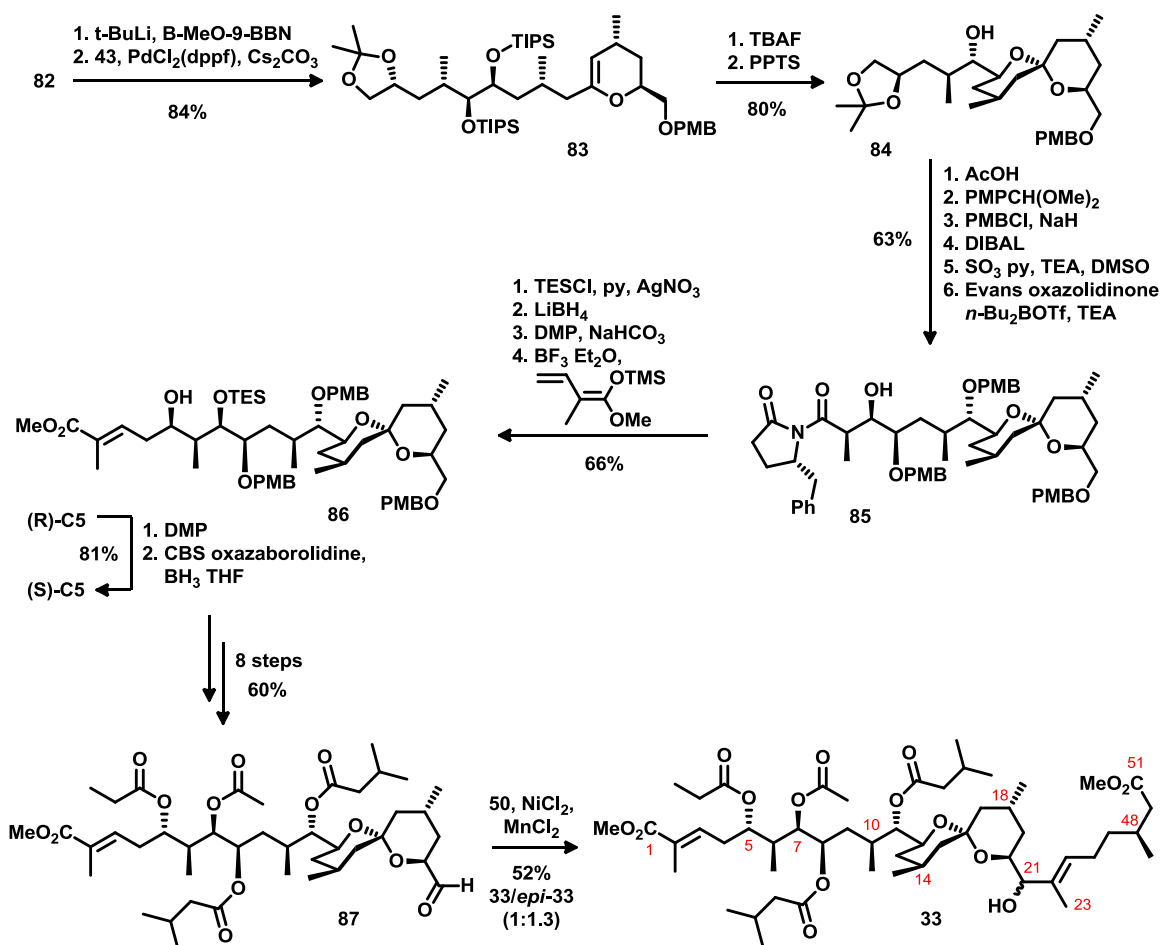
Very recently, Fuwa elaborated on this synthetic work, completing the synthesis of didemnaketol B.⁷¹ The C16-C21 (**43** in scheme 5) and the C22-C28 (**50** in scheme 1) fragments were kept the same; however, the third fragment was extended from C9 out to C7 by starting with **78**, a protecting group variant of Ito's compound **63** (shown in scheme 3). Overall, the bulk of the chemistry remains very similar to what was published before. The trityl protecting group on **78** was removed and replaced with an acetonide incorporating the C8 alcohol. The remaining primary alcohol was then tosylated and displaced in a Mitsunobu reaction, facilitating the installation of a sulfone upon oxidation (**79** in scheme 7). As before (see scheme 2), the sulfone was used in a Julia-Kocienski olefination with **57**, and then Sharpless conditions provided the diol **81**. In a sequence of

high yielding reaction, **81** was silylated then the *p*-methoxybenzyl ether was cleaved revealing a primary alcohol which was, in turn, converted to the iodide **82**.



Scheme 7. Fuwa's construction of the C7-C15 building block (**82**) for the total synthesis of didemnaketal B

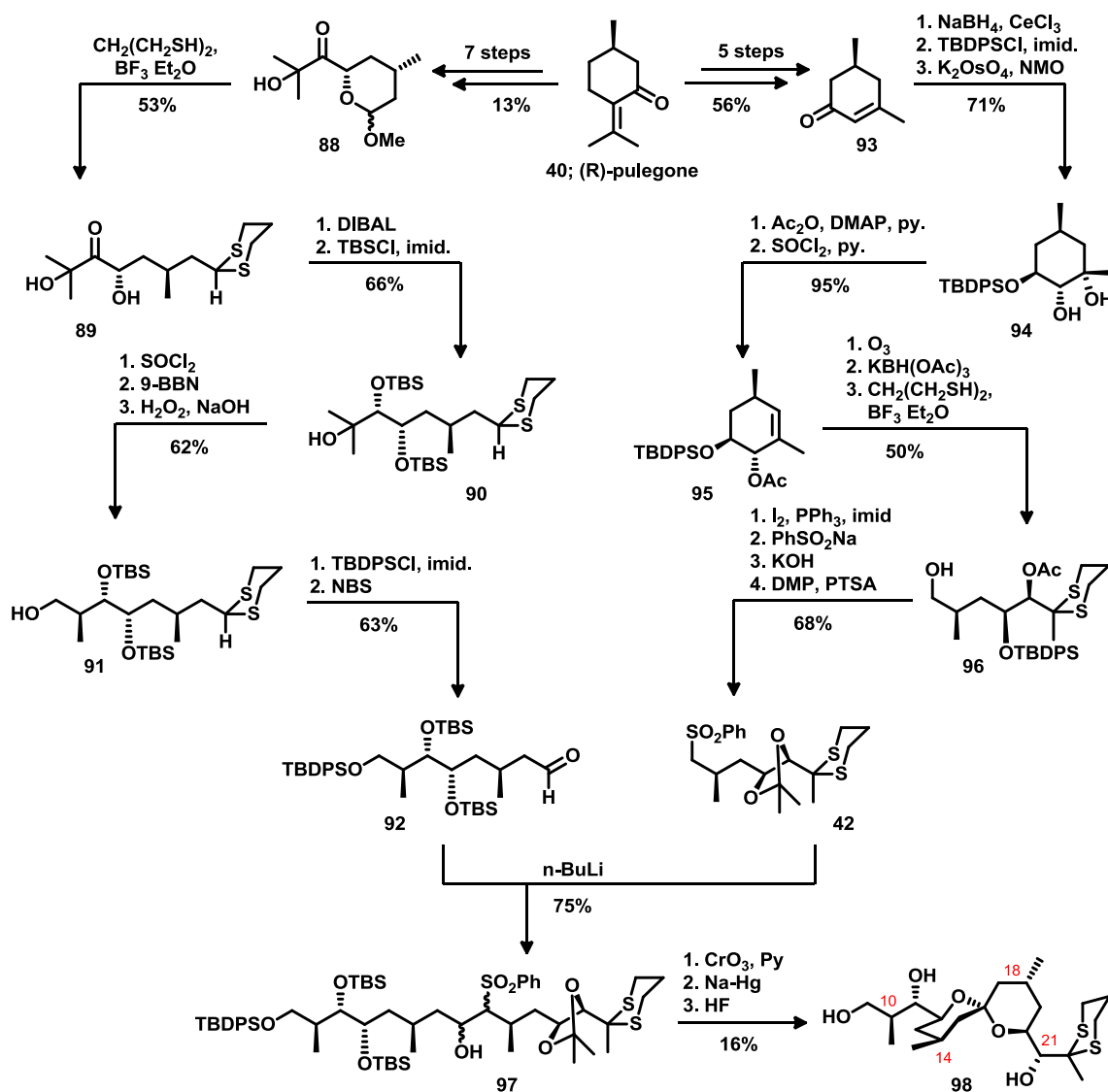
Again, a β -alkyl Suzuki-Miyaura cross-coupling was used to join the C7-C15 fragment (**82**) to the C16-C21 enol phosphate (**43**). After desilylation, PPTS catalyzed the spiroketalization onto the endocyclic enol ether, forming **84** (shown in scheme 8). Thus, having established the spiroketal architecture, Fuwa proceeded to elaborate the acyclic domains. After a series of protective group manipulations, the C7 primary alcohol was liberated and oxidized with Dess-Martin periodane. The resulting aldehyde was amenable to the Evans' syn-selective aldol reaction, simultaneously establishing the C6 and C7 stereochemistry in **85**. Following silylation, the chiral auxiliary was reductively removed and the ensuing alcohol was oxidized to an aldehyde. A subsequent vinylogous Mukaiyama aldol reaction resulted in the homoallylic alcohol **86**. Unfortunately the reaction delivered the undesired (*R*)-C5 configuration, forcing a circuitous oxidation and Corey-Bakshi-Shibata (CBS) reduction to produce the (*S*)-C5 orientation of alcohol **86**.



Scheme 8. Fuwa's completion of the total synthesis of the posited structure for didemnaketals B (**33**)

Thus, having installed the bulk of the core atoms and having completely established the correct stereochemistry, Fuwa took an additional 8 steps to deprotect and decorate the alcohols with appropriate esters. Finally, the C21 alcohol was oxidized to an aldehyde and, as described earlier (in scheme 6), the C22-C28 fragment (**50**) was added through a poorly diastereoselective NHK reaction. Thus, Fuwa obtained the proposed structure of didemnaketals B (**33**), albeit as the minor product with respect to its C21 epimer (*epi*-**33**).

Prior to Ito and Fuwa, Tu had been very prolific on the topic of the didemnaketal A synthesis, documenting his progress in a host of venues between 1998 and 2005.⁵⁹⁻⁶⁷ However, an analysis that focuses exclusively on his most recent partial synthesis will suffice as it encompasses much of what was published beforehand.⁵⁹ Like Ito and Fuwa, Tu also adopted a highly convergent approach, making use of the C16 disconnection and drawing crucial stereogenic centers from the chiral pool. In fact both the C9-C16 and the C17-C23 fragments (**92** and **42**, respectively in scheme 9) were derived from the same natural product, (*R*)-pulegone (**40**). First, using previously established methodologies, Tu prepared acetal **88** in seven steps and 13% overall yield. A transacetalization with 1,3-thiopropanol then produced the α -hydroxyketone **89**. The bulky reducing agent, DIBAL, provided good diastereoselectivity (de 82%) in securing a 1,2,3-triol, of which the two secondary alcohols were protected as TBS ethers (**90**). The remaining tertiary alcohol was effectively transposed onto an adjacent methyl group in an operation that involved an elimination of water followed by an anti-Markovnikov hydroboration of the resulting terminal olefin. Upon adding a third bulkier silyl protecting group to the newly formed primary alcohol, NBS was used to unmask the thioacetal to aldehyde **92**.



Scheme 9. Tu's convergent assembly of the spiroketal moiety of didemnaketal A starting from (R)-pulegone (40).

Toward the C17-C23 fragment, Tu prepared enone **93** in 56% yield over five steps, again starting from (R)-pulegone. The ketone was reduced with the stereochemistry controlled by the preexisting chirality. The resulting alcohol was protected as a bulky silyl ether and a diastereoselective Upjohn oxidation used to access the 1,2-diol, **94**. The acetylation of the secondary alcohol proceeded in the presence of the tertiary, allowing

for the dehydration of the latter alcohol with thionyl chloride, giving the endocyclic olefin **95**. Thus, having exploited (R)-pulegone's chiral methyl group to induce chirality in the remaining two stereogenic centers, an ozonolysis was used to cleave the ring into an open-chain keto-aldehyde. The mild reducing agent, $\text{KBH}(\text{OAc})_3$, preferentially reacted with the aldehyde over the ketone, giving an alcohol. After protecting the remaining ketone through a thioacetalization, an Appel reaction replaced the primary alcohol in **96** with an iodide, a suitable leaving group for installing phenyl sulfone. Finally, the mixed protection of the 1,2 diol was exchanged for an acetonide, giving the completed fragment (**42**).

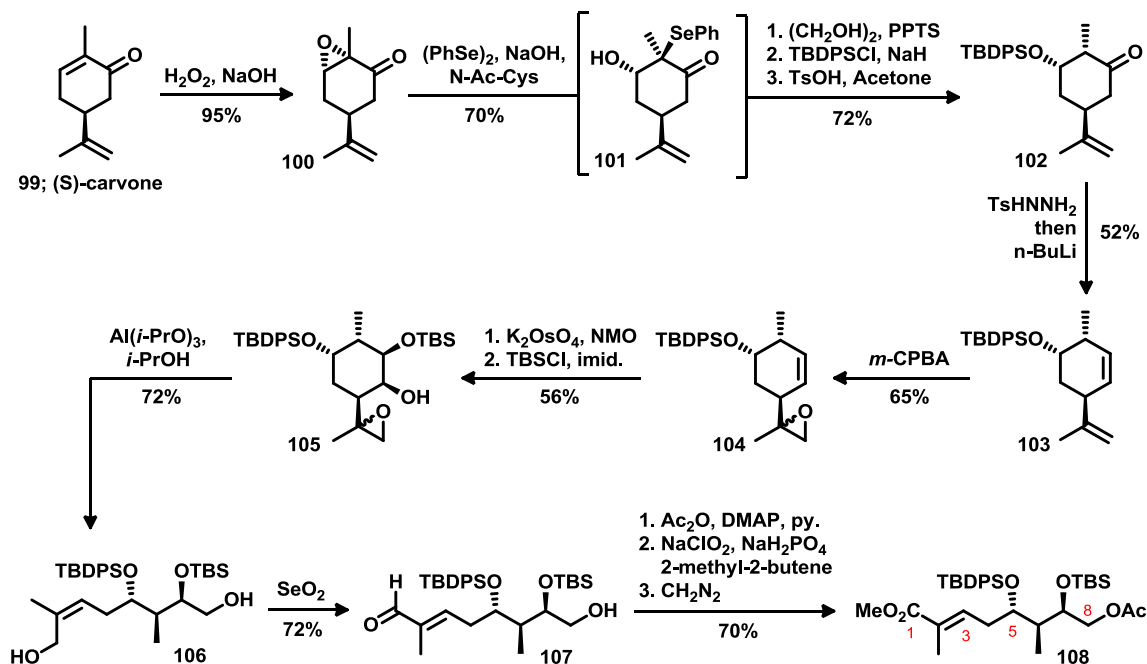
The two pieces were combined through a Julia coupling. The strong base, *n*-BuLi, was used to deprotonate **42** adjacent to the sulfone and the resulting anion reacted with aldehyde **92**, giving the alpha hydroxyl sulfone **97**. The alcohol was oxidized with Collin's reagent and the sulfone, having served its purpose, was removed in a sodium amalgam reduction. Hydrofluoric acid accomplished the concomitant double diol deprotection and spirocyclization, affording the desired product, **98**, in low yield (shown in scheme 9).

In 2004, Tu disclosed that he had assembled the C1-C8 domain of didemnaketal A, the linear branch which, when appended to **98**, would complete the synthesis of the natural product.⁶⁰ His strategy here resembles his approach to the spiroketal moiety. Once again, cyclic starting material was obtained from the chiral pool in order to exploit the ease with which chirality propagates through a rigid framework. Tu recognized that the naturally

abundant cyclic monoterpene, (S)-carvone (**99**), possesses both rigidity and the desired progenitorial chirality. As before, once this structural motif had served its purpose, the ring was opened—this time, through a meticulously orchestrated Gröb fragmentation (scheme 10).

A regio and diastereoselective epoxidation was performed across (S)-carvone's electrophilic olefin. The epoxide facilitated the installation of benzene selenide, generated *in situ* from diphenyldiselenide, at the α -position of carbonyl. Intermediate **101** was short-lived, however, as attack by another selenide anion reforms diphenyl diselenide and releases a β -hydroxyketone.⁷⁴ Unfortunately, attempts to directly protect the alcohol were met with a counterproductive elimination. Instead, it was necessary to first convert the ketone to an acetonide, address the alcohol with a silylation, and then, finally, restore ketone **102**. The subsequent Sharpito reaction using tosyl hydrazine transformed the ketone into diene **103**. A second epoxidation was performed with *m*-CPBA which, though regioselective for the terminal olefin, gave an unseparated mixture of diastereomers (**104**). Fortunately, better diastereoselectivity was observed when an Upjohn dihydroxylation was subsequently performed across the remaining olefin, thereby establishing all three of the desired stereocenters. After a selective silylation of the equatorial alcohol, treatment with aluminum isopropoxide initiated the Gröb fragmentation, opening both stereochemical configurations of the epoxide as well as the cyclohexanol ring. An ostensibly undesired Meerwein–Ponndorf–Verley reduction gave diol **106**. Fortunately, the Riley conditions used to oxidize the *Z*-allylic alcohol, restoring the aldehyde, produced a favourable geometric isomerization, giving **107**. After acylating

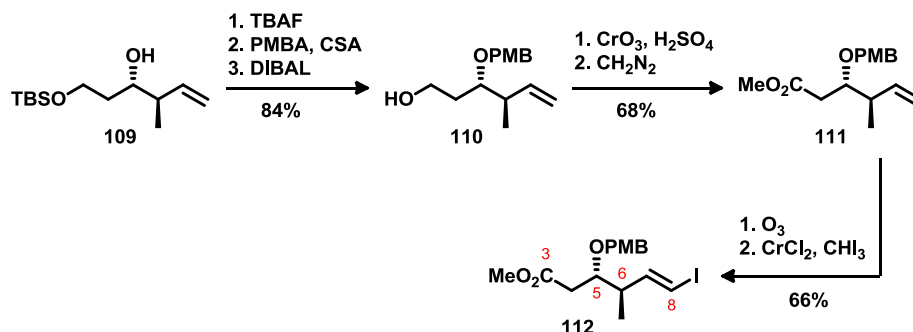
the remaining alcohol, a Pinnick oxidation and diazomethane treatment transformed the aldehyde into methyl ester **108**, an orthogonally protected a C1-C8 synthon for Tu's didemnaketol A synthesis.



Scheme 10. Tu's synthesis of the linear chain (**108**) of didemnaketol A starting from (S)-carvone (**99**)

Although he had the pieces in hand by 2005, it seems that final assembly of didemnaketol A was proving difficult. After a prodigal publication record, Tu's group was silent on the topic of didemnaketol for nearly a decade. Very recently, however, Tu announced the first total synthesis of the published structure of didemnaketol A.⁶⁸ Many aspects of the synthesis are extrapolated from his previous work. For instance, true to his original vision, this convergent synthesis can be deconstructed into three distinct fragments whose disconnections at C9 and at C16 have not changed. Again, the Julia coupling features prominently in the spiroketal assembly and many of the key stereogenic

centers are still drawn from the chiral pool. On the other hand, in some ways Tu's synthesis has also come to resemble the work published by Ito and Fuwa. Both Ito and Fuwa provide excellent demonstrations of the synthetic power β -alkyl Suzuki–Miyaura reaction. Tu, follows their lead, using this chemistry to accomplish the second of his crucial couplings. Unlike Tu's earlier work, Ito and Fuwa showed a preference for using acyclic starting materials. Tu's synthetic strategy has been to use rigid cyclic frameworks (*ie*, pulegone (**40**) and carvone (**99**)), to induce additional stereochemistry; however, as a tradeoff, this approach necessarily involves an often non-trivial C-C bond cleavage. Here, Tu abandons his former gambit, employing linear starting materials and relying more on asymmetric catalysis to compensate for the added difficulty in setting key stereogenic alcohols.

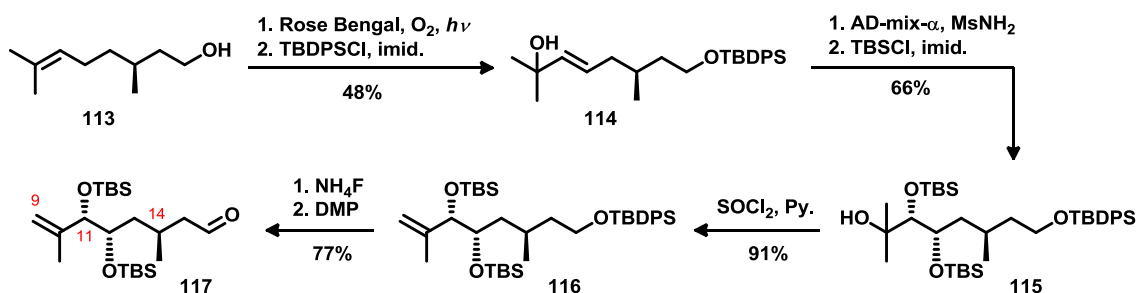


Scheme 11. Tu's assembly of the C1-C8 fragment (**112**) for the synthesis of didemnaketal A

The known alcohol **109**, assembled using a Brown crotylation, served as a very convenient starting point for the C1-C8 building block (shown in scheme 11). After removing the TBS group, the 1,3 diol was trapped as a *p*-methoxyphenyl acetal. This protecting group was reductively migrated to the secondary alcohol, freeing the primary alcohol in compound **110** for an oxidation to the acid then esterification with

diazomethane. Finally, a vinyl iodide (**112**) was installed through an ozonolysis and a subsequent Takai olefination on the resulting aldehyde.

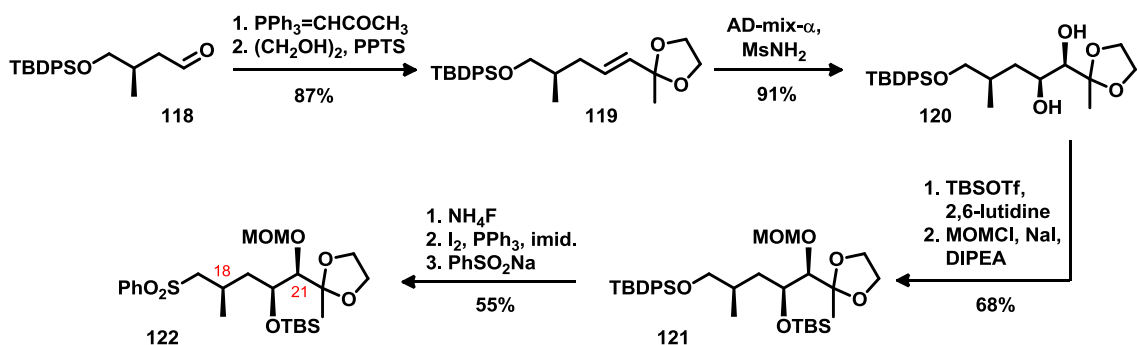
All of the carbons that constitute the backbone of the C9-C16 fragment, including the stereogenic methyl group at C14, are conveniently present in the chiral pool material, (S)-citronelle (**113**, shown in scheme 113). The chiral monoterpene reacted with oxygen, activated with rose Bengal, to give the tertiary allylic alcohol **114**. Upon protecting the primary alcohol with a bulky silyl ether, an asymmetric dihydroxylation was performed across the double bond. The resulting diol was silylated with TBS groups, preserving it through a dehydration of the tertiary alcohol. The orthogonality in the diol protection allowed the primary alcohol to be revealed and oxidized to aldehyde **117**. Tu's clever choice of starting material provided this second building block in a mere seven steps.



Scheme 12. Tu's assembly of the C9-C16 fragment (**117**) of didemnaketol A from (S)-citronelle (**113**).

The final piece, the C17-C22 fragment, was derived from a protecting group variant of Fuwa's aldehyde **57**. Whereas we saw Fuwa use this aldehyde in a Julia-Lythgoe olefination (see scheme 2), Tu installed a methyl ketone using the Wittig reaction (shown

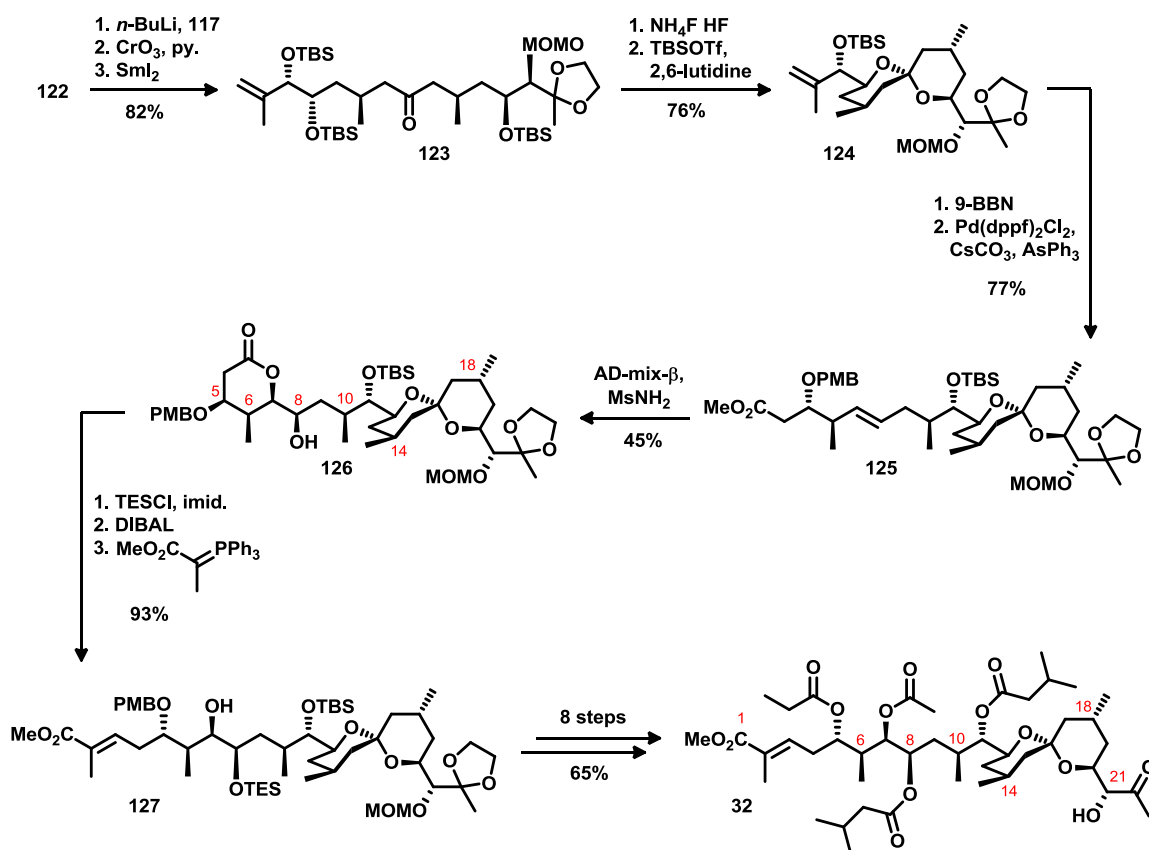
in scheme 13). The ketone was then protected as an acetonide (**119**). As with Fuwa before him, Tu used Sharpless' conditions to perform an asymmetric dihydroxylation across the resulting double bond. The less hindered of the two alcohols was protected using TBSOTf, while the remaining alcohol was converted to a MOM ether (**121**). After deprotecting the primary alcohol, Tu reverted to familiar chemistry: an Appel iodination followed by a nucleophilic displacement of the iodide giving **122**, a sulfone suitable for a Julia coupling (comparable with scheme 9).



Scheme 13. Tu's assembly of the C17-C22 fragment for the synthesis of the posited structure of didemnaketal A

The anion of **122** reacted with the aldehyde **117**, producing diastomeric alcohols, a mixture that was immediately ablated through oxidation with Collin's reagent. A one electron reduction mediated by SmI_2 removed the sulfone and completed the first coupling in 83% yield over all three steps. The linear product, **123**, was found to spiroketalize under the influence of $\text{NH}_4\text{F}\cdot\text{HF}$. The second coupling, the attachment of the linear chain, was accomplished through a β -alkyl Suzuki–Miyaura reaction between vinyl iodide **112** (refer to scheme 11) and the hydroboration product derived from compound **124**. Fortunately, the hydroboration appears to have established the correct stereochemistry at the C10 methyl group. The coupling proceeded in good yield,

conveniently creating a C7-C8 olefin, across which a third asymmetric dihydroxylation established the two remaining stereogenic alcohols. The *in situ* formation of a 6-membered lactone (**126**) differentiated the two secondary alcohols, allowing for a silylation of the C8 hydroxyl group. An equivalent of DIBAL converted the lactone to a hemiacetal—a latent aldehyde capable of reacting with a phosphonium ylide to give the α,β -unsaturated ester **127**. In this advanced intermediate all of the stereocenters have been established and all of the secondary alcohols are orthogonally protected. An 8-step sequence of selective deprotections and esterifications ultimately provided Tu with the molecule thought to be didemnaketal A.



Scheme 14. Tu's final assembly of the posited structure for didemnaketal A (**32**).

1.7 Reevaluating of the Structural Hypothesis

Generally, when a minute quantity of some substance is extracted from nature, sophisticated spectroscopic methods and X-ray crystallography permit the rapid elucidation of even highly complex structures. However, these methods are not infallible as Nicolaou and Snyder have pointed out.⁷⁵ It is total synthesis that serves as the ultimate corroboration of any structural hypothesis. If synthetically derived material matches its natural counterpart in all respects, then the proposed structure is considered to be substantiated to the limits of scientific certainty.

The synthetic work performed by Tu and Fuwa exemplifies the importance of total synthesis as a crucial check—the spectral data obtained by both groups failed to match the authentic samples discovered by Faulkner fifteen years previous. These inconsistencies call into question the structural hypothesis posited by Faulkner in 2002.⁵⁶

When the deviations between synthetic and authentic samples are plotted with respect to the proton and the carbon chemical shifts, it becomes apparent that, while large domains are in good agreement, certain regions that stand out as highly suspect (see figure 16). For instance, both Tu and Fuwa observed dramatic deviations for the ¹³C nuclei in region between C7 to C10, including the C25 and C26 methyl groups. Corroborating disparities are also found in the ¹H NMR spectrum, particularly with respect to didemnaketal B where a proton on C9 is shifted by more than 0.25 ppm from its anticipated position. The comparison strongly suggests that one or more of the three chiral centers at C7, C8, or C10 have been misassigned.

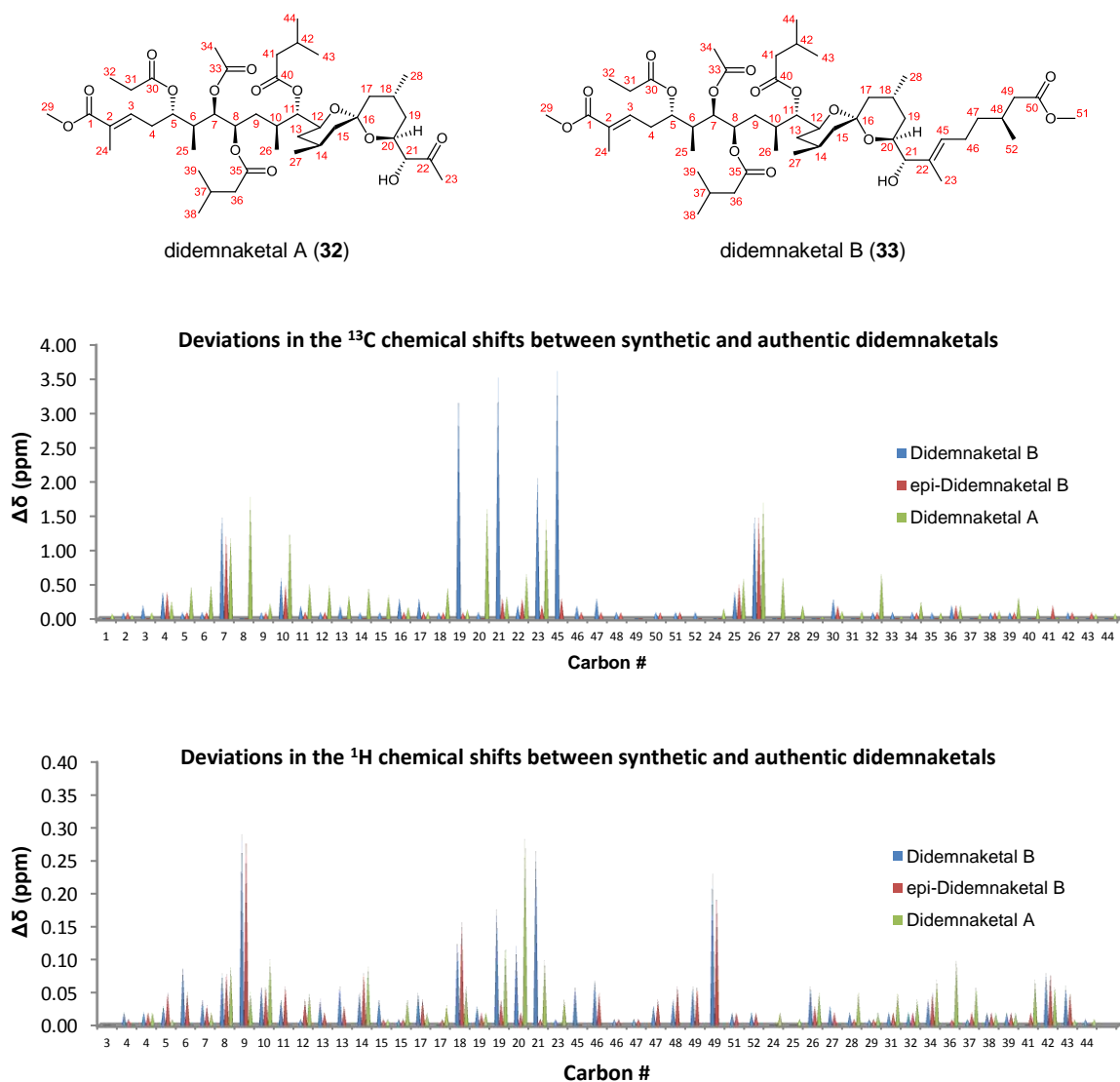


Figure 16. Discrepancies in the chemical shift of the ^1H and ^{13}C NMR spectra are plotted, comparing products discovered by Faulkner with the synthetic analogues prepared by Tu and Fuwa

A second conspicuous region occurs between C17 and C23 with the magnitude of the divergence culminating around C20 which is the mortise carbon for the polyisoprenoid branch of didemnaketals C. With respect to the C20 proton, the dissimilarity between synthetic and authentic samples is greater than 0.25 ppm for both didemnaketals A and B. Likewise, the ^{13}C nuclei flanking C20 are shifted by more than 1 ppm for didemnaketals A

and by as much as 3 ppm in the case of didemnaketal B. This spectral data makes the assumed stereochemical relationship between C20 and C21 appear very suspicious.

Interestingly, Fuwa's inelegant NHK coupling, the reaction that finalizes his synthesis of didemnaketal B, also provides a useful probe for this questionable stereochemical relationship. Recall, the nominal structure of didemnaketal B was actually the minor product of this reaction (refer to scheme 8), the bulk of the material being the C21 epimer. The proton and carbon NMR spectral data for the C17 to C23 domain of this unwanted diastereomer are in near-perfect agreement with Faulkner's authentic sample. However, other domains of Fuwa's epimer remain at variance. The protons adjacent to the chiral center at C52, for instance, remain significantly shifted in synthetic **33** and epi-**33**; likewise, the aberrant signals between C7 and C10 are not affected by the epimerization. Thus, it seems that Faulkner's structural hypothesis is plague by multiple stereochemical issues.

The fact is, however, that Faulkner never explicitly assigned the relative or absolute stereochemistry for either didemnaketal A or B. The original liquor contained only minute quantities of these decomposition products, a sufficient amount to evaluate their biological activity and to establish their gross structures, yet not enough to unambiguously characterize the subtleties of their diastereomeric configuration. By 2002, however, Faulkner did have an ample supply of didemnaketal C; thus, it was with this compound that he performed his in-depth analysis of the stereochemistry. That the same orientation should exist for both didemnaketals A and B was not shown by Faulkner, yet

his hypothesis that these compounds are derived from didemnaketal C has caused this tacit assumption to pervade the literature. It is possible that, after prolonged storage, the original sample of the natural product not only deteriorated, but also epimerized at certain chiral carbons.

Faulkner assigned the stereochemistry of didemnaketal C using degradation and derivatization experiments, chiral shift methods in conjunction with a battery of multidimensional NMR spectroscopy, and X-ray crystallography (see figure 17).⁵⁴ First, an oxidative degradation was performed on the natural product, providing a single crystal of the acid **130**. The solution of this structure by X-ray crystallography revealed the relative stereochemistry for the bulk of the spiroketal moiety. Unfortunately, the stereochemical information concerning the C21 chiral center was lost during this transformation. A second fragment was rigidified through conversion to the acetonide **128**. The relative stereochemistry between H5 and H6 was shown to be *anti* through the 12 Hz coupling constant, a value consistent with a trans-diaxial orientation. Likewise, ROESY correlations about the 7,8-acetonide ring of **129** provided strong evidence for a *syn* orientation between these two alcohols. Thus, Faulkner was able to greatly simplify the task of assigning the absolute stereochemistry by taking didemnaketal C's twelve chiral centers and grouping them in to five subsections: the spiroketal fragment; the C5 alcohol with its adjacent methyl group; the 7,8-diol; the C21 alcohol which was ablated during the oxidative cleavage; finally, the remote chiral center, C48.

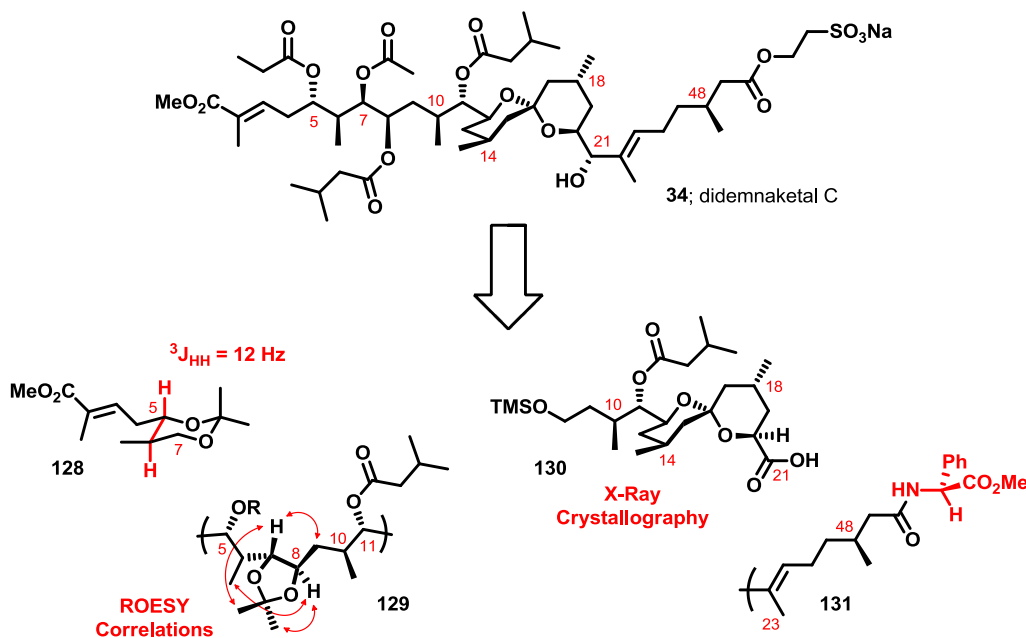


Figure 17. Faulkner's degradation analysis of didemnaketal C for assigning the relative stereochemistry of the natural product.

Faulkner proceeded to elucidate the absolute stereochemistry of these five domains using chiral derivatizing agents (CDA). An effective CDA, as the name implies, must be chiral with both *R* and *S* forms readily available in high enantiomeric purity. It must be easily appended at or near the chiral center that is to be investigated and, once added, the chiral auxiliary must strongly favor some predictable conformation. The Mosher auxiliary is a perennial favorite CDA, one that Faulkner relies on heavily for characterizing didemnaketal C. When the precursor, α -methoxy- α -(trifluoromethyl) phenylacetic acid (MTPA), is coupled with a chiral secondary alcohol, the conformational equilibrium of the resulting ester favors a particular orientation.⁷⁶ The carbonyl is found to eclipse the hydrogen of the chiral center since this geometry minimizes steric interactions. On the opposite side, the carbonyl also eclipses the CF_3 group substituent, placing this substituent orthogonal to the carbonyl's LUMO, and

thereby forestalling unfavorable donor/acceptor orbital mixing (refer to figure 18). A consequence of the coplanarity between carbonyl, the proton and the CF_3 is that, inevitably, the auxiliary's phenyl group will face one of the alcohol's substituents while the methoxy group is brought into close proximity with the opposing substituent. One side of the chiral alcohol feels the phenyl group's anisotropy and, being shielded, these protons shift upfield. Simultaneously, the other side of the alcohol is deshielded by through-space interactions with the electron withdrawing methoxy group, shifting these protons downfield. Functionalizing a substrate first with (S)- then with (R)-MTPA reveals the orientation of the alcohol. Substituent L_1 , formerly deshielded by the methoxy of (S)-MTPA, then becomes shielded by the phenyl of (R)-MTPA; thus, it follows that the change in the chemical shift ought to decrease (*ie.* $\Delta\delta_{(S-R)} < 0$). Of course, the opposite is true for the substituent L_2 (*ie.* $\Delta\delta_{(S-R)} > 0$).

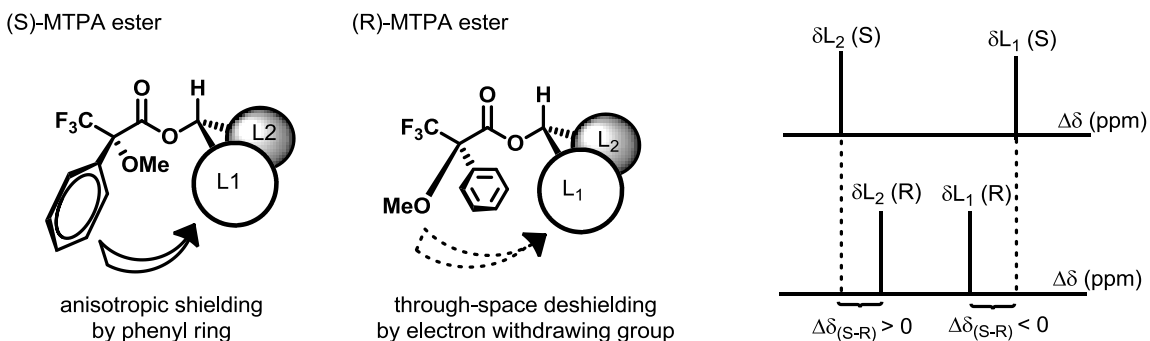


Figure 18. The Mosher method for determining the absolute stereochemistry of a chiral secondary alcohol predicts that $\Delta\delta_{(S-R)}$ is negative for the substituent L_1 and positive for L_2

Faulkner prepares fragments **129** and **132** then derivatizes the free alcohols with Mosher esters, partially isomerizing the C2-C3 double bond of **129** in the process. However, Faulkner insists that this result did not interfere with the stereochemical determination of the hydroxyl groups at C5. Meanwhile, compound **132** was used to

reveal the stereochemistry at C8 and the orientation at C21 was confirmed in both structures. The $\Delta\delta_{(S-R)}$ values are shown in blue in figure 19.

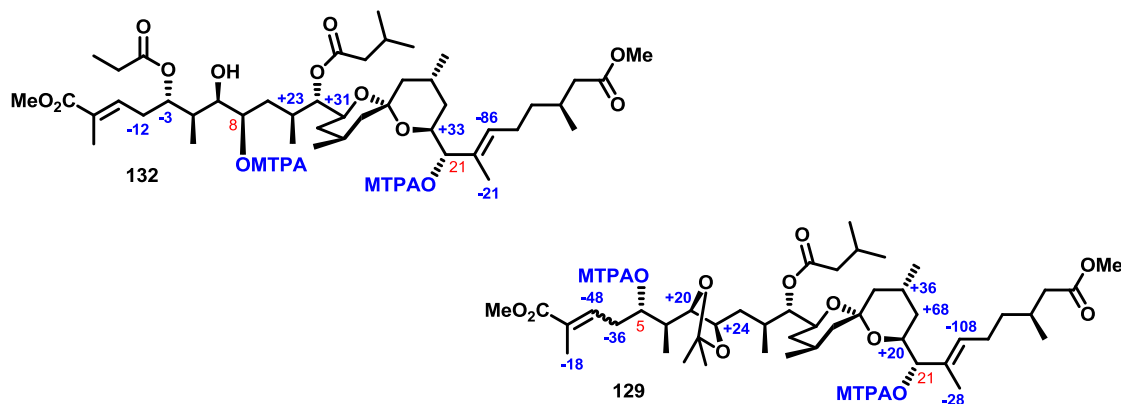


Figure 19. Faulkner's Mosher analysis for elucidating the absolute stereochemistry of didemnaketal C at C5, C8, and C21. Chiral shifts are reported in blue while atom numbers are labeled in red

An analogous method was used to determine the stereochemistry of the C26 methyl group. As this stereocenter lacks a convenient heteroatom amenable to the Mosher method, Faulkner exploited the C50 acid of **131** (in figure 17), coupling to it phenylglycine methyl ester (PGME). As is typical of peptide bonds, the chiral PGME amide adopts an s-trans conformation; consequently, the phenyl group on the auxiliary either does or does not exert anisotropy on the chiral methyl group, depending on whether (S)- or (R)-PGME is considered. Because the chiral center under investigation is at the β position with respect to the amide, this application of the CDA is somewhat dubious compared to Faulkner's earlier analysis using the Mosher method. The presence of an extra freely rotating C-C bond between the chiral center and the auxiliary diminishes the conformational preference and, thus, the magnitude and reliability of the diastereomeric

shift.⁷⁶ However, Faulkner, in an effort to allay the concerns of the critical reader, convincingly models the analysis using citronellic acid beforehand.

To complete the characterization of didemnaketal C, all that remained was to establish the absolute stereochemistry at one of the six stereogenic centers present in the spiroketal fragment **130**, inferring the remainder of the chirality from the crystallographic analysis. To accomplish this task, Faulkner returns to the Mosher method as a means of studying the C11 alcohol. However, unable to add a single auxiliary unit regioselectively to the focal hydroxyl group, he is left to analyze the chemical shift difference between the (*S*)- and (*R*)-diastereomers of the tri-MTPA derived **133** (shown in figure 20). This complication calls into question the reliability of the observations. As Seco reminds us in his authoritative review: “the fundamentals of the [Mosher] NMR method are related to aromatic shielding, which is a through space phenomenon that affects protons several bonds away from the hydroxylic carbon atom that has the auxiliary reagent. Therefore, the $\Delta\delta_{(S-R)}$ values observed in those polyderivatized compounds are, in fact, the result of the combined effects (shielding/deshielding) of all the MTPA phenyl rings and cannot be interpreted as if they were produced by just one phenyl group as in monofunctional compounds.”⁷⁷ Often when two or more MTPA esters are in relatively close proximity, as with C8 and C11 of **133**, the CDAs interfere with each other, leading to anomalous sign distributions that bear no relation to the Mosher prediction for isolated alcohols. Admittedly, the polyderivatizations of **129** and **132** do not seem to have produced spurious results, as the $\Delta\delta_{(S-R)}$ values are all large and very consistent, though the Mosher

esters in this case are better separated. Unfortunately, Faulkner does not report the $\Delta\delta_{(S-R)}$ values for **133** so it is difficult to judge how effectively the method was applied.

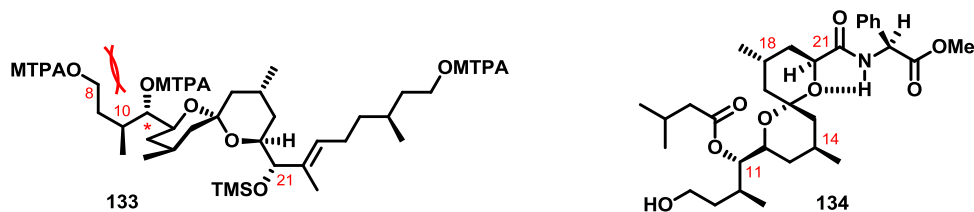


Figure 20. Faulkner's determination of the absolute stereochemistry of the spiroketal domain using the Mosher method and using PGME amide. The potential interference between the MTPA auxiliaries on C8 and C11 is indicated as well as the anomalous hydrogen bond

Ostensibly anticipating some skepticism concerning this analysis, Faulkner sought to buttress the argument for his assignment by preparing the (R)- and (S)-PGME amides **134**. Curiously, the results from this experiment appeared to contradict the original structural hypothesis rooted in the Mosher method. Faulkner addressed the disparity by proposing that amide-NH proton was strongly hydrogen bonded to the oxygen of the adjacent pyran ring, resulting in an atypical conformational preference which alters the $\Delta\delta$ sign distribution.

A critical perusal of Faulkner's work on the spiroketal domain of didemnaketals reveals the possibility that he placed too much faith in a potentially flawed Mosher analysis, an error that may have caused him to dismiss veracious results with an *ad hoc* hypothesis about an anomalous hydrogen bond. Notice that if the absolute stereochemistry had been misassigned on Faulkner's spiroketal crystal then this would result in NMR-conspicuous incongruities in both the C8/C10 and the C20/C21 relative

stereochemistry, precisely as Tu⁶⁸ and Fuwa⁷¹ observed. Though hardly conclusive, it is also worth noting that while the specific rotation for the authentic sample of didemnaketol A was levorotatory (-11),⁵³ both the synthetic samples were found to be dextrorotatory (Tu, $+20$; Fuwa, $+46$). The implication is that the flawed assumptions in the current structural hypothesis may not be limited to a mere epimerization of one or two remote centers. Instead, the issues may be far more systemic—perhaps, far more difficult to address with the current synthetic methodology.

Nevertheless, the determination of the absolute configuration of the didemnaketals is a crucial step in understanding its structure-activity relationship, knowledge that may allow us to access unique and potent inhibitors of HIV-1 protease. This was the perspective with which we proposed our own total synthesis of didemnaketol A in 2008. We recognized that we were late-comers to this synthetic enterprise behind Tu, Ito, and Fuwa; however, at the time, no one had completed the construction of any of the didemnaketol structures and we were still naïve about the latent stereochemical issues which transpired in 2012.

1.8 Our Proposed Synthesis

We envisioned a convergent synthesis where a conceptual bisection of the molecule provides logical synthetic targets: the long, highly oxygenated side-chain with its four contiguous chiral centers (**135** in figure 21); and the spiroketal with its branching methyl groups at the two β -positions (**141** in figure 22). Our lab has pursued these fragments as

two independent synthetic ventures with the intention of pairing them in a late-stage coupling reaction.

My colleague, Dr. Caleb Bromba, was tasked with the asymmetric assembly of the linear side-chain, along with a series of structural analogues intended for probing the mechanism of HIV-PR inhibition. In particular, Bromba targeted compound **135** (shown in figure 21). His strategy was to establish a central core around the C5-C7 diol, then elaborate the fragment in both directions. For instance, the α,β -unsaturated methyl ester was to be installed through an asymmetric allylation of aldehyde **136**, a reaction that establishes the stereochemistry at C5 and provides a metathesis handle for installing the terminal methyl ester. The requisite aldehyde was revealed through a reductive protecting group migration of the p-methoxybenzyl acetal **137**, followed by a mild oxidation. On the other side of the molecule, the vinyl bromide was stereoselectively installed through an expedient substrate directed allylation using allylborane **139**. The incipient fragment, **138**, a masked 1,3-diol, was accessible in four steps from Evans' chiral auxiliary. An extensive account of this synthetic work is chronicled in Bromba's 2012 thesis.⁷⁸

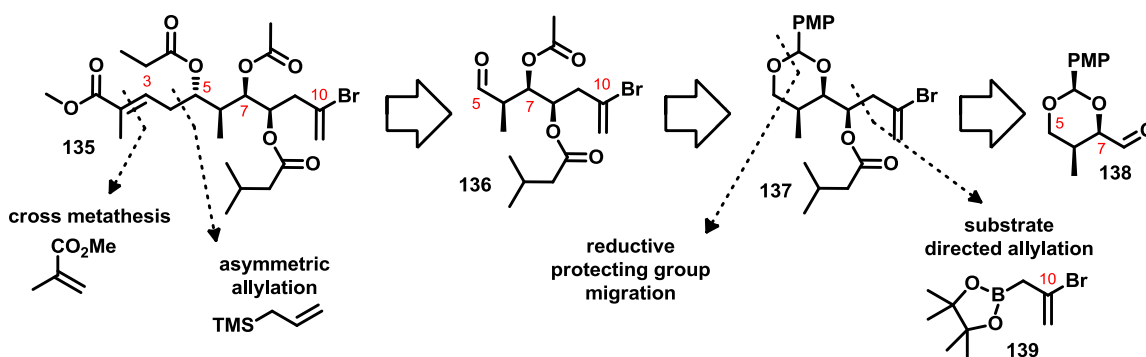


Figure 21. A retrosynthetic analysis for Dr. Caleb Bromba's assembly of the linear branch of didemnaketol A (**135**)

The vinyl bromide was incorporated into the side chain synthesis in order to facilitate an NHK coupling to the spiroketal domain, thereby forming the C10-C11 bond (shown in figure 22). The NHK approach is appealing because the reaction conditions are mild enough to tolerate esters adorning the side chain (**135**), decreasing the number of post coupling transformations. We hoped the coupling would also deliver the correct stereochemistry at the C11 alcohol. If so, this alcohol could be used to direct a stereoselective hydrogenation of the adjacent olefin (**140**) and then be converted to an isovaleric ester, completing the synthesis.

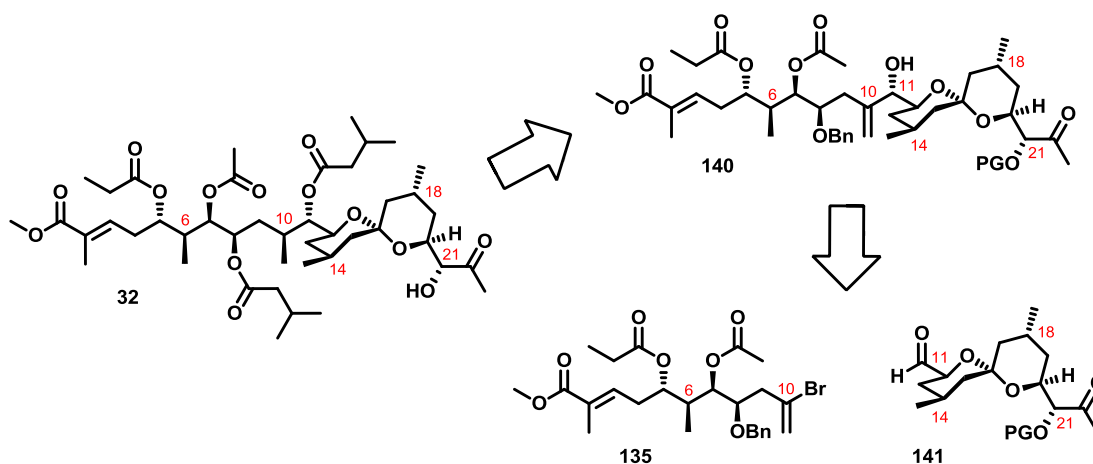


Figure 22. A retrosynthetic analysis for the late-stage coupling between the linear and spiroketal domains (**135** and **141**, respectively) of didemnaketal A (**32**)

The requisite coupling partner in the proposed NHK reaction is aldehyde **141**, a molecule that represents the principle goal of my PhD research and whose synthesis will be the focus of the remainder of this thesis (see figure 23). Although ostensibly this domain offers nothing in the way of biological activity, its spirocyclic architecture and dense arrangement of stereogenic carbons present a significant synthetic challenge. Despite the target's apparent complexity, we recognized that there is also a latent

symmetry which we hoped to use to our advantage. This aspect of symmetry is profoundly revealed in our proposed spiroketal precursor **142**, a *meso* structure due to the bisecting mirror plane. If we could desymmetrize this non-chiral material using dual asymmetric dihydroxylatons, then we would expect to be able to rapidly assemble the entire spiroketal core, correctly setting seven stereocenters, all in a single step. One of the great advantages to using a non-chiral precursor in such a late-stage transformation is that the bulk of the synthesis can be performed as a racemate. According to our vision, all enantiomers would converge on the *meso* precursor (**142**).

We intend to access this critical compound through ring opening cross metatheses performed on the 9-membered cyclic enone **143**. The metathesis will likely be undiscerning with respect to the geometry of the double bond in the starting material, producing *trans*- α,β -unsaturated ketones in either case. Thus, both *cis* and *trans* **143** are sought as keystone intermediates in our strategy. The strained nine membered ring may be accessed through an anionic oxy-cope rearrangement of the substituted cyclopentane, **144**. This precursor, in turn, is to be derived from a ring opening ring-closing metathesis of the fused cyclobutene **145**. The 5/4 ring system may be produced through a [2+2] cycloaddition of the silyl enol ether.

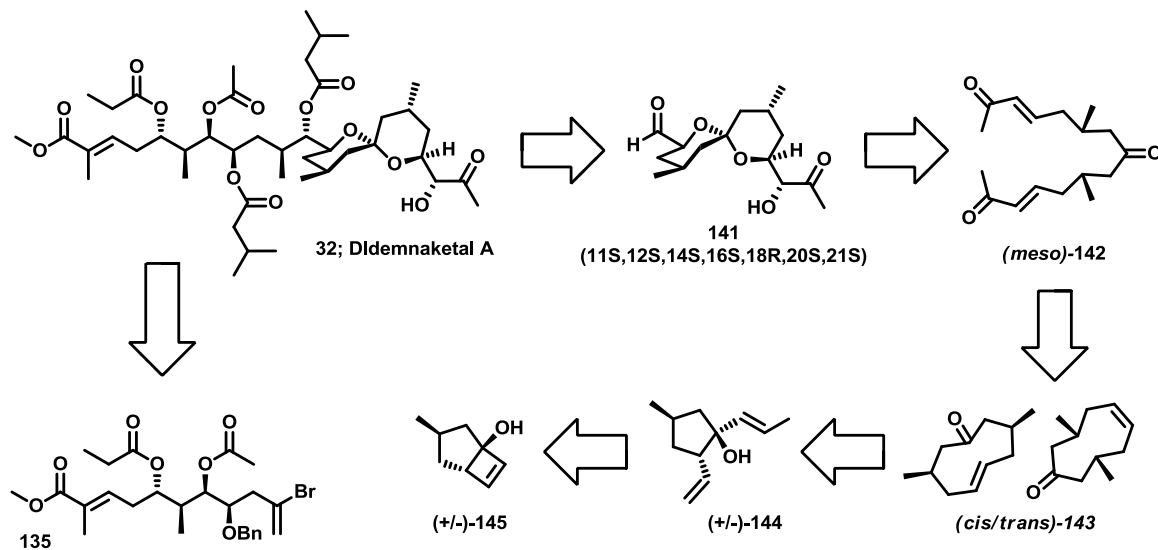


Figure 23. A retrosynthetic analysis for the synthesis of the spiroketal moiety of didemnaketal A (139)

Tu, Ito, and Fuwa, all chose to expedite their spiroketal syntheses by drawing key stereogenic centers from the chiral pool. Indeed, the chiral pool has many building blocks which allow chemists to bypass long, tortuous synthesis; however, the choice of starting material tends to shape the synthetic strategy and can severely restrict its flexibility. If the absolute stereochemistry of the entire spiroketal core has been misassigned, such a fundamental structural reorganization will likely require Tu, Ito, and Fuwa to select new starting materials and, consequently, redesign much of their synthetic methodology from the ground up. Our contrasting strategy uses asymmetric catalysis to exploit the molecules inherent symmetry. We thereby hope to avoid many of the optimization and purification issues that plague typical asymmetric syntheses. The symmetry feature also allows us to build up the molecule rapidly, performing the same reaction twice on either side of the mirror plane in a single pot. Our approach should also be far more adaptable as the chirality of the spiroketal depends on a single catalytic step; it is simple enough to

select the complementary catalyst and probe alternative structural hypotheses. Although our competitors have a head-start, our novel strategy may provide an advantage in the race to produce the first total synthesis of the *true* structure of didemnaketol A. Ultimately, we hope to develop a potent antiretroviral drug whereby dissociative inhibition can be used to buttress traditional competitive inhibitors, leading to therapies which are less susceptible to the mutations in the HIV-PR protease active site that cause drug resistance.

Chapter 2 — Photochemical Approaches

2.1 Outlook and Goals

We envisioned that the construction of the spirocyclic core of didemnaketal A would be accomplished through a desymmetrization of the *meso* precursor, **142**. We hoped to expedite access to our target by exploiting this element of symmetry, approaching the synthesis as a racemate and applying parity where possible to chemical transformations. For instance, we intended to perform two-fold Sharpless asymmetric dihydroxylations (SAD) on either side of the mirror plane of compound **142**. Likewise, **142** itself would be obtained through a ring opening cross metathesis (ROCM) of **143**, allowing us to simultaneously cap both ends of the linearized molecule with α,β -unsaturated methyl ketones. Thus, the nine-membered ring, **143**, represented a keystone structure in our synthetic strategy, and the route we developed to access these compounds is discussed here and in Chapter 4 of this thesis.

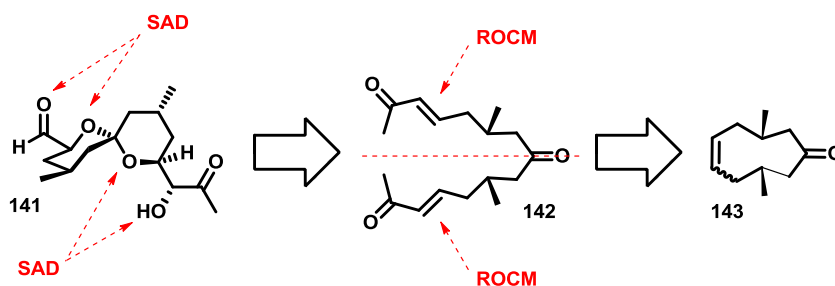


Figure 24. Use of symmetry for the expeditious assembly of the spiroketal moiety of didemnaketal A

Our preliminary target, **143**, appears to be structurally simple. The ketone and the olefin are diametrically situated around a nine-membered ring while two methyl groups flank the ketone at the β positions. The chief synthetic challenge lies in forming the nine-membered ring while ensuring a *syn* orientation between the methyl branches. Fortunately, the metathesis reaction for which compound **143** is intended does not discriminate between the two possible geometric isomers, thereby relieving us of the burden to do so.

2.2 Synthesizing 9-Membered Rings

Cycloalkanes, $(\text{CH}_2)_n$, fall into one of four categories: the small rings ($n = 3$ or 4), the common rings ($n = 5, 6$ and 7), the medium rings ($n = 8-12$), and the macrocycles ($n \geq 13$). Of these motifs, medium sized rings are often the most challenging to access, with nine-membered rings being especially difficult. Their formation is both kinetically and thermodynamically discouraged because of steep enthalpic and entropic penalties.

The rate of cyclization depends on the probability of a collision between the two termini of a linear chain; however, the likelihood of an end-to-end reaction decreases as the chain length increases. Furthermore, the formation of this cyclic transition state is impeded by severe transannular interactions. Combined, the entropic cost of preorganization and the steric penalty to the activation enthalpy ensure a high energy transition state, impeding the kinetics for the formation of medium sized rings.

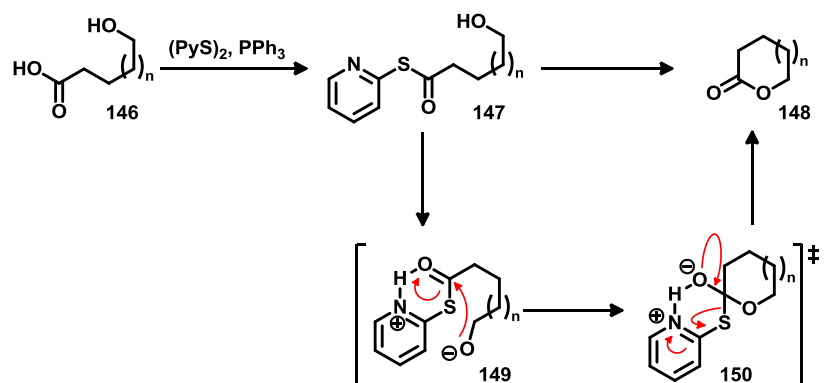
The synthesis of medium sized rings is also disadvantage with respect to thermodynamics. A cyclization involves a decrease in the torsional degrees of freedom compared to the linear chain. In other words, the reaction represents an entropically unfavourable increase in rigidity and order. These medium sized rings also produce significant transannular interactions between axial substituents. The resulting strain is accommodated through torsional and bond angle distortions which increase the heat of formation. As shown in table 1, strain energy reaches a maximum with nine-membered rings, and then diminishes as the series proceeds onward to larger macrocycles.⁷⁹

n	Strain Energy (kcal/mol)	n	Strain Energy (kcal/mol)
3	27.5	10	12.4
4	26.3	11	11.3
5	6.2	12	4.1
6	0.1	13	5.2
7	6.2	14	1.9
8	9.7	15	1.9
9	12.6	16	2.0

Table 1. Trends in ring strain for cycloalkanes, (CH₂)_n

Despite the energy amerced to both thermodynamic and kinetic factors, several strategies have been devised by which we may still access this ill-favored ring size. The most obvious approach, though perhaps the one that is also most fraught with difficulty, is the end-to-end reaction of an extended chain. Although there are several similar strategies to choose from, the Corey–Nicolaou macrolactonization nicely illustrates the general features of this transformation.⁸⁰ First, an acid (*eg.* **146** in scheme 15) is functionalized as a 2-pyrinethiol ester (**147**). As it undergoes an intramolecular proton transfer, an alkoxide nucleophile is established while simultaneously enhancing the electrophilicity of the acid derivative. The electrostatic relationship in the dipolar

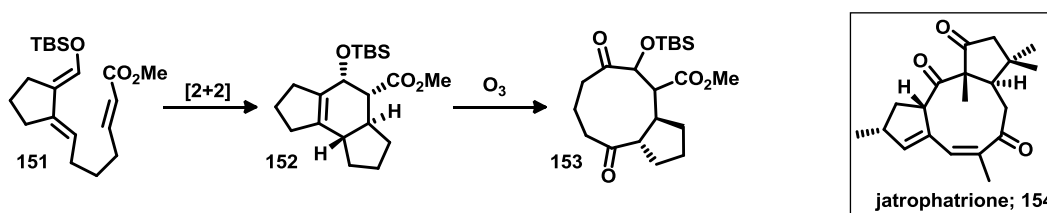
intermediate (**149**) improves the otherwise low probability of intra- over intermolecular reactivity. The attack of the alkoxide nucleophile results in a tetrahedral intermediate (**150**) which then collapses to the desired lactone (**148**). To aid in overcoming the entropic handicap associated with nine-membered ring formation, the reaction must be performed at a very high dilution. Alternatively, a high dilution may be simulated through a slow addition of the starting acid into the reaction mixture.



Scheme 15. The mechanism of the Corey–Nicolaou macrolactonization

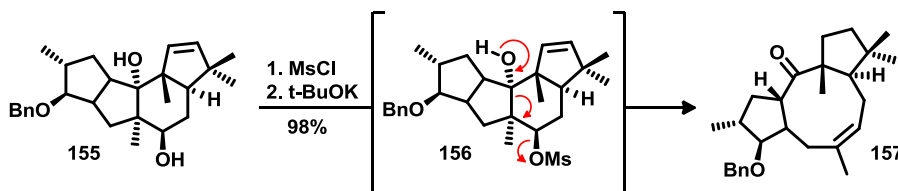
Reactions like the Corey–Nicolaou macrolactonization may be excellent for accessing medium sized cyclic esters; unfortunately, there are not many analogous method that reliably produces carbocycles. As an alternative to the end-to-end approach, it is often more efficient to prepare a bicyclic scaffold that is the fusion of two common sized rings. Then, upon selectively cleaving the bond that connects the bridgehead carbons, the larger ring is revealed. The intermediacy of the bicyclic system helps to mitigate ring strain while allowing the entropic barrier to be handled piecemeal through several discreet transformations.

Koikowski used this approach to synthesize the core of the potent antileukemic natural product, jatrophatrione (**154**).⁸¹ The 5/6 fused bicyclic precursor, **152**, was directly assembled through an intramolecular Diels Alder reaction, a transformation that conveniently provided an olefin between the bridgehead carbons. Fragmenting this double bond by ozonolysis revealed the nine-membered ring and established two pertinent ketones.



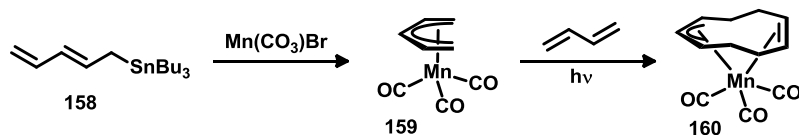
Scheme 16. Koikowski's fragmentation approach to the synthesis of the core of jatrophatrione (**154**)

Two decades later, Paquette completed the first total synthesis of jatrophatrione by adopting a similar fragmentation approach to the nine-membered ring.⁸² Rather than using an ozonolysis reaction, however, Paquette orchestrated the bond cleavage through a Gröb fragmentation. From the key intermediate, **155**, a nucleofuge was generated by mono-mesylating the less hindered of the two alcohols. Deprotonation of the remaining alcohol triggered the crucial fragmentation, forming the 5/9/5 fused tricyclic skeleton in excellent yield.



Scheme 17. Paquette's fragmentation approach in first total synthesis of jatrophatrione (**154**)

As an alternate strategy for synthesizing nine-membered rings, our lab is currently developing a formal [4+5] photochemical cycloaddition based on conditions discovered by Krieter.^{83,84} The reaction uses Mn to ligate diene precursors, bringing them into proximity of one another and facilitating the cyclization through the formation of two new carbon-carbon bonds while also potentially establishing their stereochemistry. Once optimized, this reaction should allow us to rapidly transform simple dienes into an assortment of otherwise synthetically challenging carbocycles. Although we have already prepared several $\eta^{3:2}$ Mn complexes, the simplest of which is **159** in scheme 18, the practicability of this approach as an entry into the didemnaketal A synthesis remains to be demonstrated.

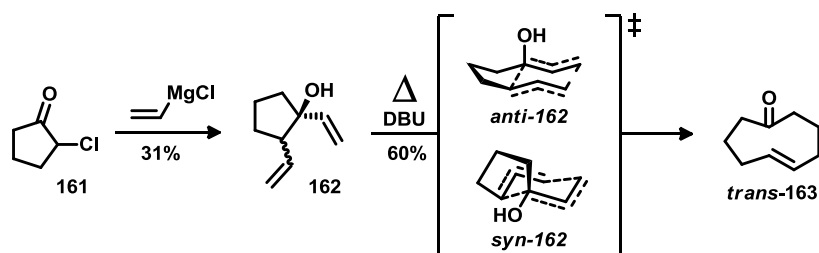


Scheme 18. Krieter based approach to the construction of nine-membered rings using a Mn-facilitated [4+5] cycloaddition

Finally, medium sized cycloalkenes can be obtainable through the expansion of smaller rings. A [3,3]-sigmatropic rearrangement, for instance, may be used to enlarge a ring by four additional carbon atoms. This approach to nine-membered rings has several appealing features. First, accessing the precursor to the cyclononene should be relatively straightforward, since five-membered rings are abundant, as are the methods for making them. This cyclopentane also provides a rigid scaffold, preorganizing the pendant alkenes into the appropriate position to react, thus circumventing the otherwise high entropy of

activation. Finally, the concerted bond formation / bond scission often proceeds with predictable diastereoselectivity which is rooted in the geometry of the transition state.

The simple Cope rearrangement is a reversible reaction, thus one might expect ring strain to drive the equilibrium towards ring contraction, not expansion. However, in the special case of the oxy-Cope modification, the rearrangement product is an enol that rapidly tautomerizes into a δ,ϵ -unsaturated carbonyl. The strength of the oxygen carbon double bond provides the thermodynamic incentive for the formation of this otherwise energetically unfavorable motif.

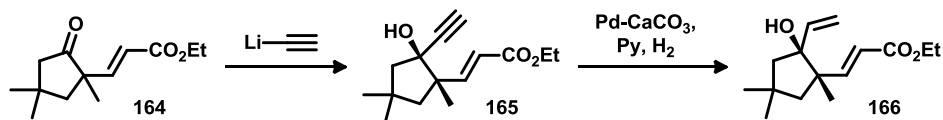


Scheme 19. Kato's two-step synthesis of nine-membered rings through an oxy-Cope ring expansion

In the early eighties, Kato reported a two-step method for producing medium sized rings using this oxy-Cope ring expansion.⁸⁵ He found that various α -chlorocycloalkanones react with vinylmagnesium chloride to give 1,2-divinylcycloalkanes (eg. **162** in scheme 19). Mechanistically, the Grignard reagent attacks the ketone resulting in an intermediate chlorohydrin which then undergoes a 1,2-migration of vinyl group, displacing the chloride and restoring the ketone for a second vinylation. The transformation, however, was poorly diastereoselective, producing a mixture of *syn* and *anti* substrates (**162**). Kato demonstrated that, when

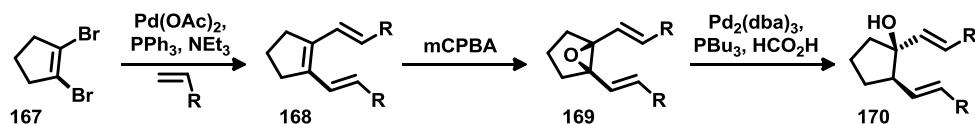
heated to between 165 and 200 °C, both stereoisomers underwent oxy-Cope rearrangements and, interestingly, both produced the *trans* isomer of nonenone **163**. Kato proposed that both substrates, *syn*- and *anti*-**162**, proceed along the reaction coordinate through 6-membered chair-like transition states. When the relative orientation between the vinyl groups is *anti*, Kato's transition state model requires the alcohol to be oriented in the axial position; as for the *syn* substrate, the alcohol must be equatorial (see scheme 19).

Kato's work convinced us of the power of the oxy-Cope rearrangement for making medium sized rings; however, the low yields and inherently poor diastereoselectivity limit the utility of this protocol. Since then, several groups have improved the precision with which one might access the 1,5-diene precursors. For instance, Janardhanam reported the diastereoselective addition of an acetylide to vinylcycloalkanone (**164** in scheme 20).⁸⁶ A partial hydrogenation of the triple bond produced a potential oxy-Cope precursor in which the vinyl groups were orientated *syn* to one another (**166**).



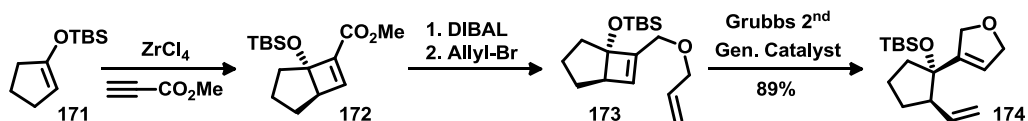
Scheme 20. Janardhanam's preparation of *syn*-1,5-diene oxy-Cope precursors

Similarly, von Zezschwitz performed two-fold Heck reactions on 1,2-dibromocycloalkene substrates (**167** in scheme 21).⁸⁷ An epoxidation across the central double bond, followed by a reductive ring opening offered diastereoselective access to other *anti*-oriented substrates (**170**).



Scheme 21. von Zezschwitz's preparation of *anti*-1,5-diene oxy-Cope precursors

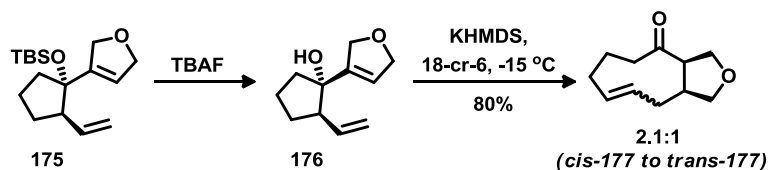
In 2003, Snapper developed a route to various *syn* precursors.⁸⁸ Using a formal [2+2] cycloaddition, Snapper fused butene rings onto a series of 5- and 6-membered cyclic silyl enol ethers. A ring-opening / ring-closing metathesis (RORCM) transformed the highly strained cyclobutenes into *syn*-1,5 dienes. The only caveat to this elegant approach is that the metathesis requires an intramolecular tether (see **173** in scheme 22); consequently, Snapper's nine- and ten-membered cycloalkanes inevitably possess a fused heterocyclic appendage adjacent to the ketone (as with **174**).



Scheme 22. Snapper's preparation of *syn*-1,5-diene oxy-Cope precursors

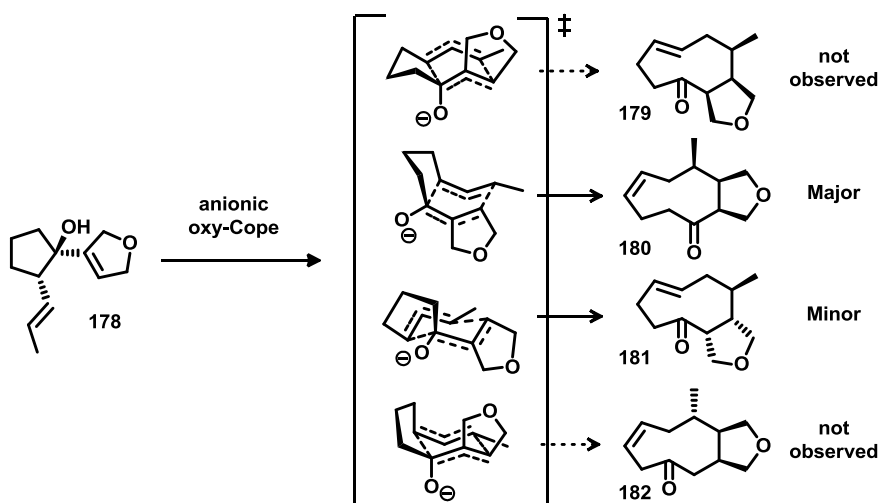
Evans discovered that simply deprotonating the alcohol of the oxy-Cope precursor causes a dramatic reduction the reaction temperature.⁸⁹ Kato's thermal rearrangement occurred at temperatures in excess of 160 °C, whereas similar dienes prepared by Snapper rearranged at -15 °C when treated with KHMDS and 18-crown-6 ether. At higher temperature, Kato's starting material, a mixture of *syn* and *anti* diastereomers, converged on a single geometric isomer of product *trans*-**163** (seen in scheme 19). Interestingly, the

analogous reaction under Snapper's milder conditions produced a mixture of geometric isomers, this time favouring *cis*-**177** by 2.1:1 (shown in scheme 23).



Scheme 23. Snapper's anionic oxy-Cope leading to a mixture of *cis* and *trans* nine-membered cyclic enones

In order to effectively apply the oxy-Cope reaction to obtain our desired diastereomer, we require a comprehensive understanding of the possible transition state geometries. However, the model posited by Kato for the thermal rearrangement fails to explain the product distribution observed under Snapper's anionic conditions. In fact, there are four possible transition states (refer to scheme 24), each one giving rise to a unique product. Specifically, the transition state may resemble either a boat or a chair and, in both conformations, the hydroxyl group may assume either an axial or an equatorial position.



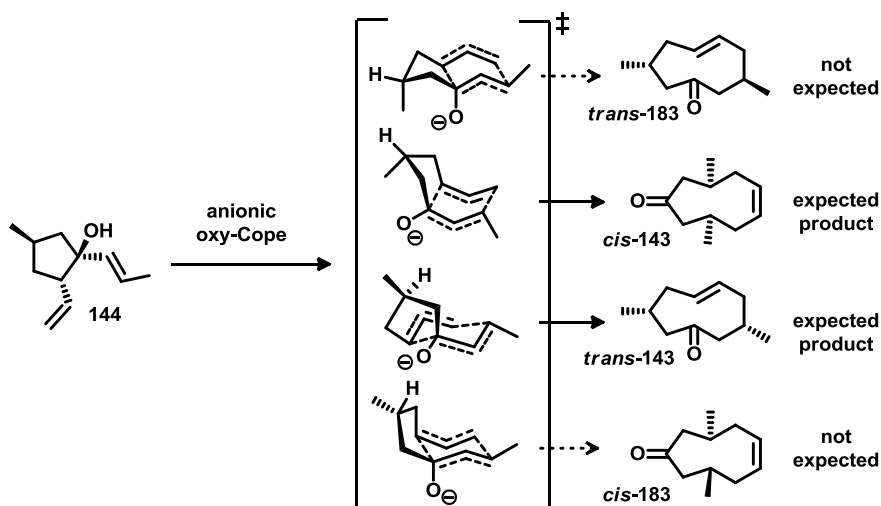
Scheme 24. Snapper's investigation of the transition state distribution for the anionic oxy-Cope ring expansion of cyclopentanes

In an elegant experiment intended to probe the transition state distribution, Snapper performed the ring-expanding rearrangement on substrate **178**. Only two products were observed, **180** and **181**—the implication being that, as long as the oxygen remains in the pseudo-equatorial position, both chair and boat transition states are energetically accessible. Those transition states where the oxygen assumes the pseudo-axial position appear to be energetically unfeasible; that is, at least when the two vinyl groups are *syn* to one another. Interestingly, Snapper's conditions, the *O*-equatorial boat appears to be lower in energy than the corresponding chair-shaped transition state.

2.3 Application of Snapper's Model

The insights gained through this transition state study revealed alkene **144** (see scheme 25) as the particular isomer that would allow us to access our targeted nine-membered ring. Establishing the correct geometry between the substituents would be crucial: the alcohol and the methyl branch have to be oriented on the same face of the cyclopentane ring; the 1,2-bisvinyl substituents must be *syn* with respect to one another; finally, *trans* geometry is required for the allylic methyl group. When compound **144** undergoes an anionic oxy-Cope reaction through either a boat or a chair transition state, as long as the alkoxide remains in the equatorial position, we expect 9-membered rings in which the β -methyl groups are to be formed *syn* to one another. The *anti* diastereomers (*cis*- and *trans*-**183**) are compounds for which we have no use and whose separation for the valuable *syn* material would likely prove challenging. Fortunately, Snapper's model suggests that these compounds arise from high energy, *O*-axial transition states, thus we expect to avoid this pitfall. Instead, we anticipate a mixture of *cis*- and *trans*-**143**,

possibly favouring the *cis* isomer arising through the boat shaped transition state. In fact, the ratio of isomers is of little consequence since the geometry about the double bond is ablated in the subsequent ring opening metathesis. With both potential products being equally valuable, the anionic oxy-Cope reaction seems perfectly suited to meet our needs.



Scheme 25. Application of Snapper's transition state predictions for the synthesis of a keystone intermediate in our didemnaketol A synthesis

Appreciating the utility of Snapper's ring opening metathesis in facilitating a rapid installation of 1,5-dienes, we sought to adapt this strategy to fit our own particular needs. However, all of Snapper's nine-membered rings invariably possess a fused heterocycle. This structural artifact originates in the necessity of a molecular tether to accomplish the ring-opening metathesis of the cyclobutene. Unfortunately, this heterocycle does not advance our goals. We recognized that we could circumvent this structural idiosyncrasy by attaching the tether through silylation of the alcohol. This subtle modification accomplishes a number of important objectives: it protects the alcohol through several transformations, saving us additional steps; it facilitates the metathesis, producing the 5 /

6 spirostructure, **184** (refer to figure 25); finally, desilylation allows us to control the installation of the allylic methyl group.

Also, we recognized that the geometry of the [3.0.2] bicyclic architecture (**185**) should allow us to direct the stereochemical outcome for the methylation of the cyclopentane ring. Unfortunately, the site for this desired alkylation is a non-activated methylene carbon. The temporary placement of a ketone adjacent to the bridgehead would greatly expand our synthetic options. Not only would this functional group facilitate the methylation through its enolate, but it could also assist us with installing cyclobutene ring since the photochemical [2+2] cycloadditions between enones and alkynes are well-known. Ultimately, after having served its purpose, the ketone would have to be fully reduced to a methylene. Though this is often a difficult transformation, we felt the advantages of incorporating the ketone would outweigh the inconvenience of its removal.

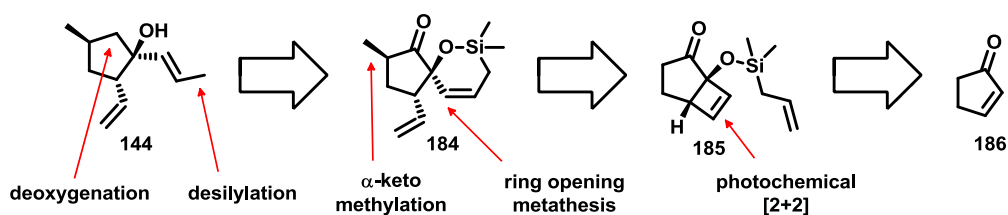
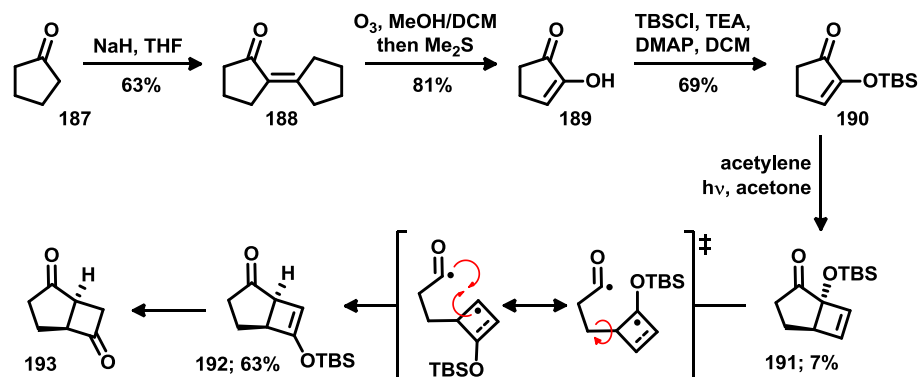


Figure 25. Retrosynthetic analysis of the anionic oxy-Cope precursor

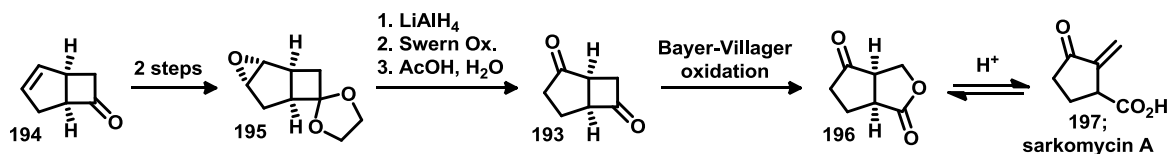
2.4 Photochemical Cycloaddition Approach

We initially attempted to access compound **185** through a photochemical [2+2] cycloaddition between acetylene and 1,2-cyclopentanedione (**189** in scheme 26). The diketone starting material was known but not conveniently purchasable. Instead, we procured the compound through a literature procedure involving the self-condensation of cyclopentanone followed by ozonolysis, then protected the free enol with TBSCl.⁹⁰ Irradiating **190** with ultraviolet light (250 nm), while using a balloon to maintain an atmosphere of acetylene, failed to transform the starting material. We did, however, observe reactivity when performing the same reaction at high pressure, condensing the gaseous acetylene into the reaction mixture at -78 °C, sealing it in a high pressure reaction vessel and allowing it to warm to room temperature. It seemed that the desired [2+2] cycloaddition was indeed occurring—except the desired compound (**191**) was not the major product. Instead, the preferred compound, present in a 9:1 ratio, was the unexpected silyl enol ether, **192** (see scheme 25). Mechanistically, it appears that upon forming the α -keto silyl ether (**190**), a Norrish Type 1 reaction homolytically fragmented cyclopentanone into an acyl radical and an allylic cyclobutenyl radical. A bond rotation allowed a new [3.0.2] ring system to form, shifting the position of the alcohol and trapping it in the enol form. The cyclobutenol configuration was not overly stable and had a tendency to decompose into the diketone **193** over time.



Scheme 26. The attempted photochemical [2+2] cycloaddition and the resulting unexpected rearrangement

This [3.0.2] diketone compound had been synthesized previously, albeit through a different route. Griengl prepared **193** in five steps from compound **194** as the penultimate compound in his brief total synthesis of sarkomycin A (**197** in scheme 27), a naturally occurring antibiotic and anti-tumor agent.⁹¹ He used the Bayer-Villiger oxidation to lactonize the four-membered ring, forming **196**, a tautomer to the natural product.



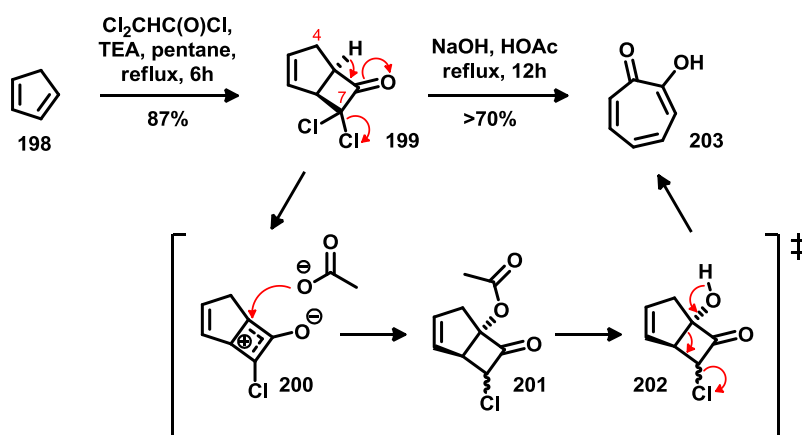
Scheme 27. The key step in Griengl's synthesis of sarkomycin A (**197**)

Optimistically, our unexpected rearrangement might be considered an accidental formal total synthesis; realistically, it was significant barrier to our entry into the didemnaketol A synthesis. After weighing the potential benefits against the challenges of optimization, along with the practical difficulties and potential dangers involved with

scaling up the high pressure reaction, this approach to compound **185** was ultimately abandoned.

2.5 Electrocyclic Ring Closure Approach

Instead, we turned to tropolone, an aromatic 7-membered alcohol which is known to undergo a four-electron electrocyclic ring closure upon irradiation, providing the [3.0.2] bicyclic scaffold we were seeking. Tropolone (**203**) is commercially available, though somewhat costly (~\$50/gram). Fortunately, there are several methods by which it can be synthesized.⁹² The most convenient and inexpensive route starts with a [2+2] cycloaddition between dichloroketene and freshly cracked cyclopentadiene (**198**). The adduct **199** can then be converted to tropolone by heating it with sodium acetate (as seen in scheme 28).

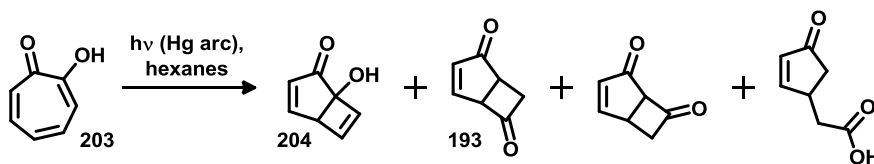


Scheme 28. Bartlett's mechanism for the formation of tropolone (**200**)

This reaction stimulated some controversy after the intuitive 4,7-elimination mechanism was disproven. The mechanistic hypothesis that has since garnered the most support was proposed by Bartlett.⁹³ The heating of compound **199** is thought to lead to

the formation of an enol allylic cation (**200**) which traps an acetate anion. Hydrolysis of the acetate then triggers a Gröb fragmentation, expelling the chloride nucleofuge and forming **203**. In our hands this transformation produced tropolone in good yield on multigram scale.

In 1970, Day published his discovery that ultraviolet light caused tropolone to undergo an electrocyclic ring closure, forming a [3.0.2] bicycle (**204** in scheme 29).⁹⁴ This small yet densely functionalized compound seems to have enormous potential for launching diverse synthetic enterprises. However, it is difficult to find even a single example where this versatile building block has been put to use; perhaps because the synthetic protocols described in the literature are not very practicable. The original paper offers no experimental procedure or product characterization, it doesn't provide any sense of reaction time, and merely reports the yield of **204** as "satisfactory" before describing a host of reaction by-products (shown in scheme 19).

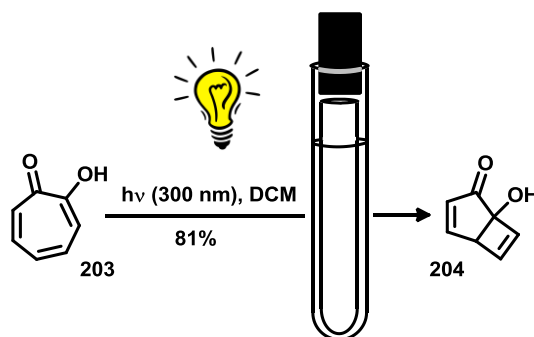


Scheme 29. Day's photochemical electrocyclization of tropolone

Indeed, our initial attempts at recreating Day's experiment were met with less than satisfactory results. The yields were low and often irreproducible and the reaction mixtures were contaminated with starting material and various undesired products. After some optimization, we found that degassed dichloromethane seemed to improve our

control over reaction output; however, we struggled to achieve rapid conversion of tropolone to **204** before losing significant amounts of the desired product to other photochemical transformations.

The key to obtaining high yields came through redesigning the reaction vessel. Rather than using a standard round bottom flask, the best results were obtained when we dissolved the tropolone with dichloromethane in a large Pyrex test tube. A smaller test tube was then inserted into the larger one, pressing the solution into a thin film between the inner and outer walls. The solvent was degassed with argon before sealing the larger test tube with a rubber stopper and irradiating at 300 nm (shown in scheme 30). With this modification, we were able to obtain consistently high yields of compound **204** after purification by silica gel chromatography. The one drawback was that the test tubes had a maximum capacity of approximately 100 mg. Although the light box could fit up to five test tubes at a time, the 500 mg per batch limit on this reaction proved to be somewhat of a bottleneck.

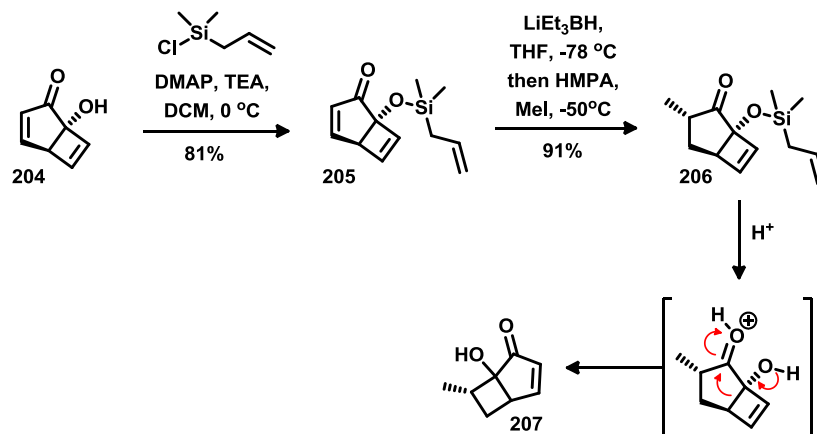


Scheme 30. A high yielding practicable photochemical electrocyclization of tropolone (**203**)

Next, we sought to functionalize the free hydroxyl group of compound **204**. We quickly discovered that the use strong bases would have to be avoided, as deprotonation of the alcohol triggered a reversion of the [3.0.2] bicycle back to tropolone. Fortunately, the substrate was found to tolerate the addition of silylchlorides upon activation with catalytic DMAP. As discussed earlier, the choice of allyldimethylsilylchloride was tactical. Not only does it protect the reactive alcohol, but it also provides an olefin tether to facilitate the pending cyclobutene ring-opening metathesis reaction. Upon excising the silicon atom, the carbons from this tether remain as the propene substituent in the oxy-Cope precursor (refer **144** in scheme 25). This alcohol protection was reliably high yielding, although the silyl group was found to be labile during chromatography, even with base-treated silica gel. Fortunately, little more than an aqueous extraction was typically necessary for obtaining clean material (**205** in scheme 31).

Treatment of **205** with lithium triethylborohydride led to a conjugate reduction of the enone. Conveniently, we found we were able use methyl iodide to trap the latent enolate which formed during the reduction. The cyclobutene ring sterically shields one face of the enolate, ensuring a diastereoselective methylation. Though often high yielding, this reaction was found to be very temperamental, sensitive to both temperature and the presence of moisture. The initial reduction had to be performed by slow addition of the lithium triethylborohydride solution at $-78\text{ }^{\circ}\text{C}$. After approximately two hours, rigorously dried HMPA was added to sequester the lithium cation, followed by addition of the alkylating iodide. The reaction was then warmed to $-50\text{ }^{\circ}\text{C}$. Within three hours the reaction would have to be quenched by quickly pouring the cold solution over a biphasic

mixture of ether and water. Failure to comply with these precise conditions resulted in a bright yellow colour change, an indication of decomposition.

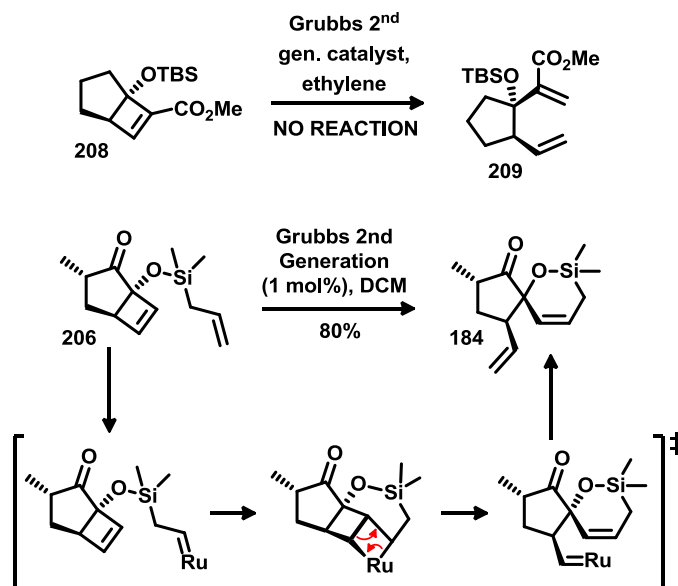


Scheme 31. Silylation, conjugate reduction, and alkylation of the [3.0.2] bicyclic core

Following the conjugate reduction / methylation sequence the overall stability the product (**206**) seemed to improve relative to compound **205**, particularly with respect to chromatography. However, we have observed that the hydrolysis of the silylether under mildly acidic conditions can trigger a semi-pinacol type rearrangement to compound **207**.

Early on, while probing the feasibility of our synthetic strategy, we prepared the simple [3.0.2] bicycle **208** and attempted to induce a ring opening metathesis under an atmosphere of ethylene (as shown in scheme 32). However, we found that the catalyst would become depleted without having affected the cyclobutene ring. With compound **206**, on the other hand, we observed excellent conversion to the 5 / 6 spiro ring system **184** with low catalyst loadings. The essential difference is that, whereas in the former reaction the metathesis is an intermolecular process, now the primary olefin can initiate the reaction by forming an alkylidene complex with the ruthenium and tethering the

catalyst directly to the molecule, thereby facilitating an intramolecular opening of the cyclobutene. The strain released when transitioning from the four- to the six-membered ring ensures that the reaction is irreversible.

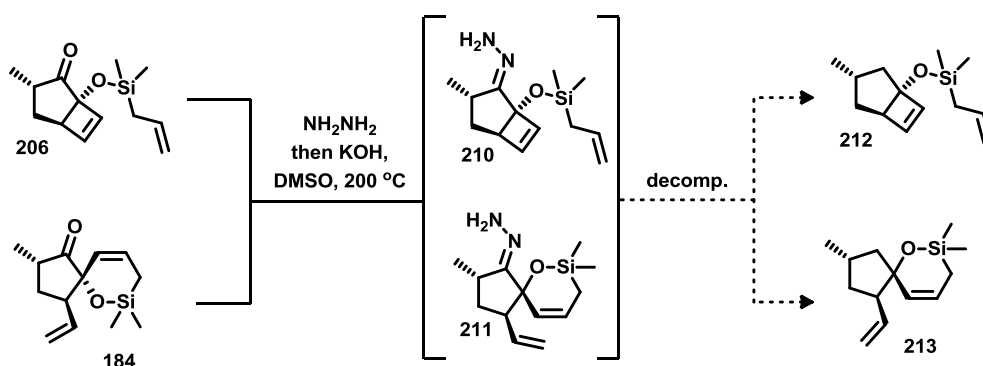


Scheme 32. Ring opening ring closing metathesis providing a 5/6 spirocyclic system

By this point in the synthesis we had fully exploited the advantages offered by the ketone functional group. Originating in our starting material, tropolone, the ketone allowed us to rapidly access the challenging [3.0.2] bicyclic architecture. Likewise, through its enolate, we were able to diastereoselectively install a methyl group on an otherwise remote methylene. The trade-off, however, is the challenge of removing it. There are several general methods for deoxygenating a ketone, but they typically involve harsh reaction conditions and high temperatures. The hindered nature of our substrate only increased the difficulty of the desired transformation. Nevertheless, we made several attempts.

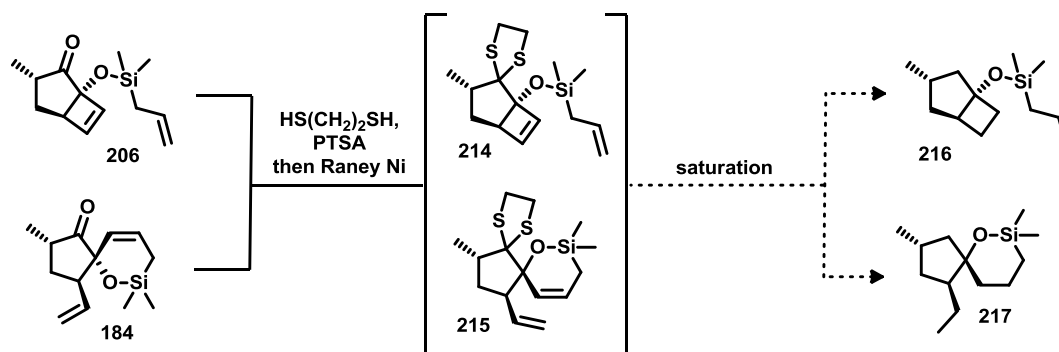
2.6 Attempted Decarboxylations

The Wolff–Kishner reduction, for instance, involves forming a hydrazone, deprotonating it with a strong base then, with high temperatures ($>200\text{ }^{\circ}\text{C}$), driving off nitrogen, leaving behind an alkyl anion for protonation. Unfortunately, when these conditions were applied to our system, we did not succeed in accomplishing the desired reduction. Neither compounds **206** nor **184** were able to withstand such severe treatment. Kishner–Leonard type eliminations, commonly observed in ketones bearing α heteroatoms, may also have contributed in our failure to obtain useful reaction products.



Scheme 33. Attempted Wolff–Kishner reduction

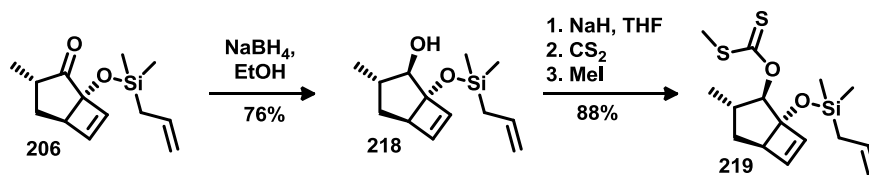
A milder alternative to the Wolff–Kishner reaction is Mozingo reduction in which a thioketalization, using 1,2-ethanedithiol, is followed by desulfurization by Raney nickel. Although the formation of the dithioketal is acid catalyzed, the desulfurization occurs under neutral conditions and at ambient temperature, making it our mildest option. We were able to form the desired dithioketal **214**, albeit with some difficulty as the silyloxy **206** had a tendency to hydrolyze. When **214** was treated with Raney nickel, we also observed desulfurization; unfortunately, these conditions also reduced the indispensable double bonds. Owing to these difficulties, the tactic was abandoned.



Scheme 34. Attempted Mozingo reduction

By reducing of the ketone to an alcohol we introduced a third option; namely, the Barton–McCombie deoxygenation. This reaction involves elaborating the alcohol into a xanthate and cleaving the *O*-alkyl bond through a radical driven β -scission. The transformation leaves behind an alkyl radical which ultimately abstracts a hydrogen atom, usually from an organotin hydride, thereby propagating the chain reaction. This method is known to be effective at removing even hindered alcohols since the thiocarbonyl group tends to be more exposed than the scissile bond itself.

We found that ketone **206** reduces diastereoselectively to alcohol **218** when treated with NaBH_4 . A subsequent deprotonation with sodium hydride provided an alkoxide which was captured using carbon disulfide and methyl iodide, producing xanthate **219** in good yield.



Scheme 35. Ketone (**206**) reduction and xanthate (**219**) formation

2.7 Unexpected Radical Cascades

The standard Barton–McCombie reaction employs stoichiometric quantities of organotin compound which are costly, highly toxic, and often complicate the purification of desired reaction products. With the goal of replacing tin reagent, Wood published an appealing protocol for the deoxygenation of xanthate esters that uses trialkylboranes as the radical source.⁹⁵ However, after applying Wood’s conditions to our substrate, we did not isolate the expected deoxygenated product. On NMR spectroscopic analysis of the crude mixture, we observed a mysterious, fully saturated compound, bearing signals which indicated the incorporation of a new ethyl group, presumably an alkyl radical originating from the triethylborane. This compound, however, could not be isolated by silica gel chromatography. Instead, our purification attempts catalyzed a second transformation where by analysis of the NMR spectra revealed the loss of the salient ethyl group signal and the appearance of a new carbonyl resonance. Using a battery of NMR experiments, including a 2-dimensional TOCSY and NOESY correlation spectroscopy, we were able to identify the final product as the cage-like lactone **220**.

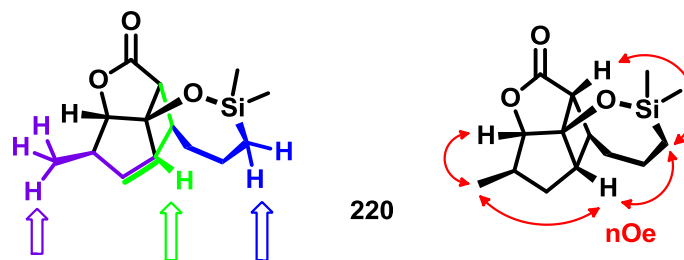
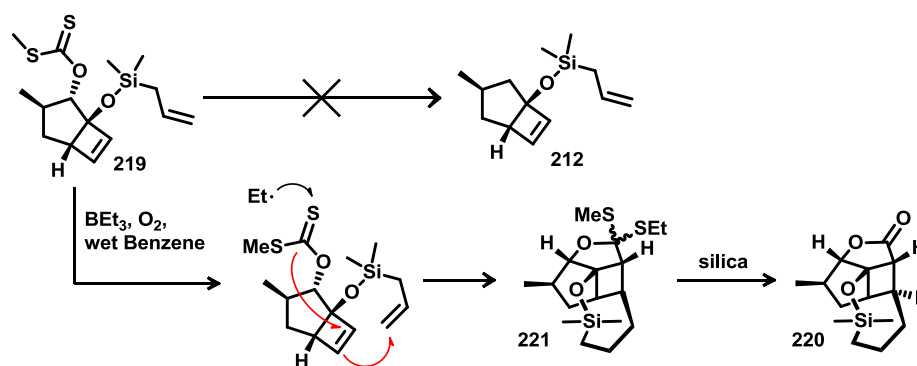


Figure 26. TOCSY spin systems (purple, green, blue) and NOESY correlations (red) used to solve the structure of **220**

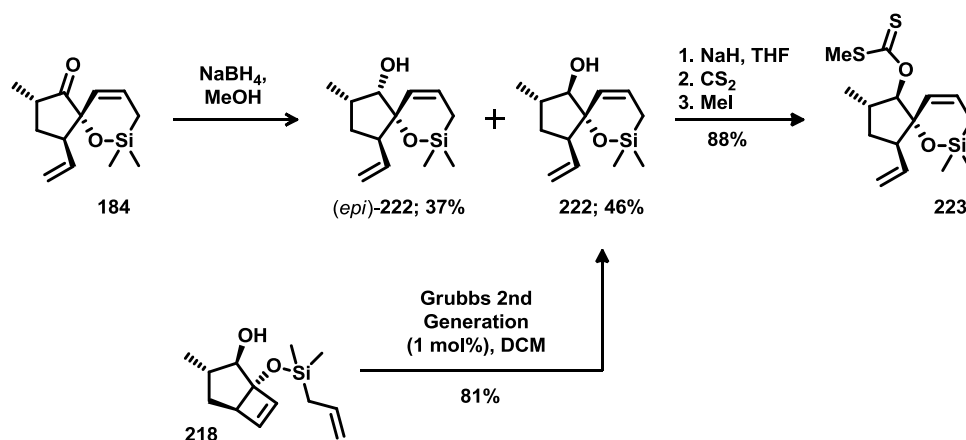
It seems that when xanthate **219** had reacted with an ethyl radical and the intermediate, rather than undergoing the expected β -scission which leads to deoxygenation, performed a cascade of cyclizations: a 5-*exo-trig* addition to the cyclobutene ring, followed by an apparent 8-*endo-trig* cyclization onto the terminal olefin tether. The short-lived penultimate compound that was observed prior to our purification attempts was likely a diastereomeric mixture of dithioorthoesters.



Scheme 36. Radical cascade observed in [3.0.2] bicycle during attempted Barton-McCombie deoxygenation

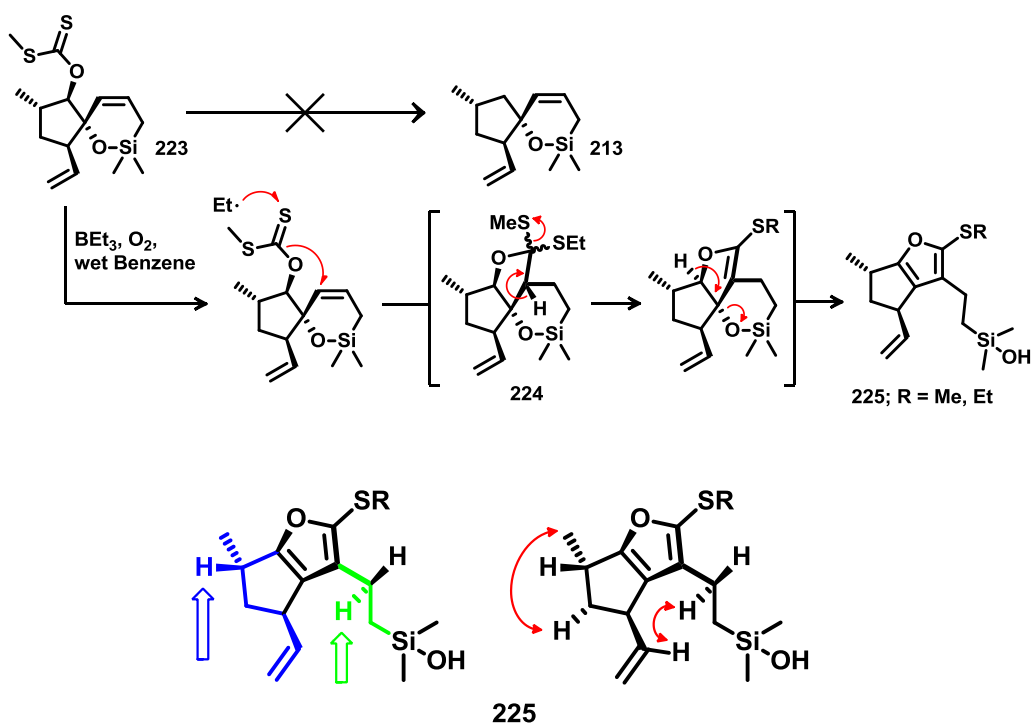
We considered that we might have more success by postponing the Barton–McCombie reduction until after the spiroketalization. In order to prepare the xanthate precursor (compound **222** in scheme 37) we attempted NaBH_4 reduction of the spiro ketone **184**.

We were successful at reducing the ketone, but the reaction produced about a 1:1 mixture of diastereomers at the alcohol center. Despite that fact that the diastereomers were separable by flash chromatography and that the poor diastereoselectivity would be obviated by the deoxygenation anyway, when we discovered that the RORCM worked equally well on the diastereomerically pure alcohol **218**, we favoured this route for its simplicity. With exclusive access to **222**, we were then able to install the xanthate functionality as described above (refer to scheme 35).



Scheme 37. Selective and non-diastereoselective access to **222** through RORCM and NaBH_4 reduction respectively for the purpose of making the Barton–McCombie substrates, **223**

When applying Wood's conditions the spiro xanthate **223**, we observed, not the reduction we were expecting, but similar *5-exo-trig* reactivity, this time leading to silanol **224**. However, unlike with the previous substrate, the dithiooesters observed in the crude NMR underwent a sequence of elimination reactions upon exposure to silica gel, producing an equimolar mixture of ethyl and methyl vinyl sulfides (**225**). Again TOCSY and NOESY NMR spectroscopy were instrumental in structural elucidation (refer to scheme 38).



Scheme 38. Radical cascade observed in 5 / 6 fused spirocyclic system during attempted Barton-McCombie deoxygenation. TOCSY spin systems (**green, blue**) and NOESY correlations (**red**) were used to solve the structure of **225**

The chemistry behind this serendipitous cascade intrigued us. We were impressed with degree of molecular complexity we were able to build into our structure and we recognized a potential utility for accessing lactones through this unconventional C-C bond forming process. For these reasons, we decided to explore this xanthate chemistry: optimizing the conditions, exploring the scope, and probing the mechanism. The results of this tangential investigation are discussed in the third chapter. Unfortunately, our failure to accomplish the deoxygenation stymied our progress toward the anionic oxy-Cope precursor **144** (refer to scheme 23). Ultimately, the decision was made to abandon this route from tropolone and redesign our approach. The continuation of our progress toward didemnaketol A will be the topic of the fourth chapter of this thesis.

Chapter 3 — Radical Lactonizations

3.1 Lactonization Strategies

Progress in our synthetic enterprise was momentarily stymied by the intractable deoxygenation of compound **219**. Our most promising strategy, the Barton–McCombie method, elicited a radical intermediate which diverted the reaction trajectory into a cascade leading to the polycyclic structure **220**. Although the transformation did not advance our goal of synthesizing didemnaketol A, we recognized in this unexpected result a potential tool for constructing complex lactones, a useful alternative to the conventional C–O bond forming approaches. Though tangential to the overarching didemnaketol synthesis, this chapter details our evaluation of dithiocarbonates as radical precursors in the synthesis of polycyclic lactones.

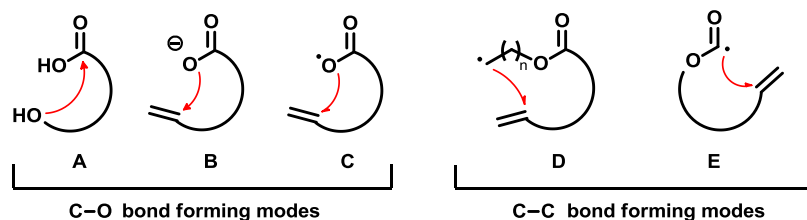
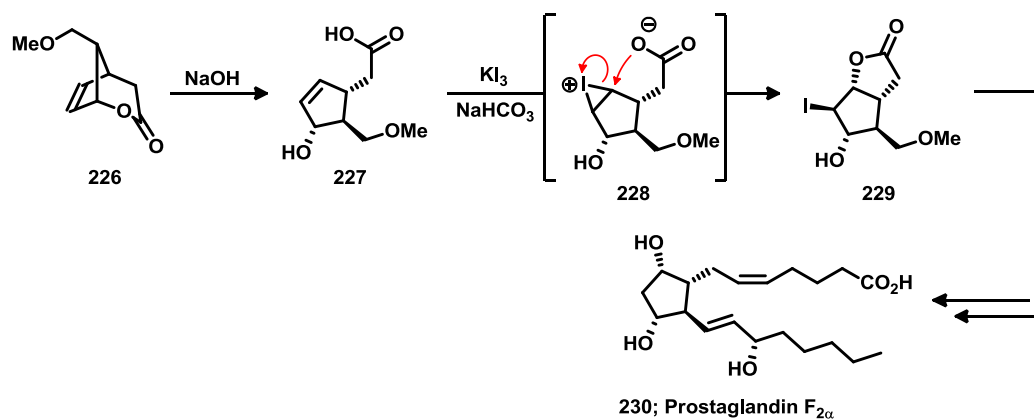


Figure 27. Some of the possible synthetic strategies for forming lactones

Lactones, particularly γ -butyrolactones, are ubiquitous among both natural products^{96,97} and drug-like molecules.⁹⁸ They are typically prepared through ionic reactions involving the formation of a new carbon–oxygen bond. The trivial example is the nucleophilic

addition of an alcohol onto a carboxylic acid or some synthetically equivalent derivative thereof (see example **A** in figure 27).

Alternatively, the ether linkage adjacent to the carbonyl may be formed through the addition of a carboxylic acid to an activated π -bond (see example **B** in figure 27). The archetypical example is the halolactonization, a reaction that has been known for over a century and is still widely used.⁹⁹ Corey's landmark prostaglandin synthesis (see **230** in scheme 39) demonstrates the power of this transformation.¹⁰⁰ After forming a positively charged halonium ion (**228**) from the existing π -bond, an intramolecular nucleophilic attack by the carboxylate anion closes the ring and forms the lactone. A host of variations have since been developed including bromolactonizations,¹⁰¹ selenolactonizations,¹⁰² tellurolactonizations,¹⁰³ and iodolactamizations.¹⁰⁴

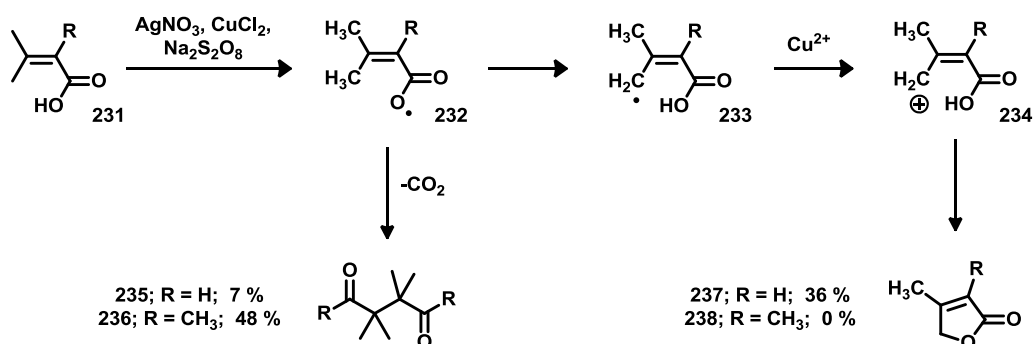


Scheme 39. Corey's use of the halolactonization for the synthesis of prostaglandin F_{2α} (**230**)

Although the conditions for this powerful cyclization are considered quite mild, the reaction does have significant limitations. For instance, the transformation is often readily reversible. Without a strong thermodynamic incentive, the use of the halolactonization is

therefore limited to the synthesis of unstrained rings. Also, in systems with competing 5-*exo* / 6-*endo* pathways, it is common to observe mixtures of regioisomers. Finally, activating the olefin to facilitate cyclization necessarily requires incorporating an additional heteroatom into the product—typically a halogen or a selenide. Occasionally this adjunct atom can serve a synthetic purpose; often, however, it is not useful and an additional step is required for ablation. In the aforementioned prostaglandin synthesis, for instance, the iodolactonization is immediately followed by radical dehalogenation of the unwanted iodide, a reaction that required stoichiometric use of an organotin hydride.

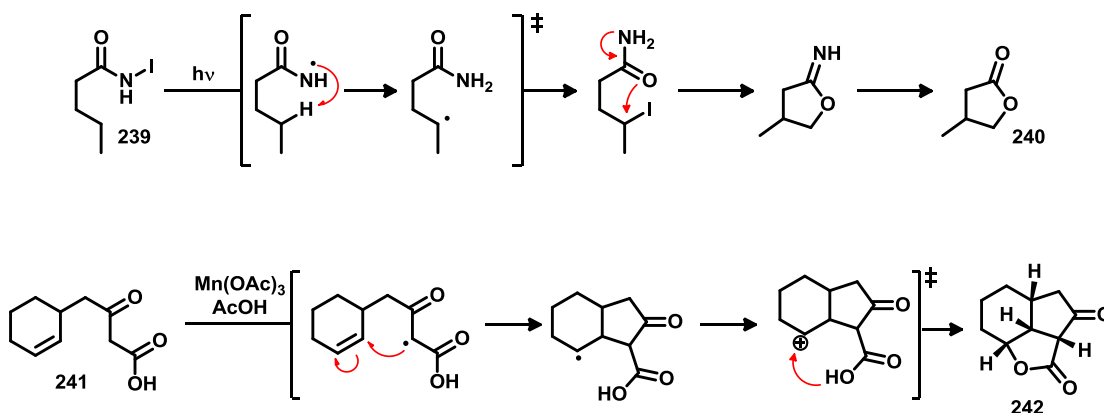
Many of these pitfalls can be circumvented by accomplishing the lactonization through a radical, rather than a polar mechanism. Radicals are high energy species, capable of driving the formation of strained systems while the reactivity is often more selective with respect to *endo* and *exo* isomers. Also, cascades are more straightforward to orchestrate, greatly increasing the amount of complexity that can be integrated per step. And, finally, since the chain reaction often terminates with a hydrogen atom transfer, the synthesis is not complicated by superfluous heteroatoms in need of removal.



Scheme 40. Lactonization involving acyloxy radical intermediates are low yielding due to competing decarboxylation pathways

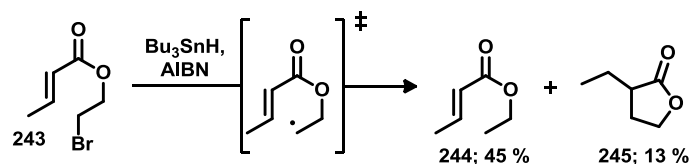
The one-electron mechanism for a cyclization that remains strictly analogous to the halolactonization reaction would need to invoke an acyloxy radical (see example **C** in figure 27). Although this transformation is not unheard-of, the acyloxy radical (eg. **232** in scheme 40) is strongly inclined toward decarboxylation, thereby diminishing yields and severely limiting the synthetic utility of this approach.¹⁰⁵

There are, however, examples where the problem of decarboxylation has been ingeniously circumvented, allowing for a radical based lactonization involving the formation of a new C–O bond. In 1965, Barton and Beckwith reported that γ -butyrolactones may be synthesized through the photolysis of *N*-iodoamides (see **239** in scheme 41).¹⁰⁶ Similarly, Corey, while attempting to synthesize the ginkgolide core, contributed to the development of an oxidative radical addition of carboxylic acids (eg. **241**) to alkenes.¹⁰⁷ In both examples, success depends on avoiding the formation of the highly unstable acyloxy radical intermediate; consequently, the actual C–O bond forming step occurs through a 2-electron process.



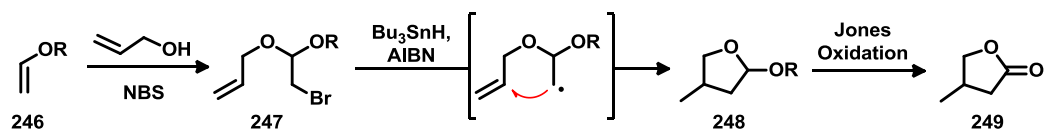
Scheme 41. Barton and Beckwith photolysis of *N*-iodoamides (**239**) and Corey's oxidative method are examples of C–O bond forming radical lactonization that avoid forming acyloxy radicals

Rather than lactonizing through a C–O bond, radical chemistry is much better suited to making C–C bonds and there are several examples of how this theme (refer to **D** in figure 27) has been developed. Walling¹⁰⁸ and Clive¹⁰⁹ were among the first to use an intramolecular addition of a nucleophilic carbon-centered radical to an α,β -unsaturated ester. However, the cyclization was largely outcompeted by premature hydrogen atom abstraction, resulting in a low yield of **245** (shown in scheme 42). Interestingly, the stabilizing effect of an adjacent carbonyl is not sufficient to overcome the preference for 5-*exo*-cyclization.



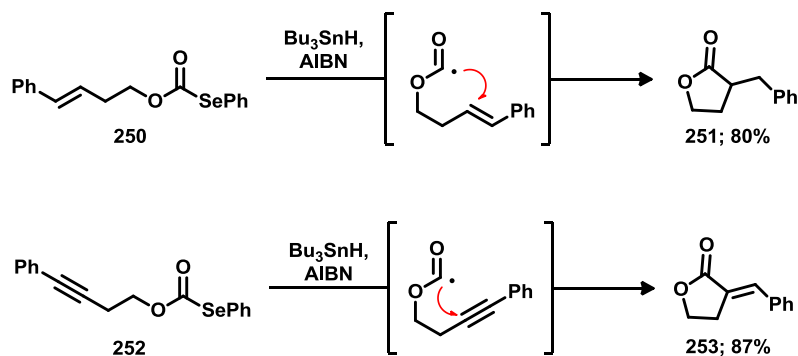
Scheme 42. Lactones formed through the intramolecular addition of a radical to an α,β -unsaturated ester

Extending the approach to carbon centered radicals that are stabilized by acyloxy groups also tends to be problematic (example **D** where $n = 0$ in figure 27). Cyclization is typically slow, possibly because the adjacent oxygen enhances the stability of the radical center, or possibly because hindered rotation about the ester retards the attainment of a conformation suitable for ring closure. The Stork–Ueno reaction (shown in scheme 43) was developed to circumvent these difficulties.^{110,111} In this reaction, an acetal acts as a surrogate for the acyloxy group during the radical cyclization. Afterward, a Jones oxidation reveals the lactone. This reaction has been used to great effect in several natural product syntheses including approaches to prostaglandins¹¹² and magellanine.¹¹³



Scheme 43. The Stork–Ueno radical lactonization method

Alternatively, by shifting the homolytic carbon by one more position, lactonizations may be accomplished through oxyacyl radicals (as in example **E** in figure 27). Barton was the first to note the synthetic potential of this radical species;¹¹⁴ however, it was Bachi who pioneered the chemistry.¹¹⁵ Using selenocarbonate precursors (eg. **250** and **252** in scheme 44) and treating them with trialkyltin hydride and AIBN, Bachi showed that oxyacyl radicals will readily undergo addition to alkenes and alkynes.¹¹⁶ Since then, several alternative functional groups have been used to initiate oxyacyl radical additions: acyl halides,¹¹⁵ tellurocarbonates,¹¹⁷ *S*-alkoxycarbonyldithiocarbonates,¹¹⁸ and xanthenoic esters,¹¹⁹ for instance.



Scheme 44. Bachi's oxyacyl radical cyclization using selenocarbonate precursors

While this method of lactone synthesis has occasionally been incorporated into natural product total syntheses,^{120,121} there are several drawbacks that can limit its applicability.

The oxyacyl radical is highly reactive and so the transformation is often complicated by competing pathways; decarboxylation, for instance, is an ever-present concern. Furthermore, the radical precursors themselves are often difficult to handle or require elaborate preparative work.

Just as Barton was able to use *N*-iodoamides as a synthetic proxy for the highly unstable acyloxy radical (scheme 41) and like Stork–Ueno reaction facilitates lactonization by masking the ester and an acetal (scheme 43), xanthates represent a more tractable synthetic equivalent to the oxyacyl radical. These substrates are easily prepared and, when reacted with tin radicals, they produce a comparatively longer lived intermediate than the oxyacyl radical. (*eg.* **255** compared to **254** in figure 28). This marked difference in reactivity is partly because radicals, as inherently electron deficient species, tend to become less stable as the *s*-character of their orbital increases. Thus **254**, where the unpaired electron resides in a sp^2 hybridized orbital, is less persistent than **255**. Here, the unpaired electron enjoys a fully *p* orbital that is also sterically protected and stabilized by surrounding donor substituents. This xanthate-derived intermediate may either fragment, as in the Barton–McCombie pathway,¹¹⁴ or cyclize, producing a thionocarbonyl product that can easily be converted to a lactone under oxidative conditions.¹²² However, owing to its enhanced stability compared to **254**, when an intramolecular pathway is available, cyclization typically out-competes the deoxygenating fragmentation.

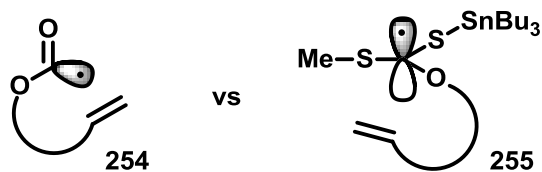
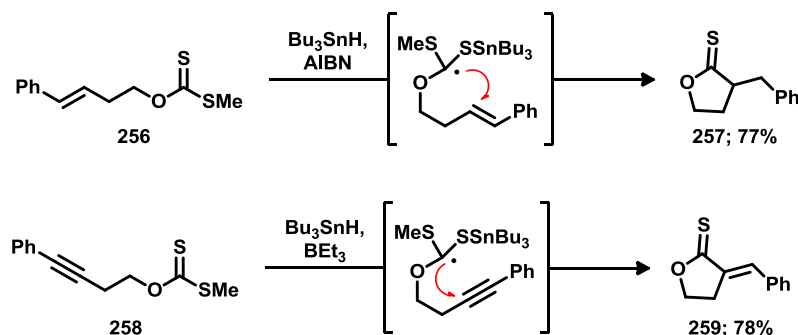


Figure 28. The oxyacyl radical compared with the xanthate derived radical intermediate in the oxygen-directed lactonization

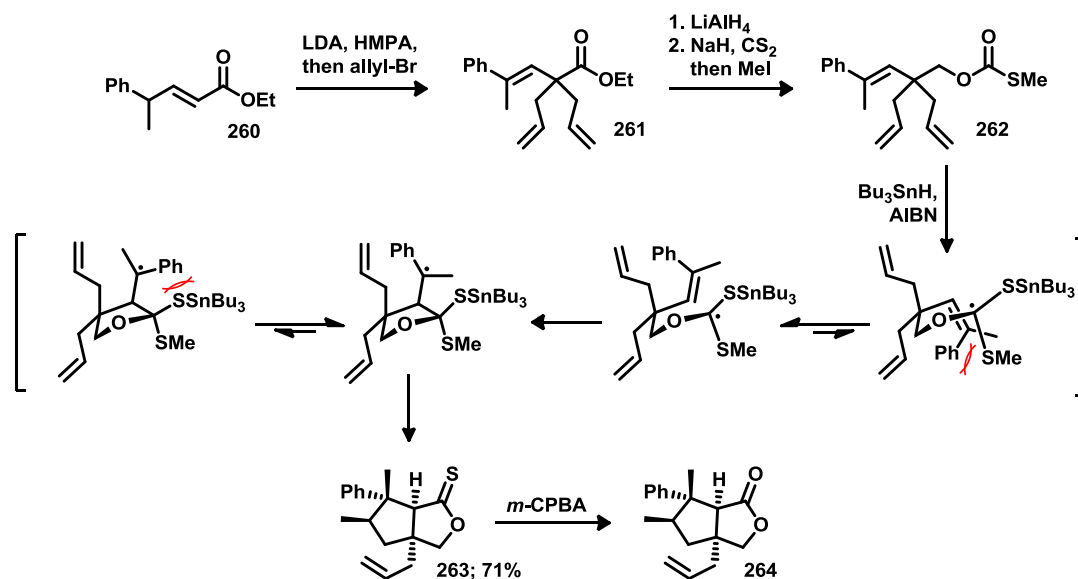
This strategy was also first explored by Bachi. When methyl xanthate **256** (shown in scheme 45) was treated with Bu_3SnH and AIBN in refluxing benzene, the thionolactone **257** was obtained in good yield.^{123,124} In fact, the reaction efficiency is comparable to the selenocarbonate based radical cyclization shown in scheme 43. Since then, there have been several contributions that have expanded this methodology. Nozaki, for instance, extended the scope of feasible substrates to include 5-*exo*-dig cyclizations onto alkynes (eg. **258** in scheme 45).¹²⁵



Scheme 45. Xanthate-based lactonizations onto alkenes (Bachi) and alkynes (Nozaki)

Yamamoto demonstrated the stereo- and regio-selective synthesis of bicyclic lactones by orchestrating a simple cascade.¹²⁶ When xanthate **262** (shown in scheme 46) was treated with tin hydride and a radical initiator, he observed the occurrence of tandem

5-*exo* cyclizations. The diastereoselectivity with which **263** was obtained appears to be under steric control as shown in scheme 46.¹²⁷ Both Yamamoto¹²² and Nozaki¹²⁵ have also provided examples of high yielding xanthate-based cyclizations of unactivated and hindered olefins.



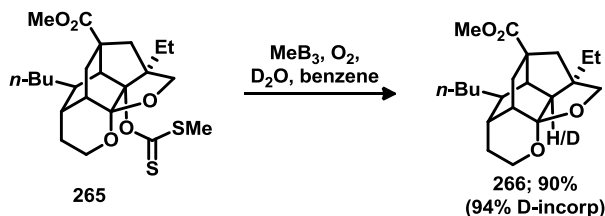
Scheme 46. Yamamoto's xanthate mediated cascade cyclization

Despite the potential usefulness of this methodology, the xanthate radical cyclization remains a largely neglected tool for lactone synthesis. Perhaps the demonstration of the scope has been too limited. Thus far, only a few monocyclic and simple bicyclic products have been prepared—examples that are easily overlooked by researchers focused on the complex architectures found among natural products. Perhaps the procedure is too involved. The initial cyclization produces thionolactone and achieving the lactone requires an additional oxidation with *m*-CPBA. Given a choice, most chemists will opt for a single step protocol. Finally, given the modern zeitgeist of environmental stewardship, perhaps researchers are less tolerant of harmful reagents. Currently, the

reaction requires a stoichiometric quantity of organotin hydride. Not only are these reagents costly and difficult to separate from desired reaction products, they are also highly toxic to humans and devastating to aquatic ecosystems. Clearly, an environmentally benign variation on this reaction would be highly desirable. The chemistry that we have developed builds on Bachi's discovery in a way that addresses all three of these important concerns. We present a simple one-pot protocol that produces complex polycyclic scaffolds resembling the cores of various natural products, all without resorting to toxic metal hydrides.

3.2 Trialkylborane and Water

It has long been known that when trialkylboranes are exposed to oxygen, alkyl radicals are produced.¹²⁸ Because this system is functional at low temperatures (down to $-78\text{ }^{\circ}\text{C}$), it is commonly used in place of AIBN or peroxides as a radical initiator, particularly in reactions that involve thermally unstable adducts or products. Indeed, this was the preferred initiator when Nozaki studied the room temperature radical cyclization of homopropargylic xanthates (refer to scheme 45).¹²⁵ In accordance with the prevailing orthodoxy, Nozaki used Et_3B in combination with Bu_3SnH , one of a few reagents that can provide a chain-terminating hydrogen radical. In 2005, however, Wood made the astonishing observation that water can replace metal hydrides as the hydrogen source.⁹⁵ He demonstrated this precept by modernizing the classic Barton–McCombie reaction so that the only reagent required was trimethylborane in wet benzene (as shown in scheme 47).



Scheme 47. Wood's tin-free conditions for the Barton–McCombie reaction

This result is very counter-intuitive. The bond dissociation energy (BDE) of an O–H bond in water is 117.6 kcal/mol, suggesting that it should be stronger than the C–H bond in the reaction solvent (the BDE for the C–H bond in benzene is 113.5 kcal/mol). Nevertheless, Wood's deuterium labeling experiments convincingly show that water was indeed the hydrogen source (shown in scheme 47). By calculating the reaction enthalpies, Wood revealed that when water forms a complex with a trialkylborane species, there is a dramatic decrease in the O–H bond strength. Overall, the homolysis of the O–H bond in $\text{H}_2\text{O}-\text{Et}_3\text{B}$ was found to be 43 kcal/mol lower than the BDE predicted for uncomplexed water, making it slightly weaker than even the Sn–H bond in tributyltin hydride.^{95,129}

3.3 Potential Natural Product Targets

Our goal was to apply Wood's insights to Bachi's lactonization strategy. Having a ready supply of bicyclo[3.3.0]octene and bicyclo[3.2.0]heptane compounds conveniently available to us, we hoped to develop a tin-free protocol for converting these substrates into tricyclic scaffolds, compounds that could provide a useful entry into a large number of natural product architectures. Picrotoxinin (**267** in figure 29), for instance, is a highly potent plant-based toxin ($\text{LD}_{50} = 3 \text{ mg/kg}$); nevertheless, it is used in western medicine as

an antidote for chloral hydrate and barbiturate intoxication.¹³⁰ Likewise, the tricyclic core of sclerocitrin (**268**), a pigment molecule of the fungus known as the common dirt ball, may be accessed from a bicyclo[3.3.0]octane derivative.¹³¹ Similarly, the bicyclo[3.2.0]heptane precursor could provide an entry into the synthesis of the Caribbean octocoral isolate, bielschowskysin (**269**),¹³² currently a highly competitive target due to its unique structure and impressive bioactivity.¹³³⁻¹³⁵ Finally, one might also envision using an oxygen-directed radical cyclization on 5-norbornen-2-ol to access the challenging polycyclic domain of nanolobatolide (**270**), a compound that is currently being sought for its anti-neuro-inflammatory properties.¹³⁶

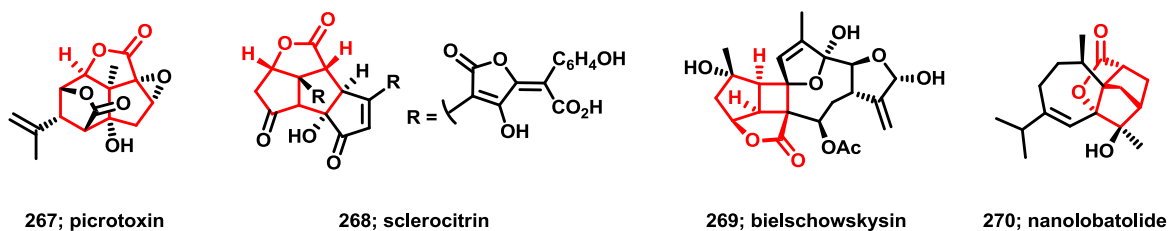
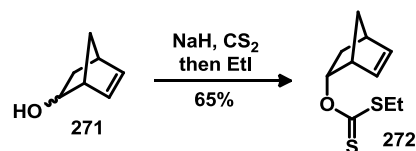


Figure 29. Natural products with lactone cores accessible through an oxygen-directed radical cyclization

3.4 Synthesis of Xanthate Precursors

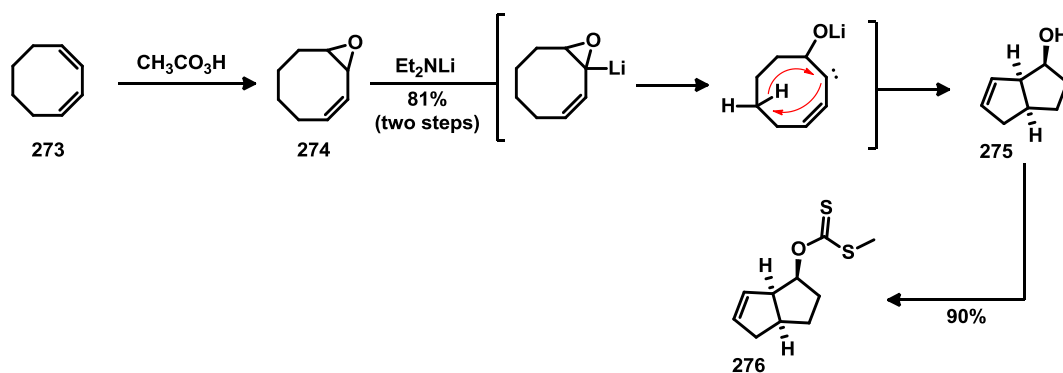
With the help of Jeremy Mason, an undergraduate laboratory assistant, we set about to test the feasibility of preparing compounds that resemble the aforementioned natural products. First, we prepared series polycyclic xanthate precursors. The 5-norbornen-2-ol based scaffold **272** was the easiest to access. The starting alcohol is commercially available, though sold as a mixture of inseparable *endo* and *exo* diastereomers. The alcohol was deprotonated with sodium hydride, and the alkoxide was trapped by carbon

disulfide. An alkylation of the resulting xanthic acid produced the desired precursor (**272** in scheme 48). Upon forming the xanthate it became possible to cleanly isolate the *endo* diastereomer.



Scheme 48. Synthesis of a lactonization precursor from 5-norbornen-2-ol

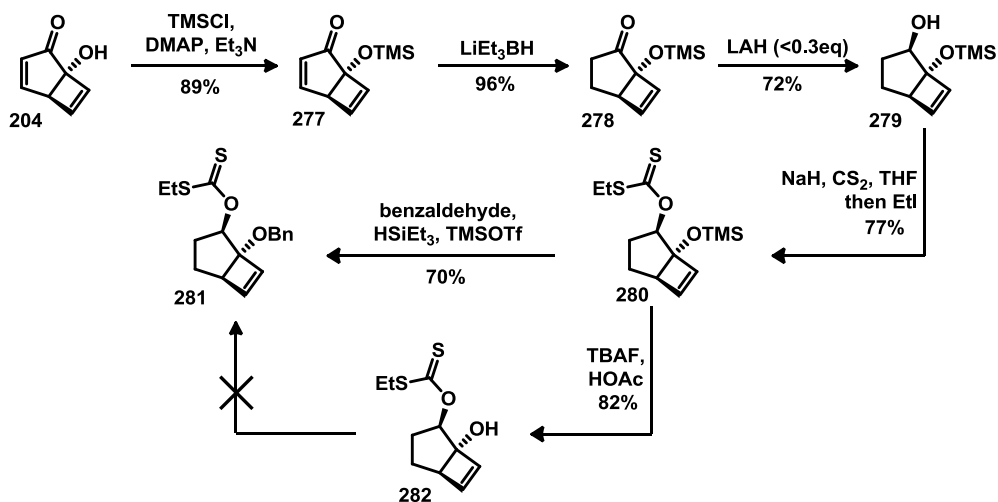
The bicyclo[3.3.0]octane scaffold (**276** in scheme 49) was accessed through the epoxidation of 1,3-cyclooctadiene. When treated with lithium diethylamide, the epoxide deprotonates, triggering an α -elimination and generating a carbenoid species. The carbene readily undergoes a transannular C–H insertion, providing alcohol **275**.¹³⁷⁻¹³⁹ This alcohol was transformed into a xanthate using the same conditions as above.



Scheme 49. Synthesis of a bicyclo[3.3.0]octane lactonization precursor (**276**)

The synthesis of bicyclo[3.2.0]heptane precursors were somewhat more involved; however, much of the chemistry was very familiar (see chapter 2). We had previously accessed compound **204** through a photochemical electrocyclic rearrangement of tropolone (refer to scheme 30).⁹⁴ The free alcohol was protected with as a trimethylsilyl

ether during the subsequent conjugate reduction. A second reduction was performed on the remaining ketone, using lithium aluminum hydride to produce alcohol **279** with excellent diastereoselectivity. As before, this alcohol was converted to xanthate **281**.



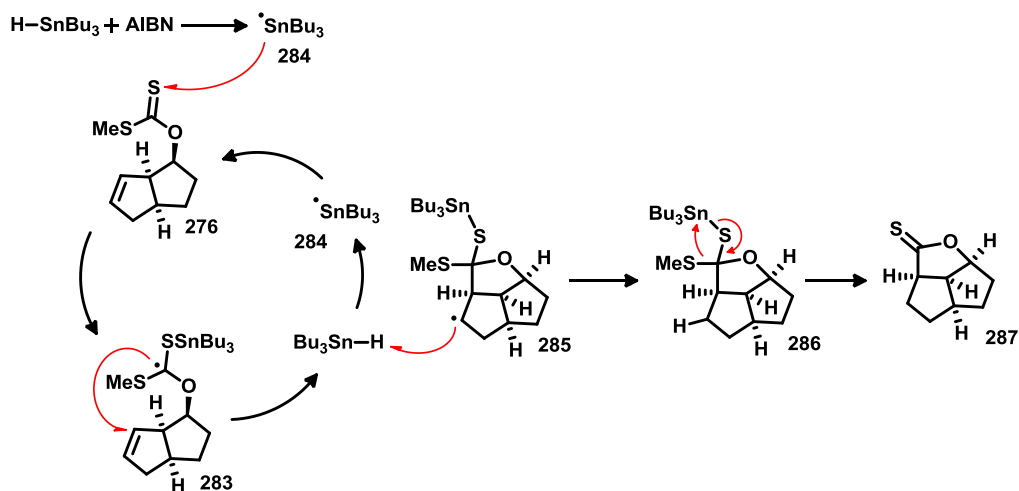
Scheme 50. Synthesis of a bicyclo[3.2.0]heptane lactonization precursor (**281**)

After installing the dithiocarbonate functional group, we found that the labile nature of the TMS protecting group had become problematic, as desilylation was accompanied by decomposition. We sought a more robust alternative. The exchange, however, proved somewhat challenging since alkoxide intermediates had a tendency to react with the neighbouring xanthate functional group. Ultimately, we found that deprotection of the silyl ether could only be accomplished with TBAF buffered in acetic acid (shown in scheme 49). Attempted methylations, allylations, and benzylation of the resulting hydroxyl group that employed basic conditions were likewise inevitably low yielding and fraught with unwanted products. Eventually we found an effective method for directly substituting the silyl ether functional group with a benzyl ether. The substrate, **280**, underwent a TMSOTf catalyzed acetalization with benzaldehyde followed by an *in situ*

trialkylsilane-reduction.¹⁴⁰ Thus, we were able to turn the highly sensitive molecule **280** into a robust substrate (**281**), suitable for testing our radical cyclization.

3.5 Radical Cyclizations

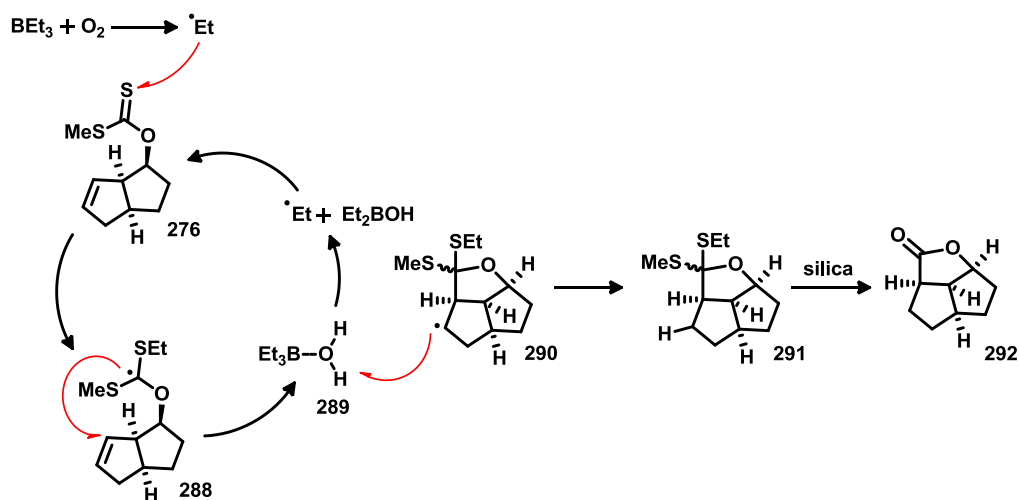
As a confirmation of the antecedent chemistry, we attempted the cyclization of **276** under Bachi's tin radical conditions.¹²³ Consistent with earlier observations, we obtained 73% of thionolactone **287** (entry 1 in table 3), a respectable yield for a reaction involving an unactivated olefin. The mechanism proposed by Bachi suggests that the tributyltin radical (**284**) adds to the thiono sulfur atom of the dithiocarbonate **276**. The adduct is a highly stabilized radical, sufficiently persistent to undergo a 5-*exo*-trig cyclization onto the double bond rather than fragmenting *as per* the Barton–McCombie reaction. The resulting intermediate, **285**, abstracts a hydrogen atom from tin hydride, propagating the chain reaction while producing the ortho thionolactone **286**. However, this compound is an ephemeral species, rapidly eliminating methyl tributylstannyl sulfide to produce the final product, thionolactone **287**.¹²⁴



Scheme 51. The proposed mechanism for the Bachi-type oxygen-directed radical lactonization

We then attempted the cyclization under tin-free conditions adapted from Wood's paper.⁹⁵ The same substrate (**276**) was dissolved in undried, though thoroughly degassed, benzene and triethylborane was added as a solution in THF. Air was then slowly introduced over the course of several hours using a syringe pump with an "empty" 60 mL syringe. As illustrated in scheme 52, air oxidation of the trialkylborane is believed to liberate ethyl radicals and, as before, these radicals appear to add to the thiono sulfur of the xanthate, prompting the same 5-exo-trig cyclization.^{95,141} The intermediate species, **290**, is then reduced by the $\text{H}_2\text{O}\cdot\text{BEt}_3$ complex (**289**) while liberating dialkyl borinic acid and an additional ethyl radical capable of propagating the chain reaction. By forgoing the customary aqueous workup and directly evaporating the reaction mixture, we observed dithiooester **291** in the crude residue as a mixture of diastereomers. Unlike compound **286**, which rapidly reverts to the thionolactone, the dithiooester (**291**) was found to hydrolyze to the corresponding lactone either gradually on the bench-top or rapidly under chromatographic conditions. Consequently, these intermediates could not be isolated effectively; instead, we found it convenient to expedite the hydrolysis in a controlled manner by stirring the crude residue in a solution of aqueous CaCO_3 and I_2 in tetrahydrofuran.¹⁴²

Ultimately, the desired lactone was isolated in 72% yield following purification (entry 2 in table 2). Thus, the cyclization appears to be at least as efficient as the pre-existing methodology. Bachi's approach, however, produces the thiocarbonyl instead of the lactone. While the conversion of thionolactones to lactones is well-known, this is now a superfluous synthetic step given our tin-free protocol.



Scheme 52. The proposed mechanism for the tin-free oxygen-directed radical lactonization

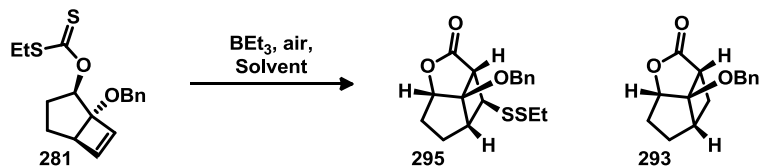
Entry	Substrate	Conditions	Product	Yield
1	 276	Ph_3SnH , AIBN, benzene, Δ	 287	73%
2	 276	Et_3B , Air, wet benzene then I_2 and CaCO_3 in wet THF	 292	72%
3	 281	Et_3B , Air, wet benzene then I_2 and CaCO_3 in wet THF	 293	51%
4	 272	Et_3B , Air, wet MeCN then I_2	 294	55%

Table 2. Xanthate-mediated radical lactonizations producing an assortment of compounds resembling natural product cores

When the same conditions were applied to the bicyclo[3.2.0]heptane precursor, **281**, the bielschowskysin-like tricyclic architecture (**293**, entry 3 in table 3) was obtained in 51% yield. Similarly, 5-norbornen-2-ol derived xanthate (**272**) produced the polycyclic nanolobatolide core in 55% yield (**294**, entry 4 in table 2).

Frequently, particularly when performing cyclizations in benzene, we observed an unexpected by-product which was eventually identified as the disulfide **295** (see table 3). The product likely arises when the radical intermediate (*eg.* **290** in scheme 52) terminates by reacting with a second xanthate rather than by abstracting a hydrogen atom from the triethylborane–water complex. The oxidation of the sulfur to a disulfide may be facilitated by iodine during the hydrolytic step.

With the hope of simplifying the purification and improving the yield, we performed some optimization of the cyclization conditions. We reasoned that the unwanted product (**295**) was emerging due to the relative unavailability of the hydrogen atom source. Thus, we attempted to modify the conditions to remedy this perceived problem. For instance, we were curious about whether or not chloroform could serve the dual function of solvent and an abundant hydrogen atom donor.¹⁴³ Unfortunately, reactions performed in chloroform were found to cause significant degradation to the substrate and / or the product (entry 2 in table 3). We also found that when we rapidly saturated the solvent with pure oxygen, rather than introducing air gradually, we shut down the reaction entirely (entry 4 in table 3). Presumably the triethylborane was being degraded before it could even react with the substrate.



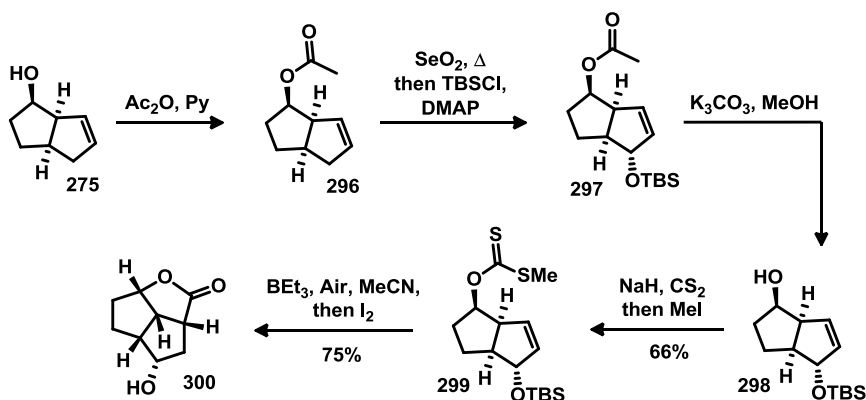
Entry	Solvent	Yield of 295	Yield of 293
1	wet benzene	16%	51%
2	chloroform	decomposition	
3	benzene / methanol	14%	43%
4	wet benzene saturated with O ₂	starting material	
5	tetrahydrofuran	decomposition	
6	acetonitrile	0%	69%

Table 3. Solvent optimization of the Xanthate-mediated radical lactonization

Thinking that perhaps the low solubility of water in benzene may be forestalling hydrogen abstraction, we substituted water for benzene-miscible methanol. This time, the desired lactone was observed, suggesting that diminishment of the O–H BDE also applies to the MeOH•BEt₃ complex; however, this modification did not greatly affect the product distribution (entry 3 in table 3). We also tried the opposite tact—rather than increasing the solubility of the hydrogen source by making it less polar and more accommodating to benzene, we attempted to make the solvent compatible with water. We found that THF was a poor solvent choice, leading to severe decomposition of the substrates and the solvent itself (entry 5 in table 3). Acetonitrile, on the other hand, completely suppressed the formation of the unwanted disulfide. When compound **281** was cyclized in this water solubilizing solvent, we observed an increase in the the yield of lactone **293** from 51 to 69% (entry 1 and entry 6 in table 3).

Thus, we have demonstrated that the increased rigidity of the bicyclo[3.2.0]heptane precursor compared to the bicyclo[3.3.0]octane version is not a barrier to efficient lactonization. We have also proven that the reaction conditions will tolerate a benzyl

protecting group. However, we were curious about the compatibility of another other key alcohol protecting strategy, silyl ethers. To this end, we prepared compound **297** through a selenium dioxide mediated allylic oxidation reaction followed by conversion to the *t*-butyldimethylsilyl ether. We found that while this substrate also cyclized effectively, the TBS group was lost under the reaction conditions. Thus, we obtained the free alcohol (**300**) in 75% yield.

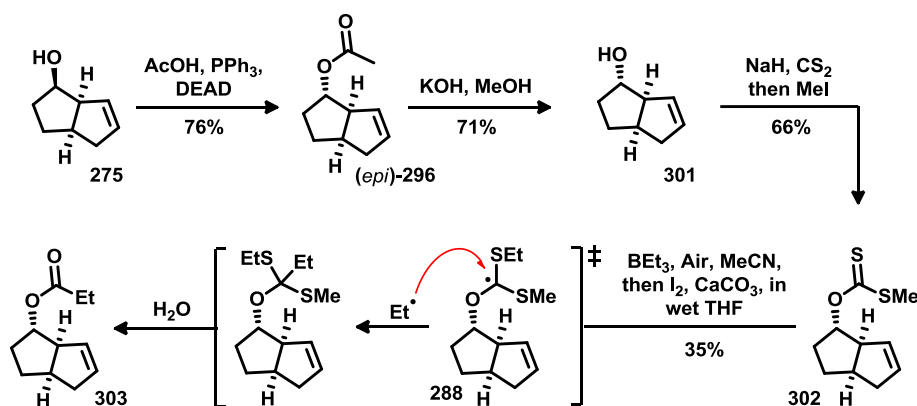


Scheme 53. Synthesis and xanthate-mediated radical lactonization of a silyl-protected precursor (**298**).

Radical reactions are often useful for introducing strained bonds into a structure. We were curious to see if we could stretch the chemistry, applying it to a strained isomer of compound **275** or if alternate pathways, like the Barton–McCombie fragmentation, would then become competitive. To position the xanthate group farther away from the alkene acceptor we used a Mitsunobu reaction to invert the secondary alcohol prior to xanthate formation (see scheme 54).

Our standard reaction conditions, however, did not result in any lactonized product. Instead, we were surprised to observe a 35% yield of propionate **303**. We hypothesize

that this compound arises from ethyl radical intercepting intermediate **288** (as shown in scheme 54). The hydrolytic loss of the two sulfur substituents converts the thioacetal to an ester. Presumably, the remainder of the substrate was deoxygenated and the volatile aliphatic product subsequently lost to evaporation following workup. However, it is a testament to the stability of the radical species **288** that when a viable intramolecular cyclization pathway is unavailable, intermolecular quenching is competitive with the fragmentation pathway.



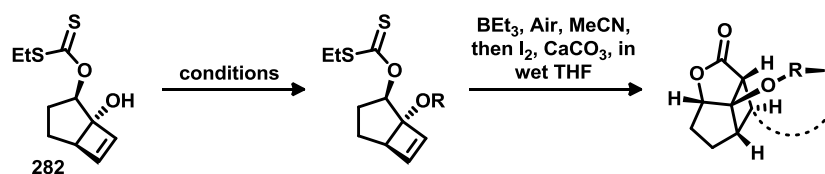
Scheme 54. Synthesis and attempted xanthate-mediated radical lactonization of a strained precursor.

The rate at which the radical intermediate is quenched is of particular interest as this will dictate the likelihood of success in radical cascade reactions. With a standard tin-mediated mechanism it is often possible to favor an intramolecular process through the slow addition of the tin hydride reagent. Analogous strategies for the tin-free system do not yet exist; indeed, it was uncertain whether they would be necessary.

3.6 Attempted Lactonization Cascades

We aimed to evaluate the feasibility of extended cascades using our bicyclo[3.2.0]heptane precursor. The tertiary alcohol provided us with a convenient handle for tethering alkenes onto the bicyclic core. For instance, a nucleophilic addition of compound **283** onto senecieryl chloride was intended to provide dimethyl acrylate **306** (refer to table 4.), a possible substrate for a 6-*exo*-trig or 7-*endo*-trig cyclization. We observed, however, that the double bond had been shifted out of conjugation with the carbonyl, resulting in a good yield of terminal alkene **305**. While we found that the olefin could be easily re-conjugated to the ester by treatment with DBU, we also recognized the potential to extend the lactonization with a 7-*exo*-trig or 8-*endo*-trig cyclization. Finally, we synthesized vinyl ether **304** using a phosphine-mediated conjugate addition to methyl propiolate^{144,145} in order to test the feasibility of a 5-*exo*-trig or 6-*endo*-trig cyclization.

Benzene was selected as the reaction solvent over acetonitrile. The logic that guided our earlier optimization suggested benzene could forestall hydrogen abstraction which would prematurely terminate the cascade. When subjected to our conditions, each of these substrates underwent a lactonization event; however, the extended cascades failed despite there being several favored pathways available (see table 4).



Entry	Conditions	Xanthate Product	Xanthate Yield	Cascade Product	Lactone Yield
1	methyl propiolate, PMe ₃	 304	72%	 307	52%
2	seneciocl chloride, Et ₃ N, DMAP	 305	69%	 308	42%
3	same as entry 2, then DBU	 306	68%	 309	47%
4	See scheme 35	 219	see scheme 35	 220	25%

Table 4. Synthesis and xanthate-mediated radical lactonization trained precursors with potential cascade pathways

This disappointing result contrasts with the analogous substrate **219** (entry 4 in table 4), bearing an allylsilane functional group, which did cyclize through an apparent 8-*endo*-trig process. It is possible that we are able to access this architecturally impressive product (**220**) only because of the silicon atom's ability to stabilize the intermediate β -radical through a mechanism analogous to the well-known β -silicon effect on carbocations. This

more accommodating tether possibly enhanced the rate of cyclization compared to the other substrates.

Our aim was to develop a tin-free radical lactonization suitable for making polycyclic structures that are relevant to natural product synthesis. We hoped to build on Bachi's concept—that the xanthate functional group could serve an oxyacyl radical stand-in—while also modernizing the approach by applying Wood's discovery that the $\text{H}_2\text{O}-\text{BEt}_3$ complex is a viable hydrogen source. Indeed, our version of the cyclization has efficiently produced the most structurally complex suite of products for which the approach has been applied. Historically stoichiometric quantities of highly toxic organotin compounds have been used to produce thionolactones. The conversion of these species to the far more synthetically relevant lactone functional group requires an additional oxidative transformation. Our contribution has been to provide an environmentally benign set of conditions capable of producing the lactones directly. Hopefully, by improving this synthetic tool, chemists will come to think of the oxygen-directed radical lactonization as a feasible alternative to the widely popular halolactonization reaction.

Chapter 4 — Nonenone Synthesis

4.1 Reevaluation of Tactics

Our investigation of xanthates as a tool for forming lactones was an interesting diversion; however, progress in our true synthetic ambition—accessing the didemnaketal core by desymmetrizing the *meso* precursor **142**—remained obstructed. The intractable deoxygenation of compound **206** (as shown in figure 30) was a barrier denying us access to the oxy-Cope precursor **144** and the resulting keystone intermediate, the nine membered carbocycle **143**. Although this troublesome ketone is absent in the final product, it was incorporated into the synthetic plan to direct crucial aspects of the early assembly. For instance, the ketone was used to facilitate the methylation of an otherwise inert carbon atom, efficiently providing us with **206**. This alkylation was highly diastereoselective because of the geometry of the [3.0.2]-bicyclic substrate (**205**), an architecture which was expediently accessed using an electrocyclic ring closure. The ketone, present in the tropolone starting material (**203**), helped to create the chromophore that enabled this photochemical transformation. However, we came to realize that we were relying on this ketone much like a crutch. Though it allowed us to rapidly develop much of the early chemistry in our synthetic plan, it ultimately became a liability, impeding our progress.

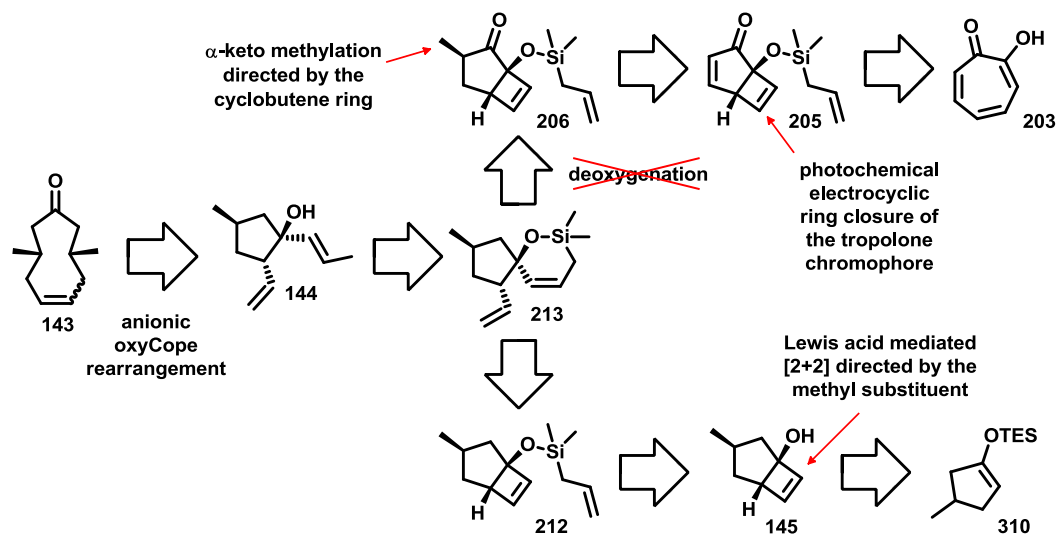
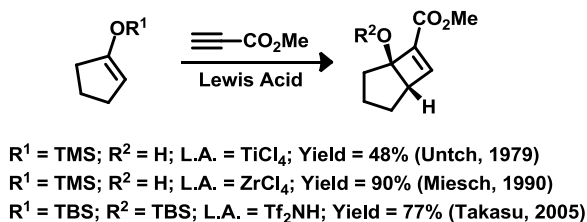


Figure 30. A retrosynthetic re-evaluation of our entry into the didemnaketal A synthesis

We needed to rethink our entry into the synthesis, eliminating our reliance on unnecessary functional groups; still, we hoped to retain much of the chemistry we had already established: namely, structural motifs, bond disconnections and optimized reaction conditions. To do so, we required an alternative route to the [3.0.2]-bicyclic alcohol **145**. We abandoned the idea of making the four-membered ring using a light-driven cyclization since this transformation typically requires an enone chromophore.¹⁴⁶ As an alternative, it is possible to access cyclobutene rings from silylenol ethers, reacting them with an electron deficient alkyne in the presence of certain Lewis acids (as shown in scheme 55). Untch provided the first example of this reaction in 1979 when he demonstrated that TiCl_4 could be used to obtain [2+2] adducts in moderate yield.¹⁴⁷ The reaction efficiency was greatly improved by Miesch, who substituted the titanium Lewis acid with ZrCl_4 ,¹⁴⁸ and then Takasu, who made the reaction catalytic using Tf_2NH .¹⁴⁹



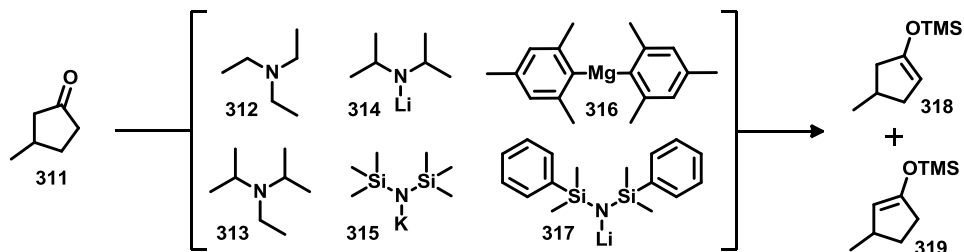
Scheme 55. Lewis acid mediated [2+2] cycloadditions

Originally, we had used the steric influence of cyclobutene ring to direct the diastereoselective installation of the methyl group (see figure 30). With this alternative route, the pre-existing methyl group on the cyclopentane ring (**310**) would have to direct the [2+2] cycloaddition. Assuming that we can access alcohol **145** in this manner, the remainder of the steps to the anionic oxy-Cope precursor (**144**) should be very straightforward. After attaching an olefin tether through the silylation of the free alcohol, a metathesis rearrangement will provide **213**, the compound that we failed synthesize through the tropolone-initiated approach. Upon cleaving the silicon atom from the spirocyclic structure, we would expect to have the oxy-Cope precursor (**144**) and thus access the nine membered intermediate **143**.

4.2 Silyl Enol Synthesis

Of course, before we could attempt any of this chemistry we required the appropriate silylenol ether. The obvious way of accessing (*eg.* **318** in table 5) is by treating commercially available 3-methyl cyclopentanone (**311**) with base then trapping the ensuing enolate with a silylchloride.¹⁵⁰ However, the transformation is complicated by

the fact that, depending on whether deprotonation occurs to the left or the right of the ketone, two regioisomers may be formed (compounds **318** and **319**).



Base	Yield	Ratio enol isomers (318:319)
312	98%	1:1
313	no reaction	n/a
314	68%	1:1
315	61%	1:1
316	decomp.	n/a
317	27%	3:2

Table 5. Attempted enolization of 3-methylcyclopentanone (**311**) using increasingly bulky bases

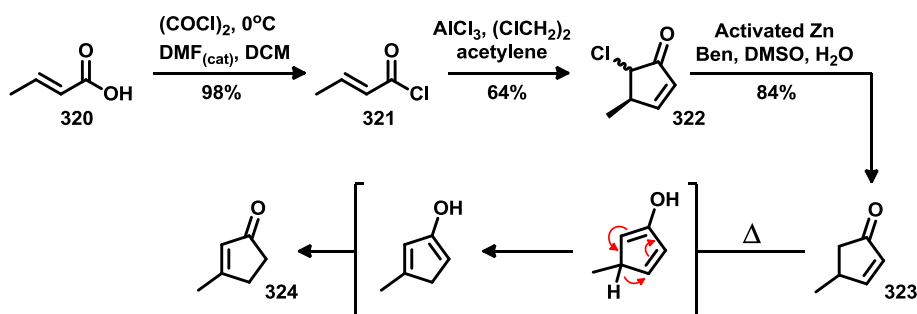
We had optimistically anticipated that the methyl side chain would exert a sufficiently large steric influence as to direct enolization to the opposite side of the ketone. Unfortunately, this proved not to be the case. Using triethyl amine with trimethylsilyl chloride, standard conditions for producing silylenol ethers,¹⁵¹ we observed excellent conversion to a 1:1 mixture of inseparable regioisomers. We proceeded to gradually increase the bulkiness of the base, hoping to encourage enolization on the less hindered side of the ketone: Hunig's base (**313**), lithium diisopropylamide (**314**), potassium hexamethyldisilazide (**315**)—increasing the size only seemed to diminish the yield without affecting the ratio of isomers. Bismesitylmagnesium (**316**) is reportedly an excellent non-nucleophilic base, capable of selectively producing silyl enol ethers in systems similar to ours.¹⁵² In our hands, however, we were unable to isolate useful

material from the reaction mixture. Finally, using Masamune's base (**317**),¹⁵³ the bulkiest reagent we could conveniently access, we obtained a 3:2 mixture of enol ethers favoring the desired regioisomer (**318**). However, this ratio was still considered to be unpragmatic and we realized we needed to consider alternative ways to access our desired precursor.

Reducing a typical non-activated alkene usually means performing a hydrogenation reaction; the olefin of an α,β -unsaturated carbonyl, on the other hand, can often be reduced by applying a suitable hydride source. For instance, we described *vide supra* the conjugate reduction of cyclopentenone **205** using LiEt_3BH (refer to scheme 31). The addition of a hydride nucleophile to the highly polarized olefin produces an enolate which we were able to exploit toward the α -methylation of ketone **206**. It occurred to us that we might be able to circumvent our selectivity issues by using a conjugate reduction and trapping the resulting enolate intermediate.

Unfortunately the requisite enone, 4-methylcyclopent-2-enone (**323** in scheme 56), was not commercially available, so we synthesized it for ourselves. Guided by the protocol developed by Smith,¹⁵⁴ acetylene was bubbled through a solution of crotonoyl chloride (**320**) in the presence of aluminum trichloride to provide the α -chloropentenone **322**. This convenient transformation occurs through a Friedel–Crafts acylation followed by an *in situ* Nazarov reaction. The conrotatory 4π -electrocyclization in the Nazarov mechanism produces a carbocation which is eventually captured by a chloride anion. Subsequently, Reformatsky-type conditions were applied for the dehalogenation of the α -chloroketone, producing the desired substrate (**323**). The purification of this volatile

ketone involved a careful vacuum distillation through a long vigreux column. Heating the compound in excess of 70 °C was found to trigger a 1,5-hydride shift, transforming the material to the useless isomer **324**. Despite this complication, we found that this sequence was amenable to scale-up and we were able to produce the desired ketone in greater than 10 g batches.

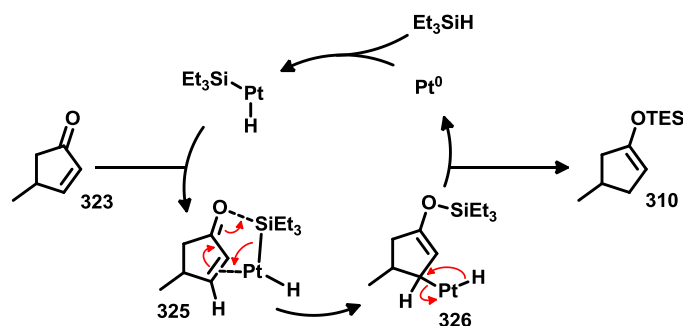


Scheme 56. Tandem Friedel–Crafts acylation / Nazarov cyclization followed by an activated Zn reduction of the resulting α -chloroketone

Similar to the formation of compound **206**, we attempted a conjugate reduction of **323** using LiEt_3BH ; however, instead of quenching the enolate with methyl iodide as before, we attempted to trap it using trimethylsilyl chloride. The olefin reduction occurred as expected but, rather than obtaining the desired silyl enol ether, we isolated only the saturated ketone (*ie.* **311** in table 5). The Birch reduction is also known to transform enones into enolates.¹⁵⁵ Unfortunately, our attempts to make use of this reaction did not yield any useful material.

Hydrosilylation chemistry provided us another avenue to explore. This reaction encompasses all catalytic addition of silanes (*ie.* Si–H) across unsaturated bonds (*eg.*

C=C, C≡C, C=O, etc.).¹⁵⁶ The catalyst is typically a transition metal—Pt, Pd, Ru, and Cu have all demonstrated efficacy—although tris(pentafluorophenyl)borane has also been used to promote the reaction.^{157,158} When a hydrosilylation reaction is applied to an α,β -unsaturated ketone, a 1,4-addition may be observed, producing a silyl enol ether. Mechanistically, the metal is believed to undergo an initial oxidative addition into the Si–H bond of the silane. The resulting intermediate forms a π -complex with the olefin (see **325** in scheme 57) in which there is also significant σ -coordination between the oxygen and the silicon atoms. The complex then rearranges with Si–metal cleavage to give **326**. Finally, a reductive elimination of the Si–C bond produces the silyl enol ether (**310**) while in the process returning the reduced metal to the catalytic cycle.¹⁵⁹



Scheme 57. The catalytic cycle for the 1,4-hydrosilylation of an enone, producing a silyl enol ether (eg. **310**)

In establishing suitable reaction conditions, we selected triethylsilane for its low cost and because the resulting silyl enol ether would be sufficiently robust to permit purification by column chromatography, yet easily removable following the [2+2] cycloaddition. Ideally, we would have performed the hydrosilylation using dimethylallyl silane as this could potentially eliminate a step from our synthesis; however, we suspected that the terminal alkene would compete with the enone in the hydrosilylation

reaction and that it may not withstand the Lewis acidic condition used in the subsequent cycloaddition.

We had four known hydrosilylation catalysts conveniently available to us: tris(pentafluorophenyl)boron (**327**),¹⁵⁸ Grubbs' 1st generation catalyst (**328**),^{160,161} Wilkinson's catalyst (**329**),¹⁶² and Karstedt's catalyst (**330**).¹⁶³

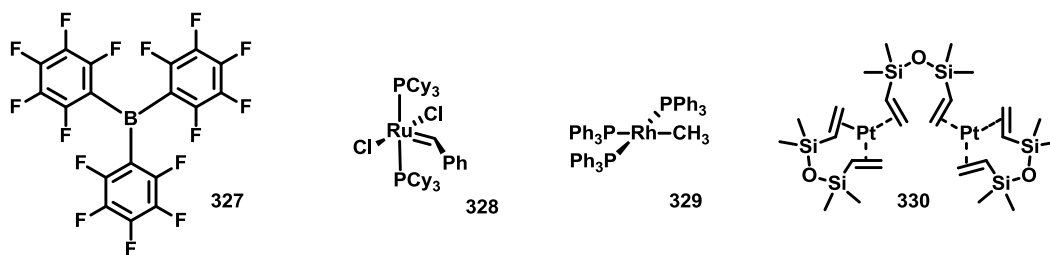


Figure 31. Commonly used hydrosilylation catalysts

In our hands, neither Grubbs' catalyst nor $B(C_6F_5)_3$ produced the desired silyl enol ether. While the former catalyst failed to convert the starting material, the latter appeared to have promoted a 1,2 addition of triethylsilane across the ketone. Fortunately both Wilkinson's (**329**) and Karstedt's (**320**) catalysts showed more promising results. The reaction catalyzed by $RhCl(PPh_3)_3$ was found to be very sluggish, giving a low conversion even after several days in refluxing benzene. When the hydrosilylation was performed using a scientific microwave, superheating the benzene to 140 °C over the course of 90 min, the conversion of starting material did not improve. However, we did achieve good conversion by conventionally heating the reaction to 110 °C within a high pressure reaction vessel.

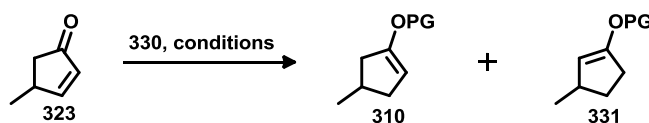
Karstead's catalyst, on the other hand, was found to perform rapidly and effectively at room temperature with minute catalyst loadings. Only a single drop of the commercially available catalyst solution (2% Pt in xylenes) was needed per 100 mg of ketone. After an initial refractory period lasting anywhere between 30 sec to 10 min, we observed a sudden exothermic reaction and a dramatic colour change—a signal that the reaction was complete.

We had originally pursued the hydrosilylation tactic in order to avoid forming enol regioisomers (*eg.* **318** and **319** in table 5). It was, therefore, aggravating to discover that both the Wilkinson's and the Karstead's catalysts were producing equimolar mixtures of these very same isomers.

Using the highly active Pt catalyst (**330** in figure 31), we attempted to vary some of the other reaction parameters in an attempt to gain control over the product distribution. The reaction solvent appeared to exert some influence, though the trends were difficult to rationalize. We found that using dichloromethane or benzene offered little selectivity (entry 1 and 2 in table 6), whereas the polar aprotic acetonitrile provided a moderate improvement (entry 4 in table 6). These gains were diminished when we substituted the polar ethereal solvent, THF (entry 3 in table 6), and yet we observed a dramatic increase in the desired product while using the less polar solvent, diethyl ether (entry 5 in table 6).

We also investigated whether the product distribution correlated with the steric size of the silane. Increasing the bulkiness of the substituents from triethyl- to dimethylphenyl-

and diphenylmethyl silane did not seem to greatly affect the outcome (entries 6, 7, and 8, respectively in table 6). However, our bulkiest reagent, triisopropyl silane, appeared to have a salient influence, favouring the desired isomer in 84:16 ratio (entry 9 in table 6). Unfortunately, owing to the hindered nature of the silane, the reaction took eight days to reach completion.



Entry	Silane	Solvent	Ratio enol isomers (310 : 331)
1	Et ₃ SiH	CH ₂ Cl ₂	51 : 49
2	Et ₃ SiH	Toluene	56 : 44
3	Et ₃ SiH	THF	66 : 34
4	Et ₃ SiH	MeCN	76 : 24
5	Et ₃ SiH	Et ₂ O	82 : 18
6	Et ₃ SiH	Neat	50 : 50
7	Me ₂ PhSiH	Neat	56 : 44
8	Ph ₂ MeSiH	Neat	54 : 46
9	<i>i</i> Pr ₃ SiH	Neat	84 : 16
10	Et ₃ SiH	neat with NaHCO ₃	46 : 44
11	Et ₃ SiH	CH ₂ Cl ₂ with Et ₃ N (1.5 eq)	99 : 1 (after 8 h)
12	Et ₃ SiH	neat with Et ₃ N (10 mol%)	97 : 3 (20 min)

Table 6. The optimization of hydrosilylation conditions aimed at eliminating enol isomerization

In his seminal paper on the synthesis and utility of silyl enol ethers, Stork reported observing similar isomerizations and he suggested that it may be caused by trace amounts of Brønsted acid.¹⁵⁰ Several publications have since demonstrated how certain protic acids can isomerize a kinetic enolate into their thermodynamically more stable isomer.^{164,165} We began to suspect that that our irksome isomerization might be due to the accidental presence of a trace of acid. Perhaps the acid was being introduced as an impurity in one of the starting materials or it may be accumulating during the reaction

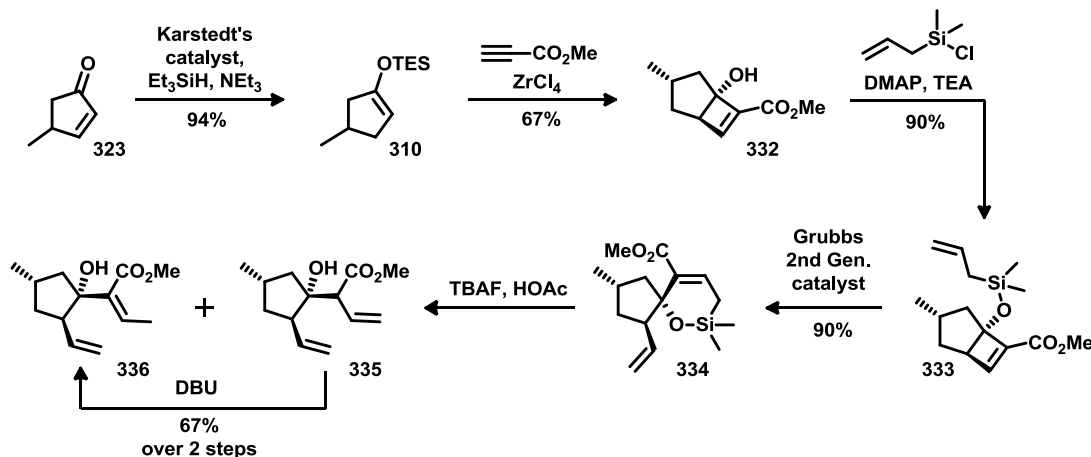
through some off-cycle process. To ensure against these possibilities, we incorporated a mild base to the reaction mixture. While the heterogeneous additive, sodium bicarbonate, had little effect (entry 10 in table 6), we found that the presence of triethylamine virtually eliminated the unwanted isomerization. Using 10 mol % of the basic additive was sufficient as larger quantities of triethylamine seemed to impede the catalyst (entries 11 and 12 in table 6).

4.3 Anionic Oxy-Cope

With compound **310** now readily available as a single isomer, we were able to attempt the Lewis acid mediated [2+2] cycloaddition developed by Miesch^{148,166} and similarly applied by Snapper.⁸⁸ We found that obtaining a good yield for this transformation depended strongly on the quality of ZrCl₄ reagent. Thus, commercial-grade ZrCl₄ was freshly sublimed before it was solubilized in dichloromethane using sonication and by adding diethyl ether as a coordinating co-solvent. Methyl propiolate and the silyl enol ether **310** were then added sequentially, causing the pale yellow solution to immediately turn dark red. After several minutes the reaction was quenched with dilute HCl overnight. The acidic treatment ensured the complete hydrolysis of the triethylsilyl protecting group. These conditions provided us with the [2.0.3] bicyclic alcohol **332** as a single diastereomer in 69% yield.

As before, we were able to tether an alkene onto the cyclic framework by reacting the alcohol with allylchlorodimethylsilane to give **333**. This straightforward and high yielding reaction would provide us with a convenient means of regioselectively installing

a carbon atom onto one of the alkene branches. Ultimately, this addition engenders one of the two *syn*-methyl substituents in the cyclononenone intermediate **143**.



Scheme 58. The synthesis of our anionic oxy-Cope precursor (**246**)

The [2.0.3] diene **333** reacted smoothly with the Grubbs 2nd generation catalyst, causing a structural rearrangement that provided the spirocyclic product **334** (as seen in scheme 58). Our next task was to excise the silicon atom. The methyl ester functional group of compound **334**, an unavoidable relic from the zirconium mediated [2+2] cycloaddition, happened to be conveniently positioned to facilitate the protodesilylation of the C–Si bond which provided our anionic oxy-Cope substrate **336**. We found that conditions involving basic fluoride anions (*eg.* KF, KHCO₃ and TBAF in THF) resulted in an assortment of unwanted product stemming from the elimination of the tertiary alcohol. However, when the basicity of tetrabutylammonium fluoride was mitigated using acetic acid as the solvent, the deleterious elimination was suppressed. Curiously, these conditions tended to move the olefin out of conjugation with the ester (see **335**). By treating the crude residue with DBU, we easily migrated the double bond, a

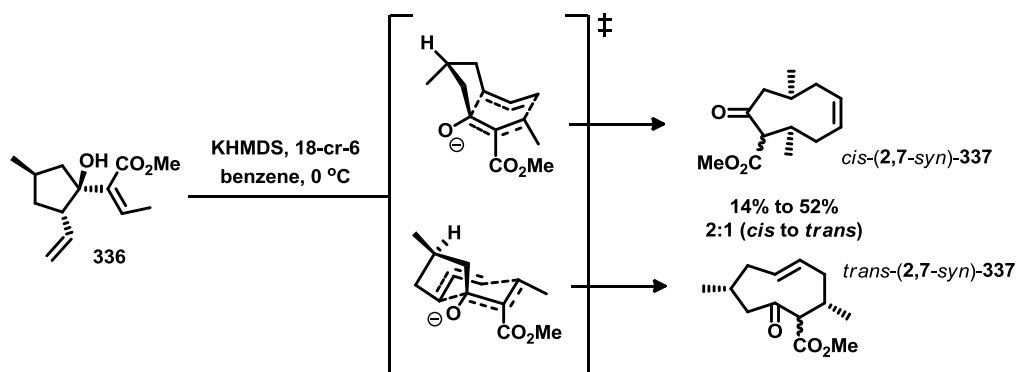
transformation which fortunately provided the *Z*-isomer as the exclusive product in 67% yield over both steps.

Our original plan was to follow Snapper's lead⁸⁸ in applying a low-temperature anionic oxy-Cope reaction to **336**, affording us our key cyclononenone intermediate. We anticipated that *cis*-(2,7-*syn*)-**337** would predominate through the boat-shaped transition state in which the oxygen anion occupies the thermodynamically favored pseudo-equatorial position. The isomer, *trans*-(2,7-*syn*)-**337** (refer to scheme 59), was expected as the minor product while the unwanted (2,7-*anti*) diastereomers would likely be excluded.

Often the outcome of the anionic oxy-Cope reaction is highly base dependent. Typical reaction conditions also incorporate additives (*e.g.* 18-crown-6, DMF, HMPA, *etc.*) to sequester the cationic counter-ion. The greater the charge separation experienced by the alkoxide anion, the greater the kinetic acceleration to the rearrangement.¹⁶⁷

Accordingly, we investigated an assortment of bases, quickly identifying several incompatible conditions. The use of potassium hydroxide, for instance, merely saponified the ester—a result we would have been satisfied with had it also accomplished the desired [3,3]-sigmatropic rearrangement. Unfortunately, it did not. Likewise, we isolated only starting material when sodium methoxide was used as the base. Both sodium and potassium hydride produced complex mixtures despite our attempts to sequester the potassium cation with DMF or 18-crown-6. We even tried potassium metal alongside

18-crown-6 ether, conditions which inadvertently led to the blue coloured solution that is characteristic of solvated electrons.¹⁶⁸ Not surprisingly, we again failed to isolate useful material.



Scheme 59. Ring expanding anionic oxy-Cope reaction to make a mixture of *cis*- and *trans*-**247**, key intermediates in our didemnaketol synthesis

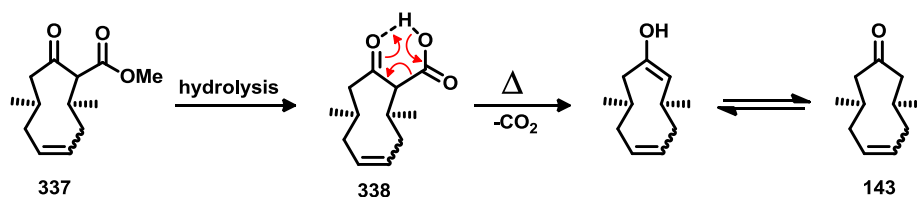
Through this process of trial and error, we found that KHMDS used with 18-crown-6 ether provided the most suitable conditions for accomplishing the low temperature anionic oxy-Cope rearrangement of compound **336**. We typically observed approximately a 2:1 mixture of *cis* and *trans* cyclononones with the desired pro-*meso* stereochemistry correctly established in both products. The favouring of the *cis*-(2,7-syn)-**337** product is consistent with Snapper's model which indicated that the lowest energy transition state is the *O*-equatorial boat.⁸⁸

While we were satisfied with the nature of the transformation, we struggled with the efficiency and reproducibility of the reaction. Upon increasing the scale, we found the yields became highly variable, depending perhaps on the quality of the KHMDS reagent or the dryness of the solvent and the crown ether. However, even with rigorously dried

benzene and freshly distilled 18-crown-6 ether, the yield of isolated cyclononenone products would often range from 14% to 52%.

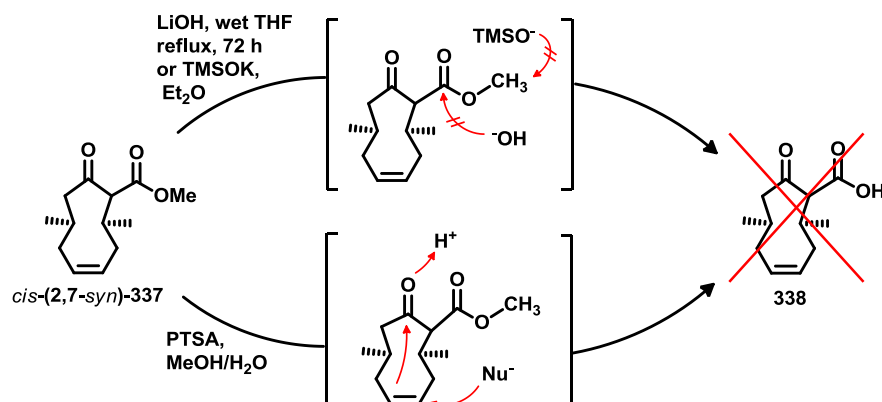
4.4 Enigmatic Decarboxylation

Nevertheless, with compound **337** in hand, we anticipated that the subsequent transformation, the decarboxylation the β -keto ester, would be trivial by comparison. Typically, these esters can be removed through hydrolysis to the acid then by warming the substrate to facilitate the loss of CO_2 through 6-membered transition state as shown in scheme 60. Unfortunately, we found that this simple transformation was fraught with even more difficulty.



Scheme 60. Mechanism for a standard decarboxylation of an β -keto ester

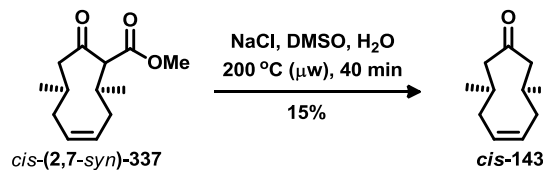
We discovered that the major product of our anionic oxy-Cope reaction, *cis*-(2,7-*syn*)-**337**, was remarkably robust toward hydrolysis. Conditions that involve either a nucleophilic attack on the ester (by a hydroxide anion, for instance) or an $\text{S}_{\text{N}}2$ type attack on the methyl ester (as with the mechanism associated with trimethylsilylanolate)¹⁶⁹—both returned starting material until heated to the point of decomposition. Acid hydrolysis was equally ineffective as the nine-membered enone had a tendency to undergo transannular Prins-type reactions (see scheme 61).



Scheme 61. Attempted hydrolysis of *cis*-(2,7-*syn*)-**337** under acidic and basic conditions

We had minor success in applying Krapcho conditions. This reaction is a one-pot decarboxylation in which the ester is refluxed with a salt (*eg.* KCN, LiCl, NaCl, *etc.*) in a wet, polar aprotic, high-boiling solvent (*eg.* DMF, DMSO).¹⁷⁰ Conventionally heating the substrate with LiCl in DMSO failed to provide the desired product; however, when we used a scientific microwave to warm *cis*-(2,7-*syn*)-**337** with NaCl in DMSO to 200 °C, we were able to isolate small quantities of the desired decarboxylated cyclononone (see scheme 62). The fact that the decarboxylation requires an elevated temperature and produces a ketone that is highly volatile likely contributed to the low yield.

Although we celebrated the fact that we had finally synthesized this keystone intermediate *en route* to the natural product core, we recognized that, in using an unreliable oxy-Cope reaction and following it with a harsh, low yielding decarboxylation, progress beyond this point would be virtually impossible. We clearly had to rethink the oxy-Cope reaction.



Scheme 62. A low yielding Krapcho decarboxylation of the *cis*-(2,7-*syn*)-**337**, giving the key intermediate *meso cis*-**143**.

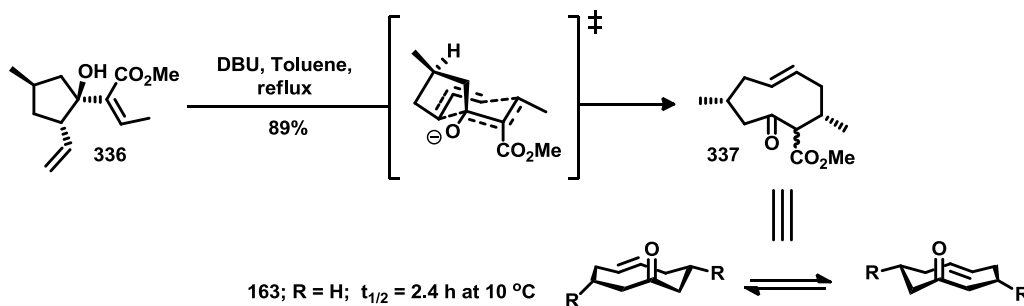
4.5 Decarboxylation Resolved

In chapter 2 of this thesis we addressed Kato's synthesis of medium sized rings using a non-anionic [3,3]-sigmatropic rearrangement.⁸⁵ This work suggested that the purely thermal oxy-Cope reaction proceeds through a chair-shaped, *O*-equatorial transition state which accounts for the *trans* geometry of the product (refer to scheme 19). As a particularly salient demonstration, when he heated the 1,2-divinylcyclopentanol substrate to 200 °C Kato obtain *trans*-**163** (shown in scheme 63) exclusively in 60% yield. Together, Snapper⁸⁸ and Kato⁸⁵ present the two extremes for approaching the oxy-Cope reaction. Full deprotonation of the alcohol with sequestering of the counter ion creates a highly reactive alkoxide species which, among other things, rearranges at low temperature. Alternatively, completely forgoing the deprotonation leaves a robust substrate that requires very high temperatures to react.

We found our optimal conditions in the middle ground between these diametrically opposed options. That is, by using a milder base, where the protonated state is likely in equilibrium with the alkoxide, we found we could exert greater control over the reaction products. However, as there is less anionic character in the oxy-Cope transition state, the

reaction temperature must increase to compensate. Thus when we performed the rearrangement under the influence of DBU in refluxing toluene—a temperature that is almost precisely midway between Snapper's bare anion approach and Kato's purely thermal conditions—we consistently observed excellent conversion of our substrate through the [3,3]-sigmatropic pathway. Interestingly, and in accordance with Kato transition state model (refer to scheme 19), we observed exclusively *trans*-(2,7-*syn*)-**337**, albeit as a mixture of diastereomers and atropisomers.

This phenomena of atropisomerism in nine-membered ring was studied by Tomooka.¹⁷¹ He estimated that the half-life for the optical activity caused by constrained bond rotation in the non-methylated cyclononenone **163** (see scheme 63) is about 2.4 h at 10 °C. Consequently, characterization of the product mixture was somewhat complicated by the number of discreet chemical entities present on the NMR timescale.



Scheme 63. DBU mediated conditions for the anionic oxy-Cope reaction producing *trans*-(2,7-*syn*)-**337** as a mixture of atropisomers and diastereomers.

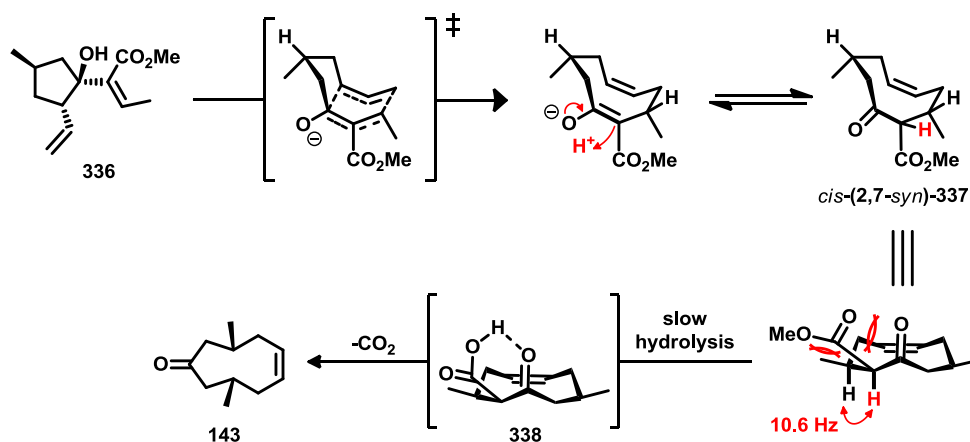
The *trans*-keto ester was found to exhibit profoundly different behavior in the hydrolysis / decarboxylation sequence compared to its geometric isomer. As discussed earlier, the hydrolysis of the ester function in *cis*-(2,7-*syn*)-**337** proceeded very slowly

even under a variety of forcing conditions (refer to scheme 61). However, the corresponding acid was never observed *en route* to the *cis* cyclononone **143**, suggesting that the decarboxylation occurs readily. By contrast, the ester group in *trans*-(2,7-*syn*)-**337** was easily hydrolyzed by stirring with potassium trimethylsilanoate in diethyl ether at room temperature. Unfortunately, the corresponding acid was highly resistant to decarboxylation, and very low conversion into *trans*-**143** was observed even after prolonged heating by either conventional or microwave methods. The seemingly complementary differences in reactivity between the two geometric isomers were as baffling as they were aggravating.

By interrogating the transition state model, we anticipated that the anionic oxy-Cope rearrangement should produce the *Z*-enolate, regardless of whether the reaction proceeds through the *O*-equatorial chair or the *O*-equatorial boat. Since the geometry of the ring obstructs one face of the enolate, there remains a single trajectory for the protonation which determines the orientation of the ester upon tautomerization to the ketone (as shown in scheme 64). Theoretically, the ester should be *syn* with respect to the methyl substituents in both the *cis* and the *trans* isomers of **337**. Admittedly, this ester is positioned on a highly epimerizable carbon and therefore the stereochemistry might not remain static; nevertheless, NMR data collected from purified samples of the major diastereomers of *cis*- and *trans*-**337** seem to confirm the prediction.

Furthermore, the lowest energy conformation of *cis*-(2,7-*syn*)-**337** can be described as an extended boat. We observed a 10.6 Hz coupling constant for the methine proton

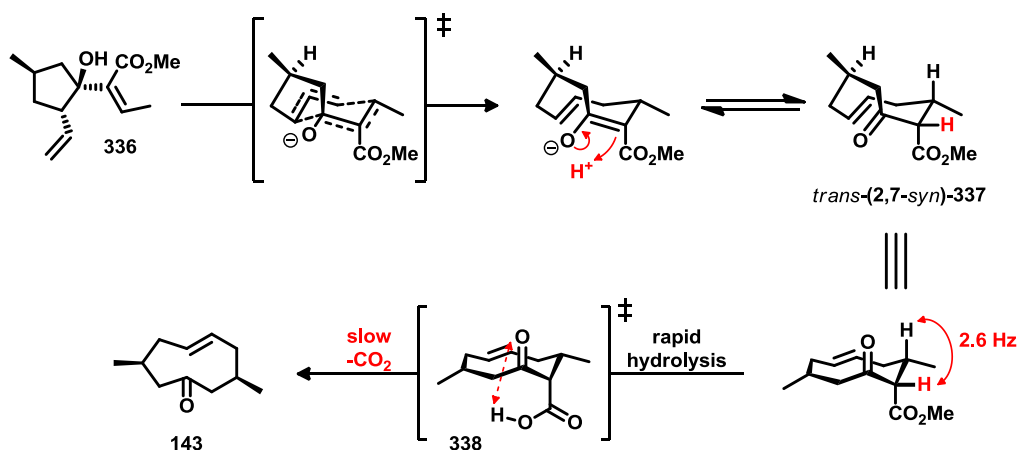
positioned between the ketone and the methyl ester (red in scheme 64). Such a large coupling constant suggests that the ester and the adjacent methyl group are both sitting in pseudo-equatorial orientations. If this assessment is correct, then the ester would be closely flanked by both the ketone and the methyl substituent. This arrangement could be sterically shielding the ester which would explain the slow rate of ester hydrolysis. However, the resulting acid would be appropriately positioned with respect to the neighbouring ketone to facilitate loss of CO₂, suggesting a rapid decarboxylation.



Scheme 64. The proposed conformation of *cis*-(2,7-*syn*)-337, accounting for the slow hydrolysis of the methyl ester.

In *trans*-(2,7-*syn*)-337, the ester is also likely to be oriented *syn* to the methyl substituents; however, to accommodate the additional strain of a *trans* double bond, this isomer probably adopts the extended chair conformation. If the two diametrical methyl groups rest in the pseudo-equatorial orientation, this conformation forces the ester into the pseudo-axial position. The 2.6 Hz coupling constant observed for proton at the α position with respect to both ketone and ester seemed to confirm this hypothesis. The ester is now directed away from the adjacent ketone and the methyl group. Being far more exposed in this orientation, we would expect the ester to hydrolyze more readily

than the *cis* counterpart. We had thought that this conformational anomaly might also explain why *trans*-(2,7-*syn*)-**337** was so slow to decarboxylate. Hydrolysis of the ester creates an acid functional group which would be pointed antiparallel with respect to the ketone. In this orientation, it would be impossible to form the 6-membered transition state which facilitates the decarboxylation of typical β -keto acids.



Scheme 65. The proposed conformation of *trans*-(2,7-*syn*)-**247**, accounting for the slow decarboxylation of the β -keto acid.

However, we were forced to rethink our interpretation of the problematic decarboxylation after obtaining a single crystal of acid *trans*-**338** and solving its structure through x-ray crystallography (shown in figure 32). The crystal structure confirms that we were indeed achieving a *syn* orientation between the methyl substituents and nicely illustrates the suspected atropisomerism. However, it also revealed that the hydrolysis conditions used on the ester were evidently epimerizing the resulting acid into the thermodynamically preferred pseudo-equatorial position. In this orientation, there is no reason why the acid should not be able to interact with the ketone and decarboxylate through a 6-membered transition state.

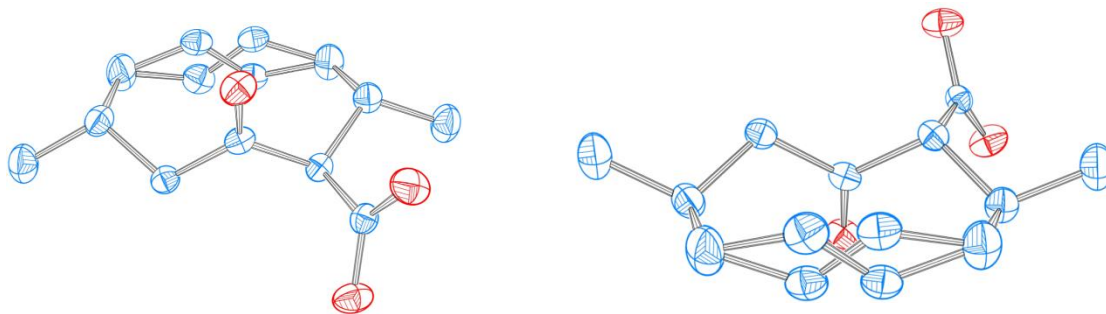
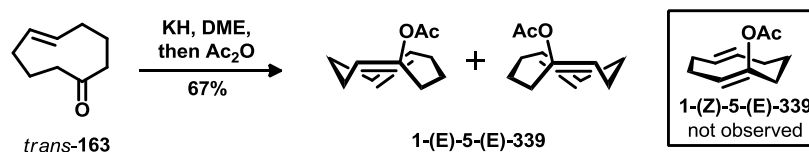


Figure 32. Crystal structure of the *trans* nine-membered cyclic ketone **338**.

With acid of *trans*-**338** now in the pseudo-equatorial position, a decarboxylation event must occur through the formation of a *Z*-enol. The fact that there is a pre-existing *trans* double bond in the ring suggests that this intermediate will be highly strained. Tomooka, while studying the stability of nonenone atropisomers, treated the non-methylated *trans*-cyclononene **163** with base and trapped the resulting enolate (shown in scheme 66). The fact that he observed exclusively 1-(*E*)-5-(*E*)-**339** seems to indicate that the 1-(*Z*)-5-(*E*)-**340** isomer may be energetically inaccessible.¹⁷¹



Scheme 66. Tomooka's enolization of *trans*-**163**, giving the less strained product, 1-(*E*)-5-(*E*)-**339** exclusively.

Furthermore, performing *ab initio* calculations on all of the relevant permutations for the double bond geometries, we found that 1-(*Z*)-5-(*E*)-**340** is the highest energy configuration (seen in table 8). The 1-(*Z*)-5(*Z*) enol through which *cis*-(2,7-*syn*)-**338** likely decarboxylates is about 17 kJ/mol lower in energy.

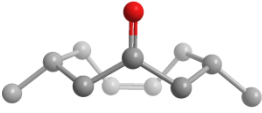
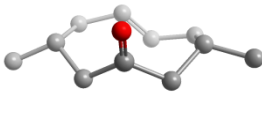
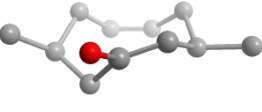
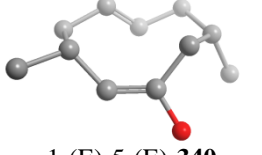
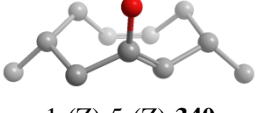
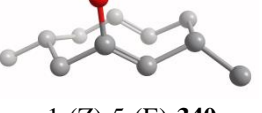
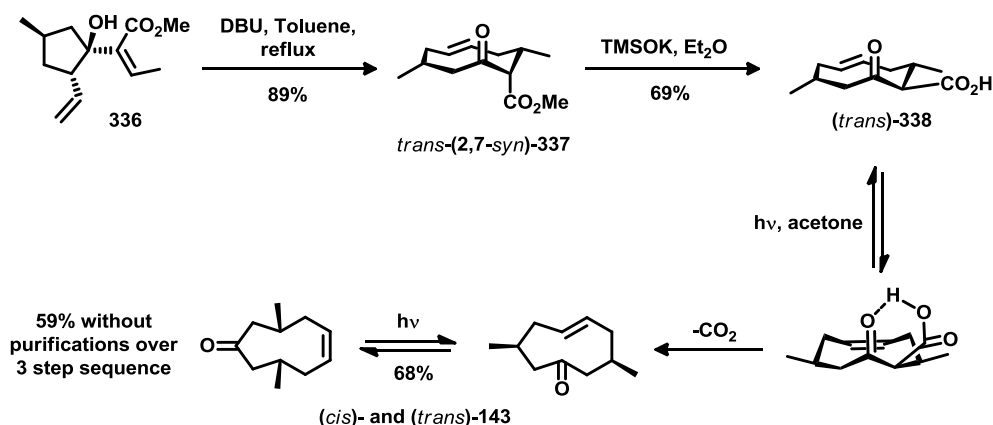
Structure	Relative Energy (kJ/mol)	Structure	Relative Energy (kJ/mol)
 <i>cis-143</i>	0.00	 <i>trans-143</i>	4.05
 1-(E)-5-(Z)- 340	65.30	 1-(E)-5-(E)- 340	88.92
 1-(Z)-5-(Z)- 340	98.65	 1-(Z)-5-(E)- 340	115.61

Table 7. Heats of formation for *cis*- and *trans*-**143**, along with their E and Z enol tautomers (**340**) calculated *ab initio* using the B3LYP 6-31 G(d) basis set.

It was by attempting to understand the structural origins of our problematic decarboxylation obstacle that we eventually arrived at an elegant solution. We simply took the readily prepared acid, *trans*-**338**, dissolved it in a sensitizing solvent, acetone, then irradiated the sample with 300 nm light, causing the alkene to isomerize. Upon converting *trans*-**338** into the lower energy *cis* isomer, the diminished ring strain permitted decarboxylation to occur readily at room temperature.

Having solved the challenges associated with the anionic oxy-Cope reaction, the ester hydrolysis, and the decarboxylation, we finally had a feasible method for transforming **336** into the nine-membered intermediate **143**. We found that it was most practical to carry out this three-step sequence without purifying the intermediate crude mixtures, most of which contain diastereomers and atropisomers that will ultimately collapse to the single *meso* compound (refer to **142** in figure 24). Hence, upon refluxing **336** with DBU

in toluene, followed by ester hydrolysis using TMSOK, and irradiation with 300 nm light, we were able to obtain a 59% overall yield of the desired product (*cis* and *trans*-**143**) as a volatile oil.



Scheme 67. Three step sequence transforming anionic oxy-Cope precursor **336** into the key intermediate **143**, isolated as an inconsequential mixture of *cis* and *trans* isomers

Although we isolated exclusively the *syn*-dimethyl isomer, the ratio of *cis* / *trans* products (**143**) varied considerably from batch to batch. It is interesting to note that the parent cyclononenone, lacking the two methyl groups (**163**), when irradiated with 300 nm light, was reported to adopt a photostationary state favoring the *trans*-isomer by a 4:1 ratio.⁸⁵ In our hands, this ratio could vary from anywhere between 5:1 favoring *cis* to 1:1.5 in which *trans* was the major isomer. Fortunately, the constitution of geometric isomers in the mixture was of no consequence, since our intended olefin metathesis step was anticipated to work with either compound. The development of this reaction and the subsequent work toward the completion of spiroketal moiety of didmentaketal A are described in following chapter.

Chapter 5 — Spiroketal

5.1 Outlook and Goals

Finally, with the crucial cyclononenone intermediate (**143** in figure 33) in hand, we felt confident of reaching our goal of assembling the spirocyclic domain of the didemnaketal A. We anticipated that we would be able to access **341** by exhaustively dihydroxylating the *meso* precursor, **142**. Performing this reaction under the influence of a chiral ligand, we intended to synchronously set all seven of the densely arranged stereogenic carbons. However, before we could encode the correct chirality, we had to ablate the preexisting stereochemical information which had accumulated during the synthesis of **143**—presently a mixture of geometric, atropic, and enantiomeric isomers. A ring opening / cross metathesis should converge 11 of the discrete isomeric constituents of compound **143** into a single, non-chiral product **142**, thereby wiping clean the stereochemical slate.

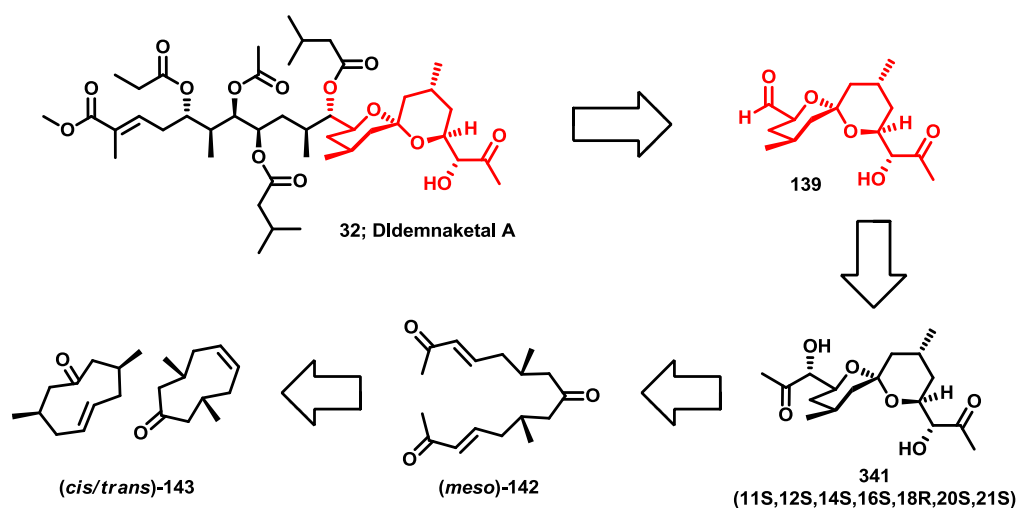
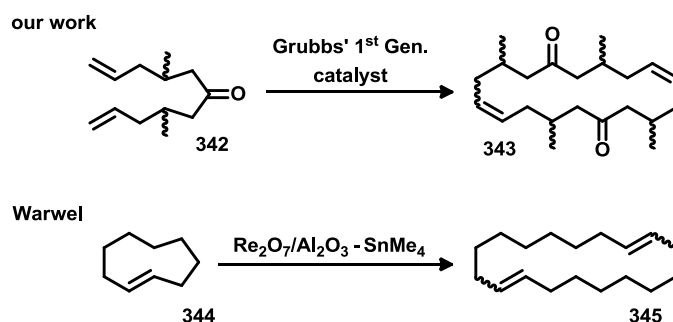


Figure 33. Our strategy for completing the synthesis of the spiroketal moiety of didemnaketal A

5.2 Ring Opening Cross Metathesis

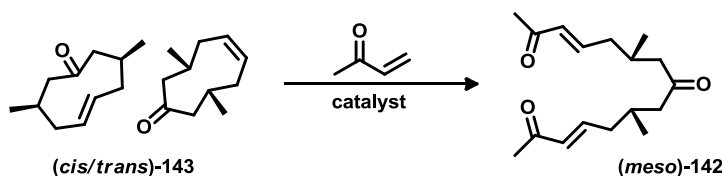
An olefin metathesis is an equilibrating reaction; the product distribution is, therefore, under thermodynamic control. We hoped to use the transannular strain inherent in *cis*- and *trans*-**143** to drive the initial ring opening step of the reaction. However, it was uncertain whether releasing this energy would be a sufficient thermodynamic incentive to ensure good conversion to the desired product. We were encouraged by the fact that the reverse reaction—the ring closing metathesis of **342**—does not appear to be an effective strategy for making nine-membered rings. We tested this reaction by preparing this linear substrate (albeit, without stereocontrol) and treating it with Grubbs' 1st generation catalyst. We observed a complex mixture of 18-membered dimeric macrocycles (eg. **343** in scheme 68), but no cyclononene products. These results were further supported by the only literature precedent that we are aware of involving the ROM of a nine-membered alkene. In 1987, Warwel treated the simple cyclononene **344** with $\text{Re}_2\text{O}_7/\text{Al}_2\text{O}_3\text{-SnMe}_4$ —metathesis conditions, predating modern Mo and Ru catalysts.¹⁷² The result was compound **345**, a mixture of 18-membered macrocycles as an assortment of *cis* and *trans* permutations, compounds that are highly analogous to the products we obtained from our linear precursor.



Scheme 68. The metathesis equilibrium appears to disfavour 9-membered rings

These observations suggested that the nine-membered ring would behave as high energy species, strongly inclined to open under thermodynamic conditions. And so we felt confident that, upon treating **143** with a metathesis catalyst in the presence of an excess of methyl vinyl ketone, we would be able to trap the linearized product **142**.

Indeed, we were pleased to find that both the *cis*- and *trans*-cyclononenones participated in the desired ROCM, affording *meso*-**142** as a single diastereomer. The reaction was initially performed using Grubbs' 2nd generation catalyst; however, acceptable yields were only achieved when applying heat with a high catalyst loading of this costly reagent. The Hoveyda–Grubbs 2nd generation catalyst is known to be more robust and performs well with electron deficient alkenes.¹⁷³ By making this switch, we were able to obtain superior yields at room temperature while cutting the catalyst loading in half. In either case, the reaction required a large excess of methyl vinyl ketone and optimal yields required this reagent to be freshly distilled after neutralizing the acidic stabilizer with bicarbonate.



Entry	Catalyst	Loading	Temp.	Yield
1	G 2 nd gen.	30%	rt	26%
2	G 2 nd gen.	30%	80°C	51%
3	H–G 2 nd gen.	15%	rt	81%
4	H–G 2 nd gen.	7%	rt	65%

Table 8. Synthesis of *meso*-**142** through the ring opening / cross metathesis of *cis* and *trans*-**143**

5.3 Asymmetric Dihydroxylations

Having thus obtained our symmetrical precursor (**142**), we were eager to attempt the critical desymmetrizing dihydroxylation; a single reaction to assemble the entire spiroketal domain of the natural product while correctly establishing all seven stereocenters. It has been known for over a century that OsO_4 reacts with olefins to give *cis* vicinal diols.¹⁷⁴ This is a robust transformation that tolerates most functional groups, yet the dihydroxylation can be sluggish when applied to sterically hindered or electron deficient olefins. Fortunately, Criegee made the important observation that this reaction is dramatically accelerated in the presence tertiary amines (*eg.* pyridine), an effect that has come to be known as ligand accelerated catalysis (LAC).^{175,176} In the early 1980's, Sharpless exploited this unique feature to develop an asymmetric version of the reaction using Chinchona alkaloids (*eg.* **346**, **347** in figure 34) as chiral ligands.¹⁷⁷ Because of the tremendous rate acceleration that accompanies binding, only catalytic quantities of the ligand are necessary.

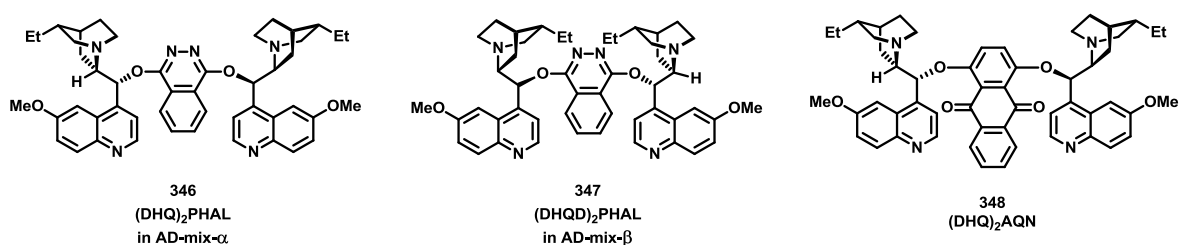


Figure 34. Chiral chinchona alkaloids used as ligands in the Sharpless asymmetric dihydroxylation

Furthermore, Sharpless discovered that when potassium ferricyanide is included as a sacrificial oxidant, the reaction also becomes catalytic with respect to OsO_4 —a great

benefit as this is a costly and extremely toxic reagent.¹⁷⁸ Sharpless' conditions are so reliable and so general that the reagents are typically purchased as pre-formulated mixtures known as AD-mix- α and AD-mix- β . Sharpless developed an empirical mnemonic to aid the chemist in predicting the appropriate AD-mix.¹⁷⁹ By applying this device (as shown in figure 35), we anticipated that AD-mix- α , operating on both enones of *meso*-**142**, would provide the (3*R*,4*S*,6*R*,10*S*,12*S*,13*R*)-tetraol **349** (refer to figure 35). We fully expected this compound to spiroketalize, if not under the basic dihydroxylation conditions, then certainly after introducing a mild acid.

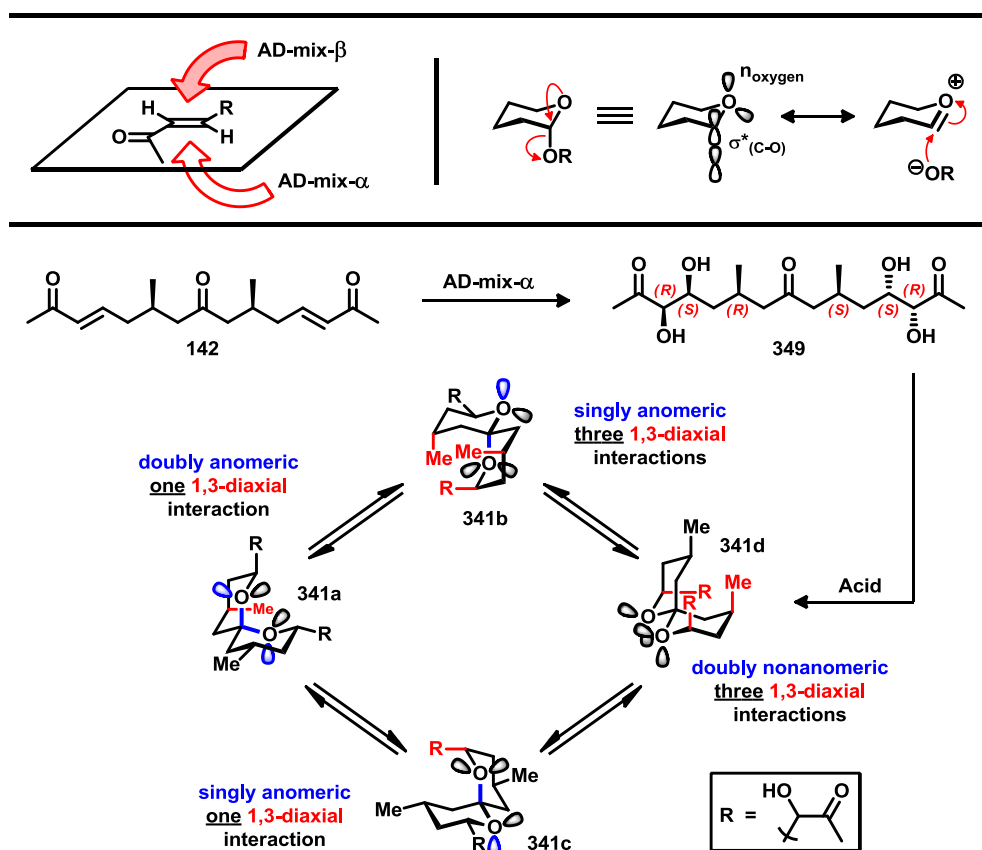


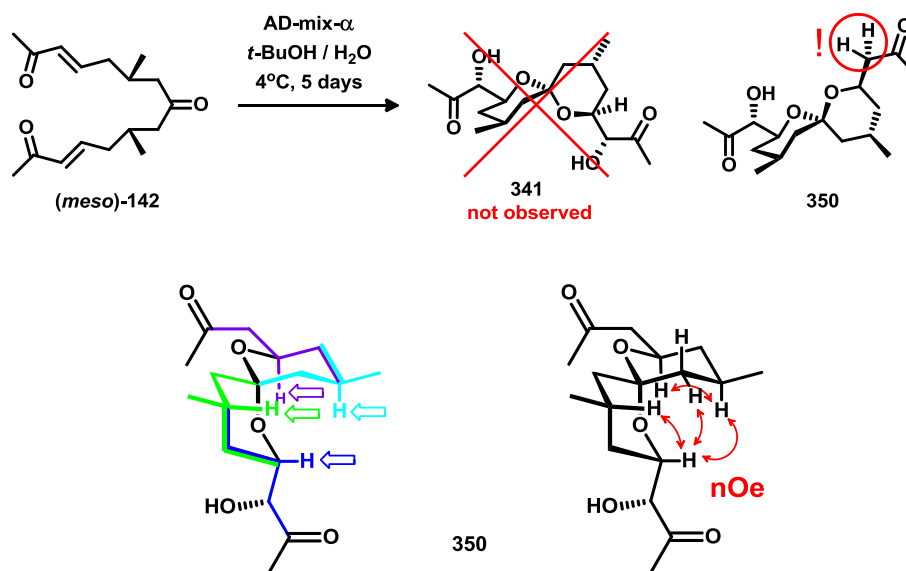
Figure 35. Sharpless' mnemonic for choosing AD-mix (top left) and the hyperconjugative resonance structures that contribute to the anomeric effect (top right). The predicted out-come for the AD-mix- α dihydroxylation of *meso*-**142** is shown along with the four hypothetical modes of spiroketalization. Favorable anomeric relationships are highlighted in blue while substituents with unfavorable 1,3-diaxial interactions are shown in red

However, the formation of the [6,6]-spiroketal creates a new chiral center about which the molecule can adopt four possible configurations: the doubly anomeric orientation (*eg.* **341a** in figure 32); the pair of geometries where either ring adopts a non-anomeric relationship (*eg.* **341b** or **341c**); or the doubly non-anomeric conformation (*eg.* **341d**). Here, our use of the term anomeric refers to the tendency of electronegative substituents at the C1 position of a pyranose ring to assume an axial orientation despite unfavorable steric interactions or dipole alignments. Instead, the axial geometry is stabilized through a hyperconjugative resonance form where one of the lone pairs from the pyranose oxygen is able to donate into the antibonding orbital of the antiperiplanar C–O bond (shown in top right of figure 35).¹⁸⁰ The anomeric effect contributes between 1.4 and 2.4 kcal/mol per interaction to the overall stability of the conformation.¹⁸¹ While this influence is significant, it can be offset by intramolecular hydrogen bonding or severe transannular strain.

Since our targeted [6,6]-spiroketal has two pyranose rings, each with oxygen substituents directly bonded to a common carbon (*ie.* the ketal carbon), the most stable conformation is expected to be the one with the maximum number of anomeric relationships and the fewest possible unfavorable steric interactions. For instance, as shown in figure 35, compound **341a** is clearly a privileged conformation—it enjoys two anomeric bonds (favourable anomeric bonds are highlighted in blue) and suffers only a single 1,3-diaxial interaction. Thus, under equilibrating conditions, we would anticipate a strong thermodynamic preference for this anomer. Unsurprisingly, this is the same arrangement that is observed in the didemnaketal family of natural products.

5.4 Singly Anomeric Spiroketal

When we attempted the dihydroxylation of *meso*-**142** with AD-mix- α , we found the reaction to be sluggish. However, it was encouraging to watch the UV-absorbing enones disappear from the TLC plate as they gradually reacted with the electrophilic osmium catalyst. After five days, the starting material was fully consumed.

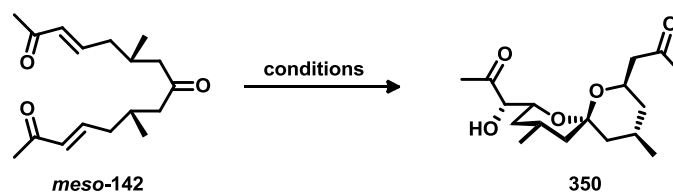


Scheme 69. Attempted dual asymmetric dihydroxylations leading to an unexpected non-anomeric spiroketal **259** as evidenced by TOCSY spin systems (blue, green, purple and cyan) and nOe correlations (red)

In fact, we did indeed isolate a single spiroketal product; however, after scrutinizing the ¹H and ¹³C NMR spectra, we were baffled by the apparent deletion of the one of the four oxygen atoms we were attempting to install. The bulk of the atom connectivity appeared to be correct according to COSY and TOCSY NMR experiments, with the conspicuous exception of the C-21 alcohol. In its place we observed matching sets of doublets of doublets at 2.56 and 2.39 ppm, the pattern and position of the signals

characteristic of a prochiral α -keto methylene. Using nOe NMR spectroscopy, we were able to unambiguously solve the structure of the singly anomeric spiroketal **350**.

While it is convenient to use commercially available AD-mix, it is often possible to achieve better results by procuring the ingredients independently. Doing so allows for control over the order and the rate of addition for any particular component as well as other subtle alterations to the conventional Sharpless protocol. For instance, hoping to influence the reaction towards the intended product, we substituted the standard AD-mix ligand, (DHQ)₂PHAL, for (DHQ)₂AQN (refer to **348** in figure 34), which is reportedly a superior alternative.¹⁸² After osmium tetroxide reacts with an alkene, it forms a glycolate complex which releases the diol upon hydrolysis which is the rate determining step in the catalytic cycle. It is known that this slow hydrolysis can be accelerated with MeSO₂NH₂, perhaps by acting as a proton shuttle.¹⁸³ Finally, commercial AD-mix contains K₂CO₃, an essential additive that facilitates the function of potassium ferricyanide, the sacrificial oxidant. Unfortunately, such basic conditions can be problematic, particularly when performing dihydroxylations across α,β -unsaturated carbonyls. The stereochemical fidelity of the product is highly susceptible to erosion through the epimerization of the α -keto alcohol. Likewise, the unwanted retroaldol cleavage of the 1,3-ketoalcohol product is a potential pitfall. To mitigate these deleterious side reactions, it is common to buffer the K₂CO₃ with an equivalent of NaHCO₃.¹⁸⁴ We attempted all of these modifications and yet compound **350** remained the only isolable product, typically obtained in 30 to 40% yield (as shown in table 11).



Entry	Conditions	Yield
1	AD-mix- α	35%
2	AD-mix- α , MeSO ₂ NH ₂	39%
3	K ₂ OsO ₄ ·2H ₂ O, (DHQ) ₂ PHAL, K ₂ CO ₃ , NaHCO ₃ , MeSO ₂ NH ₂	27%
4	K ₂ OsO ₄ ·2H ₂ O, (DHQ) ₂ AQN, K ₂ CO ₃ , NaHCO ₃ , MeSO ₂ NH ₂	41%

Table 9. Sharpless asymmetric dihydroxylations using AD-mix- α and modified conditions consistently produce the singly anomeric spiroketal **350**

These results provoked a considerable amount of ambivalence. Naturally, we were discouraged over our failure to obtain **341**. The synthesis of this doubly anomeric spiroketal was the primary goal of the research project and its completion would have represented a significant landmark in our total synthesis. On the other hand, we were intrigued by the atypical non-anomeric geometry of unexpected spiroketal product. Selectively producing these ostensibly contra-thermodynamic spiroketals remains a significant synthetic challenge.^{185,186} So, despite our initial disappointment, we were eager to learn about the chain of transformations that ultimately led to the formation of this unique product.

In nature, spiroketals typically form under equilibrating conditions, so the vast majority of them possess the maximum number of anomeric relationships. There are rare exceptions, however, where the non-anomeric configuration has a thermodynamic advantage. Generally, one or more of the following factors are often implicated: the

structure may benefit from intramolecular hydrogen bonding, a shift in conformation may result in severe steric interactions, or there may be conformational locking imposed by rigidifying macrocyclic architecture.

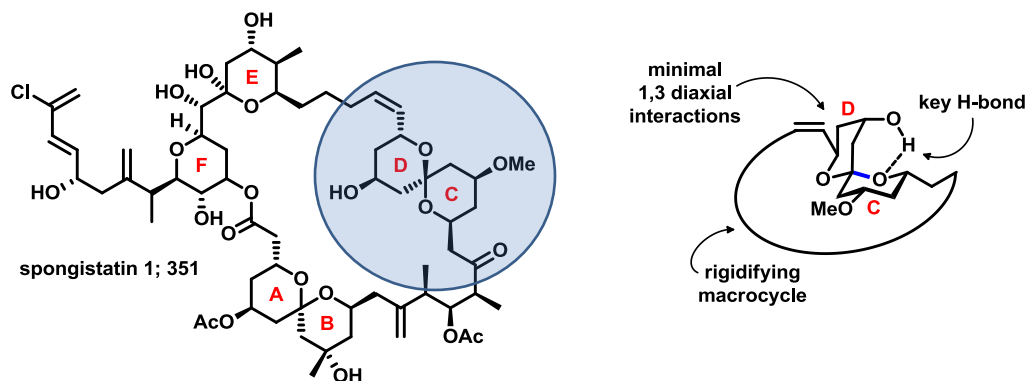


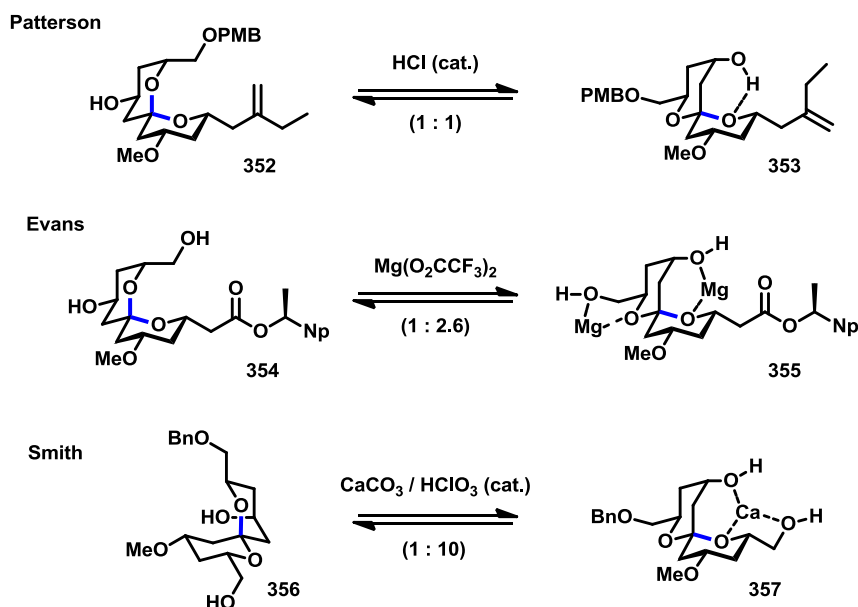
Figure 36. The cytotoxic marine macrolide, spongistatin 1 (**351**) with an expansion of the non-anomeric C / D ring system

All three of these stabilizing influences are exemplified in the singly anomeric C/D spirocycle of the marine macrolide, spongistatin A (**351** shown in figure 36).¹⁸⁷ In order for the D ring to acquire an anomeric relationship with respect to the C ring, the C ring would have to undergo a ring flip. However, this rearrangement would not only cost a beneficial hydrogen bond between the axial alcohol and the ketal oxygen, it would also invert both the methoxy substituent and the alkyl tether into sterically hindered axial orientations, while increasing ring strain throughout the 42-membered macrolactone.

Owing to this intriguing structural feature, not to mention its exceptional cytotoxicity, the spongistatins have become a favorite venue for synthetic chemists to showcase advanced methods for making non-anomeric spiroketals. In general, there are two

possible approaches; namely, those strategies that rely on thermodynamic control and those that rely on kinetic control.

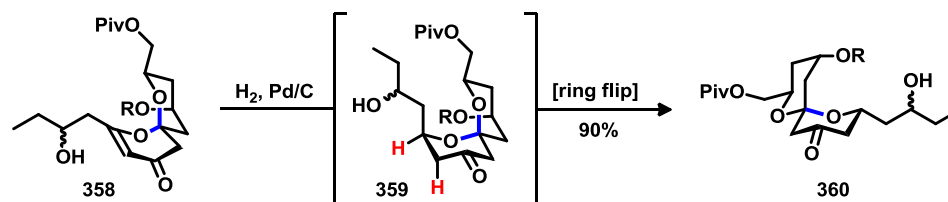
When a spiroketalization occurs under thermodynamic control the product distribution reflects the relative energies of the all interconverting configurations. Thus, the reaction conditions (*eg.* solvents, chelating additives, etc) must be carefully optimized to shift the equilibrium in an advantageous direction. Several applications of this approach with respect to spongistatin are provided in scheme 70. The strategy typically involves exploiting a favourable intramolecular hydrogen bond (as demonstrated by Patterson with **353**¹⁸⁸) or introducing metal chelation to help stabilize the non-anomeric configuration (as demonstrated by Evans with compound **355**¹⁸⁹ and Smith with compound **357**¹⁹⁰). It is, thereby, often possible to improve the ratio of the targeted spiroketal; however perfect selectivity is rarely achievable. Instead, the isomers must be separated and the undesired material recycled by reapplying the equilibrium conditions. The stronger the thermodynamic preference, the fewer of these cycles are required; nevertheless, even when there is poor thermodynamic control (but sufficient patience), good conversion to the desired isomer is often feasible. Although the reaction itself is often trivial to implement, the precise conditions can be extremely substrate specific, often requiring extensive optimization. Along with the requisite purification and the recycling, the entire process is highly labour intensive.



Scheme 70. Use of thermodynamic control in accessing the non-anomeric spiroketal domain of spongistatin

Many of these issues can be circumvented by exerting kinetic control over the reaction mechanism. With this approach, the relative heats of formation of the various products do not affect the outcome; instead, it is the transition state energy of some irreversible reaction that dictates the trajectory of spiroketalization. Under kinetic control the desired non-anomeric spiroketal is often isolated as the exclusive product, eliminating the need to purify and recycle unwanted anomers. These approaches also tend to be more broadly applicable and require less fine tuning. On the other hand, orchestrating a kinetics-based strategy is an inherently more complex endeavor. Successfully trapping the non-anomeric spiroketal requires an intimate understanding of the reaction mechanism including precise knowledge about the geometry of the transition state. Nevertheless, there are several elegant approaches to spongistatin which illustrate the point.

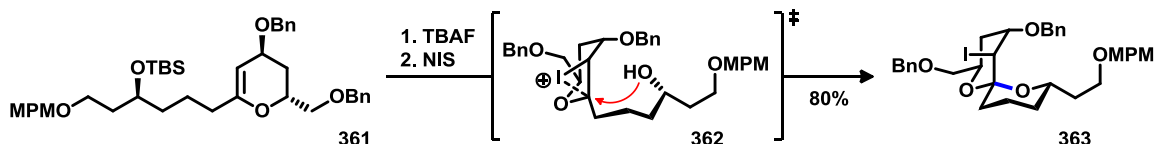
For instance, after preparing spiroketal **358** through a hetero-Michael addition, Crimmons achieved the non-anomeric anomer using a kinetically controlled catalytic hydrogenation (shown in scheme 71).¹⁹¹ Due to the enocyclic olefin, **358** preferentially adopted a chair / boat conformation while maintaining two anomeric relationships. The subsequent hydrogenation performed occurred much faster on the exposed, convex face of the bicycle. This *syn* addition of hydrogens across the alkene forced the bulky chain into an axial orientation, creating severe 1,3-diaxial strain in the doubly anomeric chair / chair conformation of **359**. A ring inversion relieved the strain at the cost one of the anomeric interactions, allowing for the isolation of the desired non-anomeric spiroketal **360** in excellent yield.



Scheme 71. Crimmons uses a catalytic hydrogenation to kinetically trap a non-anomeric spiroketal

Fuwa, who recently completed the first total synthesis of didemnaketal B (refer to scheme 8), further demonstrates his expertise in spiroketal construction by using a kinetically controlled iodo-spiroketalization to make a spongistatin precursor.¹⁹² After preparing the dihydropyran **361**, Fuwa used *N*-iodosuccinimide to activate the double bond. The bulky benzyl protecting group directed the electrophilic iodine reagent toward the opposite face of the ring, producing **362**—a fatal intermediate that determines

spiroketalization trajectory. What followed was an S_N2-type nucleophilic displacement of the iodine by the free hydroxyl group, a transformation that could only occur through an axial attack. Thus, using these thoughtfully crafted conditions, Fuwa was able to isolate the desired non-anomeric spiroketal **363** in 80% yield.

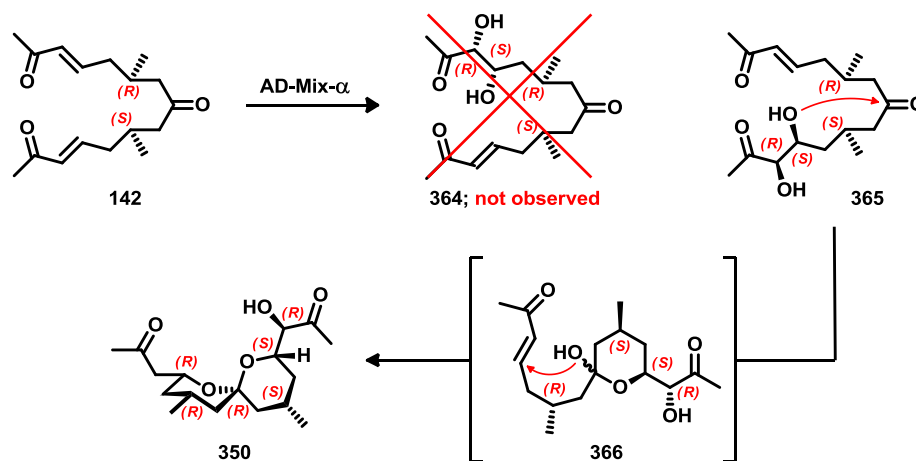


Scheme 72. Fuwa uses an iodo-spiroketalization to kinetically trap a non-anomeric spiroketal

When we observed our non-anomeric product, naturally we were curious about how it had formed. Was there some stabilizing factor that gives compound **350** a thermodynamic advantage, or had we accidentally trapped a high energy species? We had intended to perform a Sharpless asymmetric dihydroxylation and, indeed, this is likely the first step in the overall transformation. However, the chiral ligand appears to have been influenced by the stereochemistry of the adjacent methyl group, thereby allowing it to discern between the two pro-chiral enones. As a result, 1,3-*anti* product **365** is evidently formed at a greater rate than the 1,3-*syn* product **364** (as shown in scheme 73).

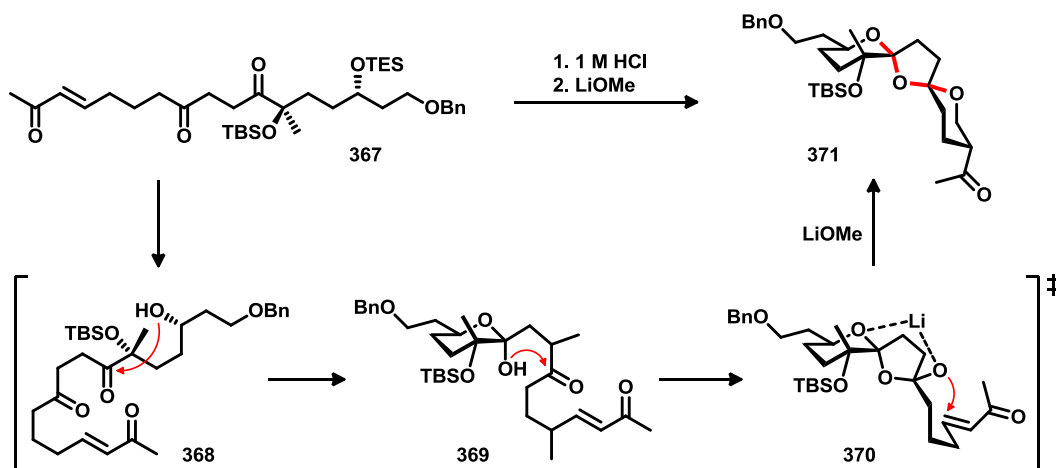
It is unlikely that we would have noticed this superlative level of selectivity had not a serendipitous cascade out-competed the second dihydroxylation reaction. First, one of the newly formed alcohols must have undergone hemiketalization with the central ketone to give **366**. The second ring of the bicyclic product then could the form through an

intramolecular hetero-Michael addition of the hemiketal onto the remaining enone, producing the end product (**350**).



Scheme 73. Observed non-anomeric spiroketal **350** arises through a cascading asymmetric dihydroxylation / hemiketalization / hetero-Michael addition sequence

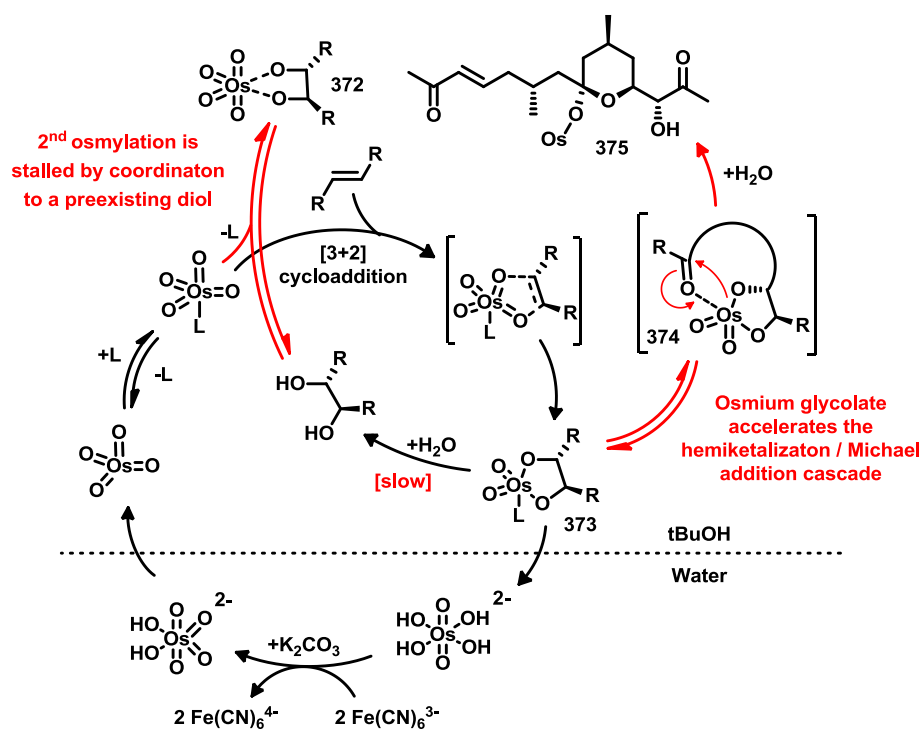
To the best of our knowledge, there had been only a single prior example of a hemiketal acting as a nucleophile in the conjugate addition. That is, when Hashimoto incorporated this transformation into an impressive cascade orchestrated for the synthesis of (+)-pinnatoxin A.¹⁹³ After having cleaved the triethylsilyl protecting group from triketone **367**, the hydrochloric acid catalyst facilitated tandem hemiketalizations, initiated by the newly liberated alcohol. When the resulting hemiketal-spiroketal product (**370**) was treated with lithium methoxide, it underwent a chelation controlled Michael addition, providing the doubly anomeric dispiroketal **371** as the major product.



Scheme 74. Hashimoto's hemiketalization / hetero-Michael addition cascade used in the synthesis of (+)-pinnatoxin A

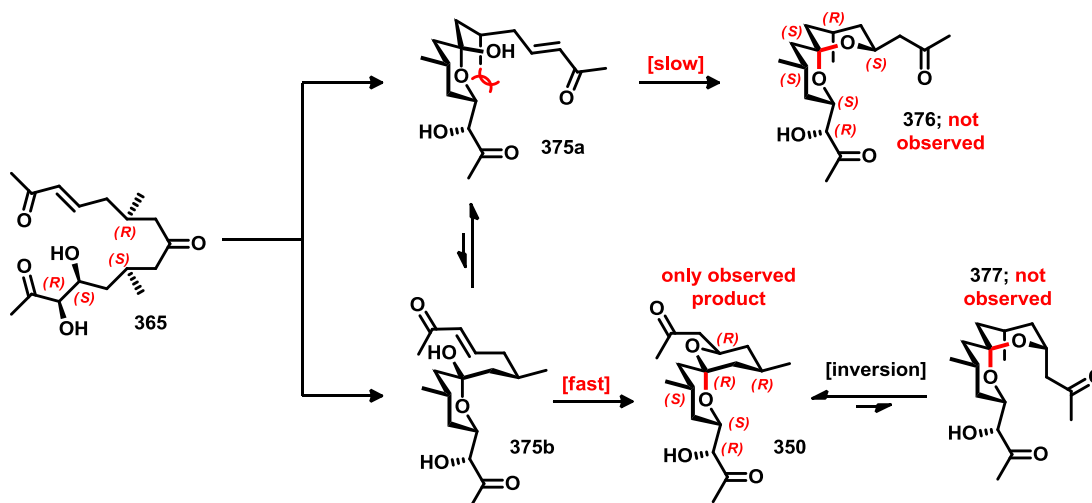
Indeed, the intramolecular conjugate addition of a hemiketal functional group appears to be a useful and yet largely unexplored strategy for synthesizing spiroketals. Perhaps chemists have been hesitant to consider this approach because hemiketals appears to be such hindered nucleophiles. In fact, we were surprised to observe the spiroketalizing Michael addition occurring faster than the second possible dihydroxylation reaction. One possible explanation is that, after installing the first diol, the alcohols then inhibits the catalysis from operating a second time. This effect has been observed previously during poly-dihydroxylation attempts,¹⁹⁴ occasionally forcing the experimenters to modify their conditions or else apply a protecting group between dihydroxylations in order to regain activity.¹⁹⁵ It may be that with particular substrates, the initial diol can coordinate the electrophilic OsO_4 catalyst, possibly displacing the ligand in the process (as in **372** shown in scheme 75). In our case, with the LAC stifled, the hemiketalization / Michael addition cascade seems to become the preferred reaction trajectory.

Alternatively, the second dihydroxylation might be delayed by the slow hydrolysis of the osmium glycolate complex **373**. This transformation is known to be the rate limiting step in the catalytic cycle.¹⁹⁶ If the regeneration of the catalyst is sufficiently sluggish, the cascade cyclization may dominate. It is even possible that the hydrolysis of compound **373** is facilitating hemiketalization by activating the ketone. An analogous mechanism was invoked by Muniz when he reported on a one-pot dihydroxylation / 1,2-diol protection strategy.¹⁹⁷ If one or more of these mechanisms are active, it would help to explain why the nor-hydroxy spiroketal **350** was observed instead of the intended didemnaketal-like compound, **341**.



Scheme 75. The catalytic cycle for the Sharpless dihydroxylation with speculative mechanistic considerations to account for the observed nor-hydroxy spiroketal **350**

The fact that we isolated a single spiroketal product—moreover, that an ostensibly contra-thermodynamic anomer was observed—suggests that an irreversible reaction was kinetically controlling the stereochemistry. We hypothesize that the initial hemiketalization resulted in a rapidly equilibrating mixture of pyranose epimers (**375a** and **375b** in scheme 76). Furthermore, it is likely that the equilibrium strongly favoured **375a** since the axial alcohol would result in anomeric stabilization. On the other hand, despite its diminished presence, the non-anomeric intermediate **375b** was probably able to cyclize more efficiently. The conjugate addition of **375a** must proceed through a transition in which one of the methyl groups assumes a pseudoaxial orientation, whereas the transition state proceeding from **375b** would need not overcome any high energy 1,3-diaxial relationships.



Scheme 76. Curtin–Hammett equilibrium kinetically trapping the non-anomeric spiroketal **350**

Since the Michael addition is likely to be irreversible under these reaction conditions, a classic Curtin–Hammett scenario emerges.¹⁹⁸ The thermodynamically disfavoured

anomer is rapidly consumed in the conjugate addition, causing a perpetual shift in the equilibrium to compensate, eventually consuming **375a**—the intermediate that would have otherwise produced the more stable, doubly-anomeric spiroketal product (**376** in scheme 76). Once formed, it is unlikely that **350** will either ring flip or epimerize into the doubly anomeric spiroketal **377** since to do so would require positioning at least one of the two alkyl substituents into axial orientations, creating considerable transannular strain.

As a further test of our hypothesis concerning kinetic control we calculated the heats of formation for structures **350** and **376**. Our calculation ruled out the observed product as the lowest energy isomer, suggesting, instead, that **376** would be thermodynamically favored by about 0.44 kcal/mol. We were not surprised to find that the energetic benefit derived from the doubly anomeric spirocenter outweighs the cost of placing a methyl group in the axial orientation. The structure of **376** is highly analogous to the spiroketal domain of didemnaketol, an architecture that emerges naturally and has also been formed synthetically under thermodynamically equilibrating conditions. Thus, we seem to have stumbled upon a novel cascade that selectively spiroketalizes a linear *meso* precursor, establishing a total of 6 stereocenters, while also incorporating a kinetic trap to access a synthetically challenging non-anomeric geometry.

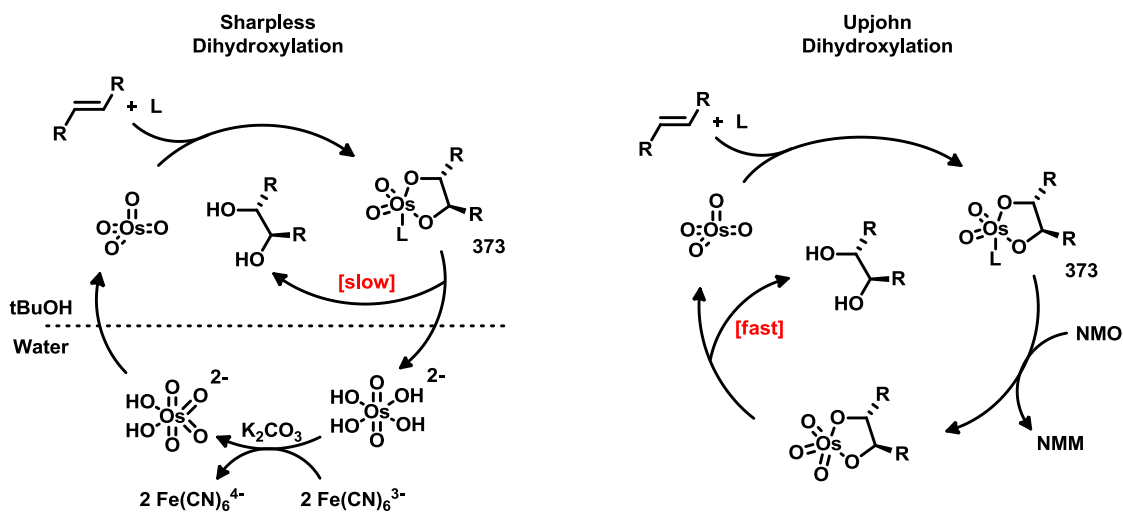
5.5 Doubly Anomeric Spiroketal

Though we were impressed by this transformation, we realized that our continued progress in the total synthesis of didemnaketal required us to subvert the kinetic control imposed by the Michael addition. As long as this irreversible reaction dominated over the second dihydroxylation, it would not be possible to access the desired doubly anomeric spiroketal. Clearly, we had to reassess our conditions.

As described earlier, in the conventional Sharpless reaction, the cleavage of the diol from the osmium glycolate complex is believed to be the rate limiting step. Not only does this slow hydrolysis stall the catalytic cycle but, as we speculated in scheme 75, **373** may even facilitate hemiketalization—the first step in diverting material to the non-anomeric product. After hydrolysis, the spent osmium must traverse the organic / aqueous interface where K_2CO_3 facilitates an oxidation by the hydrophilic $K_3Fe(CN)_6$ to regenerate the active species. Such basic conditions are also likely to augment our undesired cascade by enhancing the nucleophilicity of the hemiketal toward a subsequent Michael addition. Hashimoto's base-induced transformation lends credence to this scenario (refer the scheme 74). Unfortunately, extensive optimization by Sharpless has revealed that K_2CO_3 is an unavoidable additive when $K_3Fe(CN)_6$ is used as the stoichiometric oxidant. These are the considerations that guided our re-evaluation of the dihydroxylation conditions.

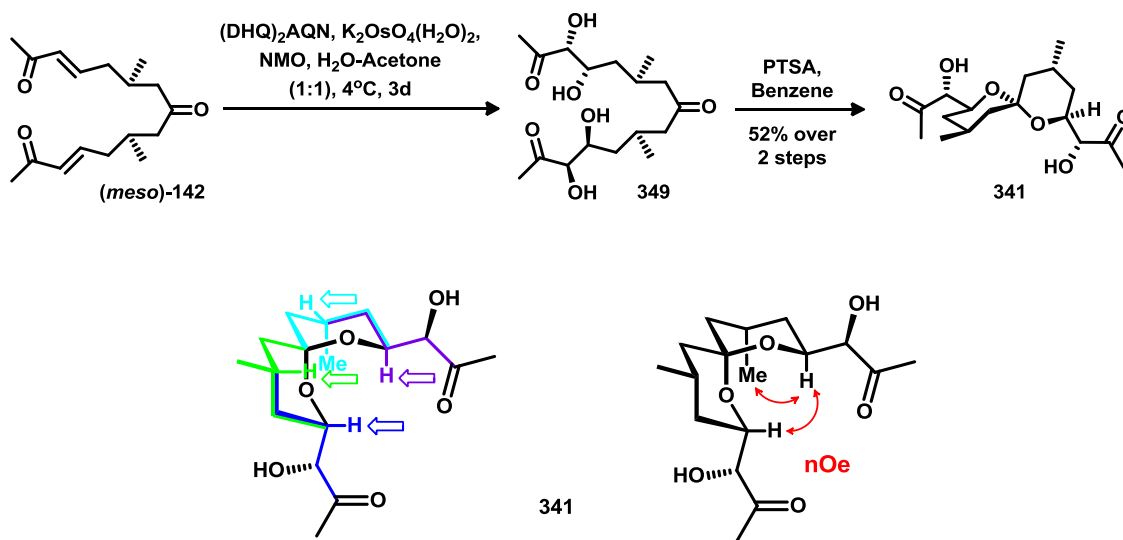
In attempting to understand the mechanism leading to the non-anomeric spiroketal, we realized that several aspects of this problematic reaction were connected to our choice for the sacrificial oxidant. There are two viable alternatives to using potassium ferricyanide:

Milas' conditions employing hydrogen peroxide¹⁹⁹ and the Upjohn reaction which uses *N*-methylmorpholine *N*-oxide (NMO).²⁰⁰ Both oxidants offer the advantage that they are active at neutral pH which should help to impede the unwanted conjugate addition. Furthermore, unlike $\text{K}_3\text{Fe}(\text{CN})_6$, both oxidants are soluble in organic solvents; consequently, both Upjohn and Milas dihydroxylations can be performed in monophasic solvent systems. This feature also has important implications. Under Sharpless' conditions, the rate of catalyst regeneration is limited by the slow hydrolysis of the osmium glycolate complex (**373** in scheme 77). Conversely, in a monophasic solvent system, the oxidant can react directly with the glycolate complex, facilitating cleavage of the diol while rapidly turning over the osmium catalyst. We reasoned that the less persistent this glycolate complex, the more competitive we could make the second dihydroxylation reaction over the undesired cascade.



Scheme 77. Catalytic cycle for biphasic Sharpless dihydroxylation and the monophasic Upjohn dihydroxylation

Of the two options, we were more wary of the Milas conditions. Hydrogen peroxide is a nucleophilic epoxidizing agent with a penchant for reacting with α,β -unsaturated ketones. Gratifyingly, we found that the Upjohn conditions delivered the desired target (**341** in scheme 78). Given our previous experiences, it took a battery of 1D and 2D NMR experiments to satisfy ourselves that we had finally isolated the correct product. The observed nOe correlations and the spin systems which we were able to isolate through TOCSY experiments were both very compelling (shown in scheme 78).



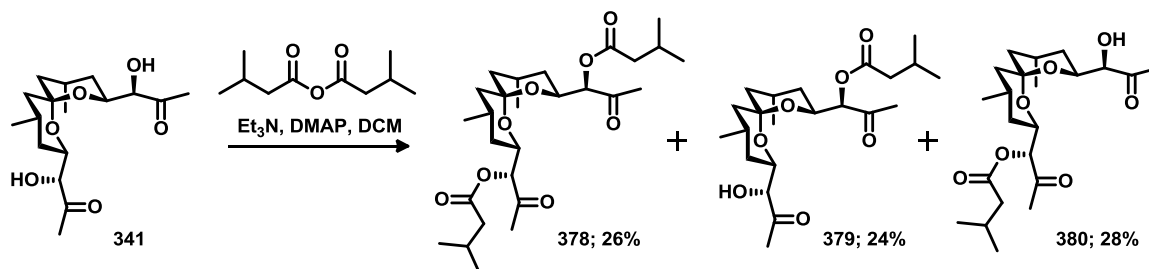
Scheme 78. Dual asymmetric dihydroxylations performed under Upjohn conditions leading to doubly anomeric spiroketal **341** as evidenced by TOCSY spin systems (blue, green, purple, and cyan) nOe correlations (red).

After repeating the experiment on larger scale, we realized that the true reaction product was the linear tetraol **349**. Previously, the chloroform used to acquire the crude NMR spectrum had been sufficiently acidic to catalyze the spiroketalization reaction. Ultimately, however, we found it more convenient to accomplish this transformation in a more controlled fashion by adding ~1 mg of *p*-TSA to a solution of the semi-purified

tetraol. The long sought doubly-anomeric spiroketal could then be isolated by column chromatography in a respectable yield.

5.6 Comparison with Didemnaketol A

Upon treating this compound with isovaleric anhydride we observed a mixture of products: the *bis*-esterified product **378**, along with the two alcohols **379** and **380**, the latter being slightly favoured under these reaction conditions. Although differentiating between these two hydroxy-ketones (*ie.* **379** and **380**) is a problem that we have not yet satisfactorily resolved, it is noteworthy that all three compounds were readily separable by column chromatography. Thus, as a worst case scenario for progressing toward the natural product, our losses at this stage could potentially be mitigated by pooling and recycling the unwanted compounds.



Scheme 79. A poorly selective esterification of our spiroketal fragment **341**

At this early stage, however, all three of these compounds provided us with valuable insights. Alcohol **380**, for instance, is a precise match for the C11-C21 domain of the posited structure of didemnaketol A. Given the recent controversy that was discussed

earlier (refer to figure 16), we were eager to learn whether our molecule would support Faulkner's claim⁵⁶ or strengthen Tu's falsification of the structural hypothesis.⁶⁸

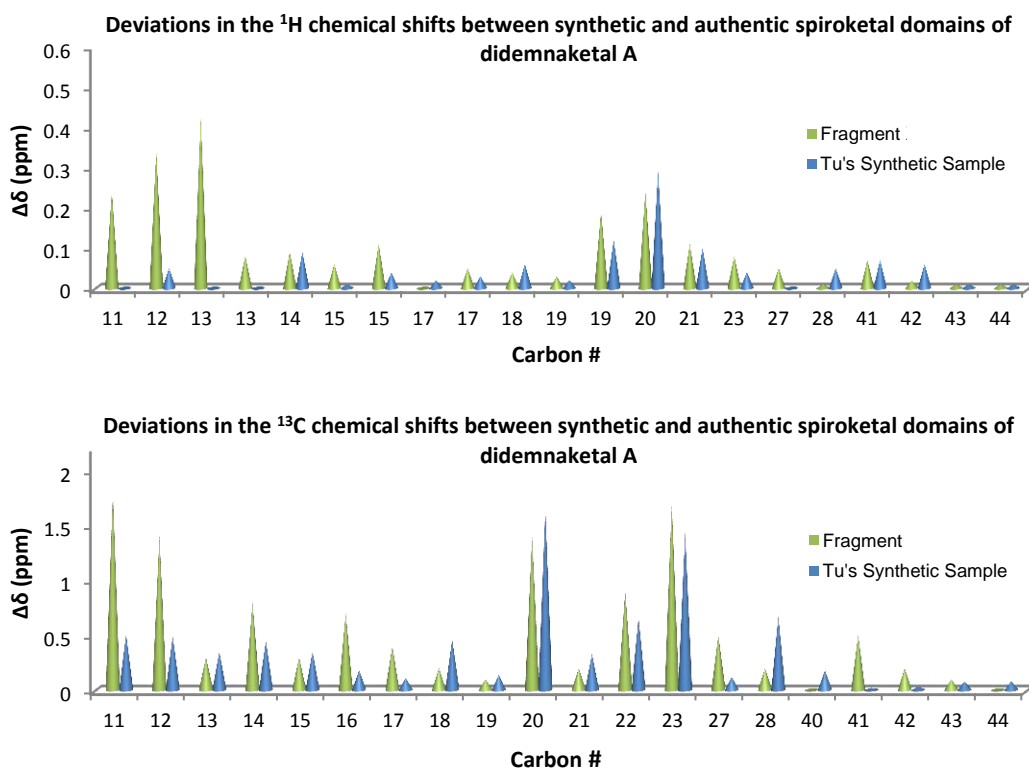
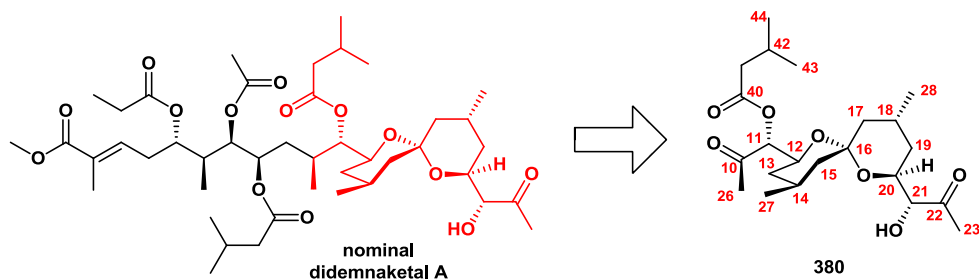
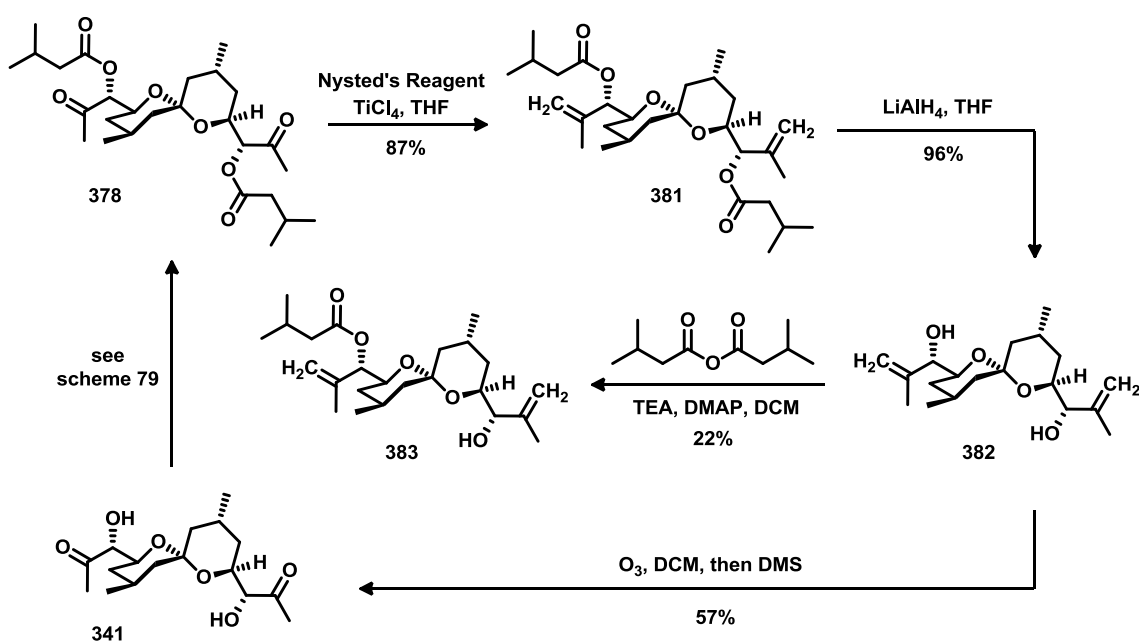


Figure 37. Discrepancies in the chemical shift of the ¹H and ¹³C NMR spectra are plotted, comparing the spiroketal domain of the authentic sample with **380** and the synthetic version prepared by Tu

We calculated the deviation in the chemical shift between the authentic sample and our synthetic fragment and plotted it alongside the deviation observed in Tu's synthetic didemnaketol A. The analysis revealed that the ¹H and ¹³C chemical shifts of our

spiroketal fragment (**380** shown above figure 37) deviate from the chemical shifts reported for the natural product, particularly in the region between C19 and C23. Moreover, we found our chemical shifts are a near perfect match with Tu's synthetic version of didemnaketal A. The only exception is between C11 and C13, where the C10 ketone in **380** is drawing the chemical shift downfield. Overall, it seems that the evidence is becoming very compelling that there is a flaw in Faulkner's structural assignments.



Scheme 80. *Bis*-olefination of **378** followed by reductive removal of the protecting esters to give the crystalline diol **382** and the restoration of **341** by ozonolysis

We wondered if we might be able to extend this analysis in order to comment on the relationship between Fuwa's synthetic version of didemnaketal B and Faulkner's ascidian isolate. To do so we made use of compound **378**, the two esters serving as protecting groups through a *bis*-olefination of the adjacent ketones. Nysted's reagent was found to be a suitably mild reagent, providing **381** in excellent yield. At this point, the esters were

reductively removed, revealing **382**, a molecule that we thought resembled a truncated version of didemnaketal B. However, the structural differences here were sufficiently significant that observed chemical shifts tracked poorly with both synthetic and authentic samples, making it difficult to offer compelling arguments for or against either structure.

Nevertheless, this effort wasn't in vain as it led us to an important structural characterization result. We were disappointed at being unable to obtain an X-ray quality crystal of **341**; fortunately, we found that the corresponding *bis*-methylene analogue **382** was far more crystalline, allowing us to solve the structure (refer to figure 38). Based on the structural data obtained for **382**, we infer that we have achieved the desired stereochemistry in the antecedent product **341**. To strengthen this claim, we performed two-fold ozonolyses on the *bis*-methylene spiroketal, returning it to spectroscopically identical version of **341**. We thus rule out the possibility of unexpected epimerization in the derivative used for structural characterization, while also demonstrating a method for recycling over-esterified product **378** back to the synthetically relevant diol **341**.

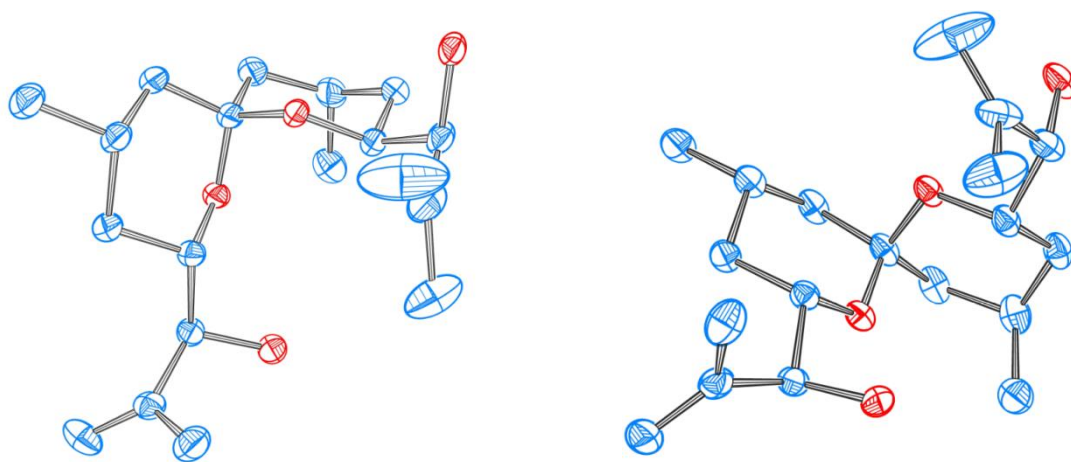
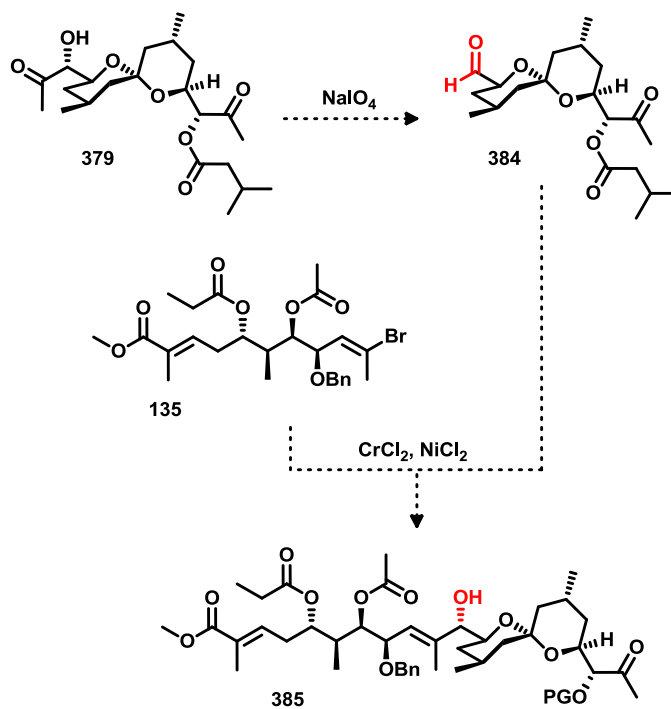


Figure 38. Crystal structure of the *bis*-allylic alcohol **382**, confirming a stereochemical arrangement that matches the spiroketal domain of nominal didemnaketal A

While **378** and **380** both led us to important structural information, compound **379** has the greatest value from a synthetic perspective. With the ester acting as a protecting group for the C21 alcohol, it becomes possible to continue building on the opposite side of the spiroketal. We intended to append the linear chain using a Nozaki-Hiyama-Kishi reaction, a mild coupling that is typically performed between a vinyl halide and an aldehyde. Now, with a free α -keto alcohol at the C11 position, it becomes very convenient to transform the spiroketal fragment into the aldehyde coupling partner. An oxidative cleavage with either lead (IV) acetate or sodium periodate should provide **384**, transitioning our campaign into the end-game (see scheme 81).



Scheme 81. The oxidative cleavage of **289** to form aldehyde **291**, a suitable NHK coupling partner for late-stage assembly of didemnaketol A

The synthesis of an asymmetrically functionalized spiroketal unit **341** was the principle goal of this doctoral research. With this compound in hand we are well positioned to take the final steps in assembling the natural product. The NHK reaction is known to be exceptionally tolerant of sensitive functional groups—the esters adorning the linear side chain, for instance. Consequently, we expect that the number of protecting group manipulations post coupling should be minimal. The remaining chapter of this thesis describes the preliminary steps we have taken toward the completion of the natural product and our opinions concerning possible directions this project could take in light of recent structural revelations.

Chapter 6 — Final Coupling

6.1 Overview and Analysis of Tactics

Our aspirations for obtaining the spirocyclic core of didemnaketal A were met by many obstacles. Our initial approach, using a photochemical transformation of tropolone, was eventually obstructed by an irresolvable deoxygenation reaction (the details of which were described in chapter 2). These vain efforts, however, did lead us to explore an unexpected radical-based lactonization through which we demonstrated the synthesis of several complex polycyclic structures (the topic of chapter 3). Ultimately, we were forced to reevaluate our tactics. We circumvented the problematic deoxygenation through the hydrosilylation of a simple cyclic enone, a strategy that provided near perfect regioselectivity in an otherwise unselective silyl enol ether synthesis. Upon resolving this issue, we made considerable headway—that is, until we were presented with an enigmatic decarboxylation. Here, the key to progressing was a light-driven olefin isomerization which granted us access to a crucial *meso* precursor **142** (as presented in chapter 4). We had anticipated that tandem asymmetric dihydroxylations would establish the correct stereochemistry of the four alcohols as well as the pair of branching methyl groups. We assumed that the remaining seventh stereocenter at the spiroketal junction would be thermodynamically controlled since the desired product was doubly anomeric. Instead, we were surprised to isolate a singly anomeric spiroketal analogue. This synthetically formidable motif was kinetically trapped in a cascade of reactions

culminating in an unusual hemiketal / Michael addition. Fortunately, after rationally reconsidering our dihydroxylation conditions, we were able to curb this unwanted reactivity and successfully assemble the bicyclic domain of the natural product, even confirming the structure and the stereochemistry through x-ray crystallography (these details are related in chapter 5).

With the spirocyclic half of our target in hand (**379**) and the linear branch approaching completion (**135**), final assembly of the natural product seemed imminent. We thus focused our attention on devising a strategy to accomplish the coupling of these two pieces. Several possibilities were considered.

One prospective route would be to use a β -alkyl Suzuki reaction. The utility of this reaction had previously been demonstrated by both Ito⁶⁹ and Fuwa⁷² (see chapter 1; schemes 2 and 5, respectively); although, admittedly, both groups placed this often temperamental transformation much earlier in their respective didemnaketal syntheses. Nevertheless, on the surface this strategy promised to be a highly efficient, requiring few post coupling transformations. Ideally, we would be able to prepare the boronate **386** (see figure 39). As we already had **379** in hand, conversion of the methyl ketone to the kinetically trapped mesyl enol ether (**387**) should provide the appropriate coupling partner. After using the Suzuki reaction to create the C9-C10 bond, the only remaining steps for the completion of the synthesis would be a selective hydrogenation of the allyl alcohol **140** followed by a moderate restructuring of some of the alcohol functionality.

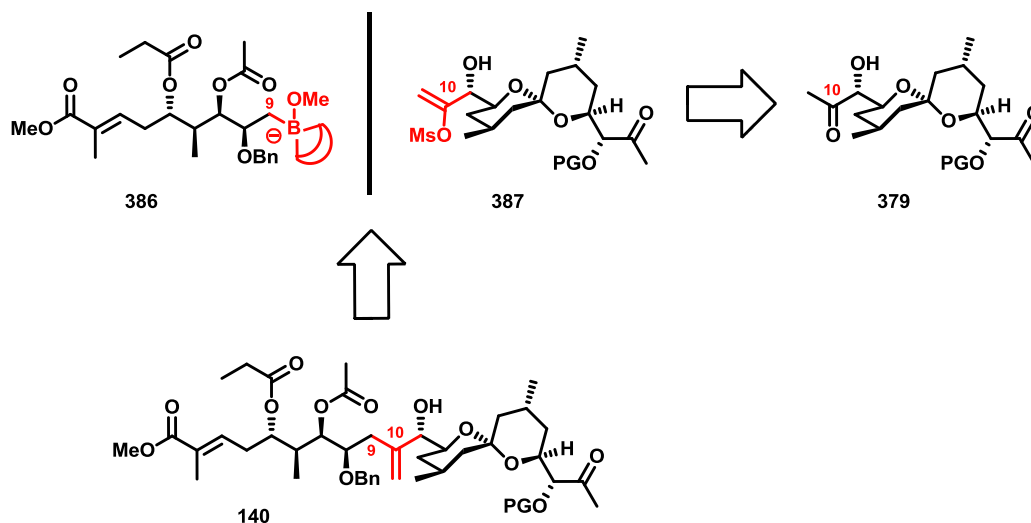


Figure 39. A retrosynthetic analysis for the final assembly of didemnaketal A featuring a Suzuki–Miyaura coupling

We realized, however, that there could be considerable pragmatic challenges associated with this proposal. For instance, both Ito and Fuwa generated their respective methoxy boronate coupling partners *in situ* using β -methoxy-9-BBN and the corresponding alkyl lithium species. Unfortunately, these highly reactive conditions are unlikely to be tolerant of the delicate esters that adorn the linear branch (consider **386**). If the esters cannot be present prior to the coupling, we would be forced to compensate with an elaborate orthogonal protecting group strategy. A milder alternative would be to use a hydroboration to prepare the alkyl borane coupling partner; unfortunately, it is difficult to imagine how we could implement this gentler approach without sacrificing the C8 stereocenter. In either case, we would find ourselves significantly burdened with a host of post-coupling transformations—not to mention that accessing the borylated substrate would likely require a fundamental reengineering of Caleb Bromba’s previous synthetic work.⁷⁸ Making matters worse, the preparation of the spiroketal coupling partner would

require a highly selective enolization of **379**. The methyl ketones are so similar that it is difficult to conceive of a basis for such a delicate discrimination. Thus, for these reasons we considered the β -alkyl Suzuki coupling to be our least viable option.

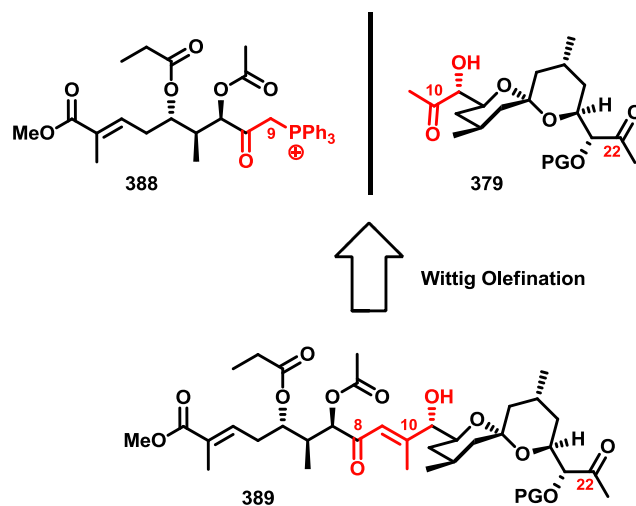


Figure 40. A retrosynthetic analysis for the final assembly of didemnaketol A, featuring a Wittig-type olefination

As an alternative, we felt that using a Wittig olefination to accomplish the coupling could circumvent several of the issues described above. For instance, the Wittig reaction targets ketones and aldehydes but typically leaves esters untouched, a great advantage as it would reduce the number of post-coupling protecting group manipulations.²⁰¹ Also, thanks to the dogged synthetic work of Caleb Bromba, elaborating the linear fragment into a phosphonium ylide (eg. **388** in figure 40) should be straight forward.⁷⁸ Likewise, our spiroketal fragment (**379**) may be employed directly without any further modifications. The immediate availability of the requisite precursors was perhaps the strongest incentive to pursue this chemistry, yet we were not ignorant of the potential complications which we were likely to encounter.

As with the β -alkyl Suzuki reaction, ostensibly the Wittig approach could suffer from poor selectivity between the two ketones that flank the bicyclic core of **379**. Fortunately, the Wittig reaction is known to be highly sensitive to the steric environment surrounding the reaction site. In this case, it is reasonable to hope that a bulky protecting group placed on the C21 alcohol could shield the adjacent ketone against undesired reactivity. Though we should be able to control the regiochemistry, it may not then be possible to guarantee the stereochemistry about resulting olefin. By incorporating an electron withdrawing group to stabilize the ylide (as in **388**), we could ensure that the E-alkene is the exclusive isomer. However, this modification would add several post-coupling transformations, including the diastereoselective reduction of an enone to a fully saturated alcohol—likely a challenging feat in the presence of the unprotected C22 ketone. Finally, the hindered nature of the two coupling partners cast doubt as to whether or not we should expect a satisfactory yield. Although this approach appeared to be superior to the β -alkyl Suzuki coupling, we maintained good reasons for skepticism.

A third possibility involved using the Nozaki-Hiyama-Kishi (NHK) reaction to couple the C11 aldehyde of the spiroketal fragment (**141** in figure 41) with a C10 vinyl bromide positioned at the terminus of the linear domain (**135**).^{202,203} These extraordinarily mild conditions should permit the bulk of the side-chain esters to be present prior to the final assembly. Furthermore, the NHK reaction is highly selective for aldehydes over ketones. Consequently, if we were to perform an oxidative cleavage of the α -hydroxy ketone of **379** to produce aldehyde **141**, it would obviate the regioselectivity issues that threatened to complicate our previous strategies.

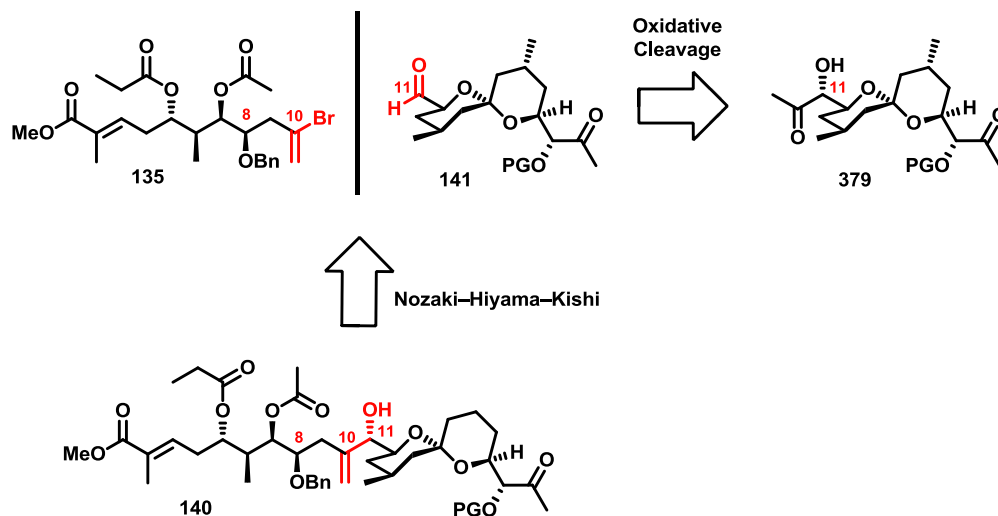


Figure 41. A retrosynthetic analysis for the final assembly of didemnaketal A, featuring an NHK coupling

Following a successful coupling, very few transformations would be left to complete the synthesis. A diastereoselective hydrogenation of the allyl alcohol **140** to set the C10 stereocenter should also liberate the C8 alcohol from its benzyl protecting group. This one-pot transformation would be very convenient since it would allow both the C8 and C11 alcohols to be synchronously converted to isovaleric esters, completing the synthesis upon final deprotection.

Although the NHK approach appears to be imminently practicable, it requires a tactical sacrifice of the C11 stereochemistry. The chirality at this stereocenter was correctly established during the desymmetrizing asymmetric dihydroxylations (see scheme 78); however, the preparation of the aldehyde coupling partner **141** requires ablating this stereochemistry, only to immediately reestablish it in the subsequent step. The fidelity of this stereocenter would then depend of the natural diastereoselectivity of the NHK

reaction. An analysis using the Felkin-Ahn model^{204,205} indicates that the preferred trajectory of the nucleophile could lead to undesired net epimerization of the C11 alcohol (column 1 in table 10). On the other hand, the presence of a heteroatom substituent at the α position of the aldehyde suggests the addition may be chelate-controlled. The Cram chelate model^{206,207} predicts a preference for the targeted diastereomer (column 2 in table 10). Naturally, we were eager to learn which model was accurate.

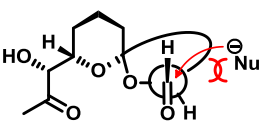
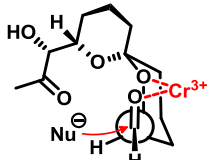
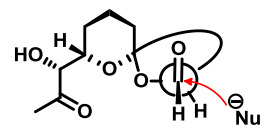
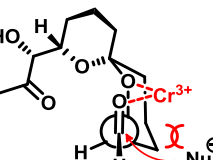
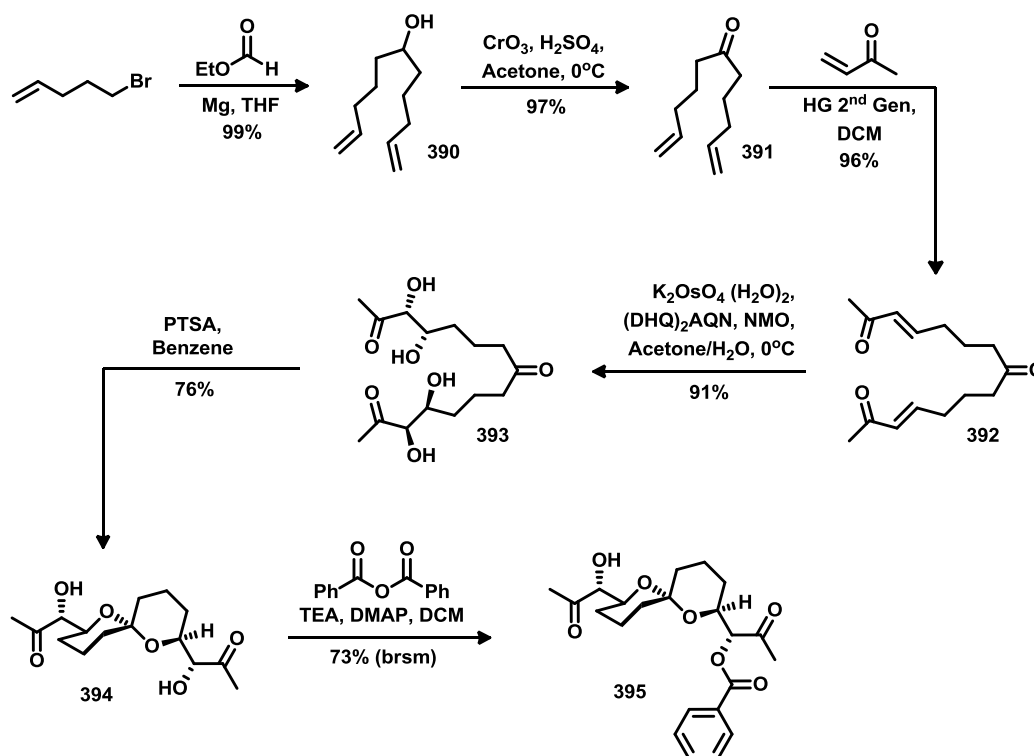
Felkin–Ahn Model	Cram Chelate Model	C11 Stereochemistry
 <p>entry 1 disfavoured</p>	 <p>entry 3 favoured</p>	<u>Correct</u>
 <p>entry 2 favoured</p>	 <p>entry 4 disfavoured</p>	<u>Incorrect</u>

Table 10. A comparison between the Felkin–Ahn and Cram Chelate models for predicting the stereochemical outcome on the C11 alcohol of **140** following an NHK coupling

6.2 Model Spiroketal

Given the foreseeable obstacles present in each of our coupling strategies, we were hesitant to rush into this enterprise and rapidly squander our reserves of the precious precursors. Instead, we hoped to explore our options using an expendable model system—ideally a close analogue which could be prepared rapidly and on gram scale.

By adapting preliminary work published by Ito⁷⁰ along with our own established methods, we were able to produce an expedient synthesis for a non-methylated analogue of didemnaketol's spirocyclic framework. First, a Grignard reagent prepared from bromopent-1-ene was added twice to ethyl formate, producing alcohol **390** in excellent yield. This alcohol was oxidized with the Jones reagent then a high yielding cross metathesis provided compound **392**, the non-methylated analogue of the long-pursued *meso* precursor **142**. As before, Sharpless asymmetric dihydroxylations under our optimized conditions delivered compound **393** in high yield. Treating this tetraol with a catalytic quantity of *p*-toluenesulfonic acid afforded the desired spiroketal (**394**) on multigram scale.



Scheme 82. An expedient synthesis of the non-methylated analogue of the spiroketal domain of didemnaketol A

We found the non-methylated spiroketal (**394**) to be highly crystalline and we were able to solve its structure by X-ray analysis, thereby confirming the relative stereochemistry and the C_2 symmetry of the product (see figure 42). Due to this higher order of symmetry compared to compound **341**, the two free alcohols were chemically equivalent. Consequently, we were able to mono-protect **394** in good yield using benzoyl anhydride with only a trivial chromatographic separation required to isolate **395** from the starting material and the difunctionalized byproduct.

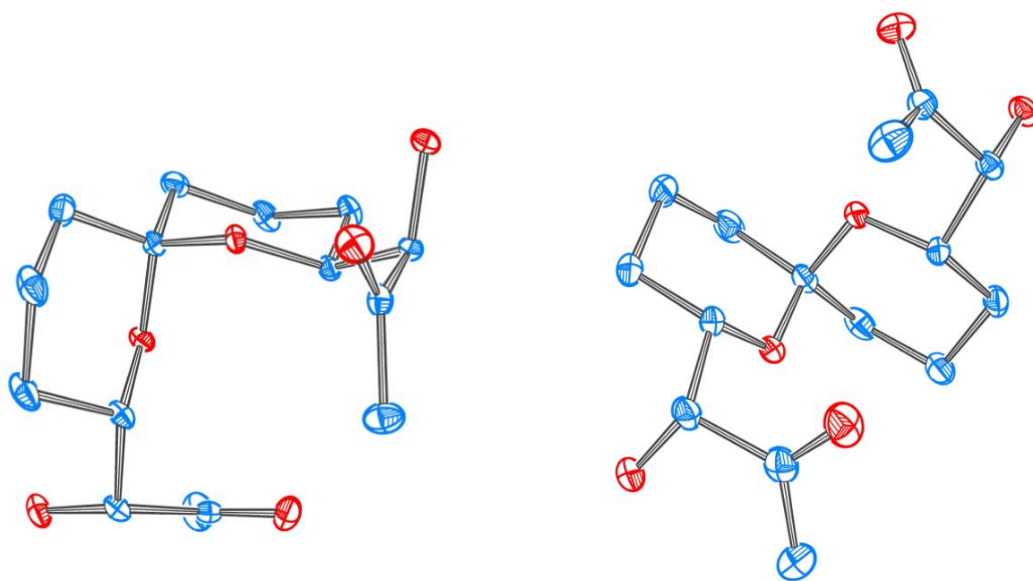
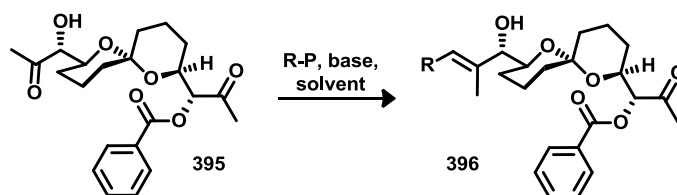


Figure 42. Crystal structure of the model spiroketal **394**

6.3 Preliminary Coupling Attempts

Initially, we used this model system to probe the Wittig-type olefination approach for accomplishing the coupling (see table 11). The benzoyl protected spiroketal **395** was treated with a series of commercially available stabilized (entry 4 in table 11) and non-stabilized ylides (entry 1-3 in table 11), as well as a stabilized alkyl phosphonate

carbanion, *as per* the Horner–Wadsworth–Emmons reaction (entry 5 in table 11). Unfortunately, in each case, we found our starting material to be unreactive. Although there is considerable precedent for performing phosphorus-mediated olefinations in the presence of unprotected alcohols,^{208,209} we suspected that the labile hydrogen adjacent to the reaction site may have contributed to the failure of these preliminary experiments. It quickly became evident that adapting this approach to suit our synthesis would not be trivial; consequently, this chemistry was deprioritized in favour of the more promising NHK coupling.

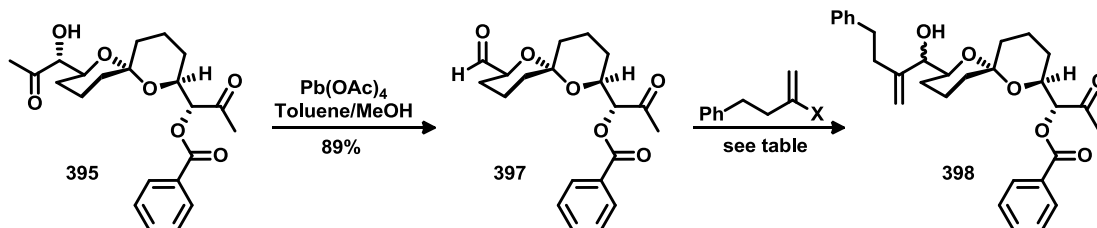


Entry	R	P	Base (equiv.)	Solvent	Result
1	<chem>Ph-CH2-CH2-CH2-CH2-</chem>	Ph_3P^+	nBuLi (1)	THF	no reaction
2	<chem>Ph-CH2-CH2-CH2-CH2-</chem>	Ph_3P^+	nBuLi (1)	DMSO	no reaction
3	<chem>Ph-CH2-CH2-CH2-CH2-</chem>	Ph_3P^+	nBuLi (3)	THF	no reaction
4	<chem>EtO-C(=O)-CH2-CH2-</chem>	Ph_3P^+	NaH (1.5)	THF	no reaction
5	<chem>CH3-C(=O)-CH2-</chem>	<chem>COP(=O)(OMe)-</chem>	NaH (1.5)	THF	no reaction

Table 11. Attempted Wittig-type olefinations aimed at probing the final assembly of didemnaketal A

Upon treating the mono-protected spiroketal **395** with lead (IV) acetate, we found we could selectively cleave between the ketone and the free alcohol. The resulting aldehyde (**397** in table 12) was isolated in good yield. We then followed literature procedures to

prepare simple vinyl halides to act as a crude surrogate for the linear fragment as we investigated the NHK reaction.^{210,211}



Entry	X (equiv.)	Conditions	Yield
1	Br (2)	NiCl ₂ , CrCl ₂ , DMSO	no rxn
2	Br (2)	NiCl ₂ , CrCl ₂ , DMF	72%
3	Br (2)	NiCl ₂ , CrCl ₂ , THF	no rxn
4	I (2)	NiCl ₂ , CrCl ₂ , LiI, THF	41%
5	Br (2)	NiCl ₂ , CrCl ₃ , LAH, THF	decomp
6	Br (2)	CrCl ₃ (cat), TMSCl, TEA, Mn, THF	no rxn
8	I (2)	NiCl ₂ , CrCl ₂ , DMF	81%
9	I (3)	NiCl ₂ , CrCl ₂ , DMF	93%

Table 12. An evaluation of NHK coupling conditions aimed at probing the final assembly of didemnaketal A

In addition to a catalytic quantity of NiCl₂, the NHK reaction typically employs an excess of CrCl₂, a salt which is extremely sensitive to both air and moisture. The nickel species, after an *in situ* reduction to Ni(0), is believed to insert into the carbon–halogen bond.^{212,213} This is followed by a transmetalation with chromium which generates the attacking nucleophile. The sensitivity and the insolubility of these salts limited our solvent choice to anhydrous DMSO, THF, or DMF. We found that the reaction failed in both DMSO and THF (entries 1 and 3 in table 12), though we were able to achieve moderate yields using THF in the presence of LiI (entry 4 in table 12).²¹⁴ Ultimately, however, DMF emerged as the superior solvent, facilitating the coupling between the

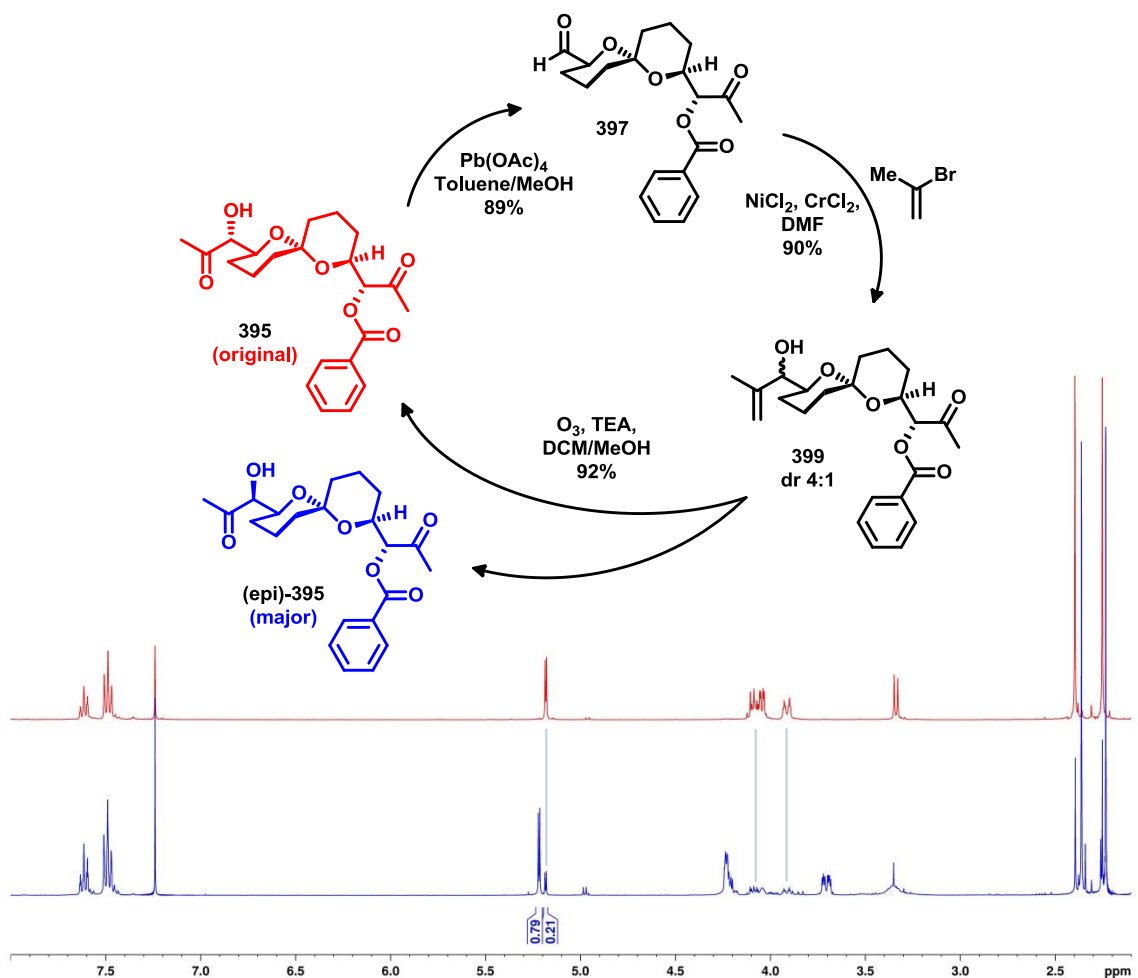
spiroketal and the vinyl bromide in good yield (entry 2 in table 12). As anticipated, the ketone was unreactive and the ester functionality remained intact.

Several groups have developed strategies to circumvent the difficulties associated with handling CrCl_2 outside of a glove-box. For instance, it is possible to generate highly reactive CrCl_2 *in situ* by reducing the far more stable CrCl_3 with lithium aluminum hydride (entry 5 in table 12).²¹⁵ Alternatively, a catalytic version of the NHK reaction has been developed which uses manganese as a stoichiometric reductant (entry 6 in table 12).²¹⁶ Unfortunately, neither of these modified approaches were successful in our hands.

Encouragingly, we found that by switching the vinyl bromide to a vinyl iodide we were able to increase our yield of **398** by almost 10% (entry 8 in table 12). Likewise, increasing the number of equivalents of the vinyl halide also improved the yield by about 10% (entry 9 in table 13). It is likely that a larger excess of the vinyl halide helps to compensate for reagent that is lost side reactions like Kumada-type homo-couplings. Combined, these two improvements allowed us to model our coupling in greater than 90% yield. Though this excellent yield creates an appearance of efficiency, we recognize that using a three-fold excess of the actual vinyl bromide precursor (*ie.* **135**) would be intolerably wasteful. Nevertheless, we were heartened by these preliminary results.

6.4 Transformation-based Assignment of Stereochemistry

The far more pressing concern was over the stereoselectivity of the reaction. Our trials using the model spiroketal consistently produced between a 3:1 and 4:1 mixture of inseparable diastereomers. It was obvious that the nucleophilic addition had a strong natural bias; however, we were not able to discern from the NMR data whether the reaction favored the orientation of the natural product or that of its C11 epimer.

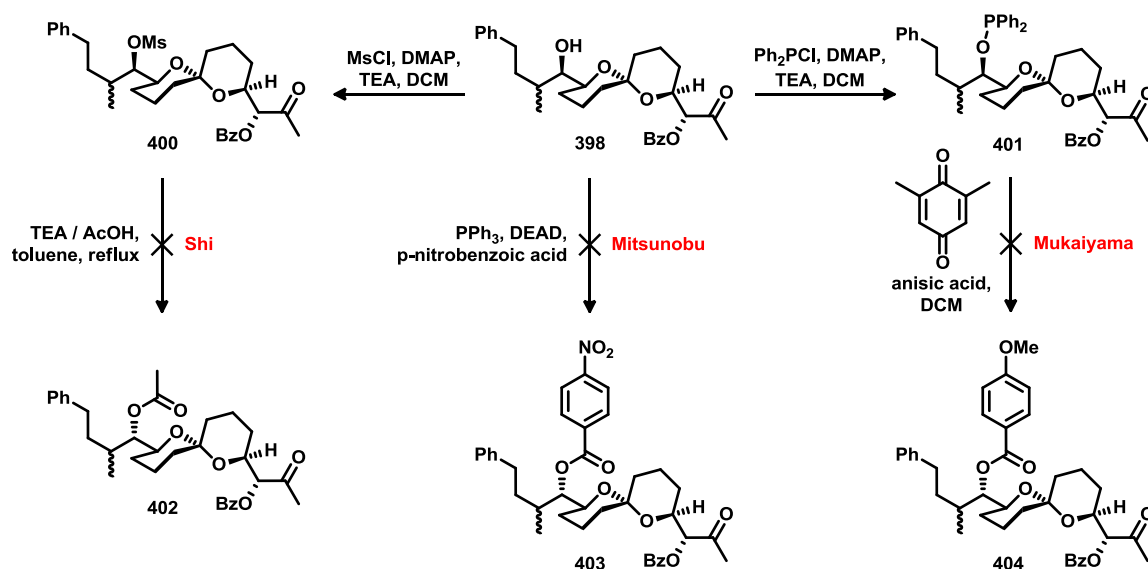


Scheme 83. ¹H NMR spectral overlay comparing the initial spiroketal starting material (**395** in red) with the diastereomeric mixture obtained after oxidative cleavage, NHC coupling using methyl vinyl bromide, then ozonolysis (in blue)

To solve this puzzle, we performed the NHK reaction using 2-bromopropene and, as expected, we once again obtained a 4:1 mixture of diastereomers about the allylic alcohol (**399** in scheme 83). We recognized that an ozonolysis of the newly installed olefin should restore the gross structure of the original mono-protected model spiroketal (**395**). In theory, if the NHK coupling had proceeded under chelate control, the mode which produces the desired stereochemical orientation at the C11, then the resulting NMR spectra of the major product should be a precise match to that of the original sample. Any discrepancies between in the NMR profile would suggest an unfortunate epimerization of the alcohol.

After performing the ozonolysis in a methanolic solution buffered with triethylamine, we found that indeed the bulk of the mixture had undergone isomerization. The spectral overlay in scheme 83 clearly shows that the original spiroketal material (spectrum shown in red) has become the minor component of the mixture following the three step sequence (spectrum shown in blue).

Our disappointment over this result was compounded by our inability to correct the stereochemistry through an inversion of the alcohol. Mitsunobu's conditions, optimized for hindered reaction sites,²¹⁷ Mukaiyama's lesser known procedure,²¹⁸ and Shi's method of mesylate substitution²¹⁹ all had no effect on the starting material (shown in scheme 84.)



Scheme 84. Three methods for inverting hindered alcohols that failed to accomplish the desired epimerization of the C11 alcohol

In point of fact, we ought to have anticipated this stereochemical outcome for the NHK coupling since it closely agrees with results previously reported by Fuwa (see scheme 6).⁷² Although he was operating on the C21 carbonyl, the pseudo symmetry about the spiroketal moiety of didemnaketal A would suggest a strong degree of analogy with our nucleophilic addition onto the C11 aldehyde. Fuwa was able to resolve his dilemma by performing a redundant oxidation / reduction sequence on the alcohol, thereby shifting the ratio of diastereomers to his advantage. It is likely that this strategy would also work in our case; however, implementing it would require an additional protection / deprotection sequence to spare our C22 ketone on top of the oxidation and reduction reactions.

6.5 Recent Developments

As we were struggling through these final steps there was a flourish of articles published on the synthesis and structure of the didemnaketals. The first syntheses for the published structures of didemnaketals A and B were both announced in close succession by Tu⁶⁸ and Fuwa,⁷¹ respectively. In both cases, however, the spectral data of the targeted compounds were found to be incongruous with the authentic samples. The weight of this evidence called into question Faulkner's original structural assignments.⁵⁶ It left us questioning the future course of this project. Clearly, there was no reason for us to continue pursuing a spurious target; however, shifting our efforts toward arbitrarily chosen isomers would likely result in an expensive and laborious wild-goose chase.

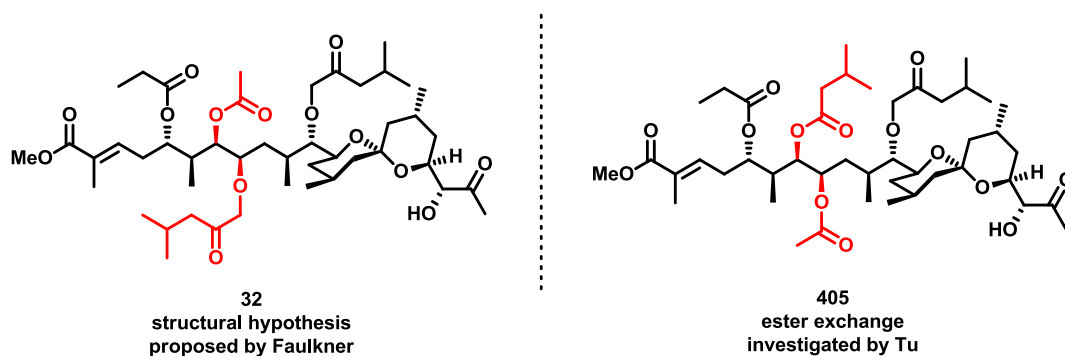


Figure 43. The original structural hypothesis proposed for didemnaketal A and a structural isomer prepared by Tu, neither of which matched the spectral data for the authentic sample

Tu, for instance, revealed one of the many spurious permutations.²²⁰ Possibly operating under the hypothesis that ester functionality had inadvertently gotten shuffled during Faulkner's characterization experiments, Tu prepared a version of didemnaketal A in which the esters derived from the C7 and C8 alcohols were switched (**405** in figure 43).

Unfortunately, the NMR data on this compound was also poor match for the data published on the natural isolate.

After scrutinizing the data, we reached an alternative hypothesis concerning the identity of the natural product. As described in chapter one, it appeared to us that Faulkner had mistakenly inverted the entire spiroketal domain which encompasses seven stereogenic centers.⁵⁶ The relative stereochemistry in this problematic region was unambiguously established using X-ray crystallography. However, the assignment of the absolute stereochemistry rested on a dubious Mosher analysis where multiple δ -perturbing auxiliaries were positioned in close enough proximity to interfere with one another. We also noted a peculiar reversal of the direction in which the synthetic didemnaketals rotated plane-polarized light compared to the natural compounds.^{68,71} It would be difficult to attribute such a dramatic discrepancy to the epimerization of one or two carbon centers; instead, the optical rotation points to a constitutional restructuring of the original molecule. Finally, we noticed that the greatest discrepancies in the NMR data occurred between C8–C10 and C20–C21. We speculated that it was not coincidental that these regions correlated with the termini of the crystalized fragment. Assuming that the absolute stereochemistry of the central domain had been inverted in the structural hypothesis, then these two junctions would be where NMR-apparent inconsistencies in the relative stereochemistry would be most obvious. Unfortunately, as we had not yet even complete the synthesis of the falsified structure, we found ourselves poorly positioned to adapt our synthetic work to this conjectural version of the natural product (**406** in figure 44).

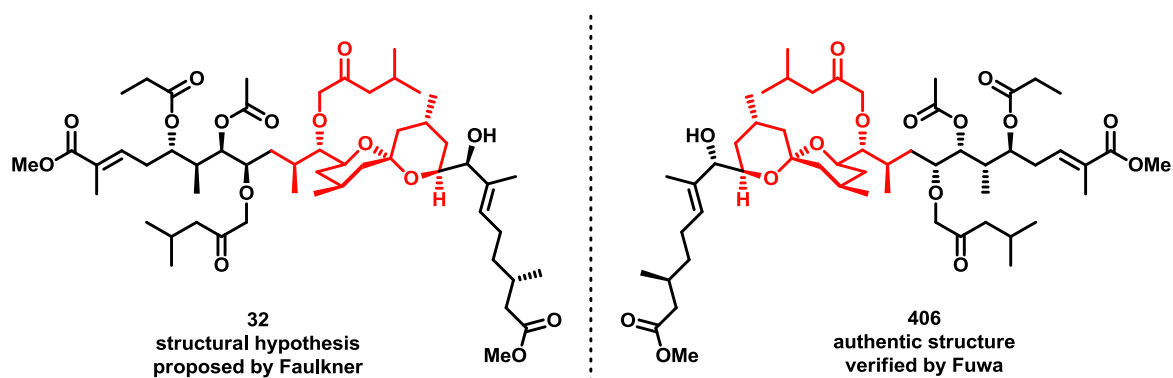


Figure 44. The original structural hypothesis proposed for didemnaketal B and the revised structure as verified by Fuwa in which the spiroketal moiety is inverted

Instead, it was Fuwa who confirmed our suspicions in a very recent publication.²²¹ Fuwa had already devised a highly convergent approach for assembling the nominal structure of didemnaketal B. While we sought to establish the bulk of the spiroketal architecture, along with its many stereocenters, in a single sweeping step; Fuwa, by contrast, opted to tackle each chiral center individually, deriving them from natural sources where possible and elaborating them into a series of simple, discreet units, then using these in a piecemeal assembly of the natural product. This strategy granted Fuwa an enviable degree of flexibility, allowing him to rapidly modify particular domains without significantly adjusting the order of assembly or the conditions used in the key coupling steps. As a result, he was able to rapidly complete the synthesis of a revised version of didemnaketal B in which the spiroketal core was enantiomeric to the nominal structure. He found that the spectral data for the synthetic product closely match the NMR profile that was reported by Faulkner. Though it remains to be seen, it is overwhelmingly likely that a similar structural revision would apply to our target, didemnaketal A.

6.6 Future Outlook

This revelation has dramatic repercussions on the future outlook of this project. It would be very simple for us to reverse the absolute stereochemistry in our synthesis by simply selecting the opposite AD-mix for the dihydroxylation step (refer to scheme 78). Unfortunately, based on Fuwa's structural amendment, we would also have to modify the relative stereochemistry between C20 and C21—an adjustment that significantly decreases the advantage of our symmetry driven approach. Thus, after recompleting the synthesis of the enantiomeric spiroketal, we would be forced to epimerize the C21 alcohol. Our previous experience with this transformation using our model spiroketal suggests that this is not a trivial task. Since Fuwa is ostensibly a mere oxidative cleavage away from also confirming the structure of didemnaketal A, we are left with very little incentive to reengineer our own synthesis.

At this point, the more interesting questions pertain to the biological activity of the natural product. For instance, by what mechanism do didemnaketals A and B trigger the dissociation of the HIV protease monomers and what structural features are important for this activity? By understanding the nature of the interaction between the natural product and the enzyme, it may be possible to develop robust molecular probes of HIV-PR dissociation, a truly understudied mode of antiretroviral activity.

The extent to which the spiroketal domain in particular contributes to molecular recognition is uncertain. Many organisms evolve the ability to generate complex molecular scaffolds to mimic or compliment small areas of a protein–protein interface.

There is a long-standing hypothesis that 2,2'-disubstituted spiroketals function as β -turn mimics, creating a rigid bend that orients the equatorial alkyl substituents into a nearly parallel geometry.¹⁸⁵ It is perhaps not coincidental that vast majority of known HIV-PR inhibitors share this distinctive tong-like aspect which allows them to destabilize the protease by disrupting a crucial β -sheet interaction.

On the other hand, there is good reason to be skeptical of this comparison. After extensive optimization, it was found that for the most potent molecular tong inhibitors are those in which the parallel peptides are separated by about 10 Å (*eg.* **23** in figure 45).^{35,40} Based on our crystallographic data, the spiroketal permits only slightly more than 5 Å space between the equatorial branches (*eg.* **407**). It would seem highly unlikely that such a tight bend would be suitable for intercalating between the *C*- and *N*- termini of the protease monomer. This theoretical inconsistency seems to support Rich's claim that the spiroketal moiety of didemnaketel A contributes nothing to molecular recognition.⁵⁵ However, Rich had naïvely tested the mirror image of the actual spiroketal moiety; consequently, his claim of inactivity may not be credible.

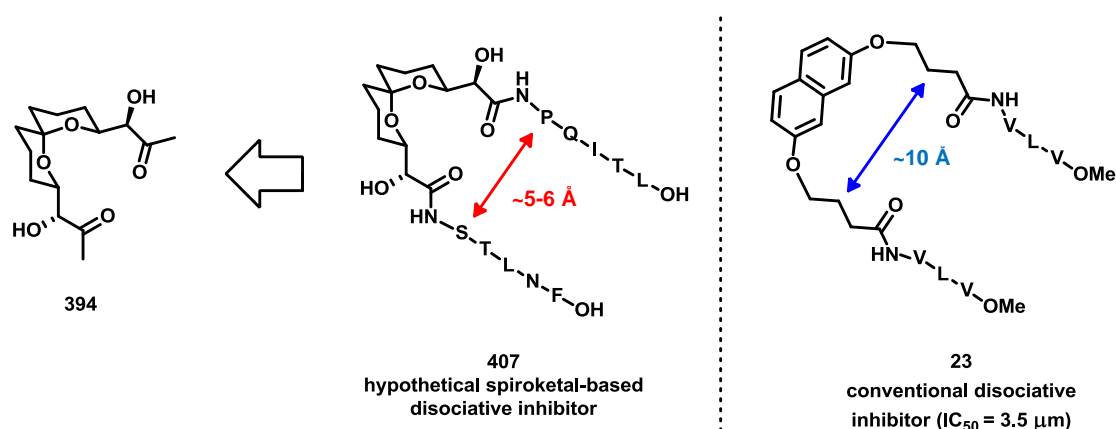


Figure 45. A possible dissociative inhibitor derived from the symmetrical didemnaketel-like spiroketal **407** compared with an established molecular tong inhibitor of HIV-PR (**23**)

We find we are now in a good position to test these opposing hypotheses. With the symmetrical spiroketal core **394** readily accessible in gram quantities, it would be trivial to graft on two peptidic sidechains with amino acid sequences that complement the *C*- and *N*- termini of the protease monomer (eg. **407**). If these molecules display any of the desired activity then it may be worthwhile to develop analogues with didemnaketel-like linear branches. The spiroketal structures developed in our research could prove to be useful scaffolds for developing robust analogues of didemnaketel A that match or even exceed the natural product's unique inhibitory activity toward HIV protease.

Chapter 7 — Experimental

7.1 General Remarks

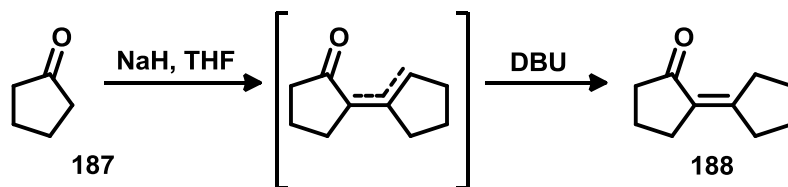
Reactions were typically carried out in flame-dried glassware fitted with rubber septa and using a rubber balloon to create a positive pressure of argon. Commercial solvents were used as received from commercial suppliers with the following exceptions: tetrahydrofuran was distilled over sodium and benzophenone; benzene was distilled over calcium hydride; finally, diethyl ether, acetonitrile, methanol, and toluene were passed through alumina column in a commercial solvent purification system (SPS). Likewise, reagents were generally used as received with several notable exceptions: methyl vinyl ketone was dried over finely ground calcium(II) chloride and potassium carbonate, filtered, and then distilled under reduced pressure (70 °C / 350 mm Hg); zirconium(IV) chloride was sublimed under reduced pressure (250 °C / 0.02 mm Hg) and stored in a glovebox; triethylamine was distilled over calcium hydride; hexamethylphosphoramide was passed through a 6 cm column of crushed 3 Å molecular sieves then distilled from calcium hydride under reduced pressure (100 °C / 2 mm Hg). Liquid reagents and solvents were transferred using either glass or rubber-free plastic syringes fitted with stainless steel needles. Organic solutions were concentrated by rotary evaporation using a water bath warmed to between 25 and 50 °C under a vacuum pressure of ~25 mm Hg. Reactions were monitored by analytical TLC, performed on aluminum plates precoated with silica gel (0.20 mm, 60 Å pore size, 230–400 mesh, Macherey-Nagel) impregnated

with a fluorescent indicator. The TLC plates were visualized by exposure to ultraviolet light (254 nm) or a *p*-anisaldehyde indicator solution and heat. Compounds were purified by flash column chromatography with either silica gel (60 Å, 63–200 µM, Caledon) or Florisil (standard grade, 100–200 mesh, Caledon) or, alternatively, using a CombiFlash Rf Teledyne ISCO fitted with SilicaSep columns according to preprogrammed gradients of ethyl acetate–hexane or methanol–dichloromethane.

¹H NMR spectra were recorded on Bruker Avance–300, –400 and –500 MHz spectrometers. The chemical shifts were reported in parts per million (ppm, δ scale) downfield from TMS, and were referenced to residual protium in the NMR solvent (CDCl₃, δ = 7.24 ppm). Standard abbreviations (s = singlet, d = doublet, t = triplet, q = quartet, m = multiplet and/or multiple resonances, br = broad, app = apparent) were used to indicate spin multiplicities. The ¹³C NMR spectra were recorded at either 75 MHz or 125 MHz and the chemical shifts were referenced to the carbon resonances of the solvent (CDCl₃, δ = 77.00 ppm). IR spectra were obtained using a Perkin-Elmer 1000 FT-IR spectrometer referenced to a polystyrene standard. The frequency of absorption (cm⁻¹) and the intensity of the signal (s = strong, m = medium, w = weak, br = broad) were noted. High-resolution mass spectra were acquired either at the UVic Proteomics Center on a Thermo scientific Orbitrap Velos system or by Prof. Aviv Amirav at Tel Aviv University using the Aviv Analytical model 5975-SMB-GC–MS. In the latter case, the empirical formulas were extracted from the true natural abundance isotope pattern around the presented molecular ion using isotope abundance analysis (IAA) software.²²² The reported matching factors indicate the goodness of fit; factors of >800 were stipulated for

acceptance of a molecular formula. All X-ray crystallography was performed by Prof. Allen Oliver using a Bruker APEX-II diffractometer at Molecular Structure Facility in the University of Notre Dame.

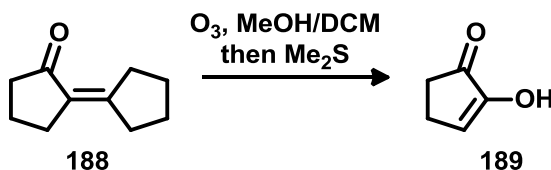
7.2 Experiments pertaining to Chapter 2



Sodium hydride (60% dispersion in mineral oil) was washed with pentane three times under an atmosphere of argon then the residual solvent was removed under high vacuum. The activated NaH (1.31 g, 0.5 equiv, 54.5 mmol) was transferred to a flame-dried round-bottom flask, suspended in freshly distilled tetrahydrofuran (60 mL) and cooled to 0 °C. The cyclopentanone was divided into two equal portions. Upon adding the first portion (4.62 g, 0.5 equiv, 55.0 mmol) vigorous bubbling was observed and the colourless solution turned light brown. After allowing the reaction to stir at 0 °C for 60 min, the second portion of cyclopentanone (4.62 g, 0.5 equiv, 55.0 mmol) was added dropwise. The reaction continued to stir overnight, acclimating to room temperature. The reaction was then quenched with a saturated solution of aqueous NH₄Cl. The crude material was extracted into ethyl ether (2 × 10 mL), washed with water (2 × 10 mL) and brine (10 mL), dried over anhydrous MgSO₄, filtered, and then concentrated. The residue was taken up in dichloromethane (10 mL) and treated with DBU (1.51 g, 0.10 equiv, 0.0110 mmol) to converge the unconjugated regioisomer with **188**. After 6 hours at room

temperature the reaction was transferred to a separatory funnel and washed with saturated solution of aqueous NH_4Cl (3×10 mL), followed by washes with water (10 mL) and brine (10 mL). The organic layer was separated and dried over anhydrous MgSO_4 , filtered, and concentrated by rotary evaporator. The resulting residue was then purified to a colourless oil by kugelrohr distillation (90 °C at 0.2 mmHg), providing the desired product, **188** (5.62 g, 63%).

188. ^1H NMR (300 MHz, CDCl_3) δ 2.79–2.67 (m, 2H), 2.47 (m, 2H), 2.28–2.17 (m, 4H), 1.91–1.78 (m, 2H), 1.71–1.58 (m, 4H); ^{13}C NMR (75 MHz, CDCl_3) δ 207.36 (C), 158.61 (C), 127.89 (C), 39.79 (CH_2), 34.28 (CH_2), 32.53 (CH_2), 29.51 (CH_2), 26.93 (CH_2), 25.22 (CH_2), 20.07 (CH_2). Spectral assignments are in good agreement with previously published data.²²³



Ketone **188** (4.03 g, 1.0 equiv, 26.8 mmol) was taken up in methanol (60 mL) and cooled to -78 °C. Para-Red (< 0.5 mg) was added to the colourless solution, causing an orange colour change. The reaction was sparged with ozone until the orange colour disappeared. Continuing the reaction past the Para-Red endpoint was found to cause over oxidation of the product; thus, at this point argon was bubbled through the solution to purge excess ozone. Dimethyl sulfide (4 mL) was then added to the mixture while at -78 °C, after which the reaction was allowed to acclimate to room temperature as it stirred

overnight. The solvent was removed by rotary evaporation and the resulting yellow oil was purified by kugelrohr distillation (45 °C at 0.2 mmHg) producing compound **189** as a colourless oil (2.13 g, 81%) that solidified to a waxy white solid upon standing.

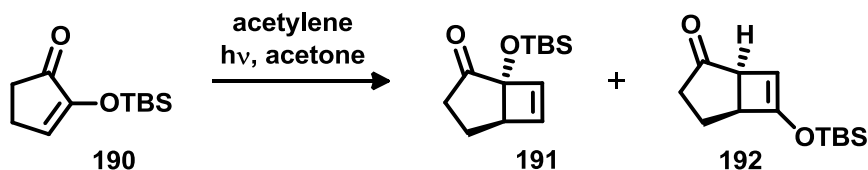
189. ^1H NMR (300 MHz, CDCl_3) δ 6.54 (t, $J = 3.1$ Hz, 1H), 5.73 (br s, 1H), 2.49 (ddd, $J = 3.5, 3.0, 1.4$ Hz, 2H), 2.43 (ddd, $J = 3.6, 2.3, 0.9$ Hz, 2H); ^{13}C NMR (75 MHz, CDCl_3) δ 204.2 (C), 153.0 (C), 129.8 (CH), 32.1 (CH_2), 21.8 (CH_2). Spectral assignments are in good agreement with previously published data.²²⁴



A flame-dried round bottom flask was charged with alcohol **189** (0.195 g, 1.0 equiv, 1.98 mmol) and 5 mL of dichloromethane. DMAP (24.1 mg, 0.10 equiv, 0.198 mmol) was added, followed by triethylamine (0.588 g, 3.0 equiv, 5.94 mmol). The reaction stirred at room temperature for 3 h and was then quenched using a saturated solution of aqueous NH_4Cl (10 mL). The aqueous phase was extracted with dichloromethane (2×15 mL) and the combined extracts were washed with water (10 mL) and brine (10 mL) then dried over MgSO_4 , filtered, and concentrated by rotary evaporation. The crude residue was purified by flash chromatography [silica, ethyl ether–hexanes, 1:4] giving compound **190** (0.287 g, 69%) as pale yellow oil.

190. ^1H NMR (300 MHz, CDCl_3) δ 6.61 (t, $J = 3.0$ Hz, 1H), 2.55–2.43 (m, 2H), 2.43–2.31 (m, 2H), 0.95 (s, 9H), 0.19 (s, 6H); ^{13}C NMR (75 MHz, CDCl_3) δ 207.0 (C), 152.8 (C), 135.6 (CH), 38.1 (CH_2), 30.9 (CH_2), 25.6 (CH_3), 18.3 (C), -4.6 (CH_3).

Spectral assignments are in good agreement with previously published data.²²⁵

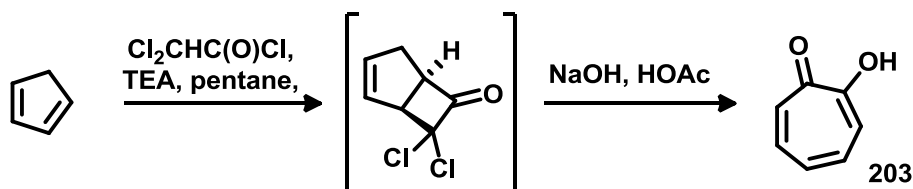


Using a high-pressure reaction flask, enone **190** (95.0 mg, 1.0 equiv, 0.448 mmol) was dissolved in acetone (6 mL) and cooled to -78 °C, then acetylene was bubbled through the solution for ~15 min. The flask was immediately crimp-sealed and allowed to gradually (!) warm to room temperature before it was irradiated at 300 nm for 72 h inside an 8-bulb photoreactor. The crude mixture was then concentrated by rotary evaporation and purified by flash chromatography [silica, ethyl ether–hexanes, 1:19 to 1:9] providing compound **192** as the major product (69.2 mg, 64%) and **191** as the minor product (7.3 mg, 7%), both colourless oils.

191. ^1H NMR (300 MHz, CDCl_3) δ 6.38 (dd, $J = 2.7, 0.7$ Hz, 1H), 6.16 (d, $J = 2.6$ Hz, 1H), 3.23 (dt, $J = 7.2, 0.7$ Hz, 1H), 2.82 (ddd, $J = 18.0, 11.7, 9.2$ Hz, 1H), 2.18 (ddt, $J = 18.0, 8.3, 0.8$ Hz, 1H), 2.07–1.84 (m, 1H), 1.73 (ddt, $J = 13.5, 9.2, 0.9$ Hz, 1H), 0.87 (s, 9H), 0.09 (s, 6H); ^{13}C NMR (76 MHz, CDCl_3) δ 217.1 (C), 143.7 (CH), 138.9 (CH), 82.3 (C), 53.4 (CH), 32.7 (CH_2), 24.7 (CH_3), 20.0 (CH_2), 18.4 (C), -3.8 (CH_3); IR (neat, cm^{-1})

2965 (s), 2929 (s), 2875 (m), 1745 (s), 1472 (m), 1253 (s), 1081 (m), 838 (s), 779 (m); HRMS (ESI) calcd for $C_{13}H_{22}OSi + H^+$ 239.1462, found 239.1461.

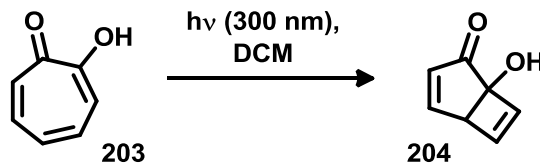
192. 1H NMR (300 MHz, $CDCl_3$) δ 4.64 (d, $J = 0.8$ Hz, 1H), 3.42 (ddd, $J = 7.6, 3.1, 0.6$ Hz, 1H), 2.86 (dddd, $J = 17.9, 11.8, 9.4, 1.2$ Hz, 1H), 2.73 (dt, $J = 2.9, 1.2$ Hz, 1H), 2.11 (ddt, $J = 17.8, 8.8, 1.4$ Hz, 1H), 1.99 (ddt, $J = 13.6, 9.5, 1.1$ Hz, 1H), 1.88–1.70 (m, 1H), 0.94 (s, 9H), 0.20 (s, 6H); ^{13}C NMR (75 MHz, $CDCl_3$) δ 217.4 (C), 153.9 (C), 102.8 (CH), 48.0 (CH), 44.0 (CH), 33.7 (CH_2), 25.5 (CH_3), 18.7 (CH_2), 18.0 (C), -4.60 (CH_3), -4.8(CH_3); IR (neat, cm^{-1}) 2962 (s), 2930 (m), 2875 (m), 1737 (s), 1485 (m), 1253 (m), 1081 (m), 765 (m); HRMS (ESI) calcd for $C_{13}H_{22}OSi + H^+$ 239.1462, found 239.1460.



A flame-dried two-necked round-bottom flask fitted with a reflux condenser was charged with dichloroacetyl chloride (31.0 mL, 1.0 equiv, 0.209 mol) and 300 mL of pentane. Freshly cracked cyclopentadiene (60.0 mL, 3.4 equiv, 0.713 mol) was then added and the solution was warmed to reflux. While refluxing, triethylamine (30.0 mL, 1.1 equiv, 0.211 mol) was added dropwise over 90 min. Heat was applied to the reaction for an additional 4h, during which time triethylamine hydrochloride salts precipitated from solution. After cooling, the salts were filtered through a pad of celite and the filtrate was washed with a

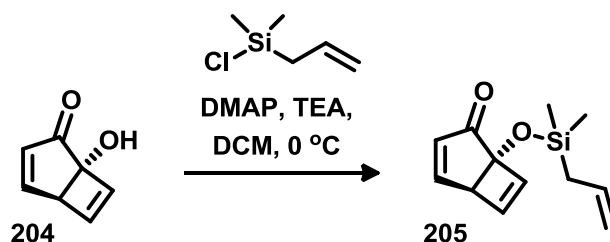
saturated solution of aqueous NH_4Cl (3×50 mL). The aqueous phase was then back-extracted with pentane (2×25 mL) and the combined organic extracts were washed with water (50 mL) and brine (50 mL) then dried over MgSO_4 , filtered, and concentrated by rotary evaporation. The resulting orange residue was purified to colourless oil (32.3g, 87%) by Kugelrohr distillation (75 °C / 2 mmHg). The purified intermediate was immediately added to round-bottom flask containing a solution of sodium hydroxide (30.0 g, 4.0 equiv, 0.750 mol) in 300 mL of glacial acetic acid and warmed to reflux. After 12 h, the reaction was cooled and acidified to a pH of ~ 1 using concentrated hydrochloric acid. The addition of benzene (300 mL) then caused a white precipitate to form which was separated by filtration through a pad of celite. After rinsing with additional benzene, the biphasic filtrate was transferred to a separatory funnel and the organic and aqueous phases were isolated. The aqueous phase was extracted with dichloromethane for 16 h using a continuous extractor. The combined organic extracts were concentrated by rotary evaporation and the resulting residue was taken up in the minimal amount of hot pentanes needed to fully solvate the oily residue. Upon cooling the solution to 4 °C overnight, amber needle-like crystals of tropolone **203** were formed (17.8g, 70% over two steps).

203. ^1H NMR (300 MHz, CDCl_3) δ 7.44–7.30 (m, 4H), 7.04 (tt, $J = 8.8, 1.7$ Hz, 1H); ^{13}C NMR (76 MHz, CDCl_3) δ 172.0 (C), 137.8 (CH), 128.4 (CH), 124.0 (CH); IR (neat, cm^{-1}) 3207 (br), 1615 (s), 1545 (m); HRMS (ESI) calcd for $\text{C}_7\text{H}_6\text{O}_2 + \text{H}^+$ 123.0441, found 123.0443.



Tropolone (0.100 g, 1.0 equiv, 0.820 mmol) was added to a 20 × 150 mm Pyrex test tube and dissolved in dichloromethane (2 mL). Degassing was accomplished by bubbling argon through the pale yellow solution for approximately ten minutes. Immediately afterwards, a second empty 16 × 100 mm Pyrex test tube was inserted into the larger test tube, pressing the solution into a thin layer between the two glass walls. The outer test tube was sealed with a rubber stopper wrapped with parafilm, then placed inside a Kimax beaker and irradiated at 300 nm for 15 h inside an eight-bulb photo-reactor. The solvent was removed by rotary evaporation and the resulting yellow oil was purified by flash chromatography [silica, ethyl ether–hexanes, 1:1 to 4:1] to provide **204** (0.083 g, 83%) as a pale yellow oil.

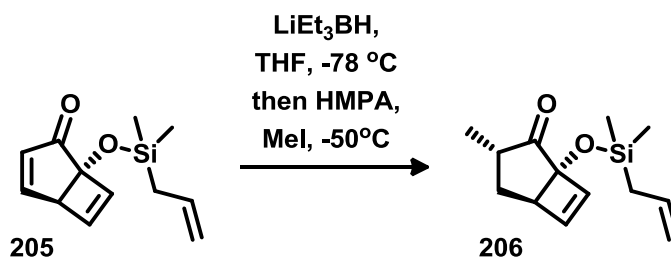
204. ^1H NMR (300 MHz, CDCl_3) δ 7.70 (dd, $J = 6.1, 2.6$ Hz, 1H), 6.76 (dd, $J = 2.7, 0.8$ Hz, 1H), 6.30 (d, $J = 2.6$ Hz, 1H), 6.15 (d, $J = 6.1$ Hz, 1H), 5.30 (s, 1H), 3.83 (d, $J = 2.7$ Hz, 1H); ^{13}C NMR (75 MHz, CDCl_3) δ 206.9, 162.1, 145.9, 138.1, 132.1, 81.2, 57.5; IR (neat, cm^{-1}) 3388 (br), 3060 (m), 2952 (m), 1669 (s), 1572 (m), 1278 (m), 1183 (m), 1060 (m); HRMS (ESI) calcd for $\text{C}_7\text{H}_6\text{O}_2 + \text{H}^+$ 123.0441, found 123.0439.



205. Alcohol **204** (0.995 g, 8.14 mmol, 1.0 eq) was added to a flame-dried round-bottom flask and dissolved in dichloromethane (50 mL). The solution was cooled to 0 °C and DMAP (100.0 mg, 0.0814 mmol, 0.10 eq), freshly distilled triethylamine (3.20 g, 16.2 mmol, 3.0eq), and dimethylallylsilyl chloride (1.31 g, 9.76 mmol, 1.2 eq), were sequentially added. The reaction stirred overnight, acclimating to room temperature. Upon quenching with saturated NaHCO₃ solution (10 mL), the crude mixture was extracted with ethyl ether (3 × 15 mL) and the combined organic layer was washed with saturated NaHCO₃ solution (20 mL), H₂O (2 × 20 mL), and brine (20 mL) then dried over MgSO₄, filtered, and concentrated by rotary evaporation. The crude material was purified by flash chromatography [florisil, dichloromethane–hexanes, (1:1)] giving compound **205** (1.49 g, 84%) as pale yellow oil.

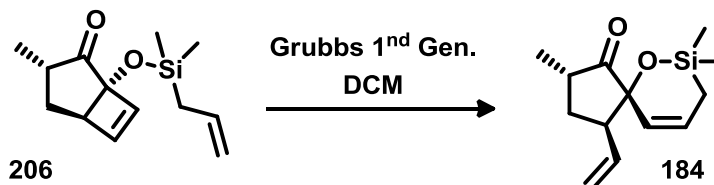
205. ¹H NMR (300 MHz, CDCl₃) δ 7.60 (dd, *J* = 6.1, 2.8 Hz, 1H), 6.73 (dd, *J* = 2.6, 1.1 Hz, 1H), 6.32 (d, *J* = 2.6 Hz, 1H), 6.21–5.99 (m, 1H), 5.79 (ddt, *J* = 17.1, 10.2, 8.1 Hz, 1H), 4.90 (ddt, *J* = 11.0, 2.2, 1.2 Hz, 1H), 4.88–4.84 (m, 1H), 3.72 (dd, *J* = 2.8, 0.9 Hz, 1H), 1.67 (ddd, *J* = 6.5, 3.8, 2.7 Hz, 2H), 0.20 (s, 3H), 0.19 (s, 3H); ¹³C NMR (75 MHz, CDCl₃) δ 205.4 (C), 160.4 (CH), 145.6 (CH), 138.4 (CH), 134.0 (CH), 132.7 (CH), 114.0

(CH₂), 113.9 (C), 58.3 (CH), 25.8 (CH₂), 0.00 (CH₃), -0.5 (CH₃); IR (neat, cm⁻¹) 3077 (m), 2960 (m), 2922 (m), 1716 (s), 1630 (m), 1283 (s), 1256 (s), 1188 (s), 1070 (m), 892 (s); HRMS (ESI) calcd for C₁₂H₁₆O₂Si + H⁺ 243.0812, found 243.0809.



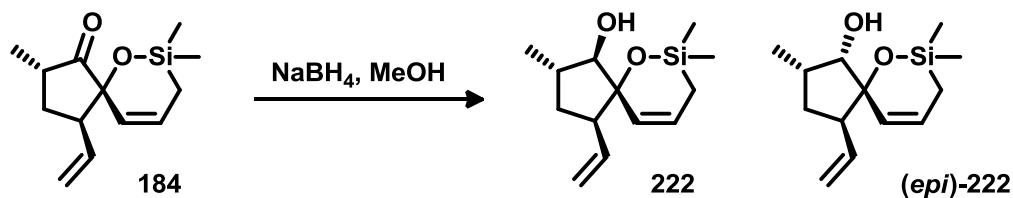
Ketone **205** (1.49 g, 1.0 equiv, 6.76 mmol) was added to a flame-dried round-bottom flask and taken up in freshly distilled tetrahydrofuran (30 mL). The mixture was cooled to $-78\text{ }^\circ\text{C}$ and a solution of LiHBEt_3 (1.0 M in THF, 7.50 mL, 1.1 equiv, 7.50 mmol) was added dropwise. After 90 min, MeI (1.92 g, 2.0 equiv, 13.5 mmol) was added followed immediately by freshly distilled HMPA (3.63 g, 3.0 equiv, 20.3 mmol). The reaction temperature was allowed to warm to $-40\text{ }^\circ\text{C}$ (caution: experience has shown that the reaction temperature should never exceed $-30\text{ }^\circ\text{C}$). After 4 h, the colourless reaction mixture was poured into a separatory funnel containing an ice cold biphasic mixture of ethyl ether (30 mL) and a saturated solution of aqueous NaHCO_3 (10 mL). When the reaction was not quenched in this particular manner, a bright yellow colour change would be observed along with severely diminished yields. The organic phase was then washed with a saturated solution of aqueous NaHCO_3 (20 mL), H_2O ($2 \times 20\text{ mL}$), and brine (20 mL) then dried over MgSO_4 , filtered, and concentrated by rotary evaporation. The resulting pale yellow oil, compound **206** (1.31 g, 82%), was satisfactorily clean, thus no further purification steps were typically performed.

206. ^1H NMR (300 MHz, CDCl_3) δ 6.44 (dd, $J = 2.7, 0.6$ Hz, 1H), 6.22 (d, $J = 2.8$ Hz, 1H), 5.79 (ddt, $J = 17.1, 10.2, 8.1$ Hz, 1H), 4.90 (ddt, $J = 11.0, 1.9, 1.1$ Hz, 1H), 4.85 (ddt, $J = 4.3, 2.2, 1.1$ Hz, 1H), 3.22 (d, $J = 7.2$ Hz, 1H), 3.10–2.76 (m, 1H), 2.01 (dd, $J = 13.2, 8.3$ Hz, 1H), 1.67 (dt, $J = 8.1, 1.3$ Hz, 2H), 1.58 (ddd, $J = 13.3, 11.9, 7.1$ Hz, 1H), 1.07 (d, $J = 6.9$ Hz, 3H), 0.16 (d, $J = 2.2$ Hz, 6H); ^{13}C NMR (75 MHz, CDCl_3) δ 216.9 (C), 142.8 (CH), 139.4 (CH), 134.2 (CH), 113.9 (CH_2), 83.7 (C), 51.8 (CH), 36.7 (CH), 29.0 (CH_2), 25.8 (CH_2), 13.5 (CH_3), -0.6 (CH_3), -0.7 (CH_3); IR (neat, cm^{-1}) 3042 (m), 2957 (s), 2933 (s), 2873 (m), 1704 (s), 1455 (m), 1288 (m), 1255 (m), 1087 (s), 985 (m), 762 (m); HRMS (ESI) calcd for $\text{C}_{13}\text{H}_{20}\text{O}_2\text{Si} + \text{H}^+$ 237.1306, found 237.1305.



Compound **206** (0.211 g, 1.0 equiv, 0.892 mmol) was added to a flame-dried round-bottom flask and dissolved in dichloromethane (15 mL). Grubbs 2nd Generation catalyst (30.0 mg, 5 mol%) was then added, causing the colourless solution to turn light brown. After stirring the reaction overnight at room temperature, the catalyst was poisoned with ~2 mL of ethyl vinyl ether, allowing an additional 30 min. The solvent was removed by rotary evaporation and the crude material was purified through a plug of silica gel [silica, ethyl ether–hexane, 1:5], providing compound **184** (0.171 g, 80%) as a colourless oil.

184. ^1H NMR (300 MHz, CDCl_3) δ 6.15–6.05 (m, 1H), 5.88 (ddd, $J = 17.8, 9.9, 6.3$ Hz, 1H), 5.55 (dd, $J = 10.5, 2.7$ Hz, 1H), 5.17 (dt, $J = 5.2, 1.7$ Hz, 1H), 5.13 (q, $J = 2.1$ Hz, 1H), 2.82–2.67 (m, 1H), 2.51–2.33 (m, 1H), 2.10 (ddd, $J = 13.6, 11.8, 9.8$ Hz, 1H), 1.76 (ddd, $J = 13.5, 7.5, 2.6$ Hz, 1H), 1.46 (dt, $J = 16.3, 3.4$ Hz, 1H), 1.32 (dd, $J = 16.7, 7.3$ Hz, 1H), 1.17 (d, $J = 7.6$ Hz, 3H), 0.35 (s, $J = 3.4$ Hz, 3H), 0.11 (s, $J = 3.2$ Hz, 3H); ^{13}C NMR (76 MHz, CDCl_3) δ 217.0 (C), 136.3 (CH), 130.4 (CH), 124.4 (CH), 116.8 (CH_2), 86.1 (C), 48.8 (CH), 37.1 (CH), 30.3 (CH_2), 17.4 (CH_2), 13.3 (CH_3), 1.1 (CH_3), 0.6 (CH_3); IR (neat, cm^{-1}) 3081 (m), 3021 (m), 2960 (s), 2931 (s), 1749 (s), 1641 (w), 1460 (w), 1250 (s), 1201 (m), 1070 (m), 975 (s), 893 (s), 848 (s), 816 (s); HRMS (ESI) calcd for $\text{C}_{13}\text{H}_{20}\text{O}_2\text{Si} + \text{H}^+$ 237.1306, found 237.1305.



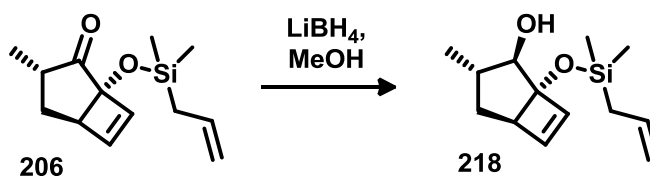
Ketone **184** (75.1 mg, 1.0 equiv. 0.317 mmol) was dissolved in methanol (6 mL) and cooled to 0 °C. Then NaBH_4 (15.0 mg, 1.2 equiv, 0.390 mmol) was added and the reaction stirred for 90 min. The solution was diluted with ethyl ether (20 mL) and washed with a saturated solution of aqueous NH_4Cl (10 mL), water (10 mL) and brine (10 mL). The organic phase was then dried over MgSO_4 , filtered, and concentrated by rotary evaporation. ^1H NMR analysis of the crude residue suggested a 1:1 ratio a diastereomers which proved to be separable by flash chromatography [silica, ethyl ether–hexanes, 1:4].

Both compound **222** (34.5 mg, 46 %) and (*epi*)-**222** (28.2 mg, 37%) were obtained as colourless oils.

222. ^1H NMR (300 MHz, CDCl_3) δ 6.20 (dt, $J = 10.8, 5.3$ Hz, 1H), 5.74 (ddd, $J = 17.0, 10.4, 7.6$ Hz, 1H), 5.54 (dt, $J = 11.0, 2.0$ Hz, 1H), 5.04 (ddd, $J = 9.1, 2.1, 1.3$ Hz, 1H), 4.99 (dq, $J = 2.3, 1.1$ Hz, 1H), 3.51 (br d, $J = 9.9$ Hz, 1H), 2.79–2.46 (m, 1H), 1.83 (ddd, $J = 11.5, 10.9, 6.2$ Hz, 1H), 1.80–1.69 (m, 1H), 1.52–1.41 (m, 2H), 1.28 (ddd, $J = 7.3, 3.4, 1.9$ Hz, 2H), 1.14 (d, $J = 6.6$ Hz, 3H), 0.21 (s, 3H), 0.14 (s, 3H); ^{13}C NMR (75 MHz, CDCl_3) δ 138.2 (CH), 129.5 (CH), 127.1 (CH), 115.8 (CH_2), 88.4 (CH), 87.0 (C), 50.3 (CH), 35.9 (CH), 32.5 (CH_2), 20.3 (CH_3), 12.7 (CH_2), 1.3 (CH_3), 0.9 (CH_3); IR (neat, cm^{-1}) 3429 (br), 2955 (m), 2927 (s), 2872 (m), 1640 (m), 1456 (m), 1398 (m), 1250 (m), 1187 (m), 1077 (m), 903 (s); HRMS (ESI) calcd for $\text{C}_{13}\text{H}_{22}\text{O}_2\text{Si} + \text{Na}^+$ 261.1281, found 261.1300.

(*epi*)-**222.** ^1H NMR (300 MHz, CDCl_3) δ 5.94 (dt, $J = 10.8, 5.4$ Hz, 1H), 5.74 (ddd, $J = 17.0, 10.2, 7.8$ Hz, 1H), 5.52 (dt, $J = 11.0, 1.9$ Hz, 1H), 5.02 (ddd, $J = 12.6, 2.1, 1.0$ Hz, 1H), 4.97 (ddd, $J = 6.0, 2.1, 1.1$ Hz, 1H), 3.50 (d, $J = 4.8$ Hz, 1H), 2.83 (dt, $J = 8.8, 7.9$ Hz, 1H), 2.23–2.11 (m, 1H), 1.74 (ddd, $J = 13.6, 10.1, 9.0$ Hz, 1H), 1.60 (dd, $J = 10.0, 6.8$ Hz, 1H), 1.56 (dd, $J = 10.0, 6.8$ Hz, 1H), 1.25 (ddd, $J = 9.5, 5.4, 1.9$ Hz, 1H), 1.17 (d, $J = 7.6$ Hz, 3H), 1.07 (d, $J = 7.0$ Hz, 3H), 0.17 (s, 2H), 0.16 (s, 3H); ^{13}C NMR (75 MHz, CDCl_3) δ 138.5 (CH), 130.0 (CH), 125.5 (CH), 115.3 (CH_2), 80.4 (CH), 51.3 (CH), 34.7 (CH), 33.8 (CH_2), 29.6 (CH_3), 12.4 (CH_2), 0.8 (CH_3), 0.3 (CH_3); IR (neat, cm^{-1}) 3550

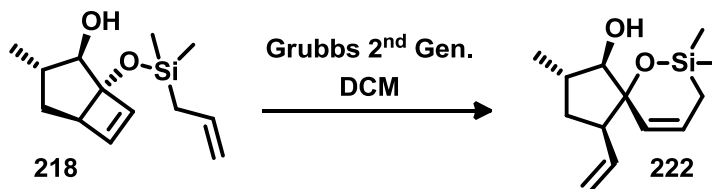
(br), 2959 (m), 2927 (m), 2873 (m), 1640 (m), 1456 (m), 1258 (m), 1105, (m), 1042 (m), 804 (m).



Ketone **206** (0.406 g, 1.0 equiv, 0.172 mmol) was dissolved in methanol (12 mL) and cooled to 0 °C. LiBH₄ (26.2 mg, 0.7 equiv, 0.120 mmol) was added and the reaction stirred for 90 min. The solution was diluted with ethyl ether (20 mL) and washed with a saturated solution of aqueous NH₄Cl (10 mL), water (10 mL) and brine (10 mL). The organic phase was then dried over MgSO₄, filtered, and concentrated by rotary evaporation. The crude residue was purified by flash chromatography [florisil, ethyl ether–hexanes, 1:8] giving compound **218** (0.311 g, 76%) as pale yellow oil.

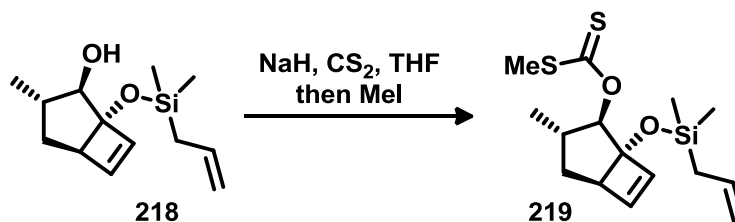
218. ¹H NMR (300 MHz, CDCl₃) δ 6.18 (d, *J* = 3.2 Hz, 1H), 6.16 (d, *J* = 2.9 Hz, 1H), 5.81 (ddt, *J* = 17.1, 10.1, 8.1 Hz, 1H), 4.97–4.88 (m, 1H), 4.86 (ddd, *J* = 4.3, 2.3, 1.0 Hz, 1H), 3.36 (d, *J* = 9.5 Hz, 1H), 2.88 (d, *J* = 7.3 Hz, 1H), 1.91–1.74 (m, 1H), 1.69 (br s, 1H), 1.65 (dt, *J* = 8.0, 1.3 Hz, 2H), 1.50 (dd, *J* = 13.2, 6.1 Hz, 1H), 1.22 (ddd, *J* = 13.2, 11.8, 6.8 Hz, 1H), 1.07 (d, *J* = 6.6 Hz, 3H), 0.16 (s, 6H). ¹³C NMR (75 MHz, CDCl₃) δ 139.1 (CH), 137.1 (CH), 134.6 (CH), 113.7 (CH₂), 89.1 (C), 84.4 (CH), 52.9 (CH), 36.4 (CH), 29.7 (CH₂), 26.0 (CH₂), 16.9 (CH₃), -0.4 (CH₃); IR (neat, cm⁻¹) 3367 (br), 3039

(w), 2954 (s), 2928 (s), 2871 (m), 1631 (m), 1456 (m), 1257 (s), 1068 (s), 841 (s), 789 (s); HRMS (EI) calcd for $C_3H_{22}O_2S_2Si^+$ 238.1389, found 238.1387



Compound **218** (0.130 g, 1.0 equiv, 0.5435 mmol) was added to a flame-dried round-bottom flask and dissolved in dichloromethane (5 mL). Grubbs 2nd generation catalyst (4.6 mg, 1 mol%) was then added, causing the colourless solution to turn light brown. After stirring overnight at room temperature, the catalyst was poisoned with ~2 mL of ethyl vinyl ether, allowing an additional 30 min before the solvent was removed by rotary evaporation and the crude material was purified through a plug of silica gel [silica, ethyl ether–hexane, 1:5], providing compound **222** (0.122 g, 94%).

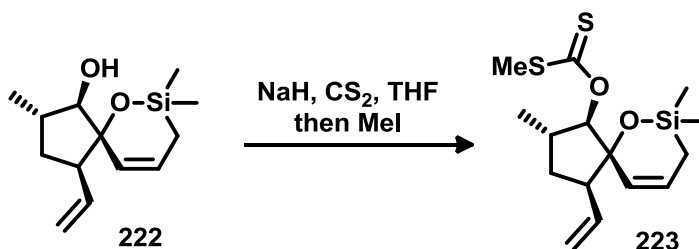
222. Identical to the spectral data obtained above.



To a solution of alcohol **218** (202 mg, 1.0 equiv, 0.851 mmol) in THF (8 mL) was added carbon disulfide (0.105 mL, 2.0 equiv, 1.70 mmol). The reaction was cooled to 0 °C and NaH (95%; 204 mg, 10 equiv, 8.51 mmol) was added. After gradually warming mixture to room temperature over 4 h, iodomethane (0.210 mL, 4 equiv, 3.40 mmol) was added and stirring continued for 12 h. A saturated solution of aqueous NH₄Cl was then added and the organic phase was separated. The aqueous phase was extracted twice with ethyl ether and the combined organic extracts were washed with brine, dried over anhydrous Na₂SO₄, filtered, concentrated, and purified by flash chromatography [silica treated with triethylamine, dichloromethane–pentane, 1:1] to give compound **219** as a foul smelling yellow oil (246 mg, 88%).

219. ¹H NMR (300 MHz, CDCl₃) δ 6.19 (d, *J* = 2.9 Hz, 1H), 6.16 (d, *J* = 2.9 Hz, 1H), 5.87 (d, *J* = 9.7 Hz, 1H), 5.71 (ddt, *J* = 10.2, 16.9, 7.9 Hz, 1H), 4.84 (ddt, *J* = 1.2, 10.4, 1.7 Hz, 1H), 4.80 (ddt, *J* = 2.2, 4.2, 1.1 Hz, 1H), 2.92 (d, *J* = 6.7 Hz, 1H), 2.55 (s, 3H), 2.18 (dq, *J* = 9.7, 6.7, 18.3 Hz, 1H), 1.58–1.54 (m, 2H), 1.59–1.52 (m, 1H), 1.39 (ddd, *J* = 12.0, 13.2, 6.7 Hz, 1H), 1.02 (d, *J* = 6.5 Hz, 3H), 0.08 (s, 6H); ¹³C NMR (75 MHz, CDCl₃) δ 216.5 (C), 138.9 (CH), 136.9 (CH), 134.1 (CH), 113.5 (CH₂), 92.5 (CH), 87.7 (C), 53.4 (CH), 35.6 (CH), 29.4 (CH₂), 25.8 (CH₂), 19.1 (CH₃), 16.6 (CH₃), -0.6

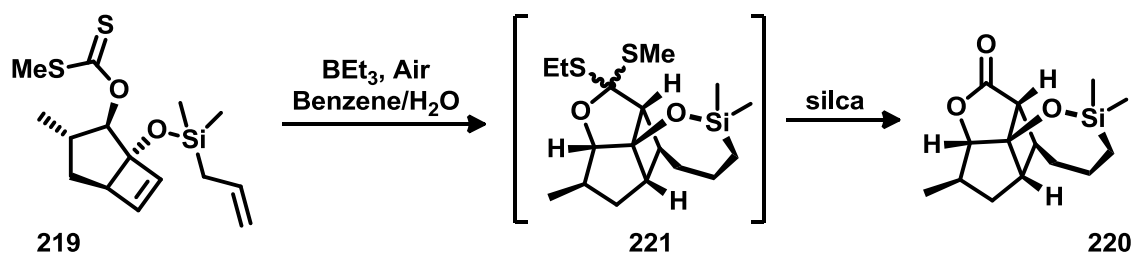
(CH₃), -0.7 (CH₃); IR (neat, cm⁻¹) 3042 (w), 2958 (s), 2982 (m), 2872 (m), 1630 (m), 1455 (w), 1299 (m), 1260 (s), 1221 (s), 1159 (s), 1109 (s), 1063 (s), 888 (m), 839 (m), 801 (m); HRMS (EI) calcd for C₁₅H₂₄O₂S₂Si⁺ 328.0987, found 328.0988.



Alcohol **222** (125 mg, 1.0 equiv, 0.524 mmol) and carbon disulfide (0.063 mL, 2.0 equiv, 1.05 mmol) were taken up in THF (4 mL) and, upon cooling the solution to 0 °C, NaH (95%; 125 mg, 10 equiv, 5.24 mmol) was added. The reaction acclimated over 4 h, at which point iodomethane (0.130 mL, 4 equiv, 2.10 mmol) was added and stirring continued for an additional 12 h. A saturated solution of aqueous NH₄Cl was used to quench the reaction and the organic phase was separated. The aqueous phase was extracted twice with ethyl ether and the combined organic extracts were washed with brine, dried over anhydrous Na₂SO₄, filtered, concentrated, and purified by flash chromatography [silica, dichloromethane–pentane, 1:1] to give compound **223** as a foul smelling yellow oil (151 mg, 88%).

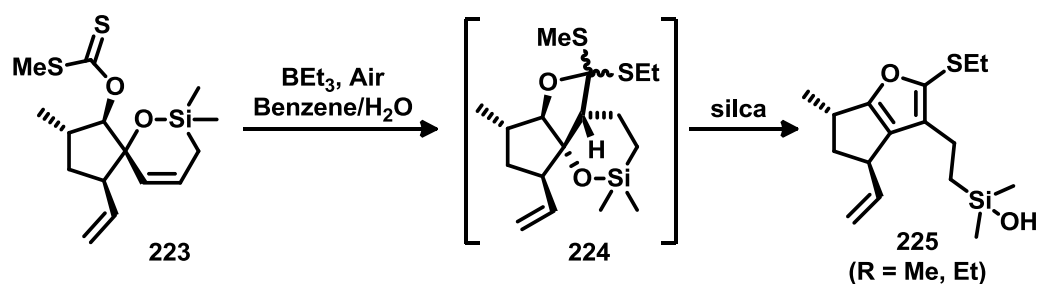
223. ¹H NMR (300 MHz, CDCl₃) δ 6.09 (dt, *J* = 10.8, 5.3 Hz, 1H), 5.94 (d, *J* = 8.0 Hz, 1H), 5.73 (ddd, *J* = 17.0, 10.4, 7.7 Hz, 1H), 5.65 (dt, *J* = 11.0, 1.9 Hz, 1H), 5.06 (ddd, *J* = 8.8, 2.0, 1.0 Hz, 1H), 5.03–4.98 (m, 1H), 2.54 (s, 3H), 2.15 (m, 1H), 2.02–1.87 (m, 1H),

1.63–1.53 (m, 2H), 1.23 (ddd, $J = 5.4, 1.9, 1.0$ Hz, 2H), 1.17 (d, $J = 6.9$ Hz, 3H), 0.10 (s, 3H), 0.08 (s, 3H). ^{13}C NMR (125 MHz, CDCl_3) δ 216.1 (C), 137.4 (CH), 127.7 (CH), 127.1 (CH), 116.4 (CH_2), 95.9 (CH), 86.2 (C), 51.4 (CH), 34.5 (CH), 33.4 (CH_2), 20.4 (CH_3), 18.9 (CH_3), 12.4 (CH_2), 0.9 (CH_3), 0.3 (CH_3); IR (neat, cm^{-1}) 3077 (w), 2958 (s), 2874 (m), 1640 (w), 1456 (w), 1395 (w), 1228 (s), 1061 (s), 901 (m); HRMS (EI) calcd for $\text{C}_{15}\text{H}_{24}\text{O}_2\text{S}_2\text{Si}^+$ 328.0987, found 328.0987.



A solution of xanthate **219** (21.0 mg, 1.0 equiv, 0.0640 mmol) in 5 mL of benzene was sparged with argon for 20 min. Triethylborane (1 M in hexanes; 0.320 mL, 5.0 equiv, 0.319 mmol) was then added dropwise. A 60-mL syringe was filled with air, and a syringe pump was used to slowly inject the air (ca. 5 mL/h) into the mechanically stirred reaction mixture. Upon completion of the injection, the solution was concentrated by rotary evaporation. Spectroscopic analysis indicated that the crude mixture was predominantly composed of the dithioortho ester **221**; however, after purification by flash chromatography [triethylamine treated silica, ethyl ether–pentane, 1:5 to 1:1], lactone **220**, obtained as a colourless oil, was sole isolated product (4.3 mg, 25% yield).

220. ^1H NMR (300 MHz, CDCl_3) δ 4.33 (s, 1H), 2.84 (dd, $J = 2.5, 3.6$ Hz, 1H), 2.66–2.57 (m, 1H), 2.42 (qd, $J = 7.1, 7.4$ Hz, 1H), 2.08 (ddd, $J = 1.4, 13.8, 9.6$ Hz, 1H), 2.05–2.02 (m, 1H), 2.00–1.85 (m, 4H), 1.78 (td, $J = 6.4, 13.8$ Hz, 1H), 0.92 (d, $J = 7.5$ Hz, 3H), 0.85–0.78 (m, 2H), 0.14 (s, 3H), 0.12 (s, 3H); ^{13}C NMR (75 MHz, CDCl_3) δ 178.6 (C), 94.9 (CH), 87.3 (C), 46.3 (CH), 45.1 (CH), 41.9 (CH), 40.7 (CH), 39.8 (CH_2), 33.7 (CH_2), 19.0 (CH_2), 17.0 (CH_2), 16.8 (CH_3), 0.3 (CH_3), 0.1 (CH_3); IR (neat, cm^{-1}) 2962 (s), 2919 (s), 2873 (s), 1771 (s), 1463 (m), 1342 (m), 1259 (s), 1192 (m), 1154 (m), 1102 (m), 1020 (s), 905 (m), 829 (m), 750 (m); HRMS (EI) calcd for $\text{C}_{14}\text{H}_{22}\text{O}_3\text{Si}^+$ 266.1338, found 266.1338.

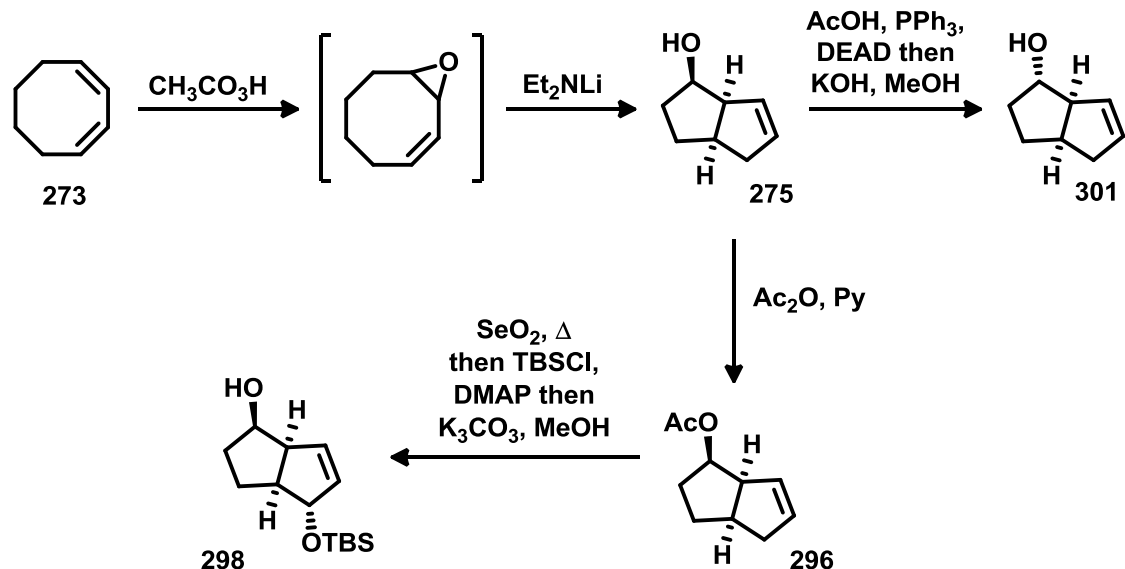


A solution of xanthate **223** (31.2 mg, 1.0 equiv, 0.0578 mmol) in 5 mL of benzene was sparged with argon for 20 min. Triethylborane (1 M in hexanes; 0.300 mL, 5.0 equiv, 0.300 mmol) was then added dropwise. A 60-mL syringe was filled with air, and a syringe pump was used to slowly inject the air (ca. 5 mL/h) into the mechanically stirred reaction mixture. Upon completion of the injection, the crude mixture was concentrated by rotary evaporation. Spectroscopic analysis indicated that the crude mixture was predominantly composed of the dithio ortho ester **224**; however, after purification by

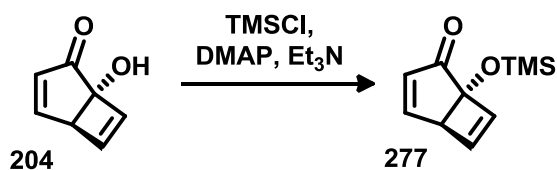
flash chromatography [triethylamine treated silica, ethyl ether–pentane, 1:5 to 1:1], an inseparable 1:1 mixture of lactones **225** were the sole isolated products (10.3 mg, 58% yield) as a colourless oil.

225. ^1H NMR (300 MHz, CDCl_3) δ 5.88–5.64 (m, 1H), 5.04 (ddd, $J = 17.0, 2.9, 1.4$ Hz, 1H), 4.96 (dd, $J = 10.0, 2.0$ Hz, 1H), 3.74–3.49 (m, 1H), 3.27–3.01 (m, 1H), 2.69 (q, $J = 7.5$ Hz, 1Hi), 2.64–2.41 (m, 2H), 2.36 (ddd, $J = 12.9, 8.3, 4.6$ Hz, 1H), 2.31 (s, 1.5H), 2.20 (ddd, $J = 13.0, 6.4, 3.4$ Hz, 1H), 1.21 (t, $J = 7.2$ Hz, 1.5H), 1.18 (d, $J = 6.9$ Hz, 3H) 0.96–0.72 (m, 2H), 0.12 (s, 3H), 0.12 (s, 3H); ^{13}C NMR (75 MHz, CDCl_3) δ 165.1 (C), 159.4 (C), 141.6 (CH), 141.6 (CH), 133.3 (C), 131.9 (C), 127.2 (CH_2), 127.1 (CH_2), 113.4 (C), 113.4 (C), 44.8 (CH_2), 40.7 (CH), 32.2 (CH), 30.9 (CH_2), 20.0 (CH), 19.1 (CH), 18.7 (CH_2), 18.6 (CH_2), 18.2 (CH_2), 15.2 (CH_3), -0.3 (CH_3); IR (neat, cm^{-1}) 3420 (br), 2959 (s), 2926 (s), 2855 (s), 1634 (w), 1455 (m), 1376 (w), 1252 (s), 1179 (m), 1053 (m), 913 (m), 839 (s). HRMS (ESI) calcd for $\text{C}_{10}\text{H}_{14}\text{OS}_2 - \text{H}_2 + \text{H}^+$ 295.1188, found 295.1175.

7.3 Experiments pertaining to Chapter 3



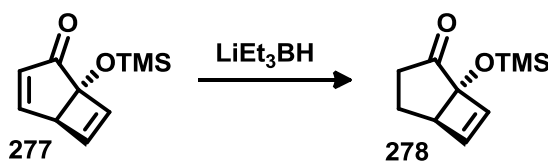
Compounds **273**, **275**, **296**, **298**, and **301** were prepared by Jeremy Mason and the details of his synthetic efforts are disclosed within the patent on the synthesis of bicyclic compounds and methods for their use as therapeutic agents.²²⁶



A flame-dried round-bottom flask was charged with alcohol **204** (0.511 g, 1 equiv, 4.18 mmol), taken up in dichloromethane (12 mL) and the solution was cooled to 0 °C. Next DMAP (30.0 mg, 0.6 equiv, 0.251 mmol) and triethylamine (1.26 g, 3 equiv, 12.5 mmol) were added, resulting in a bright yellow solution. The colour then changed to pale yellow

with the dropwise addition of trimethylsilyl chloride (0.676 g, 1.5 equiv, 4.18 mmol). The reaction stirred at 0 °C for 4 h, at which point it was diluted with ethyl ether (20 mL), precipitating ammonium chloride salts. The white solids were removed by filtration through a pad of celite and the filtrate was washed with a saturated NaHCO₃ solution (20 mL), H₂O (2 × 20 mL), and brine (20 mL) then dried over MgSO₄, filtered, and concentrated by rotary evaporation. The crude material was purified by flash chromatography [florisil, dichloromethane–hexanes, 1:1] giving compound **277** (0.721 g, 89%) as pale yellow oil.

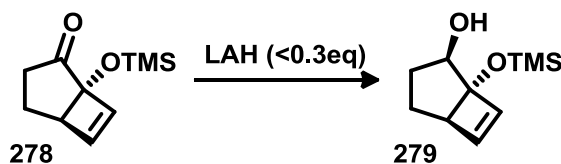
277. ¹H NMR (300 MHz, CDCl₃) δ 7.59 (dd, *J* = 6.3, 2.8 Hz, 1H), 6.71 (dd, *J* = 2.6, 0.8 Hz, 1H), 6.31 (dd, *J* = 2.6, 0.8 Hz, 1H), 6.07 (d, *J* = 6.3 Hz, 1H), 3.71 (dt, *J* = 2.8, 1Hz, 1H), 0.16 (s, 6H); ¹³C NMR (75 MHz, CDCl₃) δ 205.7 (C), 160.1 (CH), 145.2 (CH), 138.5 (CH), 132.6 (CH), 81.9 (C), 58.2 (CH), -3.2 (CH₃); IR (neat, cm⁻¹) 3056 (m), 2959 (s), 2854 (m), 1716 (s), 1575 (m), 1343 (m), 1254 (s), 1188 (s), 1070 (s), 897 (s), 845 (s).



A flame-dried round-bottom flask was charged with enone **277** (0.721 g, 1.0 equiv, 3.71 mmol) and taken up in freshly distilled tetrahydrofuran (12 mL) and the reaction was cooled to -78 °C. A solution of LiHBEt₃ in tetrahydrofuran (1 M in THF, 4.5 mL, 1.2 equiv, 4.45 mmol) was added dropwise. Monitoring the reaction by TLC, the UV-active

starting material had been fully consumed within 90 min. At this point, the cold reaction mixture was poured directly into a separatory funnel containing an ice cold biphasic mixture of ethyl ether (30 mL) and a saturated solution of aqueous NaHCO₃ (10 mL). The aqueous phase was extracted with ethyl ether (10 mL) and the combined organic phase was washed with water (10 mL) and brine (10 mL) then dried over anhydrous MgSO₄, filtered, and concentrated by rotary evaporation. The resulting pale yellow oil, compound **278** (0.701 g, 96%), was satisfactorily clean, thus no further purification steps were performed.

278. ¹H NMR (300 MHz, CDCl₃) δ 6.41 (dd, J = 2.8, 0.8 Hz, 1H), 6.20 (d, J = 2.8 Hz, 1H), 3.32 (dd, J = 6.7, 0.7 Hz, 1H), 2.84 (ddd, J = 18.1, 11.7, 9.2 Hz, 1H), 2.21 (ddt, J = 18.2, 8.5, 1.0 Hz, 1H), 2.06–1.90 (m, 1H), 1.77 (ddt, J = 13.1, 9.3, 0.9 Hz, 1H), 0.17 (s, J = 3.4 Hz, 9H); ¹³C NMR (76 MHz, CDCl₃) δ 215.5 (C), 142.1 (CH), 139.1 (CH), 83.1 (C), 53.4 (CH), 33.3 (CH₂), 19.6 (CH₂), 1.5 (CH₃); IR (neat, cm⁻¹) 3050 (m), 2958 (m), 1744 (s), 1414 (m), 1283 (s), 1081 (s), 894 (m).



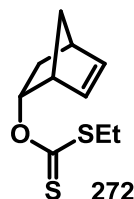
Ketone **278** (0.764 g, 1.0 equiv, 3.89 mmol) was dissolved in 12 mL of freshly distilled tetrahydrofuran and the solution was cooled to 0 °C. Lithium aluminum hydride (44.0 mg, 0.3 equiv, 1.16 mmol) was suspended in 1 mL of dry tetrahydrofuran and added to the reaction dropwise. After 30 min, the reaction was quenched with 3 mL of a saturated

solution of aqueous NaHCO₃. The mixture was extracted with ethyl ether (2 × 10 mL) and the combined organic extracts were washed with water (2 × 5 mL) and brine (5 mL), then dried over anhydrous MgSO₄, filtered, concentrated. The residue was purified by flash chromatography [florisil, ethyl ether–hexanes, (1:4)] giving compound **279** (0.652 g, 85%) as a colourless oil.

279. ¹H NMR (300 MHz, CDCl₃) δ 6.15 (s, 2H), 3.95–3.84 (m, 1H), 2.92 (dd, *J* = 6.2, 1.8 Hz, 1H), 1.98–1.86 (m, 1H), 1.61 (dd, *J* = 5.2, 2.3 Hz, 1H), 1.50 (dd, *J* = 12.4, 6.6 Hz, 1H), 1.37–1.31 (m, 1H), 0.15 (s, 9H); ¹³C NMR (76 MHz, CDCl₃) δ 138.3 (CH), 136.8 (CH), 88.8 (CH), 78.4 (C), 54.0 (CH), 29.8 (CH₂), 20.6 (CH₂), 1.8 (CH₃); IR (neat, cm⁻¹) 3429 (br), 2956 (s), 2926 (s), 2855 (s), 1456 (w), 1250 (s), 1072 (m), 900 (s), 842 (s).

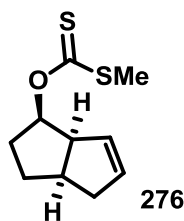
General Procedure for Xanthate Formation.

To a solution of alcohol (1.0 equiv) in THF (0.5 M) was added carbon disulfide (2.0 equiv). The resulting solution was cooled to 0 °C and NaH (95%; 1.1 equiv) was added, followed by a gradual acclimation to room temperature over 4 h. Iodoethane or iodomethane (4.0 equiv) was added, and the solution stirred at room temperature for an additional 12 h. The reaction was quenched with a saturated solution of aqueous NH₄Cl and the organic phase was separated. The aqueous phase was extracted twice with ethyl ether and the combined organic extracts were washed with brine, dried over anhydrous MgSO₄, filtered, concentrated, and purified by flash chromatography.



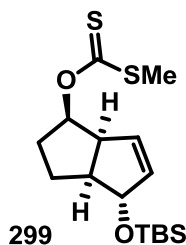
Xanthate **272** was prepared from commercially available 5-norbornen-2-ol (mixture of endo and exo isomers) using the general procedure given above then purified by flash chromatography [silica, ethyl acetate–hexanes 1:40] to give the product **272** as a yellow oil in 70%.

272. ^1H NMR (300 MHz, CDCl_3) δ 6.38 (dd, $J = 5.6, 2.9$ Hz, 1H), 6.02 (dd, $J = 5.6, 2.9$ Hz, 1H), 5.97 (ddd, $J = 8.0, 2.8, 3.8$ Hz, 1H), 3.35–3.29 (m, 1H), 3.03 (q, $J = 7.4$ Hz, 2H), 2.92–2.87 (m, 1H), 2.25 (ddd, $J = 12.9, 7.9, 3.8$ Hz, 1H), 1.52 (dddd, $J = 8.8, 3.8, 2.1, 2.0$ Hz, 1H), 1.40–1.34 (m, 1H), 1.30 (t, $J = 7.4$ Hz, 3H), 1.11 (ddd, $J = 12.9, 2.6, 3.8$ Hz, 1H); ^{13}C NMR (90 MHz, CDCl_3) δ 214.6 (C), 139.0 (CH), 131.8 (CH), 84.8 (CH), 47.7 (CH_2), 46.0 (CH), 42.4 (CH), 35.1 (CH_2), 29.9 (CH_2), 13.8 (CH_3); IR (neat, cm^{-1}) 3065 (m), 1219 (s), 1066 (s), 726 (s); HRMS (ESI) calcd for $\text{C}_{10}\text{H}_{14}\text{OS}_2 + \text{H}^+$ 215.0564, found 215.0564.



Xanthate **276** was prepared according to the general procedure given above and purified by flash chromatography [silica, ethyl acetate–hexanes. 1:40] to give the product as a yellow oil in 90% yield.

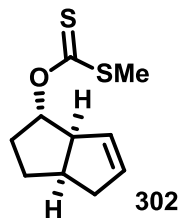
276. ^1H NMR (300 MHz, CDCl_3) δ 5.84 (dd, $J = 12.4, 6.2$ Hz, 1H), 5.75 (dt, $J = 5.8, 2.2$ Hz, 1H), 5.45 (dt, $J = 8.0, 2.2$ Hz, 1H), 3.61–3.51 (m, 1H), 2.80–2.60 (m, 2H), 2.51 (s, 3H), 2.12 (ddd, $J = 14.0, 5.1, 2.5$ Hz, 1H), 2.00–1.74 (m, 3H), 1.46 (ddd, $J = 15.6, 10.0, 5.3$ Hz, 1H); ^{13}C NMR (75 MHz, CDCl_3) δ 215.4 (C), 132.7 (CH), 128.3 (CH), 87.1 (CH), 53.6 (CH), 41.5 (CH_2), 39.6 (CH), 30.9 (CH_2), 30.9 (CH_2), 18.8 (CH_3); IR (neat, cm^{-1}) 3051 (w), 1231 (s), 1213 (s), 1057 (s), 713 (m); HRMS (ESI) calcd for $\text{C}_{10}\text{H}_{14}\text{OS}_2 + \text{H}^+$ 215.0564, found 215.0560.



Xanthate **299** was prepared according to the general procedure given above and purified by flash chromatography [silica, ethyl acetate–hexanes 1:40] to give the product as a yellow oil in 66% yield.

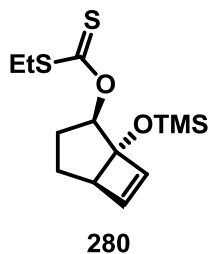
299. ^1H NMR (300 MHz, CDCl_3) δ 5.85–5.74 (m, 2H), 5.69 (ddd, $J = 5.7, 2.3, 0.9$ Hz, 1H), 4.58 (dt, $J = 2.9, 2.2$ Hz, 1H), 3.75 (ddt, $J = 7.5, 10.0, 2.3$ Hz, 1H), 2.53 (s, 3H), 2.52–2.45 (m, 1H), 2.03–1.91 (m, 1H), 1.90–1.79 (m, 1H), 1.79–1.68 (m, 1H), 1.67–1.56

(m, 1H), 0.90 (s, 9H), 0.09 (s, 6H); ^{13}C NMR (75 MHz, CDCl_3) δ 215.4 (C), 135.9 (CH), 132.4 (CH), 86.5 (CH), 85.8 (CH), 52.3 (CH), 50.7 (CH), 30.2 (CH_2), 27.3 (CH_2), 26.1 (CH), 19.0 (CH_3), 18.4 (C), -4.3 (CH_3); IR (neat, cm^{-1}) 3058 (w), 1252 (s), 1212 (s), 1056 (s), 667(m); HRMS (ESI) calcd for $\text{C}_{16}\text{H}_{28}\text{O}_2\text{S}_2\text{Si} + \text{Na}^+$ 367.1198, found 367.1190.



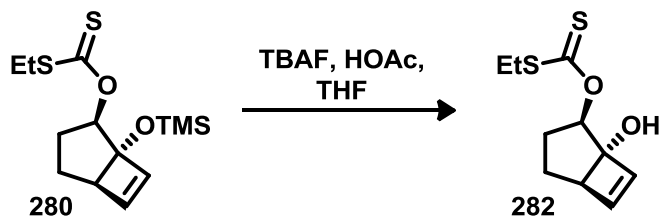
Xanthate **302** was prepared according to the general procedure given above and purified by flash chromatography [silica, ethyl acetate–hexanes, 1:40] to give the product as a yellow oil in 66%.

302. ^1H NMR (360 MHz, CDCl_3) δ 5.71 (ddd, $J = 5.6, 4.4, 2.1$ Hz, 1H), 5.64 (ddd, $J = 5.6, 4.6, 2.2$ Hz, 1H), 5.59 (d, $J = 2.3$ Hz, 1H), 3.33 (d, $J = 7.1$ Hz, 1H), 2.90 (ddt, $J = 17.3, 8.3, 2.9$ Hz, 1H), 2.70 (dddd, $J = 17.2, 9.4, 4.1, 2.1$ Hz, 1H), 2.55 (s, 3H), 2.13–1.98 (m, 2H), 1.97–1.87 (m, 1H), 1.80 (dddd, $J = 13.8, 11.7, 4.7, 6.9$ Hz, 1H), 1.52 (dddd, $J = 12.4, 6.6, 2.9, 2.7$ Hz, 1H); ^{13}C NMR (90 MHz, CDCl_3) δ 215.1 (C), 132.9 (CH), 130.0 (CH), 90.3 (CH), 58.2 (CH), 41.5 (CH_2), 39.1 (CH), 32.8 (CH_2), 30.6 (CH_2), 19.1 (CH_3); IR (neat, cm^{-1}) 3050 (w), 1221 (s), 1081 (s), 1047 (s), 716 (m); HRMS (ESI) calcd for $\text{C}_{10}\text{H}_{14}\text{OS}_2 + \text{H}^+$ 215.0564, found 215.0564.



Xanthate **280** was prepared according to the general procedure given above and purified by flash chromatography [silica treated with triethylamine, dichloromethane] to give the product as a yellow oil in 77% yield.

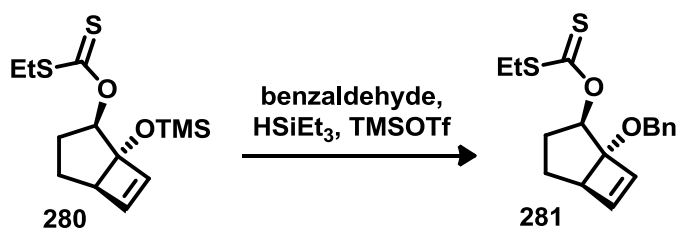
280. ^1H NMR (300 MHz, CDCl_3) δ 6.22 (d, $J = 2.9$ Hz, 1H), 6.17 (d, $J = 2.9$ Hz, 1H), 5.55 (dd, $J = 9.6, 7.0$ Hz, 1H), 3.10 (q, $J = 7.5$ Hz, 2H), 2.94 (dd, $J = 6.2, 1.1$ Hz, 1H), 2.51–2.31 (m, 1H), 1.73–1.58 (m, 2H), 1.44 (dd, $J = 11.6, 6.1$ Hz, 1H), 1.35 (t, $J = 7.4$ Hz, 3H), 0.13 (s, 9H); ^{13}C NMR (76 MHz, CDCl_3) δ 215.1 (C), 138.1 (CH), 137.2 (CH), 88.6 (CH), 87.1 (C), 53.6 (CH), 30.3 (CH_2), 29.8 (CH_2), 26.7 (CH_2), 13.6 (CH_3), 1.6 (CH_3); IR (neat, cm^{-1}); 2927 (s), 2854 (s), 1646 (w), 1456 (w), 1252 (m), 1212 (s), 1071 (s), 898 (m), 842 (m).



Xanthate **280** (0.153 g, 1.0 equiv, 0.507 mmol) was dissolved in 6 mL of freshly distilled tetrahydrofuran and the reaction was cooled to 0 °C. A solution of TBAF (1 M in THF,

1.60 mL, 3.0 equiv, 1.60 mmol) and acetic acid (0.120 mL, 4.0 equiv, 2.00 mmol) was then added dropwise. After stirring for 2 h at 0 °C, the reaction was quenched with a saturated solution of NH₄Cl (2 mL), the crude mixture was extracted with ethyl ether (3 × 5 mL), and the combined organic layer was washed with H₂O (2 × 10 mL) and brine (10 mL), dried over MgSO₄, filtered, and the filtrate was concentrated by rotary evaporation. The crude residue was purified by flash chromatography [silica, ethyl ether–hexanes, 1:3] to afford compound **282** (95.7 mg, 82%) as a yellow oil.

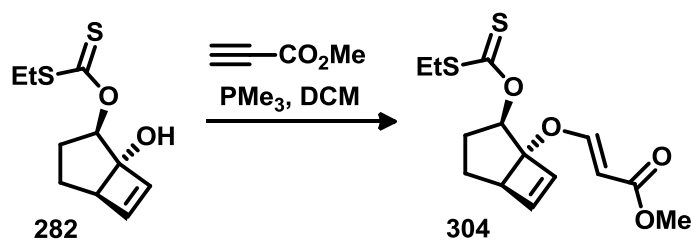
282. ¹H NMR (300 MHz, CDCl₃) δ 6.24 (d, *J* = 3.0 Hz, 1H), 6.13 (d, *J* = 2.9 Hz, 1H), 5.69 (dd, *J* = 9.9, 7.1 Hz, 1H), 3.11 (q, *J* = 7.5 Hz, 3H), 2.99 (d, *J* = 7.5 Hz, 1H), 2.43–2.22 (m, 1H), 2.06–1.80 (m, 1H), 1.80–1.58 (m, 1H), 1.52 (dd, *J* = 15.0, 8.0 Hz, 1H), 1.35 (t, *J* = 7.4 Hz, 3H). ¹³C NMR (75 MHz, CDCl₃) δ 211.9 (C), 139.1 (CH), 136.5 (CH), 87.5 (CH), 78.8 (C), 53.8 (CH), 30.4 (CH₂), 28.0 (CH₂), 20.8 (CH₂), 13.4 (CH₃); IR (neat, cm⁻¹); 3366 (br), 2925 (s), 2854 (m), 1455 (w), 1222 (s), 1080 (s), 1063 (s).



Silyl ether **280** (122 mg, 0.403 mmol, 1.0 equiv) and benzaldehyde (59.1 mg, 0.504 mmol, 1.3 equiv) were taken up in dry dichloromethane (6 mL), and the reaction was cooled in an ice bath. The subsequent addition of TMSOTf (2 drops) at 0°C caused the pale yellow solution to turn reddish brown. After 1 h, triethylsilane (59.1 mg, 0.504

mmol, 1.3 equiv) was added and the reaction continued to stir overnight, acclimating to room temperature. Upon quenching with saturated NH_4Cl solution (5 mL), the crude mixture was extracted with ethyl ether (3×10 mL), and the combined organic layer was washed with H_2O (2×10 mL) and brine (10 mL), dried over MgSO_4 , filtered, and concentrated by rotary evaporation. The crude material was purified by flash chromatography [silica, benzene–hexanes, 1:3 to 1:1] to afford compound **281** (90.4 mg, 70%) as a yellow oil.

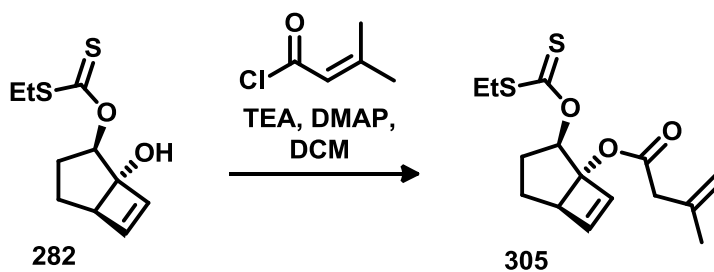
281. ^1H NMR (300 MHz, CDCl_3) δ 7.30–7.15 (m, 5H), 6.20 (d, $J = 2.9$ Hz, 1H), 6.18 (d, $J = 2.9$ Hz, 1H), 5.76 (dd, $J = 7.1, 9.5$ Hz, 1H), 4.60 (d, $J = 12.2$ Hz, 1H), 4.55 (d, $J = 12.2$ Hz, 1H), 3.13 (dd, $J = 0.9, 5.9$ Hz, 1H), 3.07 (q, $J = 7.4$ Hz, 2H), 2.47–2.38 (m, 1H), 1.73–1.40 (m, 3H), 1.32 (t, $J = 7.4$ Hz, 3H); ^{13}C NMR (75 MHz, CDCl_3) δ 214.6 (C), 139.2 (CH), 139.1 (C), 135.6 (CH), 128.3 (CH), 127.4 (CH), 127.2 (CH), 91.2 (C), 86.1 (CH), 67.7 (CH_2), 49.8 (CH), 30.1 (CH_2), 26.9 (CH_2), 20.8 (CH_2), 13.5 (CH_3); IR (neat, cm^{-1}) 3088 (w), 3033 (m), 2947 (m), 2864 (m), 1454 (m), 1313 (m), 1211 (s), 1137 (m), 1071 (s), 768 (m); HRMS (ESI) calcd for $\text{C}_{17}\text{H}_{20}\text{O}_2\text{S}_2 + \text{Na}^+$ 343.0797, found 343.0795.



A solution of methyl propiolate (87.8 mg, 1.05 mmol, 4.0 equiv) in dry dichloromethane (3 mL) was added dropwise to a mixture of alcohol **282** (60.2 mg, 0.261 mmol, 1.0

equiv) and trimethylphosphine (1 M in THF, 0.130 mL, 0.50 equiv) in dry dichloromethane (5 mL). The clear colorless reaction turned dark brown as it stirred over 4 h. The reaction was concentrated by rotary evaporation and purified by flash chromatography (silica treated with triethylamine, dichloromethane) to afford product **304** (59.4 mg, 72%) as yellow oil:

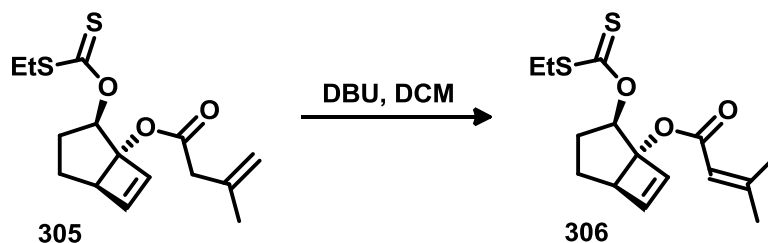
304. ^1H NMR (300 MHz, CDCl_3) δ 7.59 (d, $J = 12.1$ Hz, 1H), 6.36 (d, $J = 2.9$ Hz, 1H), 6.24 (d, $J = 2.9$ Hz, 1H), 5.73 (dd, $J = 9.4, 7.0$ Hz, 1H), 5.41 (d, $J = 12.1$ Hz, 1H), 3.67 (s, 3H), 3.15 (d, $J = 5.7$ Hz, 1H), 3.09 (q, $J = 7.4$ Hz, 2H), 2.53–2.44 (m, 1H), 1.70–1.59 (m, 1H), 1.73–1.50 (m, 2H), 1.32 (t, $J = 7.4$ Hz, 3H); ^{13}C NMR (75 MHz, CDCl_3) δ 214.6 (C), 168.2 (C), 157.9 (CH), 141.4 (CH), 133.7 (CH), 100.0 (CH), 92.7 (C), 84.6 (CH), 51.3 (CH), 51.1 (CH_3), 30.4 (CH_2), 26.9 (CH_2), 20.7 (CH_2), 13.4 (CH_3); IR (neat, cm^{-1}) 2951 (m), 1717 (s), 1645 (s), 1435 (m), 1316 (m), 1257 (s), 1205 (s), 1176 (s), 1138 (s), 1081 (s), 957 (w), 771 (w); HRMS (ESI) calcd for $\text{C}_{14}\text{H}_{18}\text{O}_4\text{S}_2 + \text{Na}^+$ 337.0539, found 337.0545.



Alcohol **282** (67.0 mg, 0.290 mmol, 1.0 equiv) was added to a flame-dried round-bottom flask and dissolved in 10 mL of dichloromethane. The solution was cooled to 0 °C then

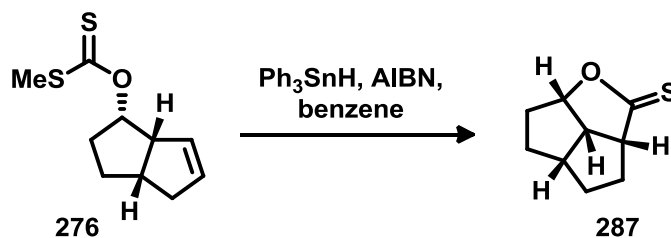
DMAP (3.5 mg, 0.0290 mmol, 0.10 equiv), freshly distilled triethylamine (88.3 mg, 0.873 mmol, 3.0 equiv), and 3,3-dimethylacryloyl chloride (51.7 mg, 0.436 mmol, 1.5 equiv) were sequentially added. After acclimating to room temperature during an overnight stir, the reaction was quenched with saturated NH_4Cl solution (5 mL), the crude mixture was extracted with ethyl ether (3×10 mL), and the combined organic layer was washed with H_2O (2×10 mL) and brine (10 mL), dried over MgSO_4 , filtered, and concentrated by rotary evaporation. The crude material was purified by flash chromatography [silica, dichloromethane–hexanes, 3:7 to 1:1] to afford product **305** (62.4 mg, 69%; containing 16% of compound **306**) as a yellow oil.

305. ^1H NMR (300 MHz, CDCl_3) δ 6.24 (d, $J = 2.9$ Hz, 1H), 6.23 (d, $J = 2.9$ Hz, 1H), 6.15 (dd, $J = 7.4, 9.3$ Hz, 1H), 4.89 (apparent pen, $J = 1.6$ Hz, 1H), 4.82 (oct, $J = 1.0$ Hz, 1H), 3.27 (d, $J = 7.1$ Hz, 1H), 3.08 (dq, $J = 2.4, 7.4$ Hz, 2H), 3.00 (d, $J = 1.0$ Hz, 2H), 2.42–2.25 (m, 1H), 1.87–1.73 (m, 1H), 1.82–1.71 (m, 1H), 1.77 (t, $J = 1.2$ Hz, 3H), 1.50 (dd, $J = 5.4, 11.5$ Hz, 1H), 1.32 (t, $J = 7.4$ Hz, 3H); ^{13}C NMR (75 MHz, CDCl_3) δ 214.8 (C), 170.7 (C), 140.0 (CH), 138.3 (C), 133.8 (CH), 114.9 (CH_2), 89.7 (C), 83.3 (CH), 51.4 (CH), 43.5 (CH_2), 30.1(CH_2), 27.9 (CH_2), 22.4 (CH_3), 21.4 (CH_2), 13.5 (CH_3); IR (neat, cm^{-1}) 3079 (w), 2933 (m), 2871 (m), 1738 (s), 1652 (m), 1447 (m), 1279 (m), 1207 (s), 1143 (s), 1083 (s), 1069 (s), 898 (w), 764 (w); HRMS (ESI) calcd for $\text{C}_{15}\text{H}_{20}\text{O}_3\text{S}_2 + \text{Na}^+$ 335.0746, found 335.0744.



The unconjugated ester **305** (9.8 mg, 0.0313 mmol, 1.0 equiv) was dissolved in 3 mL of dichloromethane along with DBU (50.0 mg, 0.313 mmol, 10 equiv). The reaction was stirred at room temperature overnight prior to quenching with saturated NH_4Cl solution (2 mL). The crude mixture was extracted with ethyl ether (3×5 mL), and the combined organic layer was washed with H_2O (2×5 mL) and brine (5 mL), dried over MgSO_4 , filtered, and concentrated by rotary evaporation. The crude material (9.8 mg, 99%), a yellow oil, did not require additional purification.

306. ^1H NMR (300 MHz, CDCl_3) δ 6.24 (d, $J = 2.9$ Hz, 1H), 6.23 (d, $J = 2.9$ Hz, 1H), 6.12 (dd, $J = 9.3, 7.2$ Hz, 1H), 5.63 (apparent sep, $J = 1.4$ Hz, 1H), 3.31 (d, $J = 6.0$ Hz, 1H), 3.08 (dq, $J = 1.4, 7.4$ Hz, 2H), 2.47–2.38 (m, 1H), 2.12 (d, $J = 1.2$ Hz, 3H), 1.95 (qt, $J = 12.5, 6.3$ Hz, 1H), 1.86 (d, $J = 1.3$ Hz, 3H), 1.86–1.73 (m, 1H), 1.51 (dd, $J = 12.6, 6.5$ Hz, 1H), 1.32 (t, $J = 7.4$ Hz, 3H); ^{13}C NMR (75 MHz, CDCl_3) δ 214.6 (C), 165.7 (C), 157.4 (C), 139.8 (CH), 134.1 (CH), 116.0 (CH), 89.9 (C), 83.8 (CH), 51.4 (CH), 30.1 (CH_2), 27.9 (CH_2), 27.4 (CH_3), 21.4 (CH_2), 20.2 (CH_3), 13.5 (CH_3); IR (neat, cm^{-1}) 2962 (m), 2929 (s), 2855 (m), 1716 (s), 1649 (m), 1445 (w), 1234 (s), 1207 (s), 1142 (s), 1069 (s), 1035 (m); HRMS (ESI) calcd for $\text{C}_{15}\text{H}_{20}\text{O}_3\text{S}_2 + \text{Na}^+$ 335.0746, found 335.0744.

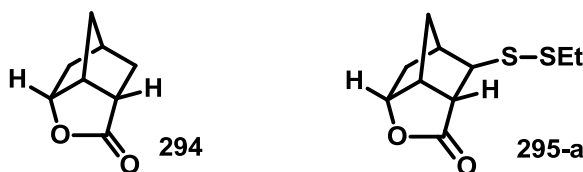


A solution containing 30 mg (0.14 mmol, 1.0 equiv) of **276** in 15 mL of benzene (freshly distilled over CaH and degassed) was heated to reflux. A separate solution containing Ph₃SnH (74 mg, 0.21 mmol, 1.5 equiv) and AIBN (2.3 mg, 0.014 mmol, 0.10 equiv) in 2 mL of benzene (also distilled and degassed) was slowly injected via syringe pump (0.35 mL / h) into the refluxing solution of **276**. After 8 h, the reaction mixture was cooled to room temperature, concentrated under reduced pressure, and purified by flash chromatography [silica, hexanes–ethyl acetate, 9:1] to afford product **287** (17.0 mg, 73%) as a light yellow oil.

287. ¹H NMR (300 MHz, CDCl₃) δ 5.38–5.32 (m, 1H), 3.52 (ddt, *J* = 0.6, 9.7, 6.7 Hz, 1H), 3.22 (dt, *J* = 9.2, 7.0 Hz, 1H), 2.63 (ddt, *J* = 16.1, 5.4, 7.7 Hz, 1H), 2.34–2.17 (m, 3H), 1.98–1.79 (m, 3H), 1.53–1.45 (m, 1H), 1.45–1.35 (m, 1H); ¹³C NMR (90 MHz, CDCl₃) δ 229.1 (C), 95.8 (CH), 61.5 (CH), 52.3 (CH), 46.4 (CH), 36.3 (CH₂), 34.7 (CH₂), 31.8 (CH₂), 29.3 (CH₂); IR (neat, cm⁻¹) 1298 (s), 1255 (s), 1206 (s), 1154 (s); HRMS (ESI) calcd for C₉H₁₂OS + H⁺ 169.0687, found 169.0684.

General Procedure for Tin-Free Xanthate Lactonization.

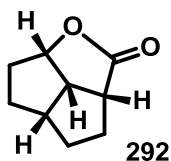
A solution of xanthate (1.0 equiv) in MeCN–H₂O (4:1, 8 mM) was sparged with argon. Triethylborane (1 M in hexanes; 5.0 equiv) was added dropwise. A 60-mL syringe was filled with air and a syringe pump was used to slowly inject the air (ca. 5 mL/h) into the mechanically stirred reaction mixture. Upon completion of the injection, iodine (3.0 equiv) was added to the reaction mixture, causing a dark brown colour change, and the solution was stirred open to air for a minimum of 3 h. The dark brown solution became colourless after the addition of a 0.5 M solution of aqueous Na₂S₂O₃ (approximately twice the reaction volume), and the mixture stirred for an additional 30 min. Finally, the solution was extracted twice with dichloromethane, and the organic extracts were washed with brine, dried over anhydrous Na₂SO₄, filtered, and concentrated under reduced pressure. Products were purified by flash chromatography.



Lactone **294** was prepared from xanthate **272** according to the general procedure given above. The product was isolated as a white solid in 55% yield following flash chromatography [silica, dichloromethane–hexanes, 4:1]. The byproduct, lactone **295-a**, was also isolated as a pale yellow oil in 33% yield.

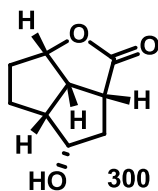
294. ^1H NMR (300 MHz, CDCl_3) δ 4.78 (dd, $J = 7.9, 5.3$ Hz, 1H), 3.22–3.16 (m, 1H), 2.53 (ddt, $J = 11.4, 4.7, 1.5$ Hz, 1H), 2.48–2.42 (m, 1H), 1.96 (ddt, $J = 13.0, 11.3, 3.3$ Hz, 1H), 1.80–1.69 (m, 2H), 1.61–1.49 (m, 3H); ^{13}C NMR (75 MHz, CDCl_3) δ 181.6 (C), 81.0 (CH), 46.6 (CH), 39.2 (CH), 38.2 (CH_2), 38.0 (CH_2), 36.6 (CH), 34.6 (CH_2); IR (KBr, cm^{-1}) 1770 (s), 1187 (s), 1166 (s), 1002 (s), 983 (s); HRMS (ESI) calcd for $\text{C}_8\text{H}_{10}\text{O}_2 + \text{Na}^+$ 161.0578, found 161.0578.

295-a. ^1H NMR (300 MHz, CDCl_3) δ 4.80 (dd, $J = 7.9, 4.7$ Hz, 1H), 3.24–3.17 (m, 2H), 2.75 (q, $J = 7.3$ Hz, 2H), 2.64–2.58 (m, 2H), 2.09 (dtd, $J = 11.4, 0.9, 3.5$ Hz, 1H), 1.94 (ddd, $J = 14.3, 7.9, 3.8$ Hz, 1H), 1.59–1.50 (m, 2H), 1.34 (t, $J = 7.3$ Hz, 3H); ^{13}C NMR (75 MHz, CDCl_3) δ 178.4 (C), 80.3 (CH), 55.4 (CH), 46.5 (CH), 46.2 (CH), 42.2 (CH), 38.4 (CH_2), 35.4 (CH_2), 32.8 (CH_2), 14.6 (CH_3); IR (neat, cm^{-1}) 1772 (s), 1172 (m), 1028 (m), 987 (m); HRMS (ESI) calcd for $\text{C}_{10}\text{H}_{14}\text{O}_2\text{S}_2 + \text{Na}^+$ 253.0333, found 253.0333.



Lactone **292** was prepared from xanthate **276** according to the general procedure given above. The product was purified to a colourless oil in 72% yield by flash chromatography [silica, dichloromethane–hexanes, 1:1].

292. ^1H NMR (300 MHz, CDCl_3) δ 4.98–4.89 (m, 1H), 3.17 (ddd, $J = 9.5, 9.1, 7.2$ Hz, 1H), 3.04 (ddd, $J = 9.9, 8.4, 5.1$ Hz, 1H), 2.69–2.55 (m, 1H), 2.19–2.02 (m, 3H), 1.94–1.76 (m, 3H), 1.57–1.36 (m, 2H); ^{13}C NMR (75 MHz, CDCl_3) δ 181.3 (C), 84.9 (CH), 51.0 (CH), 46.4 (CH), 45.5 (CH), 34.8 (CH_2), 32.1 (CH_2), 32.0 (CH_2), 29.1 (CH_2); IR (neat, cm^{-1}) 1760 (s), 1179 (s), 1001 (s); HRMS (ESI) calcd for $\text{C}_9\text{H}_{12}\text{O}_2 + \text{Na}^+$ 175.0735, found 175.0733.



Lactone **300** was prepared from xanthate **299** according to the general procedure given above. The product was isolated as colourless oil in 75% yield following flash chromatography [silica, ethyl acetate–hexanes 1:2].

300. ^1H NMR (300 MHz, CDCl_3) δ 5.01 (dd, $J = 5.4, 6.6$ Hz, 1H), 4.30 (s, 1H), 3.49 (ddd, $J = 7.5, 8.3, 10.2$ Hz, 1H), 3.28 (ddd, $J = 10.2, 6.7, 10.0$ Hz, 1H), 2.60–2.47 (m, 1H), 2.37–2.19 (m, 2H), 2.16–2.05 (m, 1H), 1.96–1.83 (m, 1H), 1.82–1.66 (m, 1H), 1.32–1.15 (m, 1H); ^{13}C NMR (75 MHz, CDCl_3) δ 181.1 (C), 84.9 (CH), 78.3 (CH), 55.4 (CH), 49.4 (CH), 43.5 (CH), 40.0 (CH_2), 34.7 (CH_2), 26.9 (CH_2); IR (neat, cm^{-1}) 3407 (m), 1760 (s), 1191 (m), 989 (m); HRMS (ESI) calcd for $\text{C}_9\text{H}_{12}\text{O}_3 + \text{Na}^+$ 191.0684, found 191.0685.

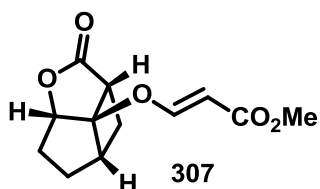


Lactone **293** was prepared from xanthate **281** according to the general procedure given above. The product was isolated as a colourless oil in 69% yield following flash chromatography [silica, dichloromethane–hexanes, 1:1 to 1:0]. Lactone **295**, a light yellow oil, was isolated as a byproduct during the synthesis of **293** (16% yield).

293. ^1H NMR (300 MHz, CDCl_3) δ 7.40–7.25 (m, 5H), 4.92 (dd, $J = 3.1, 6.3$ Hz, 1H), 4.49 (s, 2H), 3.14 (ddd, $J = 1.7, 4.2, 11.4$ Hz, 1H), 2.94–2.82 (m, 1H), 2.70 (ddd, $J = 10.1, 11.4, 12.9$ Hz, 1H), 2.30–2.14 (m, 1H), 2.21–2.03 (m, 1H), 2.07–1.97 (m, 1H), 1.78–1.66 (m, 1H), 1.54 (dt, $J = 12.9, 4.2$ Hz, 1H); ^{13}C NMR (75 MHz, CDCl_3) δ 177.9 (C), 137.2 (C), 128.6 (CH), 128.1 (CH), 127.4 (CH), 92.4 (C), 88.3 (CH), 67.5 (CH), 39.1 (CH), 37.8 (CH_2), 32.8 (CH_2), 31.2 (CH_2), 23.7 (CH_2); IR (neat, cm^{-1}) 3033 (w), 2958 (m), 2866 (m), 1771 (s), 1455 (m), 1350 (m), 1298 (m), 1267 (m), 1190 (m), 1102 (m), 1029 (m), 739 (m), 702 (m); SMB-IAA-GC-MS (EI) confirmed molecular formula $\text{C}_{15}\text{H}_{16}\text{O}_3$ with a matching factor of 998.31.

295. ^1H NMR (300 MHz, CDCl_3) δ 7.38–7.25 (m, 5H), 4.92 (dd, $J = 6.1, 2.8$ Hz, 1H), 4.57 (s, 2H), 3.25 (dd, $J = 2.0, 3.5$ Hz, 1H), 2.97 (t, $J = 3.7$ Hz, 1H), 2.95–2.88 (m, 1H), 2.75 (q, $J = 7.3$ Hz, 2H), 2.32–2.19 (m, 1H), 2.23–2.11 (m, 1H), 2.04 (dddd, $J = 5.9, 7.7,$

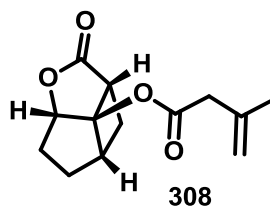
13.7, 3.1 Hz, 1H), 1.91–1.81 (m, 1H), 1.32 (t, $J = 7.3$ Hz, 3H); ^{13}C NMR (75 MHz, CDCl_3) δ 175.0 (C), 137.1 (C), 128.6 (CH), 128.1 (CH), 127.4 (CH), 90.1 (C), 88.6 (CH), 68.3 (CH_2), 48.2 (CH), 46.4 (CH), 45.4 (CH), 32.7 (CH_2), 32.6 (CH_2), 30.5 (CH_2), 14.6 (CH_3); IR (neat, cm^{-1}) 3032 (w), 2957 (m), 2925 (m), 2854 (m), 1771 (s), 1455 (m), 1374 (w), 1350 (m), 1295 (m), 1256 (m), 1182 (m), 1137 (m), 1096 (m), 1041 (m), 1002 (m), 736 (m), 698 (m); SMB-IAA-GC-MS (EI) confirmed molecular formula $\text{C}_{17}\text{H}_{20}\text{O}_3\text{S}_2$ with a matching factor of 992.31.



Lactone **307** was prepared from xanthate **304** according to the general procedure given above. The product was isolated as a colourless oil in 52% yield following flash chromatography [silica, dichloromethane].

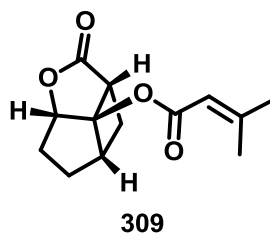
307. ^1H NMR (300 MHz, CDCl_3) δ 7.35 (d, $J = 12.3$ Hz, 1H), 5.36 (d, $J = 12.3$ Hz, 1H), 4.91 (dd, $J = 3.2, 6.2$ Hz, 1H), 3.65 (s, 3H), 3.23 (ddd, $J = 1.7, 4.3, 11.5$ Hz, 1H), 3.00–2.91 (m, 1H), 2.80 (ddd, $J = 10.2, 11.4, 12.8$ Hz, 1H), 2.35–2.19 (m, 1H), 2.22–2.13 (m, 1H), 2.12–2.01 (m, 1H), 1.81 (dddd, $J = 2.8, 5.7, 7.0, 12.6$ Hz, 1H), 1.59 (td, $J = 4.3, 12.9$ Hz, 1H); ^{13}C NMR (75 MHz, CDCl_3) δ 176.2 (C), 167.2 (C), 156.2 (CH), 101.9 (CH), 93.5 (C), 88.1 (CH), 51.4 (CH_3), 40.3 (CH), 38.5 (CH), 32.9 (CH_2), 31.2 (CH_2), 23.8 (CH_2); IR (neat, cm^{-1}) 2953 (m), 2870 (m), 1778 (s), 1716 (s), 1646 (s),

1437 (m), 1331 (m), 1293 (m), 1267 (m), 1192 (m), 1135 (s), 1030 (m), 970 (w), 843(w); SMB-IAA-GC-MS (EI) confirmed molecular formula $C_{12}H_{14}O_5$ with a matching factor of 998.31.



Lactone **308** was prepared from xanthate **305** according to the general procedure given above. The product was isolated as colourless oil 42% yield (containing 20% of **309**) following flash chromatography [silica, dichloromethane].

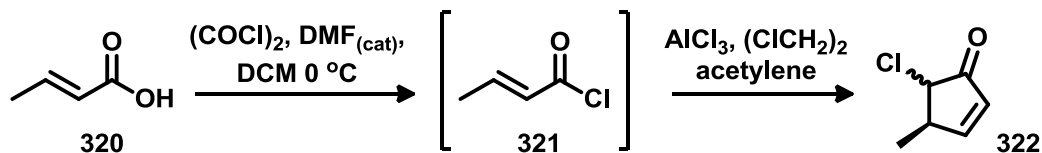
308. 1H NMR (300 MHz, $CDCl_3$) δ 4.93 (br s, 1H), 4.84 (br s, 1H), 3.23 (ddd, $J = 1.8, 4.5, 11.2$ Hz, 1H), 3.02 (d, $J = 1.0$ Hz, 2H), 3.00–2.92 (m, 1H), 2.85 (ddt, $J = 10.0, 0.9, 11.6$ Hz, 1H), 2.46–2.34 (m, 1H), 2.31 (ddd, $J = 13.4, 6.5, 16.1$ Hz, 1H), 2.08 (ddd, $J = 3.2, 7.2, 14.5$ Hz, 1H), 1.81–1.76 (m, 1H), 1.78 (t, $J = 1.0$ Hz, 3H), 1.57 (td, $J = 4.4, 12.4$ Hz, 2H); ^{13}C NMR (75 MHz, $CDCl_3$) δ 176.9 (C), 170.4 (C), 137.6 (C), 115.4 (CH_2), 90.3 (C), 89.0 (CH), 43.0 (CH_2), 40.9 (CH), 38.9 (CH), 33.0 (CH_2), 31.5 (CH_2), 24.5 (CH_2), 22.4 (CH_3); IR (neat, cm^{-1}) 3081 (w), 2949 (m), 2866 (m), 1778 (s), 1741 (s), 1650 (m), 1445 (m), 1346 (m), 1267 (m), 1224 (m), 1151 (s), 1033 (s), 974 (m); SMB-IAA-GC-MS (EI) confirmed molecular formula $C_{13}H_{16}O_4$ with a matching factor of 997.31.



Lactone **309** was prepared from xanthate **306** according to the general procedure given above. The product was purified by flash chromatography [silica, dichloromethane] to colourless oil in 47% yield.

309. ^1H NMR (300 MHz, CDCl_3) δ 5.63 (sep, $J = 1.3$ Hz, 1H), 4.95 (dd, $J = 3.2, 6.9$ Hz, 1H), 3.24 (ddd, $J = 1.8, 11.2, 4.5$ Hz, 1H), 3.00–2.92 (m, 1H), 2.84 (ddd, $J = 9.9, 11.2, 12.4$ Hz, 1H), 2.44 (dddd, $J = 5.2, 7.0, 9.1, 14.3$ Hz, 1H), 2.31 (tdd, $J = 6.8, 13.5, 9.3$ Hz, 1H), 2.14 (d, $J = 1.3$ Hz, 3H), 2.09–2.00 (m, 1H), 1.90 (d, $J = 1.4$ Hz, 3H), 1.76 (dddd, $J = 7.9, 2.3, 5.4, 13.2$ Hz, 1H), 1.57 (td, $J = 4.5, 12.4$ Hz, 1H); ^{13}C NMR (75MHz, CDCl_3) δ 177.4 (C), 165.3 (C), 159.8 (C), 114.8 (CH), 89.5 (C), 89.1 (CH), 40.9 (CH), 39.1 (CH), 33.1 (CH_2), 31.5 (CH_2), 27.6 (CH_3), 24.7 (CH_2), 20.4 (CH_3); IR (neat, cm^{-1}) 2943 (m), 2861 (m), 1777 (s), 1719 (s), 1646 (m), 1445 (m), 1343 (m), 1266 (m), 1224(m), 1141 (s), 1032 (m); SMB-IAA-GC-MS (EI) confirmed molecular formula $\text{C}_{13}\text{H}_{16}\text{O}_4$ with a matching factor of 978.31.

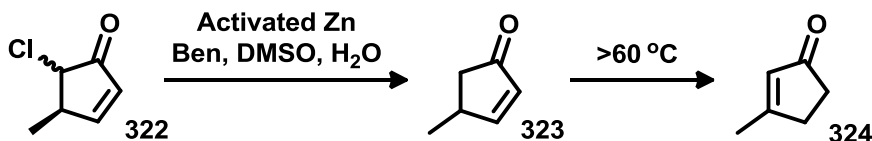
7.4 Experiments pertaining to Chapter 4



Enone **322** was prepared by adapting the procedure developed by Amos.¹⁵⁴ A flame-dried Schlenk flask was charged with crotonic acid (17.6 g, 1.0 equiv, 0.204 mol) and dissolved in dry dichloroethane (120 mL). The solution was cooled to $0\text{ }^\circ\text{C}$ and oxalyl chloride was added followed by a catalytic amount of DMF ($\sim 0.3\text{ mL}$). The reaction bubbled vigorously as it stirred at $0\text{ }^\circ\text{C}$ over the next 4 h. The stirring reaction mixture was warmed to room temperature and placed under a weak vacuum (200 mmHg) for 2 h, thereby removing any volatile by-products, leaving behind the pure crotonyl chloride. The reaction was then returned to $0\text{ }^\circ\text{C}$ and AlCl_3 (27.0 g, 1.0 equiv, 0.204 mol) was added over a 15 min period. After acclimating to room temperature, the solution pale yellow was warmed to $35\text{ }^\circ\text{C}$ over 75 min and acetylene was bubbled through at a rate of approximately 1 bubble per second. Over the next 10 h, the solution thickened considerably and a dark brown colour change was observed. The viscous product mixture was then poured over 700 mL of ice in a large beaker. The mixture was extracted with dichloromethane ($3 \times 60\text{ mL}$) and the combined organic extracts were washed with a saturated solution of aqueous NaHCO_3 solution ($2 \times 50\text{ mL}$), water ($2 \times 50\text{ mL}$), and brine (50 mL) then dried over MgSO_4 , filtered, and concentrated by rotary evaporation. The crude material was purified by flash chromatography [silica, ethyl ether–pentane, 0:1 to 1:4] giving diastereomers **322** (37.6 g, 64%) as colourless oil.

321. ^1H NMR (300 MHz, CD_2Cl_2) δ 7.26 (dq, $J = 15.2, 7.0$ Hz, 1H), 6.12 (dq, $J = 15.2, 1.7$ Hz, 1H), 2.02 (dd, $J = 7.0, 1.7$ Hz, 3H); ^{13}C NMR (75 MHz, CDCl_3) δ 165.6 (C), 152.5 (CH), 127.8 (CH), 18.3 (CH_3). Spectral assignments are in good agreement with previously published data.¹⁵⁴

322. ^1H NMR (300 MHz, CDCl_3) δ 7.64 (dd, $J = 6.0, 2.8$ Hz, 1H), 6.23 (dd, $J = 6.0, 1.9$ Hz, 1H), 4.42 (d, $J = 6.4$ Hz, 1H), 3.36–3.17 (m, 1H), 1.24 (d, $J = 7.3$ Hz, 1H). ^{13}C NMR (75 MHz, CDCl_3) δ 202.3 (C), 167.4 (CH), 130.4 (CH), 59.4 (CH), 39.9 (CH), 16.6 (CH_3). Spectral assignments are in good agreement with previously published data.¹⁵⁴

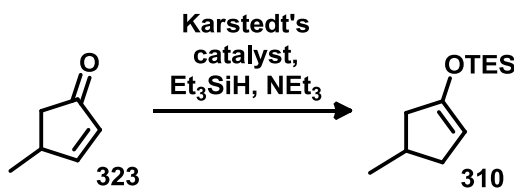


Compound **323** was prepared by adapting the reaction conditions also developed by Amos.¹⁵⁴ The enone **322** (13.1 g, 1.0 equiv, 0.101 mol) was dissolved in a mixture of benzene (140 mL), DMSO (14 mL), and water (5.5 mL) then stirred over activated zinc (33.0 g, 5.0 equiv, 0.505 mol) for 15 h. The crude mixture was filtered through a pad of celite, using pentane for rinsing. The filtrate was washed with brine (2×60 mL), dried with MgSO_4 , and filtered. The bulk of the solvent was removed by distillation (400 mmHg) through a one meter long vigeroux column, taking care to keep the temperature below $60\text{ }^\circ\text{C}$ in order to prevent the product from rearranging to **324**. The remaining

solute was purified by flash chromatography [silica, pentane (to elute residual benzene) then dichloromethane (to elute the product)]. The dichloromethane fractions were combined and concentrated by distillation through a vigorous column as described earlier. The residue was purified by short-path fractional distillation, giving **323** (8.05 g, 84%) as a colourless volatile oil.

323. ^1H NMR (300 MHz, CDCl_3) δ 7.59 (dd, $J = 5.6, 2.6$ Hz, 1H), 6.13 (dd, $J = 5.6, 2.0$ Hz, 1H), 3.21–2.85 (m, 1H), 2.60 (dd, $J = 18.8, 6.4$ Hz, 1H), 1.94 (dd, $J = 18.8, 2.1$ Hz, 1H), 1.21 (d, $J = 7.2$ Hz, 3H). 210.4 (C), 169.9 (CH), 133.2 (CH), 42.7 (CH), 36.1 (CH_2), 19.9 (CH_3). Spectral assignments are in good agreement with previously published data.¹⁵⁴

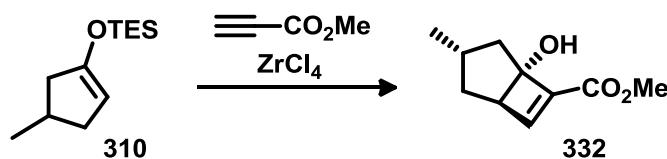
324. ^1H NMR (300 MHz, CDCl_3) δ 5.94 (dq, $J = 2.7, 1.3$ Hz, 1H), 2.60–2.57 (m, 1H), 2.56 (tt, $J = 2.2, 1.2$ Hz, 1H), 2.44–2.38 (m, 2H), 2.13 (d, $J = 1.1$ Hz, 3H). ^{13}C NMR (75 MHz, CDCl_3) δ 210.2 (C), 178.8 (CH), 130.7 (CH), 35.7 (CH_2), 33.0 (CH_2), 19.4 (CH_3). Spectral assignments are in good agreement with commercial source.



Triethylsilane (2.73 g, 23.5 mmol, 1.1 eq), freshly distilled triethylamine (0.220 g, 2.14 mmol, 0.10 eq), and ketone **323** (2.05 g, 21.3 mmol, 1.0 eq) were added via syringe into flame-dried 20 mL Biotage microwave reactor vial under an atmosphere of Ar. The vial

was immersed in a room temperature water bath and Karstedt's catalyst (0.07 mL, 2% Pt in xylenes) was added, causing the pale yellow solution to turn deep yellow. Within 30 minutes, the colour suddenly changed to dark brown and the reaction warmed considerably. After stirring for an additional 2 h, the volatile components were removed under high vacuum and the residue was purified by flash chromatography [florisil, hexanes], to give silyl enol ether **310** (4.28 g, 94%) as a pale yellow oil.

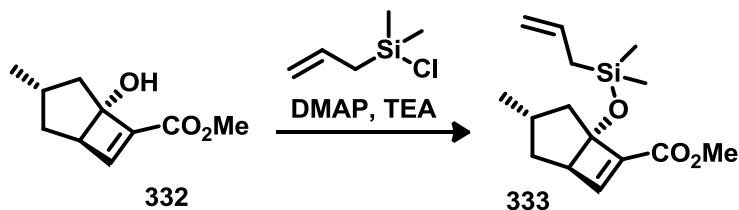
221. ^1H NMR (300 MHz, CDCl_3) δ = 4.54–4.51 (m, 1H), 2.46–2.20 (m, 2H), 2.32–2.22 (m, 1H), 1.93–1.86 (m, 1H), 1.02 (d, J = 6.6 Hz, 3H), 0.96 (t, J = 7.9 Hz, 9H), 0.65 (q, J = 7.9 Hz, 6H); ^{13}C NMR (75 MHz, CDCl_3) δ = 154.0 (C), 101.4 (CH), 41.8 (CH_2), 37.2 (CH_2), 30.1 (CH), 22.2 (CH_3), 6.6 (CH_3), 4.8 (CH_2). IR (neat, cm^{-1}): 2955 (s), 2914 (m), 2845 (w), 1646 (s), 1458 (m), 1338 (m), 1261 (m), 1241 (m), 1215 (m), 1074 (m), 1005 (m), 921 (m), 813 (m), 746 (s).



A flame-dried round-bottom flask was charged with freshly sublimed ZrCl_4 (6.00 g, 25.7 mmol, 1.2 eq) inside a glovebox, then transferred to the fumehood under a nitrogen atmosphere. Solvents dichloromethane (100 mL) and ethyl ether (10 mL) were added via syringe and the ZrCl_4 was sonicated into solution. Upon cooling to 0 °C, methyl propiolate (3.06 g, 36.4 mmol, 1.7 eq) was added, causing the cloudy white solution to turn yellow. After 10 min, the silyl enol ether **310** (4.28 g, 20.1 mmol, 1.0 eq) was added

at 0 °C, and the solution immediately turned reddish brown. After 20 min, 10% HCl (25 mL) was added and the reaction stirred overnight, acclimating to room temperature. The reaction was extracted with ethyl ether (3 × 40 mL) and the combined organic layer was washed with saturated NaHCO₃ solution (20 mL), H₂O (20 mL), and brine (20 mL) then dried over MgSO₄, filtered, and concentrated by rotary evaporation. The crude material was purified by flash chromatography [silica, ethyl ether–hexanes, 3:7], giving alcohol **332** (2.42 g, 67%) as a pale yellow oil.

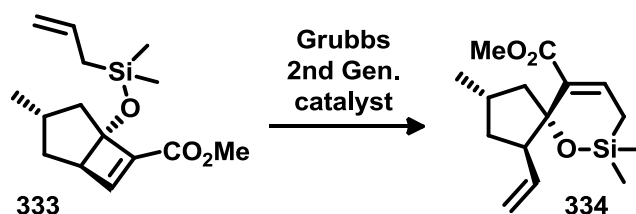
332. ¹H NMR (300 MHz, CDCl₃) δ = 6.76 (br s, 1H), 3.69 (s, 3H), 2.84 (d, *J* = 7.5 Hz, 1H), 2.10 (dd, *J* = 5.7, 12.6 Hz, 1H), 1.87–1.73 (m, 1H), 1.53 (dd, *J* = 5.8, 12.9 Hz, 1H), 1.19 (ddd, *J* = 12.9, 11.9, 7.6 Hz, 1H), 1.15 (t, *J* = 12.0 Hz, 1H), 0.98 (d, *J* = 6.5 Hz, 3H); ¹³C NMR (75 MHz, CDCl₃): δ = 161.7 (C), 147.9 (CH), 139.7 (C), 86.3 (C), 54.1 (CH₃), 52.2 (CH), 41.0 (CH₂), 33.5 (CH₂), 32.3 (CH), 18.6 (CH₃); IR (neat, cm⁻¹): 3427 (s), 2953 (s), 2927 (s), 2871 (m), 2849 (m), 1720 (s), 1456 (m), 1463 (m), 1274 (s), 1192 (m), 1102 (m), 1067 (m), 767 (m), 746 (m); HRMS (EI): calcd for C₁₀H₁₄O₃⁺ 182.09429, found 182.09440.



Alcohol **332** (0.902 g, 4.95 mmol, 1.0 eq) was added to a flame-dried round-bottom flask and taken up in dichloromethane (50 mL). The solution was cooled to 0 °C and DMAP

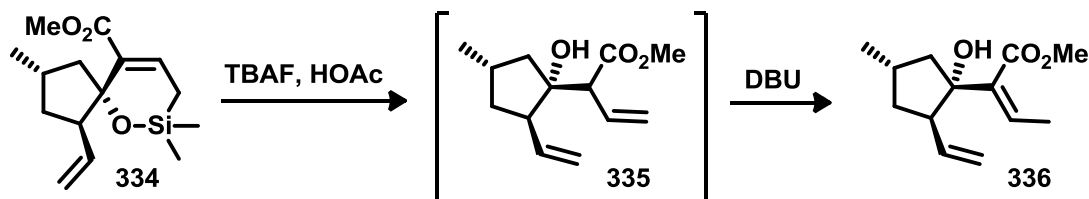
(60.0 mg, 0.494 mmol, 0.10 eq), freshly distilled triethylamine (1.50g, 14.8 mmol, 3.0 eq), and dimethylallylsilyl chloride (0.865 g, 6.42 mmol, 1.3 eq), were sequentially added. The reaction stirred overnight, acclimating to room temperature. Upon quenching with saturated NaHCO₃ solution (10 mL), the crude mixture was extracted with ethyl ether (3 × 15 mL) and the combined organic layer was washed with saturated NaHCO₃ solution (20 mL), H₂O (2 × 20 mL), and brine (20 mL) then dried over MgSO₄, filtered, and concentrated by rotary evaporation. The crude material was purified by flash chromatography [florisil, dichloromethane–hexanes, 1:1] giving compound **333** (1.24 g, 90%) as pale yellow oil.

333. ¹H NMR (300 MHz, CDCl₃) δ = 6.73 (br s, 1H), 5.75 (ddt, *J* = 16.8, 10.2, 8.1 Hz, 1H), 4.82 (ddd, *J* = 11.3, 2.2, 1.1 Hz, 1H), 4.84 (ddd, *J* = 15.6, 2.3, 1.3 Hz, 1H), 3.72 (s, 3H), 2.91 (d, *J* = 7.3 Hz, 1H), 2.19 (dd, *J* = 12.6, 5.7 Hz, 1H), 1.82–1.66 (m, 1H), 1.58 (d, *J* = 8.3 Hz, 2H), 1.55 (dd, *J* = 13.1, 6.0 Hz, 1H), 1.19 (ddd, *J* = 12.9, 11.8, 7.4 Hz, 1H), 1.15 (t, *J* = 12.0 Hz, 1H), 0.99 (d, *J* = 6.5 Hz, 3H), 0.09 (s, 6H). ¹³C NMR (75 MHz, CDCl₃): δ = 162.3 (C), 147.6 (CH), 141.3 (C), 134.7 (CH), 114.0 (CH₂), 88.2 (C), 54.9 (CH₃), 51.5 (CH), 42.7 (CH₂), 34.0 (CH₂), 32.1 (CH), 26.2 (CH₂), 19.1 (CH₃), -0.18 (CH₃), -0.23 (CH₃); IR (neat, cm⁻¹): 2953 (s), 2927 (m), 2851 (w), 1726 (s), 1630 (w), 1435 (m), 1315 (m), 1255 (m), 1189 (m), 894 (m), 838 (m), 798 (m); HRMS (EI): calcd for C₁₅H₂₄O₃Si⁺ 280.14947, found 280.14954.



Compound **333** (2.21 g, 7.91 mmol, 1.0 eq) was added to a flame-dried round-bottom flask and dissolved in dichloromethane (100 mL). Grubbs 2nd Generation catalyst (20.2 mg, 0.3 mol%) was then added, causing the colourless solution to turn brown. After stirring overnight at room temperature, the catalyst was poisoned with ~2 mL of ethyl vinyl ether, stirring for an additional 30 min. The solvent was removed by rotary evaporation and the crude material was purified through a plug of silica gel [silica, ethyl ether–hexane, 1:9], providing compound **334** (2.01 g, 90%) as a pale yellow oil.

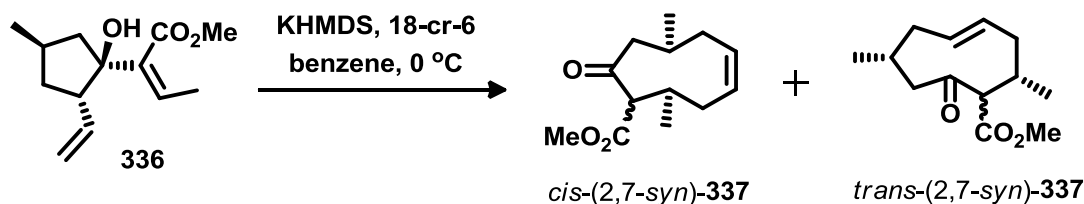
334. ¹H NMR (300 MHz, CDCl₃) δ = 6.96 (t, *J* = 6.1 Hz, 1H), 5.73 (ddd, *J* = 17.1, 10.2, 8.8 Hz, 1H), 4.83 (ddd, *J* = 10.1, 2.2, 0.7 Hz, 1H), 4.89 (ddd, *J* = 17.1, 2.2, 1.1 Hz, 1H), 3.63 (s, 3H), 2.83 (dd, *J* = 15.3, 7.4 Hz, 1H), 2.71 (dd, *J* = 13.6, 8.7 Hz, 1H), 2.36–2.20 (m, 1H), 1.84 (dt, *J* = 12.4, 7.1 Hz, 1H), 1.63 (ddd, *J* = 12.6, 7.0, 5.8 Hz, 1H), 1.46 (dd, *J* = 13.6, 5.1 Hz, 1H) 1.41 (d, *J* = 6.1 Hz, 2H), 1.07 (d, *J* = 6.9 Hz, 3H), 0.19 (s, 3H), 0.08 (s, 3H); ¹³C NMR (75 MHz, CDCl₃) δ = 168.2 (C), 139.5 (CH), 137.9 (C), 137.4 (CH), 114.3 (CH₂), 88.2 (C), 58.6 (CH₃), 51.4 (CH), 48.6 (CH₂), 39.3 (CH₂), 31.7 (CH), 22.3 (CH₃), 14.0 (CH₂), 1.04 (CH₃), 0.09 (CH₃); IR (neat, cm⁻¹) 2952 (m), 2869 (m), 1717 (s), 1609 (w), 1435 (m), 1258 (s), 1035 (s), 840 (m), 804 (m); HRMS (EI): calcd for C₁₅H₂₄O₃Si⁺ 280.1495, found 280.1496.



Compound **334** (1.07 g, 3.81 mmol, 1.0 eq) was taken up in glacial acetic acid (10 mL) in a round-bottom flask. TBAF (1M in THF, 19.0 mL, 19.0 mmol, 5 eq) was added and the solution stirred at room temperature for 90 min. The reaction was diluted with ethyl ether (50 mL) and washed twice with water (20 mL). The organic phase was carefully neutralized using saturated NaHCO_3 solution and the combined basic aqueous layer was extracted three times with ethyl ether (20 mL). The combined organic extracts were then washed twice water (20 mL) and brine (20 mL) then dried over MgSO_4 , filtered, and concentrated by rotary evaporation. ^1H NMR analysis of the crude residue typically revealed a variable mixture of predominately compounds **335** and **336**. Stirring the neat crude oil with DBU (5 mL) overnight effectively induced the migration of the alkene of **335** into conjugation with the ester. The reaction mixture was then diluted in ethyl ether (30 mL) and washed with a saturated solution of aqueous NH_4Cl solution (3×15 mL). The aqueous washing were back extracted with ethyl ether (20 mL) and the combined organic layer was washed with an addition 20 mL of water and 20 mL of brine, then dried over MgSO_4 , filtered, and concentrated by rotary evaporation. The crude material was purified by flash chromatography [silica, dichloromethane–hexane, 1:1 to 1:0], giving alcohol **336** (0.573 g, 67%) as colourless oil.

335. ^1H NMR (300 MHz, CDCl_3) δ 6.43 (ddd, $J = 17.6, 11.3, 0.8$ Hz, 1H), 5.76 (ddd, $J = 17.0, 10.2, 6.3$ Hz, 1H), 5.23 (dt, $J = 17.6, 1.1$ Hz, 1H), 5.12 (dt, $J = 11.2, 1.2$ Hz, 1H), 5.02 (dt, $J = 10.1, 1.4$ Hz, 1H), 4.95 (dt, $J = 17.1, 1.5$ Hz, 1H), 3.79 (s, 3H), 3.55–3.45 (m, 1H), 2.81–2.71 (m, 1H), 2.19–2.09 (m, 2H), 1.82–1.73 (m, 1H), 1.55–1.42 (m, 1H), 1.07 (dd, $J = 14.1, 6.2$ Hz, 1H), 1.00 (d, $J = 6.3$ Hz, 3H).

336. ^1H NMR (300 MHz, CDCl_3) δ = 6.14 (q, $J = 7.2$ Hz, 1H), 5.51 (ddd, $J = 17.1, 10.3, 8.8$ Hz, 1H), 4.88 (ddd, $J = 10.3, 2.1, 0.6$ Hz, 1H), 4.90 (ddd, $J = 17.1, 2.0, 1.1$ Hz, 1H), 3.8 (s, 3H), 3.60 (br s, 1H), 2.81 (dt, $J = 9.0, 2.4$ Hz, 1H), 2.31–2.22 (m, 1H), 1.87 (d, $J = 7.1$ Hz, 3H), 2.24–2.15 (m, 1H), 1.83–1.78 (m, 2H), 1.44 (ddd, $J = 12.6, 3.4, 1.6$ Hz, 1H), 1.10 (d, $J = 6.6$ Hz, 3H); ^{13}C NMR (75 MHz, CDCl_3) δ = 169.9 (C), 138.8 (CH), 135.7 (C), 134.6 (CH), 114.9 (CH_2), 85.4 (C), 55.5 (CH_3), 51.3 (CH), 42.6 (CH_2), 38.4 (CH_2), 29.4 (CH), 23.1 (CH_3), 15.7 (CH_3); IR (neat, cm^{-1}): 3514 (m), 2952 (s), 2930 (s), 2869 (m), 1727 (s), 1697 (s), 1437 (m), 1386 (m), 1266 (m), 1212 (m), 1159 (m), 994 (m), 913 (m); HRMS (ESI): calcd for $\text{C}_{13}\text{H}_{20}\text{O}_3 + \text{Na}^+$ 247.1305, found 247.1306.

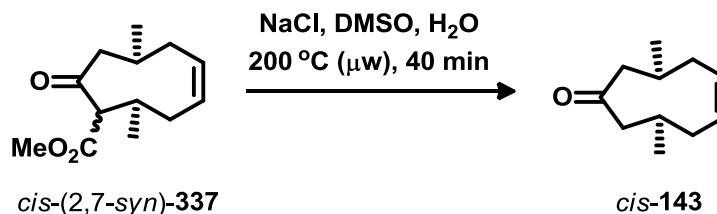


A flame-dried round bottom flask was charged with freshly distilled 18-crown-6 ether (0.300 g, 2 equiv, 1.11 mmol) and alcohol **336** (0.125 g, 1.0 equiv, 0.557 mmol) and

freshly distilled THF (20 mL). The solution was cooled to $-40\text{ }^{\circ}\text{C}$ and a solution of KHMDS (0.5 M in toluene, 3.35 mL, 3.0 equiv, 1.67 mmol) was added dropwise. After 2 h the reaction was warmed to $-20\text{ }^{\circ}\text{C}$ and stirred for an additional 6 h. The reaction was quenched with a saturated solution of aqueous NH_4Cl (5 mL). The aqueous layer was extracted with ethyl ether ($2 \times 15\text{ mL}$) and the combined organic extracts were washed with water (15 mL) and brine (15) then dried over MgSO_4 , filtered and concentrated by rotary evaporation. The crude residue was purified by flash chromatography [silica, ethyl ether–pentane; 1:19] giving a mixture of nonenone products of which *cis*-(2,7-*syn*)-**337** (25.3 mg, 20%) and *trans*-(2,7-*syn*)-**337** (19.8 mg, 15%) are the major isolable products.

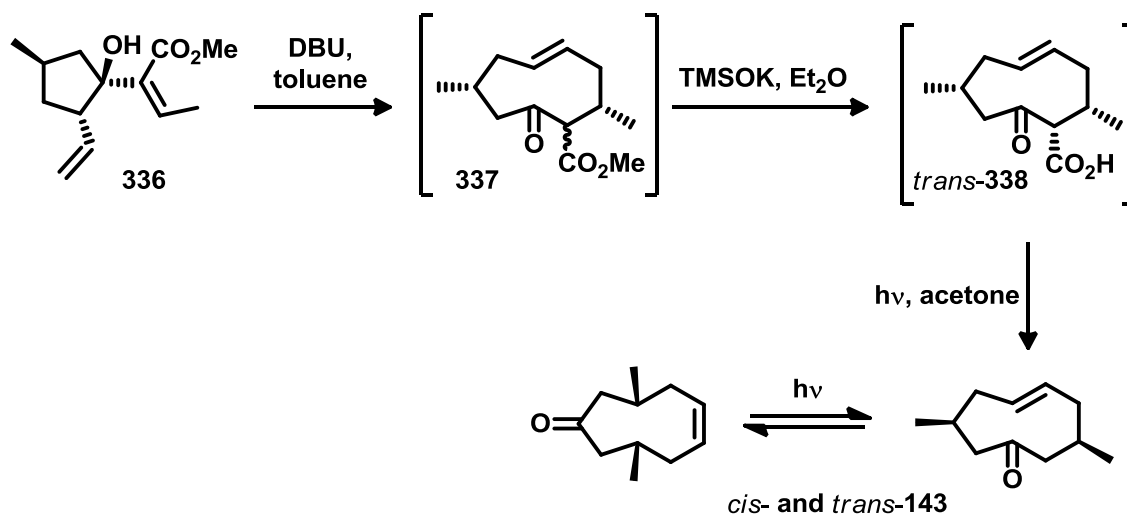
cis-(2,7-*syn*)-**337**. ^1H NMR (300 MHz, CDCl_3) δ 5.45 – 5.25 (m, 2H), 3.70 (s, $J = 1.9$ Hz, 3H), 3.35 (d, $J = 8.6$ Hz, 1H), 2.51 – 2.23 (m, 2H), 2.11 – 1.95 (m, 1H), 1.95 – 1.80 (m, 2H), 1.64 (br d, $J = 5.8$ Hz, 2H), 0.91 (d, $J = 6.7$ Hz, 3H), 0.86 (d, $J = 6.6$ Hz, 3H). ^{13}C NMR (75 MHz, CDCl_3) δ 204.6 (C), 169.7 (C), 129.1 (CH), 128.3 (CH), 127.8 (CH), 127.2 (CH), 64.7 (CH), 52.2 (CH_3), 49.4 (CH_2), 39.8 (CH_2), 37.8 (CH_2), 33.07 (CH), 28.9 (CH), 19.7 (CH_3), 17.0 (CH_3).

trans-(2,7-*syn*)-**337**. ^1H NMR (300 MHz, CDCl_3) δ 5.79 (dt, $J = 16.3, 7.5$ Hz, 1H), 5.25 – 5.12 (m, 1H), 3.74 (s, 3H), 3.13 (dd, $J = 2.6, 0.9$ Hz, 1H), 2.83 – 2.68 (m, 1H), 2.52 – 2.39 (m, 1H), 2.33 – 2.21 (m, 3H), 2.20 – 2.05 (m, 2H), 1.98 (ddd, $J = 14.5, 2.0, 1.2$ Hz, 1H), 1.10 (d, $J = 6.9$ Hz, 3H), 1.01 (d, $J = 6.7$ Hz, 3H); ^{13}C NMR (75 MHz, CDCl_3) δ 208.4 (C), 170.9 (C), 136.9 (CH), 133.7 (CH), 64.2 (CH), 51.7 (CH_3), 48.0 (CH_2), 43.2 (CH), 41.6 (CH_2), 35.5 (CH), 32.4 (CH_2), 21.67 (CH_3), 21.32 (CH_3).



The β -keto ester *cis*-(2,7-*syn*)-**337** (14.0 mg, 1.0 equiv, 0.0624 mmol) was dissolved in DMSO in a Biotage microwave reactor vial. Sodium chloride was added (12.0 mg, 2.5 equiv, 0.156 mmol) along with 3 drops of water. The vial was crimp-sealed and warmed to 200 °C for 3 min using a scientific microwave reactor. The crude reaction mixture was diluted in ethyl ether (3 mL) and washed with brine (3 \times 3 mL). The organic phase was dried over MgSO₄, filtered, and carefully concentrated using a gentle stream of air. The resulting residue was purified by column chromatography (silica, ethyl ether–pentane 1:19). The relevant fractions were again concentrated under a gentle stream of air, producing the desired *cis*-**143** (1.5 mg, 14%).

cis-**143**. ¹H NMR (300 MHz, CDCl₃) δ 5.56 – 5.39 (m, 2H), 2.39 (dd, $J = 12.2, 1.5$ Hz, 2H), 2.32 – 2.24 (m, 2H), 2.28 – 2.16 (m, 4H), 2.09 – 2.00 (m, 2H), 1.04 (d, $J = 6.6$ Hz, 6H).



Using a flame-dried round-bottom flask, fitted with an oven-dried condenser and under an argon purge, alcohol **336** (0.320 g, 1.43 mmol, 1.0 eq) and DBU (0.261 g, 1.71 mmol, 1.2 eq) were dissolved in toluene (60 mL) and refluxed for 18 h. The reaction mixture was transferred to a separatory funnel and washed with saturated NH₄Cl solution (2 × 20 mL), then with water (20 mL) and brine (20 mL). The organic layer was dried over MgSO₄, filtered, and concentrated by rotary evaporation. The crude oil (0.271 g) was taken up with ethyl ether (10 mL) in a flame-dried round-bottom flask, along with TMSOK (0.460 g, 3.60 mmol, 3 eq) and the mixture stirred at room temperature overnight, turning a deep yellow colour. The crude reaction mixture was transferred to a separatory funnel and the acidic intermediates extracted with 10% NaOH solution (3 × 5 mL). The combined basic aqueous washings were then back-extracted with 10 mL of ethyl ether before acidification (pH of 1–2) using 10% HCl solution. The aqueous layer was re-extracted with ethyl ether (3 × 10 mL) and the combined organic layer was washed with an additional 5 mL of water and 5 mL of brine, dried over MgSO₄, filtered,

then concentrated by rotary evaporation, giving *trans*-**338** as a white solid (0.183 mg). Slow diffusion of hexanes into a solution of this material in dichloromethane provided X-ray quality crystals. The remainder was taken up in acetone (5 mL) and the solution was irradiated for 15 h at 256 nm using inside an 8-bulb light box. The acetone was *carefully* removed by rotary evaporation and the residual oil purified by flash chromatography [silica, ethyl ether–pentane 1:9]. Ketones **143** (0.141 mg; 59%) were obtained as an unseparated 1:1.5 mixture of *cis* and *trans* isomers; however, this ratio was found to vary from batch to batch.

trans-(2,7-*syn*)-**337**. Identical to the spectral data obtained above.

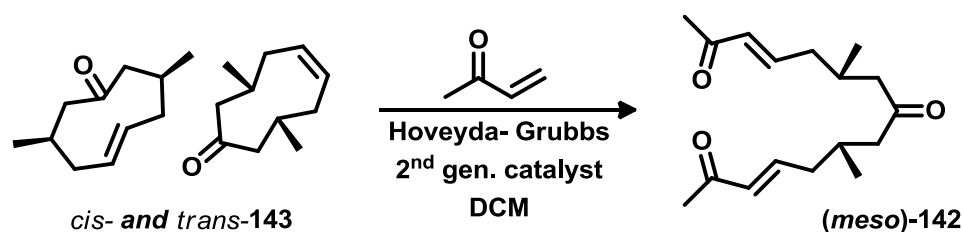
trans-**338**. ^1H NMR (300 MHz, CDCl_3) δ 5.82 – 5.67 (m, 1H), 5.70 – 5.57 (m, 1H), 5.31 – 5.19 (m, 1H), 5.20 – 5.08 (m, 1H), 3.43 (d, $J = 10.5$ Hz, 1H), 3.29 (d, $J = 10.7$ Hz, 1H), 2.87 – 2.58 (m, 1H), 2.48 – 2.32 (m, 3H), 2.12 (dd, $J = 12.9, 2.0$ Hz, 1H), 1.82 – 1.70 (m, 1H), 1.70 – 1.40 (m, 3H), 1.10 (d, $J = 6.7$ Hz, 4H), 1.08 (d, $J = 6.4$ Hz, 6H), 1.07 (d, $J = 6.8$ Hz, 5H), 1.06 (d, $J = 6.7$ Hz, 5H); HRMS (ESI): calcd for $\text{C}_{12}\text{H}_{18}\text{O}_3 - \text{H}^+$ 209.1183, found 209.1177.

cis- and *trans*-**143**. ^1H NMR (300 MHz, CD_2Cl_2) δ = 5.66 (dt, $J = 15.8, 7.9$ Hz, 0.43H), 5.45–5.32 (m, 0.87H), 5.07 (dddd, $J = 15.7, 11.3, 4.4, 0.8$ Hz, 0.54H), 2.49–1.90 (m, 9.1H), 1.51–1.29 (m, 1.1H), 0.98–0.93 (3 sets of d, 6.1H) [0.95 ($J = d, 6.7$ Hz), 0.94 (d, $J = 6.6$ Hz), 0.93 (d, $J = 6.6$ Hz)]; ^{13}C NMR (75 MHz, CDCl_3) δ = 214.4 (*cis*-C), 213.5 (*trans*-C), 137.2 (*trans*-CH), 133.7 (*trans*-CH), 132.74 (*cis*-CH), 52.0 (*cis*-CH₂), 51.45

(*trans*-CH₂), 50.96 (*trans*-CH₂), 41.9 (*trans*-CH₂), 40.2 (*cis*-CH₂), 39.2 (*trans*-CH), 37.1 (*trans*-CH), 34.9 (*trans*-CH₂), 33.6 (*cis*-CH), 23.2 (*trans*-CH₃), 22.8 (*cis*-CH₃), 21.6 (CH₃-*trans*); IR (neat, cm⁻¹) 2954 (s), 2926 (s), 2869 (m), 2854 (m), 1703 (s), 1699 (s), 1693 (s), 1456 (s), 1348 (s), 1296 (m), 1139 (m), 979 (m).

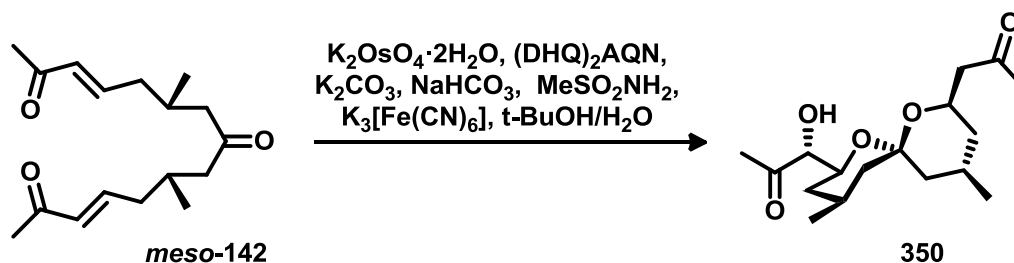
Ab initio calculations for the heats of formation for *cis*- and *trans*-**143**, along with their E and Z enol tautomers (**340**) were performed using Wavefunction Inc's Spartan 2010 mechanics software with the B3LYP 6-31 G(d) basis set.

7.5 Experiments pertaining to Chaper 5



A mixture of cis and trans ketones (**143**) (47.9 mg, 0.288 mmol, 1.0 eq) was added to a flame-dried round-bottom flask and dissolved in dichloromethane (20 mL), along with Hoveyda-Grubbs 2nd Generation catalyst (27.0 mg, 0.0432 mmol, 15 mol%), which caused the colourless solution to become green, and finally freshly distilled methyl vinyl ketone (0.84 g, 11.5 mmol, 40 eq) was added. The reaction proceeded at room temperature overnight and was quenched by adding ~2 mL of ethyl vinyl ether with an additional 30 min of stirring. The solvent was removed by rotary evaporation and the crude material was purified by flash chromatography [silica, ethyl ether–hexanes, 1:1], providing ketone **142** (68.4 mg, 81%) as a pale brown oil.

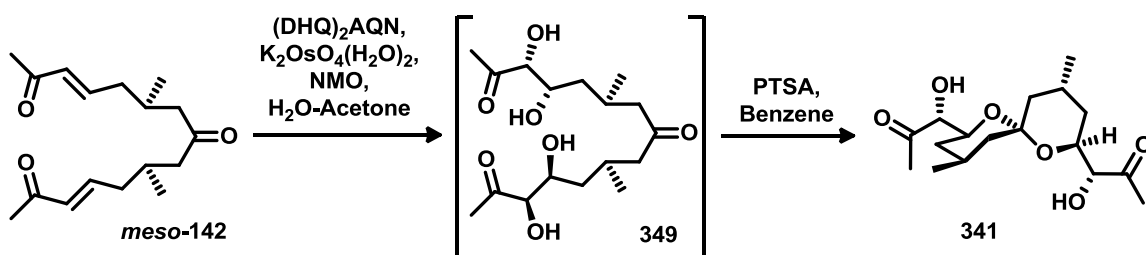
meso-**142**. ¹H NMR (300 MHz, CDCl₃) δ = 6.69 (td, *J* = 7.2, 15.9 Hz, 2H), 6.02 (td, *J* = 1.3, 15.8 Hz, 2H), 2.40–2.11 (m, 4H), 2.21 (s, 6H), 2.20–1.96 (m, 4H), 0.90 (d, *J* = 5.9 Hz, 6H); ¹³C NMR (75 MHz, CDCl₃) δ = 209.0 (C), 198.4 (2C), 145.9 (2CH), 132.8 (2CH), 49.9 (2CH₂), 39.5 (2CH₂), 28.4 (2CH₃), 27.0 (2CH), 19.9 (2CH₃); IR (neat, cm⁻¹) 2958 (m), 2927 (m), 2876 (m), 1709 (s), 1699 (s), 1674 (s), 1627 (m), 1458 (m), 1432(m), 1363 (s), 1254 (s), 982 (m); HRMS (ESI): calcd for C₁₇H₂₆O₃ + H⁺ 279.1955, found 279.1954.



Ketone *meso*-143 (13.2 mg, 0.0474 mmol, 1.0 eq), NaHCO_3 (24.0 mg, 0.286 mmol, 6.0 eq), K_2CO_3 (46.2 mg, 0.334 mmol, 7.0 eq), MeSO_2NH_2 (9.0 mg, 0.0950 mmol, 2.0 eq), $(\text{DHQ})_2\text{AQN}$ (2.0 mg, 0.00240 mmol, 5 mol%), and $\text{K}_3[\text{Fe}(\text{CN})_6]$ (34.8 mg, 0.296 mmol, 6.2 eq) were dissolved in $t\text{BuOH-H}_2\text{O}$ (1:1, 2 mL) in a round-bottom flask. To the yellow heterogeneous solution was added $\text{K}_2\text{OsO}_4 \cdot 2\text{H}_2\text{O}$ (1.1 mg/mL in H_2O , 0.250 mL, 0.000746 mmol, 1.6 mol%). The reaction stirred at 4 °C for 3 days. Acetone (1.0 mL) was then added and the reaction stirred at room temperature for an additional 24 h. Saturated Na_2SO_3 (2 mL) was added and the reaction stirred for an hour before it was transferred to a separatory funnel and extracted exhaustively with 5 mL portions of ethyl ether. The combined organic extracts were washed with brine, dried over MgSO_4 , filtered, and concentrated by rotary evaporation. The crude residue was adsorbed onto silica gel and purified by flash chromatography [silica, ethyl ether–hexanes, 20:80 to 60:40], giving **350** (5.9 mg, 41%).

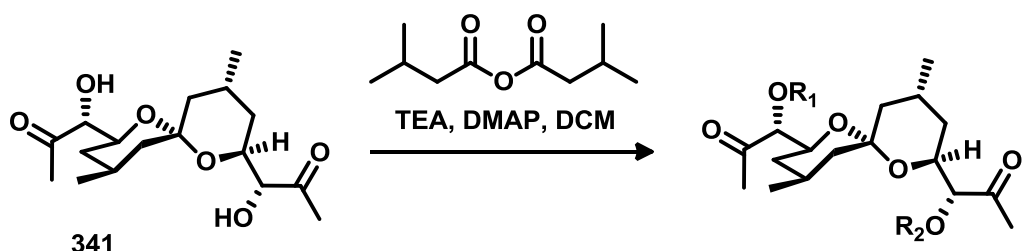
350. ^1H NMR (500 MHz, CDCl_3) δ = 4.32 (dddd, J = 11.5, 7.8, 5.4, 2.2 Hz, 1H), 4.03 (br s, 1H), 3.85 (td, J = 2.64, 11.93 Hz, 1H), 3.42 (br s, 1H), 2.56 (dd, J = 15.5, 7.8 Hz, 1H), 2.39 (dd, J = 15.4, 5.2 Hz, 1H), 2.29 (s, 3H), 2.15 (s, 3H), 2.12 (ddd, J = 13.9, 3.7, 1.7 Hz,

1H), 1.80–1.72 (m, 1H), 1.70–1.62 (m, 1H), 1.64–1.59 (m, 1H), 1.60–1.55 (m, 1H), 1.59–1.48 (m, 1H), 1.09 (d, $J = 12.8$ Hz, 1H), 1.04 (d, $J = 12.1$ Hz, 1H), 0.91 (d, $J = 6.5$ Hz, 3H), 0.87 (d, $J = 6.5$ Hz, 3H), 0.86–0.79 (m, 1H), 0.80–0.74 (m, 1H); ^{13}C NMR (125 MHz, CDCl_3) $\delta = 210.2$ (C), 207.3 (C), 96.7 (C), 79.3 (CH), 73.4 (CH), 67.1 (CH), 49.8 (CH₂), 44.5 (CH₂), 39.3 (CH₂), 36.9 (CH₂), 34.4 (CH₂), 30.9 (CH₃), 27.2 (CH₃), 26.4 (CH), 25.0 (CH), 22.4 (CH₃), 22.0 (CH₃); IR (neat, cm^{-1}) 3466 (s), 2952 (s), 2926 (s), 2871 (m), 1715 (s), 1456 (m), 1374 (m), 1366 (m), 1308 (m), 1196 (m), 1093 (m), 1010 (m), 888 (w); HRMS (ESI) calcd for $\text{C}_{17}\text{H}_{28}\text{O}_5 + \text{H}^+$ 313.2010, found 313.2009.



A solution of the ketone (*meso*-**142**) (60.0 mg, 0.215 mmol) in 5 mL of acetone was added slowly via syringe pump to a solution of NMO (0.125 g, 1.08 mol), $\text{DHQ}(\text{AQN})_2$ (9.2 mg, 0.0110 mol), and potassium osmate dihydrate (1 mg, 0.003 mmol) in acetone– H_2O (9:1, 5 mL) at 0 °C. A reaction temperature of 4 °C was maintained for three days using a refrigerated stir plate. The reaction was quenched with the addition of ~1 mL of sat. Na_2SO_3 solution which was allowed to stir for 30 min before the crude mixture was concentrated by rotary evaporation. The residue was taken up in benzene (6.0 mL) along with a spatula tip of PTSA. After stirring at room temperature overnight, then the crude mixture was concentrated by rotary evaporation, and purified by flash chromatography [silica, ethyl acetate–hexanes, 2:1 to 1:0] giving **341** as a white solid (36.7 mg, 52%).

341. ^1H NMR (300 MHz, CDCl_3) δ = 4.12 (dt, J = 2.6, 11.8 Hz, 1H), 3.98 (dt, J = 2.8, 6.5 Hz, 1H), 3.98 (dt, J = 2.5, 11.9 Hz, 1H), 3.96 (dd, J = 2.8, 6.8 Hz, 1H), 3.21 (d, J = 7.1 Hz, 1H), 3.13 (d, J = 6.5 Hz, 1H), 2.34 (s, 3H), 2.33 (s, 3H), 2.02 (m, 1H), 1.87 (m, 1H), 1.81 (ddd, J = 13.4, 11.8, 5.4 Hz, 1H), 1.59 (ddd, J = 11.0, 3.9, 1.9 Hz, 1H), 1.55 (dd, J = 13.7, 5.2 Hz, 1H), 1.52 (br d, J = 12.9 Hz, 1H), 1.44, (ddd, J = 13.8, 2.9, 1.4 Hz, 1H), 1.30 (br d, J = 14.0 Hz, 1H), 1.12 (q, J = 13.3 Hz, 1H), 1.07 (d, J = 7.3 Hz, 3H), 0.97 (t, J = 12.6 Hz, 1H), 0.85 (d, J = 6.7 Hz, 3H); ^{13}C NMR (75 MHz, CDCl_3) δ = 210.1 (C), 209.6 (C), 98.7 (C), 79.5 (CH), 79.2 (CH), 70.8 (CH), 66.0 (CH), 44.1 (CH_2), 39.8 (CH_2), 34.2 (CH_2), 31.4 (CH_2), 27.0 (CH_3), 26.8 (CH_3), 24.5 (CH), 24.4 (CH), 21.9 (CH_3), 20.3 (CH_3); IR (neat, cm^{-1}) 3467 (br), 2922(s), 2852 (m), 1713 (s), 1455 (m), 1376 (m), 1261 (m), 1182 (m), 1112 (m), 999 (m), 873 (m); HRMS (ESI) calcd for $\text{C}_{17}\text{H}_{28}\text{O}_6 + \text{Na}^+$ 351.1778, found 351.1778.



378; R_1 = isovalerate; R_2 = isovalerate
379; R_1 = H; R_2 = isovalerate
380; R_1 = isovalerate; R_2 = H

Using a flame dried round bottom flask, **341** (27.3 mg, 0.0830 mmol) was dissolved in dry dichloromethane (30 mL). DMAP (1 mg, 0.00830 mmol), TEA (0.060 mL, 0.420 mmol) and isovaleric anhydride (31.8 mg, 0.166 mmol) were added sequentially at room

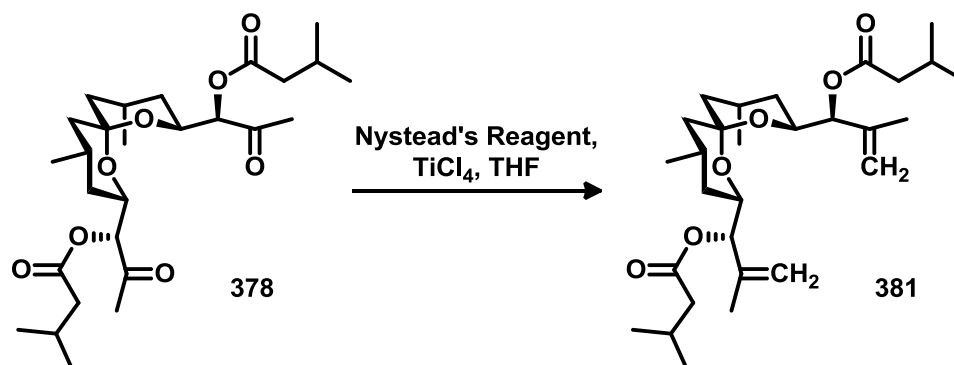
temperature. The reaction stirred for 72 h before quenching with a saturated NaHCO_3 solution (2 mL). The organic phase was extracted into ethyl acetate (30 mL), washed with H_2O (2×15 mL) and brine (15 mL), then dried over MgSO_4 , filtered, and concentrated by rotary evaporation. The residue was purified by flash chromatography [silica, dichloromethane–ethyl ether–hexanes; 4:1:5] providing the disubstituted spiroketal **378** (10.8 mg, 26%), and both monosubstituted compounds **379** (8.1 mg, 24%) and **380** (9.5 mg, 28%), all as clear colourless oils.

378. ^1H NMR (300 MHz, CDCl_3) δ = 4.98 (d, J = 3.8 Hz, 1H), 4.96 (d, J = 3.4 Hz, 1H), 4.19 (dt, J = 11.7, 3.0 Hz, 1H), 3.98 (ddd, J = 11.9, 3.7, 2.3 Hz, 1H), 2.30 (dd, J = 2.8, 1.1 Hz, 2H), 2.28 (d, J = 2.6 Hz, 2H), 2.19 (s, 3H), 2.17 (s, 3H), 2.10 (sept, J = 6.7 Hz, 2H), 2.00–1.91 (m, 1H), 1.86–1.74 (m, 1H), 1.66 (ddd, J = 13.1, 11.9, 5.4 Hz, 1H), 1.59 (dd, J = 13.5, 2.6 Hz, 1H), 1.54 (dd, J = 13.9, 5.9 Hz, 1H), 1.44 (br d, J = 13.3 Hz, 1H), 1.40 (br d, J = 10.9 Hz, 1H), 1.20 (br d, J = 13.1 Hz, 1H), 1.07 (d, J = 7.4 Hz, 3H), 0.97 (d, J = 6.6 Hz, 12H), 0.89 (t, J = 13.2 Hz, 1H), 0.87 (q, J = 13.2 Hz, 1H), 0.82 (d, J = 6.4 Hz, 3H); ^{13}C NMR (75 MHz, CDCl_3) δ 205.1 (C), 204.9 (C), 172.7 (C), 172.6 (C), 98.5 (C), 80.2 (CH), 79.8 (CH), 69.6 (CH), 65.0 (CH), 43.8 (CH_2), 43.0 (CH_2), 42.9 (CH_2), 39.5 (CH_2), 34.1 (CH_3), 31.1 (CH_3), 27.9 (CH), 27.7 (CH), 25.6 (CH), 24.5 (CH), 22.4 ($4 \times \text{CH}_3$), 22.0 (CH_3), 20.3 (CH_3); IR (neat, cm^{-1}) 2957 (s), 2930 (s), 2873 (m), 1738 (s), 1733 (s), 1456 (m), 1372 (m), 1295 (m), 1186 (m), 1102 (m), 998 (m), 980 (m); HRMS (ESI) calcd for $\text{C}_{27}\text{H}_{44}\text{O}_8 + \text{H}^+$ 497.3109, found 497.3108.

379. ^1H NMR (500 MHz, CDCl_3) δ 4.95 (d, $J = 3.1$ Hz, 1H), 4.17 (dt, $J = 11.9, 2.8$ Hz, 1H), 4.02 (dd, $J = 6.6, 1.9$ Hz, 1H), 3.94 (td, $J = 11.8, 2.2$ Hz, 1H), 3.39 (d, $J = 6.9$ Hz, 1H), 2.38 (s, 3H), 2.35 (d, $J = 7.0$ Hz, 2H), 2.19 (s, 3H), 2.17 (m, 1H), 2.02–1.99 (m, 1H), 1.88–1.79 (m, 1H), 1.64 (td, $J = 12.8, 6.2$ Hz, 1H), 1.60 (dd, $J = 13.5, 4.1$ Hz, 1H), 1.52 (dd, $J = 13.9, 5.5$ Hz, 1H), 1.52 (br d, $J = 12.3$ Hz, 1H), 1.43 (br d, $J = 14.1$ Hz, 1H), 1.24 (q, $J = 12.2$ Hz, 1H), 1.17 (br d, $J = 12.7$ Hz, 1H), 1.03 (d, $J = 7.2$ Hz, 3H), 0.99 (d, $J = 6.4$ Hz, 6H), 0.96 (t, $J = 12.8$ Hz, 1H), 0.86 (d, $J = 6.4$ Hz, 3H); ^{13}C NMR (100 MHz, CDCl_3) δ 208.4 (C), 207.2 (C), 172.7 (C), 98.7 (C), 80.4 (CH), 70.5 (CH), 69.1 (CH), 65.9 (CH), 43.8 (CH_2), 43.1 (CH_2), 39.5 (CH_2), 34.5 (CH_2), 31.2 (CH_2), 30.4 (CH_3), 29.6 (CH_3), 27.9 (CH), 26.1 (CH), 25.6 (CH), 24.6 (CH_3), 22.4 ($2 \times \text{CH}_3$), 20.1 (CH_3); IR (neat, cm^{-1}) 3468 (br), 2954 (s), 2928 (s), 2873 (m), 1721 (s), 1372 (m), 1294 (m), 1186 (m), 1109 (m), 997 (m), 885 (m) cm^{-1} ; HRMS (ESI) calcd for $\text{C}_{22}\text{H}_{36}\text{O}_7 + \text{Na}^+$ 435.2353, found 435.2350.

380. ^1H NMR (500 MHz, CDCl_3) δ = 5.02 (d, $J = 3.7$ Hz, 1H), 4.13 (dt, $J = 11.7, 2.5$ Hz, 1H), 4.03 (dt, $J = 12.1, 2.4$ Hz, 1H), 4.03 (dt, $J = 12.1, 2.4$ Hz, 1H), 3.31 (br d, $J = 7.2$ Hz, 1H), 2.40 (s, 3H), 2.35 (d, $J = 7.0$ Hz, 2H), 2.18–2.14 (m, 1H), 2.17 (s, 3H), 2.03 (m, 1H), 1.90 (dt, $J = 12.5, 4.7$ Hz, 1H), 1.84 (m, 1H), 1.56 (br d, $J = 13.6$ Hz, 1H), 1.54 (dd, $J = 14.1, 5.8$ Hz, 1H), 1.45 (br d, $J = 14.0$ Hz, 1H), 1.37 (br d, $J = 12.3$ Hz, 1H), 1.31 (br d, $J = 12.3$ Hz, 1H), 1.25–1.22 (m, 1H), 1.09 (d, $J = 7.2$ Hz, 3H), 0.99 (d, $J = 6.4$ Hz, 6H), 0.92 (q, $J = 12.3$ Hz, 1H), 0.81 (d, $J = 6.7$ Hz, 3H); ^{13}C NMR (100 MHz, CDCl_3) δ 208.4 (C), 206.7 (C), 172.5 (C), 99.1 (C), 80.0 (CH), 79.3 (CH), 70.6 (CH), 66.1 (CH), 44.2 (CH_2), 43.1 (CH_2), 39.6 (CH_2), 34.2 (CH_2), 31.9 (CH_2), (CH), 25.7 (CH), 24.5 (CH), 22.5

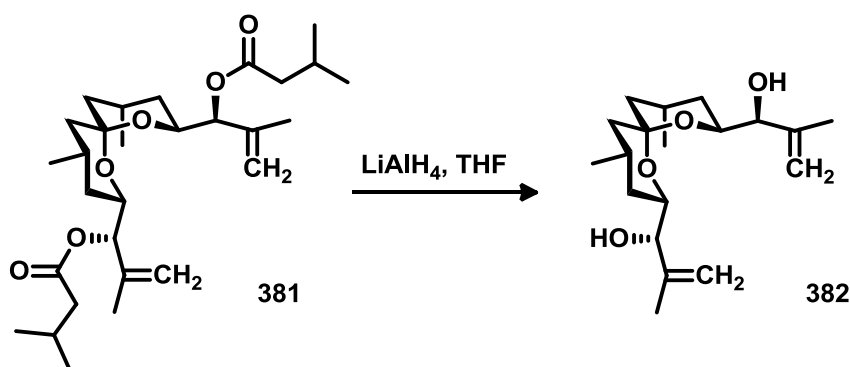
(CH₃), 22.4 (2 × CH₃), 20.4 (CH₃); IR (neat, cm⁻¹): 3476 (m), 2954 (s), 2873 (m), 1721 (s), 1356 (m), 1185 (m), 1109 (m), 1000 (m), 976 (m), 888 (m) cm⁻¹; HRMS (ESI) calcd for C₂₂H₃₆O₇ + Na⁺ 435.2353, found 435.2354.



Using flame dried glassware, TiCl₄ (1 M in dichloromethane, 0.390 mL, 0.390 mmol) was added dropwise to a suspension of Nysted's Reagent (20 wt% in THF, 0.890 g, 0.390 mmol) in freshly distilled THF (10 mL) at 0 °C. After stirring for 30 min, a solution of **378** (32.2 mg, 0.0649 mmol) in THF (1 mL) was also added. The reaction stirred for 20 h, acclimating to room temperature before it was quenched with aqueous solution of HCl (1 M, 2 mL). The crude mixture was extracted into ethyl acetate (30 mL), washed with H₂O (2 × 15 mL) and brine (15 mL), then dried over MgSO₄, filtered, and concentrated by rotary evaporation. The residue was purified by flash chromatography [silica, ethyl ether–hexanes, 1:9] providing **381** as colourless oil (27.5 mg, 86%).

381. ¹H NMR (300 MHz, CDCl₃) δ 5.13 (d, *J* = 7.7 Hz, 1H), 5.05 (d, *J* = 8.0 Hz, 1H), 5.03 (br s, 2H), 4.95 (br s, 2H), 4.00 (ddd, *J* = 11.9, 7.5, 2.3 Hz, 1H), 3.89 (ddd, *J* = 11.8, 8.0, 2.1 Hz, 1H), 2.19–2.14 (m, 4H), 2.13–2.07 (m, 2H), 2.03–1.96 (m, 1H), 1.93–1.85 (m, 1H), 1.76 (s, 3H), 1.74 (s, 3H), 1.60 (dd, *J* = 12.6, 3.9 Hz, 1H), 1.55 (dd, *J* = 13.9, 5.8

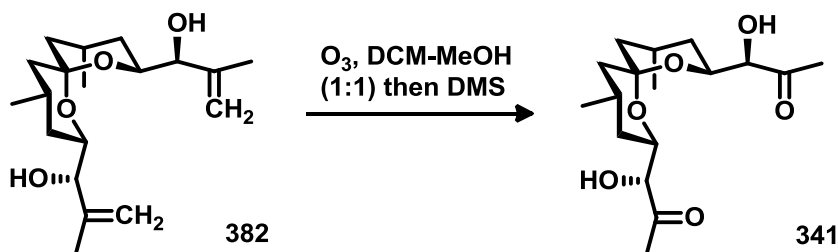
Hz, 1H), 1.47 (td, $J = 12.6, 5.6$ Hz, 1H), 1.43, (br d, $J = 12.3$ Hz, 1H) 1.37 (br d, $J = 12.6$ Hz, 1H), 1.18 (br d, $J = 12.6$ Hz, 1H), 1.12 (d, $J = 7.2$ Hz, 3H), 0.97 (t, $J = 12.7$ Hz, 1H), 0.95–0.91 (m, 12H), 0.82 (d, $J = 6.3$ Hz, 3H), 0.78 (q, $J = 12.7$ Hz, 1H); ^{13}C NMR (75 MHz, CDCl_3) δ 172.4 (C), 172.2 (C), 141.0 (C), 140.9 (C), 115.2 (CH_2), 115.1 (CH_2), 97.9 (C), 79.6 (CH), 79.5 (CH), 69.4 (CH), 64.8 (CH), 43.8 (CH_2), 43.7 (CH_2), 39.5 (CH_2), 34.8 (CH_2), 32.3(CH_2), 25.7 (CH_3), 25.6 (CH_3), 24.9 (CH_3), 24.8 (CH_3), 22.4 (CH), 22.1 (CH), 20.4 (CH_3), 18.8 (CH), 18.7 (CH); IR (neat, cm^{-1}): 2952 (s), 2922 (s), 2872 (m), 1738 (s), 1662 (m), 1455 (m), 1368 (m), 1188 (m), 999(m), 911 (m); HRMS (ESI) calcd for $\text{C}_{29}\text{H}_{48}\text{O}_6 + \text{Na}^+$ 515.3343, found 515.3345.



Using a flame dried round bottom flask, **381** (27.4mg; 0.0556 mmol) was dissolved in freshly distilled THF (5 mL) and cooled to -78 °C. Lithium aluminum hydride (25.0 mg, 0.556 mmol) was added and the reaction was allowed to stir for 16 h, acclimating to room temperature. A saturated solution of Rochelle salt (2 mL) was used to quench the excess reducing agent. The crude mixture was extracted with ether (15 mL) and the extracts were washed with water (2×10 mL) and brine (10 mL), then dried over MgSO_4 , filtered, and concentrated by rotary evaporation. The residue was purified by flash chromatography [silica, ethyl ether–hexanes; 1:5 to 1:0] providing the diol **382** as a white

solid (17.3 mg, 96%). Single crystals were obtained by slow evaporation of dichloromethane.

382. ^1H NMR (300 MHz, CDCl_3) δ 4.99 (br s, 1H), 4.97 (br s, 1H), 4.92 (br s, 2H), 3.86, (d, $J = 6.5$ Hz, 1H), 3.83 (d, $J = 5.6$ Hz, 1H), 3.73 (ddd, $J = 11.6, 6.9, 2.7$ Hz, 1H), 3.69 (ddd, $J = 11.8, 6.0, 2.2$ Hz, 1H), 2.55 (br s, 2H), 2.00 (m, 1H), 1.96 (m, 1H), 1.74 (s, 6H), 1.65, (br d, $J = 12.7$ Hz, 1H), 1.61 (dd, $J = 13.3, 6.3$ Hz, 1H), 1.56 (dd, $J = 11.2, 5.7$ Hz, 1H), 1.53 (dd, $J = 11.8, 5.6$ Hz, 1H), 1.48 (br d, $J = 13.4$ Hz, 1H), 1.23 (br d, $J = 13.4$ Hz, 1H), 1.13 (d, $J = 7.2$ Hz, 3H), 1.03 (t, $J = 12.8$ Hz, 1H), 0.96 (q, $J = 12.2$ Hz, 1H), 0.87 (d, $J = 6.5$ Hz, 3H); ^{13}C NMR (75 MHz, CDCl_3): $\delta = 144.1$ (C), 144.0 (C), 113.8 (CH_2), 113.1 (CH_2), 98.7 (C), 78.9 (CH), 78.2 (CH), 70.8 (CH), 66.3 (CH), 44.2 (CH_2), 40.3 (CH_2), 35.5 (CH_2), 32.5 (CH_2), 24.9 (CH), 24.5 (CH), 22.0 (CH_3), 21.0 (CH_3), 18.2 (CH_3), 17.9 (CH_3); IR (neat, cm^{-1}): 3468 (br), 2924 (s), 2853 (s), 1652 (m), 1456 (m), 1374 (m), 1210 (m), 1046 (m), 1009 (m), 980 (m), 898 (m); LRMS (ESI) calcd for $\text{C}_{19}\text{H}_{32}\text{O}_4 + \text{H}^+$ 325.24, found 325.47.

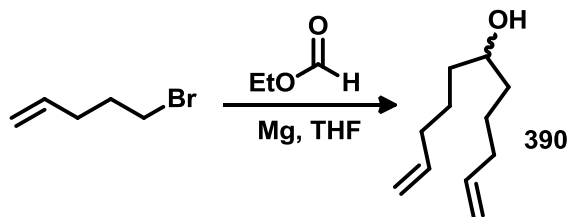


The *bis*-methylene spiro ketal (8.3 mg, 1.0 equiv, 0.0256 mmol) was taken up in dichloromethane–methanol (1:1, 4 mL) and the solution was cooled to -78 °C. Ozone was bubbled through the solution until a pale blue colour change was observed. The

reaction was quenched with dimethyl sulfide and allowed to stir overnight, acclimating to room temperature. The solvents were removed by rotary evaporation and the crude residue was purified by flash chromatography [silica, ethyl acetate–hexanes, 2:1 to 1:0], providing the desired product as a white solid (4.5 mg, 57%).

341. Identical to the spectral data obtained above.

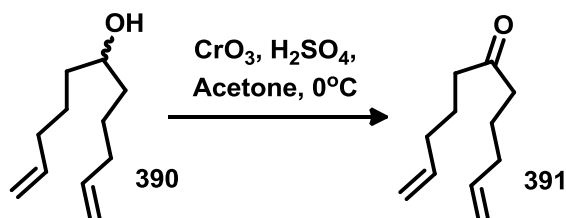
7.6 Experiments pertaining to Chapter 6



Mg turnings (2.6 g, 4.0 equiv, 0.108 mol) were added to an oven dried 250 mL 3-necked flask, followed by 10 mL of dry THF and a single chip of iodine. Approximately, 2 mL of a solution of 1-bromopent-4-ene (50 mL of dry THF, 10.06 g, 2.5 equiv, 0.0675 mol) were added. Upon observing decolouration, the remainder of the bromide solution was added drop-wise to the reaction over 45 min, maintaining a gentle reflux. After an additional hour of stirring, the reaction was cooled to 0 °C and ethyl formate (2.00 g, 1.0 equiv, 27.0 mmol) was added drop-wise. The reaction acclimated to room temperature as it stirred for 2 h. After quenching with MeOH, the crude mixture was filtered through a pad of celite, and diluted with ethyl ether (100 mL). The filtrate was washed with a saturated NH₄Cl solution (20 mL) and brine (20 mL), dried over MgSO₄, filtered and concentrated by rotary evaporation. The resulting clear, colourless oil **390** did not require additional purification (4.48 g, 98%).

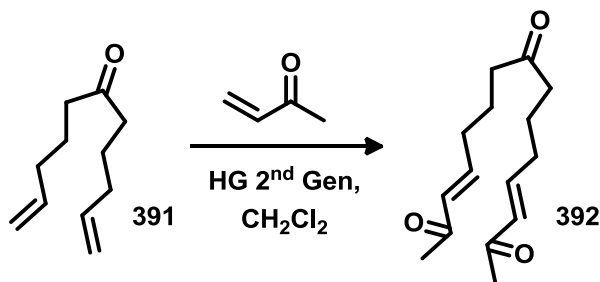
390. ¹H NMR (400 MHz, CDCl₃) δ 5.79 (ddt, *J* = 17.0, 10.2, 6.7 Hz, 2H), 4.99 (dq, *J* = 17.1, 1.8 Hz, 2H), 4.93 (ddt, *J* = 10.2, 2.0, 1.1 Hz, 2H), 3.60–3.56 (m, 1H), 2.10–2.02 (m, 4H), 1.56–1.37 (m, 8H); ¹³C NMR (100 MHz, CDCl₃) δ 138.7 (CH), 114.6 (CH₂), 71.7 (CH), 36.9 (CH₂), 33.7 (CH₂), 24.9 (CH₂); IR (neat, cm⁻¹) 3351 (br), 3077 (m), 2931 (s),

2859 (m), 1641 (m), 1459 (m), 1441 (m), 1416 (m), 994 (m), 910 (s); HRMS (ESI) calcd for $C_{11}H_{20}O + H^+$ 169.1587, found 169.1586.



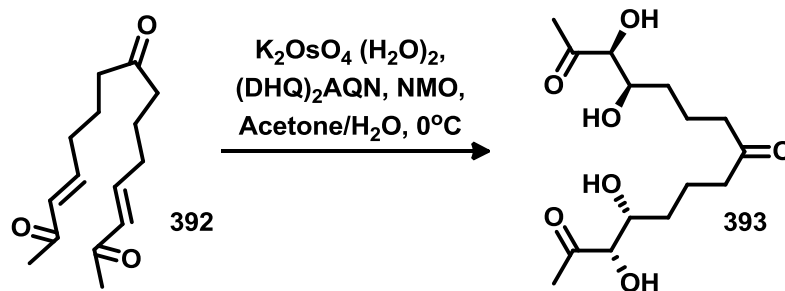
Jones reagent was freshly prepared (2.7 g of CrO_3 in 4.0 mL of H_2SO_4 and 12.0 mL H_2O) and added drop-wise to a solution of **390** (3.99 g, 1.0 equiv, 23.7 mmol) in 10 mL of acetone at -10°C until the green to orange colour change persisted for more than 5 min. The reaction mixture was filtered through a pad of celite and the filtrate was washed with a saturated NaHCO_3 solution (10 mL), H_2O (10 mL), and brine (10 mL), then dried over MgSO_4 , filtered and concentrated by rotary evaporation. The resulting clear colourless oil **391** did not require additional purification (3.01 g, 97%).

391. ^1H NMR (400 MHz, CDCl_3): δ = 5.74 (ddt, J = 17.0, 10.2, 6.7 Hz, 2H), 4.98 (dq, J = 17.1, 1.7 Hz, 2H), 4.95 (ddt, J = 10.4, 2.1, 1.1 Hz, 2H), 2.34 (t, J = 7.4 Hz, 4H), 2.03 (q, J = 7.1 Hz, 4H), 1.65 (quin, J = 7.3 Hz, 4H); ^{13}C NMR (100 MHz, CDCl_3) δ 210.9 (C), 138.0 (CH), 115.2 (CH_2), 41.9 (CH_2), 33.1 (CH_2), 22.8 (CH_2); IR (neat, cm^{-1}) 3079 (m), 2931 (s), 2858 (m), 1713 (s), 1641 (m), 1440 (m), 1414 (m), 1372 (m), 1245 (m), 996 (m), 912 (m).



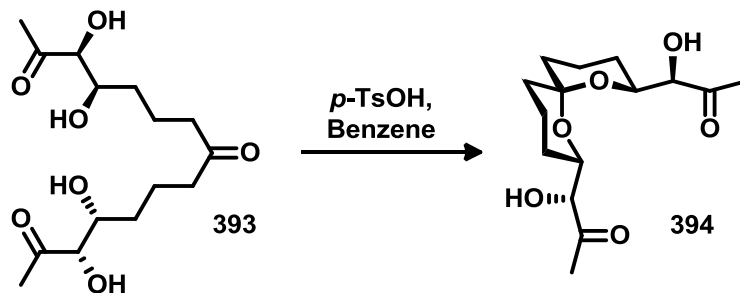
Methyl vinyl ketone was dried over K_2CO_3 and CaCl_2 for 2 h, filtered, then distilled under reduced pressure using a kugelrohr apparatus. This freshly distilled reagent (18.0 mL, 30 equiv, 0.217 mol) was then added to a solution of **391** (1.20 g, 1.0 equiv, 7.22 mmol) in dry dichloromethane (150 mL). Hoveyda-Grubbs 2nd generation catalyst (315.0 mg, 0.07 equiv, 0.361 mmol) was added and the reaction stirred overnight at room temperature, changing colour from green to brown. The reaction was quenched with methyl vinyl ether (~3 mL), concentrated by rotary evaporation, and purified by combiflash [silica, ethyl acetate–hexanes, 1:1 to 1:0] giving the product as a light brown oil (1.80 g, 98%).

392. ^1H NMR (400 MHz, CDCl_3) δ 6.72 (dt, $J = 15.9, 6.8$ Hz, 2H), (dt, $J = 15.9, 1.4$ Hz, 2H), 2.40 (t, $J = 7.2$ Hz, 4H), 2.24–2.18 (m, 4H), 2.21 (s, 6H), 1.73 (quin, $J = 7.3$ Hz, 4H); ^{13}C NMR (100 MHz, CDCl_3) δ 209.5 (C), 198.7 (C), 147.2 (CH), 131.7 (CH), 41.8 (CH_2), 31.7 (CH_2), 26.9 (CH_2), 21.8 (CH_3); IR (neat, cm^{-1}) 2941 (s), 2866 (m), 1713 (s), 1674 (s), 1626 (m), 1422 (m), 1362 (m), 1256 (m), 1182 (m), 1088 (m), 981 (m); HRMS (ESI) calcd for $\text{C}_{15}\text{H}_{22}\text{O}_3 + \text{Na}^+$ 273.1461, found 273.1462.



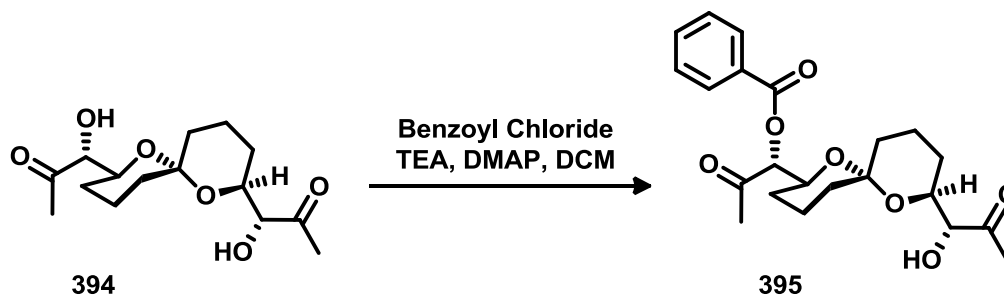
A solution of **392** (0.768 g, 1.0 equiv, 3.07 mmol) in 20 mL of acetone was added slowly via syringe pump to a solution of NMO (9.03 g, 2.5 equiv, 7.71 mmol), (DHQ)₂AQN (396 mg, 0.15 equiv, 0.463 mmol), and potassium osmate dihydrate (28.4 mg, 0.025 equiv, 0.0771 mmol) in acetone–H₂O (9:1, 5 mL) at 0 °C. A cryostat was used to maintain a bath temperature as the reaction stirred for 4 days. The reaction was quenched with the addition of a saturated Na₂SO₃ solution (2 mL). The crude mixture was concentrated by rotary evaporation, and purified by CombiFlash [silica, MeOH–dichloromethane, 0:1 to 1:5] giving product **393** as a pale yellow oil (4.46 g, 91%).

393. ¹H NMR (400 MHz, CDCl₃) δ 4.08 (d, *J* = 1.6 Hz, 2H), 3.98 (dt, *J* = 1.6, 6.6 Hz, 2H), 2.51 (t, *J* = 6.8 Hz, 4H), 2.29 (s, 6H), 1.84–1.62 (m, 8H); ¹³C NMR (100 MHz, CDCl₃) δ 210.9 (C), 208.0 (C), 79.3 (CH), 71.6 (CH), 42.3 (CH₂), 29.6 (CH₂), 25.3 (CH₂), 19.8 (CH₃); IR (neat, cm⁻¹): 3449 (br), 2964 (s), 1712 (s), 1354 (m), 1224 (m), 1112 (s), 983 (m) cm⁻¹; HRMS (ESI) calcd for C₁₅H₂₆O₇ + Na⁺ 341.1571, found 341.1575.



Tetraol, **393**, (0.895 g, 1.0 equiv, 0.00281 mol) was dissolved in benzene (6.0 mL) along with a spatula tip of *p*-TSA. The reaction stirred at room temperature overnight then the crude mixture was concentrated by rotary evaporation, and the residue was purified by CombiFlash [silica, ethyl acetate–hexanes; 1:1 to 1:0] giving **394** as a white solid (0.644 g, 76%). The slow evaporation of dichloromethane from this material provided X-ray quality crystals.

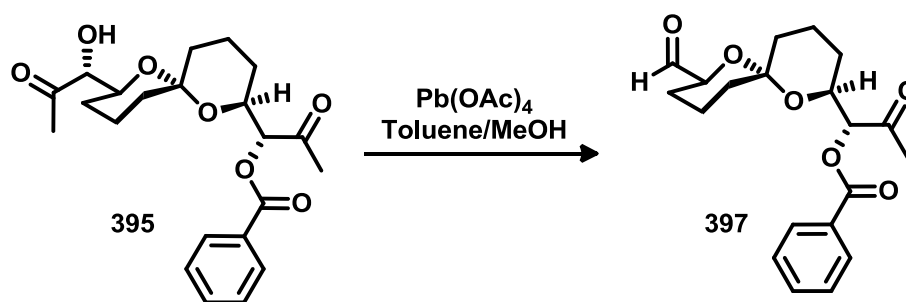
394. ^1H NMR (300 MHz, CDCl_3) δ 3.95 (dd, $J = 7.8, 2.2$ Hz, 2H), 3.90 (dt, $J = 7.0, 2.3$ Hz, 2H), 3.17 (d, $J = 7.8$ Hz, 2H), 2.32 (s, 6H), 1.77–1.65 (m, 2H), 1.60–1.48 (m, 8H), 1.31 (dt, $J = 13.5, 4.4$ Hz, 2H); ^{13}C NMR (75 MHz, CDCl_3) δ 210.1 (C), 97.0 (C), 79.3 (CH), 70.4 (CH), 34.9 (CH_2), 26.9 (CH_2), 25.9 (CH_2), 18.0 (CH_3); IR (neat, cm^{-1}) 3462 (br), 2949 (s), 2870 (m), 1712 (s), 1353 (m), 1223 (m), 1111 (s), 983 (s), 875 (m); HRMS (ESI) calcd for $\text{C}_{15}\text{H}_{24}\text{O}_6 + \text{Na}^+$ 323.1465, found 323.1466.



Using an oven dried round bottom flask, spiroketal **394** (0.450 g, 1.0 equiv, 1.50 mmol) was dissolved in dry dichloromethane (30 mL). DMAP (18.3 mg, 0.10 equiv, 0.150 mmol), TEA (0.626 mL, 3.0 equiv, 4.50 mmol) and benzoic anhydride (0.678 g, 2.0 equiv, 3.00 mol) were added sequentially at room temperature. The reaction stirred for 72 h before quenching with a saturated solution of NaHCO₃ (15 mL). The organic phase was extracted into ethyl acetate (60mL), washed with H₂O (2 x 30 mL) and brine (30 mL), then dried over MgSO₄, filtered, and concentrated by rotary evaporation. The residue was purified by combiflash [silica, ethyl acetate–hexanes, 1:5 to 1:0] providing product **395** (0.384 g, 62%; 73% based on recoverd starting material) as clear colourless oil.

395. ¹H NMR (400 MHz, CDCl₃) δ 8.14 (dd, *J* = 8.3, 1.6 Hz, 2H), 7.63 (t, *J* = 7.4 Hz, 1H), 7.50 (t, *J* = 7.6 Hz, 2H), 5.20 (d, *J* = 3.1 Hz, 1H), 4.09 (ddd, *J* = 9.1, 7.1, 3.1 Hz, 1H), 4.06 (d, *J* = 1.6 Hz, 1H), 3.93 (dt, *J* = 4.5, 2.4 Hz, 1H), 3.38 (d, *J* = 6.3 Hz, 1H), 2.41 (s, 3H), 2.27 (s, 3H), 1.77–1.44 (m, 10H), 1.38 (m, 2H); ¹³C NMR (101 MHz, CDCl₃) δ 208.6 (C), 207.4 (C), 166.3 (C), 133.8 (CH), 130.1 (CH), 129.4 (C), 128.8 (CH), 97.2 (C), 80.8 (CH), 79.4 (CH), 70.8 (CH), 69.9 (CH), 34.9 (CH₂), 34.8 (CH₂) 28.1 (CH₃), 26.4 (CH₃), 26.2 (CH₂), 26.2 (CH₂), 18.3 (CH₂), 18.3 (CH₂); IR (neat, cm⁻¹) 3485

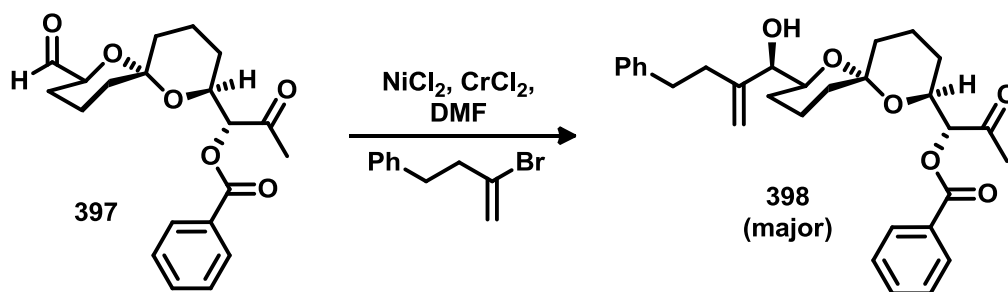
(br), 3008 (m), 2955 (m), 1716 (s), 1353 (m), 1275 (s), 1260 (s), 1106 (m), 982 (m), 750 (s), 764 (s); HRMS (ESI) calcd for $C_{22}H_{28}O_7 + H^+$ 405.1913, found 405.1914.



The alcohol **395** (2.01 g, 1.0 equiv, 4.97 mmol) was dissolved in toluene–MeOH (1:1; 120 mL) and $Pb(OAc)_4$ (6.61 g, 3.0 equiv, 14.9 mmol) was added at rt. The reaction stirs for 72 h, changing from yellow to orange to colourless. Upon quenching with a saturated solution of NH_4Cl (10 mL), the organic phase was extracted into ethyl acetate (2×25 mL), washed with H_2O (10 mL), and brine (10 mL), dried over $MgSO_4$, filtered, and concentrated by rotary evaporation. The crude residue was purified by CombiFlash [silica, ethyl acetate–hexanes, 0:1 to 2:1] providing aldehyde **397** (1.55 g; 87%) as a clear colourless oil.

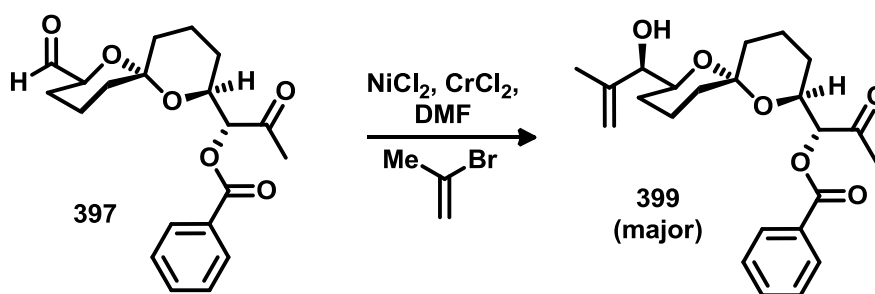
397. 1H NMR (400 MHz, $CDCl_3$) δ 9.64 (s, 1H), 8.15 (dd, $J = 8.4, 1.7$ Hz, 2H), 7.64 (tt, $J = 7.5, 1.5$ Hz, 1H), 7.52 (tt, $J = 1.9$ Hz, 2H), 5.24 (d, $J = 3.1$ Hz, 1H), 4.29 (dt, $J = 10.6, 3.1$ Hz, 1H), 3.93 (dd, $J = 12.3, 2.9$ Hz, 1H), 2.26 (s, 3H), 2.12–1.96 (m, 2H), 1.84 (ddd, $J = 8.5, 6.4, 3.9$ Hz, 1H), 1.80–1.39 (m, 8H), 1.30 (ddd, $J = 16.4, 12.3, 4.6$ Hz, 1H); ^{13}C

NMR (101 MHz, CDCl₃) δ 206.7 (C), 201.6 (C), 166.3 (C), 133.8 (CH), 130.1 (CH), 129.4 (C), 128.8 (CH), 97.2 (C), 80.7 (CH), 76.8 (CH), 74.5 (CH), 70.6 (CH), 35.0 (CH₂), 34.7 (CH₂), 28.2 (CH₃), 26.1 (CH₂), 25.2 (CH₂), 18.2 (CH₂), 18.2 (CH₂); IR (neat, cm⁻¹) 2948 (m), 1718 (s), 1452 (m), 1261 (s), 1109 (m), 987 (s), 713 (s); HRMS (ESI) calcd for C₂₀H₂₄O₆ + Na⁺ 383.1471 found 383.1479.



A solution of aldehyde **397** (48.0 mg, 1.0 equiv, 0.133 mmol) and vinyl iodide (0.103 g, 3.0 equiv, 0.400 mmol) in dry DMSO (1 mL) was added to an oven dried microwave vial containing a solution of CrCl₂ (78.4 mg, 4.8 equiv, 0.638 mmol), and NiCl₂ (< 0.5 mg) in DMSO (4 mL). The blue solution stirred at rt overnight then the reaction was diluted with ethyl acetate, washed with a saturated solution of NH₄Cl (5 mL), the organic phase was extracted into ethyl acetate, washed with H₂O (3 × 5 mL), and brine (5 mL), dried over MgSO₄, filtered, and concentrated by rotary evaporation. The crude residue was then purified by CombiFlash [silica, ethyl acetate–hexanes, 0:1 to 2:1] providing **398**, a 3:1 diastereomeric mixture of alcohols (60.6 mg; 93%).

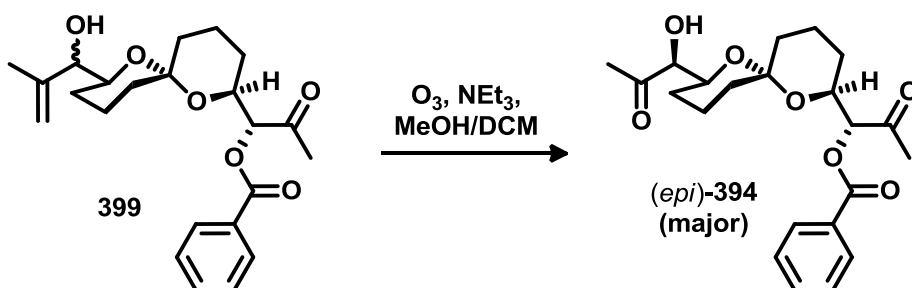
398. ^1H NMR (400 MHz, CDCl_3) δ 8.14 (ddd, $J = 7.9, 4.3, 1.4$ Hz, 2H), 7.63 (t, $J = 8.2$ Hz, 1H), 7.50 (t, $J = 7.6$ Hz, 2H), 7.34–7.23 (m, 4H), 7.17 (m, 1H), 5.22 (d, $J = 8.9$ Hz, 1H), 5.21 (br s, 1H), 5.15 (minor diastereomer, s, 0.25H), 5.04 (minor diastereomer, br s, 0.25H) 5.04 (br s, 1H), 4.26 (ddd, $J = 8.4, 6.8, 3.5$ Hz, 1H), 4.19 (d, $J = 4.2$ Hz, 1H), 3.92 (minor diastereomer, d, $J = 6.6$ Hz, 0.25H), 3.77 (minor diastereomer, s, 0.25H), 3.58 (ddd, $J = 11.3, 7.0, 3.9$ Hz, 1H), 3.50 (minor diastereomer, ddd, $J = 11.7, 6.3, 2.5$ Hz, 0.25H), 2.98–2.77 (m, 2H), 2.64–2.54 (minor diastereomer, m, 0.5H), 2.53–2.36 (m, 2H), 2.23 (s, 3H), 2.17 (bs s, 1H), 1.99–1.82 (m, 1H), 1.71–1.21 (m, 11H); ^{13}C NMR (101 MHz, CDCl_3) δ 206.3 (C), 166.2 (C), 147.5 (CH), 142.1 (C), 133.6 (CH), 129.9 (CH), 129.4 (C), 128.6 (CH), 128.5 (CH), 128.3 (CH), 125.8 (CH), 110.7 (CH₂), 97.2 (C), 80.9 (CH), 75.7 (CH), 71.3 (CH), 70.3 (CH), 35.1 (CH₂), 34.9 (CH₂), 34.6 (CH₂), 34.5 (CH₂), 28.0 (CH₃), 26.1 (CH₂), 23.1 (CH₂), 18.3 (CH₂); ^{13}C NMR (101 MHz, CDCl_3 , minor diastereomer) δ 205.6 (C), 162.1 (C), 147.9 (CH), 142.1 (C), 133.6 (CH), 129.9 (CH), 129.4 (C), 128.6 (CH), 128.5 (CH), 128.3 (CH), 125.8 (CH), 112.5 (CH), 96.8 (C), 80.7 (CH), 78.6 (CH), 71.3 (CH), 70.0 (CH), 35.0 (CH₂), 34.9 (CH₂), 34.3 (CH₂), 33.4 (CH₂), 27.9 (CH₃), 26.9 (CH₂), 26.0 (CH₂), 18.3 (CH₂); IR (neat, cm^{-1}) 3503 (br), 2944 (m), 2873 (m), 1719 (s), 1453 (m), 1274 (s), 1261 (s), 1097 (m), 982 (s), 750 (m), 712 (s); HRMS (ESI) calcd for $\text{C}_{30}\text{H}_{36}\text{O}_6 + \text{H}^+$ 493.2590, found 493.2588.



A solution of aldehyde **397** (36.0 mg, 1.0 equiv, 0.100 mmol) and vinyl bromide (40.1 mg, 3.3 equiv, 0.334 mmol) in dry THF (0.3 mL) was added to an oven dried microwave vial containing a solution of CrCl_2 (58.6 mg; 4.8 equiv, 0.480 mmol), and NiCl_2 (< 0.5 mg) in DMSO (4 mL) at -10°C . The blue solution stirred at room temperature overnight, at which point, the reaction was diluted with ethyl acetate (5 mL) and quenched with a saturated NH_4Cl solution (5 mL). The aqueous layer was extracted with ethyl acetate (2×5 mL), washed with H_2O (3×5 mL), and brine (5 mL), dried over MgSO_4 , filtered, and concentrated by rotary evaporation. The crude residue was purified by Combilash [silica, ethyl acetate–hexanes, 0:1 to 2:1] providing **399**, a 4:1 mixture of inseparable diastereomeric alcohols (36.2 mg; 90%).

399. ^1H NMR (400 MHz, CDCl_3) δ 8.14 (dd, $J = 6.7, 4.8$ Hz, 2H), 7.63 (t, $J = 7.6$ Hz, 1H), 7.51 (t, $J = 7.8$ Hz, 2H), 5.22 (minor diastereomer, d, $J = 3.2$ Hz, 0.3H), 5.21 (d, $J = 3.1$ Hz, 1H), 5.10 (br s, 1H), 5.00 (minor diastereomer, d, $J = 1.8$ Hz, 0.3H), 4.95 (dq, $J = 3.2, 1.6$ Hz, 1H), 4.26 (ddd, $J = 13.8, 6.6, 3.1$ Hz, 1H), 4.16 (d, $J = 3.8$ Hz, 1H), 3.88 (minor diastereomer, d, $J = 6.6$ Hz, 1H), 3.48 (ddd, $J = 11.3, 6.6, 2.5$ Hz, 1H), 3.57 (ddd, $J = 11.3, 6.5, 3.6$ Hz, 1H), 2.26 (minor diastereomer, 0.9H), 2.25 (s, 3H), 2.03–1.88 (m,

1H), 1.85 (minor diastereomer, 0.9H) 1.82 (s, 3H), 1.74–1.30 (m, 11H); ^{13}C NMR (101 MHz, CDCl_3) δ 206.52 (C), 166.25 (C), 143.50 (C), 133.60 (CH), 129.92 (CH), 129.38 (C), 128.62 (CH), 111.24 (CH_2), 97.22 (C), 80.90 (CH), 76.39 (CH), 70.82 (CH), 70.33 (CH), 35.10 (CH_2), 34.91 (CH_2), 27.91 (CH_3), 26.14 (CH_2), 22.89 (CH_2), 19.72 (CH_3), 18.31 (CH_2), 18.30 (CH_2); ^{13}C NMR (101 MHz, CDCl_3 , minor diastereomer) δ 205.8 (C), 166.2 (C), 144.2 (C), 133.6 (CH), 129.9 (CH), 129.4 (C), 128.6 (CH), 113.6 (CH_2), 96.8 (C), 80.7 (CH), 79.0 (CH), 70.7 (CH), 70.0 (CH), 35.0 (CH_2), 34.8 (CH_2), 27.8 (CH_3), 26.8 (CH_2), 26.0 (CH_2), 18.3 (CH_2), 18.0 (CH_3); IR (neat, cm^{-1}) 3514 (br), 2946 (m), 2873 (m), 1719 (s), 1452 (m), 1262 (s), 1224 (s), 1098 (m), 982 (s), 712 (s); LRMS (ESI) calcd for $\text{C}_{23}\text{H}_{30}\text{O}_6 + \text{H}^+$ 403.20, found 403.20.



Olefin **399** (as a 4:1 mixture of diastereomers; 10.2 mg, 1.0 equiv, 0.251 mmol) and triethylamine (~ 0.01 mL) were dissolved in MeOH–dichloromethane (1:1; 3 mL) and cooled to -78 °C. Ozone was bubbled through the solution for approximately 2 min, at which point a faint blue colour change was observed. The reaction was quenched at -78 °C with the addition of dimethyl sulfide (0.5 mL) and the reaction was allowed to acclimate as it stirred overnight. After diluting the solution with ethyl acetate (5 mL), the organic phase was washed with a saturated solution of NH_4Cl (5 mL), H_2O (2×5 mL)

and brine (5 mL), then dried over MgSO₄, filtered, and concentrated by rotary evaporation. The residue was purified by column chromatography [silica, ethyl ether–hexanes, 1:5 to 1:0] providing the product (9.4 mg; 92%), a clear colourless oil, as a 4:1 mixture of diastereomers (the minor of which was a spectral match to **394**).

(epi)-**394**. ¹H NMR (400 MHz, CDCl₃) δ 8.20–8.09 (m, 2H), 7.69–7.61 (t, *J* = 7.4 Hz, 1H), 7.51 (t, *J* = 7.6 Hz, 2H), 5.24 (d, *J* = 3.0 Hz, 1H), 4.30–4.20 (m, 2H), 3.73 (ddd, *J* = 11.6, 3.9, 2.4 Hz, 1H), 3.38 (br s, 3H), 2.39 (s, 3H), 2.26 (s, 1H), 2.01–1.84 (m, 1H), 1.78–1.25 (m, 11H).

Bibliography

- (1) *Global Report: UNAIDS report on the global AIDS epidemic*, Joint United Nations Programme on HIV/AIDS (UNAIDS), **2012**.
- (2) *WHO case definitions of HIV for surveillance and revised clinical staging and immunological classification of HIV-related disease in adults and children*, World Health Organization, **2007**.
- (3) Chu, C.; Selwyn, P. A. *American Family Physician*, **2011**, 83, 395.
- (4) Dalgleish, A. G.; Beverley, P. C. L.; Clapham, P. R.; Crawford, D. H.; Greaves, M. F.; Weiss, R. A. *Nature*, **1984**, 312, 763.
- (5) Zhu, P.; Winkler, H.; Chertova, E.; Taylor, K. A.; Roux, K. H. *PLoS Pathogens*, **2008**, 4, e1000203.
- (6) Qadir, M. I.; Malik, S. A. *Reviews in Medical Virology*, **2010**, 20, 23.
- (7) Sarafianos, S. G.; Marchand, B.; Das, K.; Himmel, D. M.; Parniak, M. A.; Hughes, S. H.; Arnold, E. *Journal of Molecular Biology*, **2009**, 385, 693.
- (8) Erickson, J. W.; Burt, S. K. *Annual Review of Pharmacology and Toxicology*, **1996**, 36, 545.
- (9) Chiu, T. K.; Davies, D. R. *Current Topics in Medicinal Chemistry*, **2004**, 4, 965.
- (10) Flexner, C. N. *The New England Journal of Medicine*, **1998**, 338, 1281.
- (11) Miller, M. *Biopolymers*, **2010**, 94, 521.
- (12) Pokorna, J.; Machala, L.; Rezacova, P.; Konvalinka, J. *Viruses*, **2009**, 1, 1209.
- (13) Navia, M. A.; Fitzgerald, P. M.; McKeever, B. M.; Leu, C. T.; Heimbach, J. C.; Herber, W. K.; Sigal, I. S.; Darke, P. L.; Springer, J. P. *Nature*, **1989**, 337, 615.
- (14) Thompson, M. A.; Aberg, J. A.; Hoy, J. F.; Telenti, A.; Benson, C.; Cahn, P.; Eron, J. J.; Gunthard, H. F.; Hammer, S. M.; Reiss, P.; Richman, D. D.; Rizzardini, G.; Thomas, D. L.; Jacobsen, D. M.; Volberding, P. A. *The Journal of the American Medical Association*, **2012**, 308, 387.

- (15) McCoy, C. *Clinical Therapeutics*, **2007**, 29, 1559.
- (16) Kozal, M. *AIDS Patient Care and STDS*, **2004**, 18, 199.
- (17) Campo, R. E.; Lichtenberger, P. N.; Rosa, I.; Suarez, G.; Rivera, F. A.; Rodriguez, A. E.; Jayaweera, D. T.; Wahlay, N. A.; Kolber, M. A. *Journal of Clinical Microbiology*, **2003**, 41, 3376.
- (18) Weber, I. T. *Journal of Biological Chemistry*, **1990**, 265, 10492.
- (19) Meek, T. D.; Dayton, B. D.; Metcalf, B. W.; Dreyer, G. B.; Strickler, J. E.; Gorniak, J. G.; Rosenberg, M.; Moore, M. L.; Magaard, V. W.; Debouck, C. *Proceedings of the National Academy of Sciences*, **1989**, 86, 1841.
- (20) Darke, P. L.; Jordan, S. P.; Hall, D. L.; Zugay, J. A.; Shafer, J. A.; Kuo, L. C. *Biochemistry*, **1994**, 33, 98.
- (21) Xie, D.; Gulnik, S.; Gustchina, E.; Yu, B.; Shao, W.; Qoronfleh, W.; Nathan, A.; Erickson, J. W. *Protein Science*, **1999**, 8, 1702.
- (22) Sousa, S. F.; Tamames, B.; Fernandes, P. A.; Ramos, M. J. *Journal of Physical Chemistry B*, **2011**, 115, 7045.
- (23) Winslow, D. L.; Stack, S.; King, R.; Scarnati, H.; Bincsik, A.; Otto, M. J. *AIDS Research and Human Retroviruses*, **1995**, 11, 107.
- (24) Gustchina, A.; Weber, I. T. *Proteins*, **1991**, 10, 325.
- (25) Davis, D. A.; Tebbs, I. R.; Daniels, S. I.; Stahl, S. J.; Kaufman, J. D.; Wingfield, P.; Bowman, M. J.; Chmielewski, J.; Yarchoan, R. *Biochemical Journal*, **2009**, 419, 497.
- (26) Todd, M. J.; Semo, N.; Freire, E. *Journal of Molecular Biology*, **1998**, 283, 475.
- (27) Zhang, Z. Y.; Poorman, R. A.; Maggiora, L. L.; Heinrikson, R. L.; Kezdy, F. J. *Journal of Biological Chemistry*, **1991**, 266, 15591.
- (28) Schramm, H. J.; Boetzel, J.; Buttner, J.; Fritsche, E.; Gohring, W.; Jaeger, E.; Konig, S.; Thumfart, O.; Wenger, T.; Nagel, N. E.; Schramm, W. *Antiviral Research*, **1996**, 30, 155.
- (29) Schramm, H. J.; Nakashima, H.; Schramm, W.; Wakayama, H.; Yamamoto, N. *Biochemical and Biophysical Research Communications*, **1991**, 179, 847.
- (30) Babe, L. M.; Rose, J.; Craik, C. S. *Protein Science*, **1992**, 1, 1244.

- (31) Shultz, M. D.; Bowman, M. J.; Ham, Y. W.; Zhao, X.; Tora, G.; Chmielewski, J. *Angewandte Chemie International Edition*, **2000**, *39*, 2710.
- (32) Song, M.; Rajesh, S.; Hayashi, Y.; Kiso, Y. *Bioorganic & Medicinal Chemistry Letters*, **2001**, *11*, 2465.
- (33) Breccia, P.; Boggetto, N.; Perez-Fernandez, R.; Van Gool, M.; Takahashi, M.; Rene, L.; Prados, P.; Badet, B.; Reboud-Ravaux, M.; de Mendoza, J. *Journal of Medicinal Chemistry*, **2003**, *46*, 5196.
- (34) Bowman, M. J.; Chmielewski, J. *Bioorganic & Medicinal Chemistry*, **2009**, *17*, 967.
- (35) Merabet, N.; Dumond, J.; Collinet, B.; Van Baelinghem, L.; Boggetto, N.; Ongeri, S.; Ressay, F.; Reboud-Ravaux, M.; Sicsic, S. *Journal of Medicinal Chemistry*, **2004**, *47*, 6392.
- (36) Zutshi, R.; Franciskovich, J.; Shultz, M.; Schweitzer, B.; Bishop, P.; Wilson, M.; Chmielewski, J. *Journal of the American Chemical Society*, **1997**, *119*, 4841.
- (37) Lee, S. G.; Chmielewski, J. *Chemistry and Biology*, **2006**, *13*, 421.
- (38) Bannwarth, L.; Kessler, A.; Pethe, S.; Collinet, B.; Merabet, N.; Boggetto, N.; Sicsic, S.; Reboud-Ravaux, M.; Ongeri, S. *Journal of Medicinal Chemistry*, **2006**, *49*, 4657.
- (39) Song, M.-c.; Rajesh, S.; Hayashi, Y.; Kiso, Y. *Peptide Science*, **2002**, *38*, 211.
- (40) Bouras, A.; Boggetto, N.; Benatalah, Z.; de Rosny, E.; Sicsic, S.; Reboud-Ravaux, M. *Journal of Medicinal Chemistry*, **1999**, *42*, 957.
- (41) Bannwarth, L.; Rose, T.; Dufau, L.; Vanderesse, R.; Dumond, J.; Jamart-Gregoire, B.; Pannecouque, C.; De Clercq, E.; Reboud-Ravaux, M. *Biochemistry*, **2009**, *48*, 379.
- (42) Dufau, L.; Marques Ressurreicao, A. S.; Fanelli, R.; Kihal, N.; Vidu, A.; Milcent, T.; Soulier, J.-L.; Rodrigo, J.; Desvergne, A.; Leblanc, K.; Bernadat, G.; Crousse, B.; Reboud-Ravaux, M.; Ongeri, S. *Journal of Medicinal Chemistry*, **2012**, *55*, 6762.
- (43) Ko, E.; Raghuraman, A.; Perez, L. M.; Ioerger, T. R.; Burgess, K. *Journal of the American Chemical Society*, **2013**, *135*, 167.
- (44) Rosen, J.; Gottfries, J.; Muresan, S.; Backlund, A.; Oprea, T. I. *Journal of Medicinal Chemistry*, **2009**, *52*, 1953.

- (45) Cardellina, J. H., 2nd; Munro, M. H.; Fuller, R. W.; Manfredi, K. P.; McKee, T. C.; Tischler, M.; Bokesch, H. R.; Gustafson, K. R.; Beutler, J. A.; Boyd, M. R. *Journal of Natural Products*, **1993**, *56*, 1123.
- (46) Gochfeld, D. J.; El Sayed, K. A.; Yousaf, M.; Hu, J. F.; Bartyzel, P.; Dunbar, D. C.; Wilkins, S. P.; Zjawiony, J. K.; Schinazi, R. F.; Schlueter Wirtz, S.; Tharnish, P. M.; Hamann, M. T. *Mini-Reviews in Medicinal Chemistry*, **2003**, *3*, 401.
- (47) Tziveleka, L. A.; Vagias, C.; Roussis, V. *Current Topics in Medicinal Chemistry*, **2003**, *3*, 1512.
- (48) Lee, K. H. *Journal of Natural Products*, **2004**, *67*, 273.
- (49) Quere, L.; Wenger, T.; Schramm, H. J. *Biochemical and Biophysical Research Communications*, **1996**, *227*, 484.
- (50) Liu, J.-S.; Huang, M.-F.; Arnold, G. F.; Arnold, E.; Clardy, J.; Ayer, W. A. *Tetrahedron Letters*, **1983**, *24*, 2351.
- (51) El Dine, R. S.; El Halawany, A. M.; Ma, C.-M.; Hattori, M. *Journal of Natural Products*, **2008**, *71*, 1022.
- (52) El Dine, R. S.; El Halawany, A. M.; Ma, C.-M.; Hattori, M. *Journal of Natural Products*, **2009**, *72*, 2019.
- (53) Potts, B. C. M.; Faulkner, D. J.; Chan, J. A.; Simolike, G. C.; Offen, P.; HemLing, M. E.; Francis, T. A. *Journal of the American Chemical Society*, **1991**, *113*, 6321.
- (54) Baglin, I.; Mitaine-Offer, A. C.; Nour, M.; Tan, K.; Cave, C.; Lacaille-Dubois, M. A. *Mini-Reviews in Medicinal Chemistry*, **2003**, *3*, 525.
- (55) Fan, X.; Flentke, G. R.; Rich, D. H. *Journal of the American Chemical Society*, **1998**, *120*, 8893.
- (56) Salomon, C. E.; Williams, D. H.; Lobkovsky, E.; Clardy, J. C.; Faulkner, D. J. *Organic Letters*, **2002**, *4*, 1699.
- (57) Brik, A.; Wong, C.-H. *Organic & Biomolecular Chemistry*, **2003**, *1*, 5.
- (58) Li, X.-Q.; He, Q.; Tu, Y.-Q.; Zhang, F.-M.; Zhang, S.-Y. *Chinese Journal of Chemistry*, **2007**, *25*, 1357.
- (59) Zhao, X. Z.; Peng, L.; Tang, M.; Tu, Y. Q.; Gao, S. H. *Tetrahedron Letters*, **2005**, *46*, 6941.

- (60) Zhao, X. Z.; Tu, Y. Q.; Peng, L.; Li, X. Q.; Jia, Y. X. *Tetrahedron Letters*, **2004**, *45*, 3713.
- (61) Li, X. Q.; Zhao, X. Z.; Liu, P. N.; Tu, Y. Q. *Chinese Journal of Chemistry*, **2004**, *15*, 757.
- (62) Jia, Y. X.; Li, X.; Wu, B.; Zhao, X. Z.; Tu, Y. Q. *Tetrahedron*, **2002**, *58*, 1697.
- (63) Jia, Y.; Li, X.; Wang, P.; Wu, B.; Zhao, X.; Tu, Y. *Journal of the Chemical Society, Perkin Transactions 1*, **2002**, 565.
- (64) Jia, Y. X.; Wu, B.; Li, X.; Ren, S. K.; Tu, Y. Q.; Chan, A. S. C.; Kitching, W. *Organic Letters*, **2001**, *3*, 847.
- (65) Jia, Y. X.; Wu, B.; Wang, P. Z.; Tu, Y. Q. *Chinese Chemical Letters*, **2000**, *11*, 509.
- (66) Wang, P. Z.; Jia, Y. X.; Tu, Y. Q.; Wu, B. *Chinese Chemical Letters* **1999**, *10*, 749.
- (67) Wang, P. Z.; Tu, Y. Q.; Yang, L.; Dong, C. Z.; Kitching, W. *Tetrahedron Asymmetry*, **1998**, *9*, 3789.
- (68) Zhang, F.-M.; Peng, L.; Li, H.; Ma, A.-J.; Peng, J.-B.; Guo, J.-J.; Yang, D.; Hou, S.-H.; Tu, Y.-Q.; Kitching, W. *Angewandte Chemie International Edition*, **2012**, *51*, 10846.
- (69) Ito, H.; Inoue, T.; Iguchi, K. *Organic Letters*, **2008**, *10*, 3873.
- (70) Ito, H.; Kawabe, C.; Iguchi, K. *Heterocycles*, **2006**, *67*, 695.
- (71) Fuwa, H.; Sekine, K.; Sasaki, M. *Organic Letters*, **2013**.
- (72) Fuwa, H.; Noji, S.; Sasaki, M. *Organic Letters*, **2010**, *12*, 5354.
- (73) Fuwa, H.; Naito, S.; Goto, T.; Sasaki, M. *Angewandte Chemie International Edition*, **2008**, *47*, 4737.
- (74) Engman, L.; Stern, D. *Journal of Organic Chemistry*, **1994**, *59*, 5179.
- (75) Nicolaou, K. C.; Snyder, S. A. *Angewandte Chemie International Edition*, **2005**, *44*, 1012.
- (76) Seco, J. M.; Quinoa, E.; Riguera, R. *Chemical Reviews*, **2012**, *112*, 4603.
- (77) Seco, J. M.; Quiñoá, E.; Riguera, R. *Chemical Reviews*, **2004**, *104*, 17.

- (78) Bromba, C.; Wulff, J. E. *Synthesis of bicyclic compounds and method for their use as therapeutic agents*, Department of Chemistry, University of Victoria, 2012.
- (79) Anslyn, E. V.; Dougherty, D. A. *Modern Physical Organic Chemistry*, University Science: Sausalito, Calif., 2006.
- (80) Corey, E. J.; Nicolaou, K. C. *Journal of the American Chemical Society*, **1974**, *96*, 5614.
- (81) Kozikowski, A. P.; Jung, S. H. *Tetrahedron Letters*, **1986**, *27*, 3227.
- (82) Paquette, L. A.; Yang, J.; Long, Y. O. *Journal of the American Chemical Society*, **2002**, *124*, 6542.
- (83) Kreiter, C. G.; Hellmann, T. *Journal of Organometallic Chemistry*, **1991**, *405*, C6.
- (84) Kreiter, C. G.; Lehr, K.; Leyendecker, M.; Sheldrick, W. S.; Exner, R. *Chemische Berichte*, **1991**, *124*, 3.
- (85) Kato, T.; Kondo, H.; Nishino, M.; Tanaka, M.; Hata, G.; Miyake, A. *Bulletin of the Chemical Society of Japan*, **1980**, *53*, 2958.
- (86) Janardhanam, S.; Shanmugam, P.; Rajagopalan, K. *Synthetic Communications*, **1993**, *23*, 311.
- (87) Von Zezschwitz, P.; Voigt, K.; Noltemeyer, M.; De Meijere, A. *Synthesis*, **2000**, 1327.
- (88) White, B. H.; Snapper, M. L. *Journal of the American Chemical Society*, **2003**, *125*, 14901.
- (89) Evans, D. A.; Golob, A. M. *Journal of the American Chemical Society*, **1975**, *97*, 4765.
- (90) Wrobel, J.; Cook, J. M. *Synthetic Communications*, **1980**, *10*, 333.
- (91) Konigsberger, K.; Griengl, H. *Bioorganic & Medicinal Chemistry*, **1994**, *2*, 595.
- (92) Minns, R. A. *Organic Synthesis*, **1977**, *57*, No pp given.
- (93) Bartlett, P. D.; Ando, T. *Journal of the American Chemical Society*, **1970**, *92*, 7518.

- (94) Day, A. C.; Ledlie, M. A. *Journal of the Chemical Society D: Chemical Communications*, **1970**, 1265.
- (95) Spiegel, D. A.; Wiberg, K. B.; Schacherer, L. N.; Medeiros, M. R.; Wood, J. L. *Journal of the American Chemical Society*, **2005**, *127*, 12513.
- (96) Seitz, M.; Reiser, O. *Current Opinion in Chemical Biology*, **2005**, *9*, 285.
- (97) Kitson, R. R.; Millemaggi, A.; Taylor, R. J. *Angewandte Chemie International Edition*, **2009**, *48*, 9426.
- (98) Singh, P.; Mittal, A.; Bhardwaj, A.; Kaur, S.; Kumar, S. *Bioorganic & Medicinal Chemistry Letter*, **2008**, *18*, 85.
- (99) Dowle, M. D.; Davies, D. I. *Chemical Society Reviews*, **1979**, *8*, 171.
- (100) Corey, E. J.; Weinshenker, N. M.; Schaaf, T. K.; Huber, W. *J. Amer. Chem. Soc.* **1969**, *91*, 5675.
- (101) Rood, G. A.; DeHaan, J. M.; Zibuck, R. *Tetrahedron Letters*, **1996**, *37*, 157.
- (102) Ranganathan, S.; Muraleedharan, K. M.; Vaish, N. K.; Jayaraman, N. *Tetrahedron*, **2004**, *60*, 5273.
- (103) Campos, M. d. M.; Petragnani, N. *Tetrahedron*, **1962**, *18*, 521.
- (104) Hu, T.; Liu, K.; Shen, M.; Yuan, X.; Tang, Y.; Li, C. *Journal of Organic Chemistry*, **2007**, *72*, 8555.
- (105) Bertrand, M. P.; Oumar-Mahamat, H.; Surzur, J. M. *Tetrahedron Letters*, **1985**, *26*, 1209.
- (106) Barton, D. H. R.; Beckwith, A. L. J.; Goosen, A. *Journal of the American Chemical Society*, **1965**, 181.
- (107) Corey, E. J.; Kang, M. C. *Journal of the American Chemical Society*, **1984**, *106*, 5384.
- (108) Walling, C.; Cooley, J. H.; Ponaras, A. A.; Racah, E. J. *Journal of the American Chemical Society*, **1966**, *88*, 5361.
- (109) Clive, D. L. J.; Beaulieu, P. L. *Journal of the Chemical Society, Chemical Communications*, **1983**, 307.
- (110) Ueno, Y.; Chino, K.; Watanabe, M.; Moriya, O.; Okawara, M. *Journal of the American Chemical Society*, **1982**, *104*, 5564.

- (111) Stork, G.; Mook, R., Jr.; Biller, S. A.; Rychnovsky, S. D. *Journal of the American Chemical Society*, **1983**, *105*, 3741.
- (112) Zanoni, G.; Re, S.; Meriggi, A.; Castronovo, F.; Vidari, G. *Tetrahedron: Asymmetry*, **2001**, *12*, 1785.
- (113) Kozaka, T.; Miyakoshi, N.; Mukai, C. *Journal of Organic Chemistry*, **2007**, *72*, 10147.
- (114) Barton, D. H. R.; Jang, D. O.; Jaszberenyi, J. C. *Tetrahedron Letters*, **1990**, *31*, 3991.
- (115) Bachi, M. D.; Bosch, E. *Tetrahedron Letters*, **1986**, *27*, 641.
- (116) Bachi, M. D.; Bosch, E. *Journal of Organic Chemistry*, **1992**, *57*, 4696.
- (117) Lucas, M. A.; Schiesser, C. H. *Journal of Organic Chemistry*, **1996**, *61*, 5754.
- (118) Forbes, J. E.; Saicic, R. N.; Zard, S. Z. *Tetrahedron*, **1999**, *55*, 3791.
- (119) Plessis, C.; Derrer, S. *Tetrahedron Letters*, **2001**, *42*, 6519.
- (120) Trost, B. M.; Waser, J.; Meyer, A. *Journal of the American Chemical Society*, **2007**, *129*, 14556.
- (121) Trost, B. M.; Nguyen, H. M.; Koradin, C. *Tetrahedron Letters*, **2010**, *41*, 6232.
- (122) Iwasa, S.; Yamamoto, M.; Kohmoto, S.; Yamada, K. *Journal of the Chemical Society, Perkin Transactions 1*, **1991**, 1173.
- (123) Bachi, M. D.; Bosch, E. *Journal of Organic Chemistry*, **1989**, *54*, 1234.
- (124) Bachi, M. D.; Bosch, E.; Denenmark, D.; Girsh, D. *Journal of Organic Chemistry*, **1992**, *57*, 6803.
- (125) Nozaki, K.; Oshima, K.; Utimoto, K. *Tetrahedron Letters*, **1988**, *29*, 6127.
- (126) Yamamoto, M.; Uruma, T.; Iwasa, S.; Kohmoto, S.; Yamada, K. *Journal of the Chemical Society, Chemical Communications*, **1989**, 1265.
- (127) Iwasa, S.; Yamamoto, M.; Kohmoto, S.; Yamada, K. *Journal of Organic Chemistry*, **1991**, *56*, 2849.
- (128) Ollivier, C.; Renaud, P. *Chemical Reviews*, **2001**, *101*, 3415.

- (129) Povie, G.; Renaud, P. *Chimia*, **2013**, *67*, 250.
- (130) Goessinger, E. *Progress in the Chemistry of Organic Natural Products*, **2010**, *93*, 71.
- (131) Winner, M.; Gimenez, A.; Schmidt, H.; Sontag, B.; Steffan, B.; Steglich, W. *Angewandte Chemie International Edition*, **2004**, *43*, 1883.
- (132) Marrero, J.; Rodriguez, A. D.; Baran, P.; Raptis, R. G.; Sanchez, J. A.; Ortega-Barria, E.; Capson, T. L. *Organic Letters*, **2004**, *6*, 1661.
- (133) Himmelbauer, M.; Farcet, J.-B.; Gagnepain, J.; Mulzer, J. *European Journal of Organic Chemistry*, **2013**, *2013*, 8214.
- (134) Meyer, M. E.; Phillips, J. H.; Ferreira, E. M.; Stoltz, B. M. *Tetrahedron*, **2013**, *69*, 7627.
- (135) Townsend, S. D.; Sulikowski, G. A. *Organic Letters*, **2013**, *15*, 5096.
- (136) Tseng, Y.-J.; Wen, Z.-H.; Dai, C.-F.; Chiang, M. Y.; Sheu, J.-H. *Organic Letters*, **2009**, *11*, 5030.
- (137) Crandall, J. K.; Chang, L.-H. *Journal of Organic Chemistry*, **1967**, *32*, 532.
- (138) Bedekar, A. V.; Patel, H. A.; Nair, K. B.; Soman, R. *Indian Journal of Chemistry -Section B*, **1994**, *33B*, 668.
- (139) Oger, C.; Brinkmann, Y.; Bouazzaoui, S.; Durand, T.; Galano, J.-M. *Organic Letters*, **2008**, *10*, 5087.
- (140) Hatakeyama, S.; Mori, H.; Kitano, K.; Yamada, H.; Nishizawa, M. *Tetrahedron Letters*, **1994**, *35*, 4367.
- (141) Povie, G.; Marzorati, M.; Bigler, P.; Renaud, P. *Journal of Organic Chemistry*, **2013**, *78*, 1553.
- (142) Kikelj, V.; Plantier-Royon, R.; Portella, C. *Synthesis*, **2006**, 1200.
- (143) Ho, J.; Zheng, J.; Meana-Paneda, R.; Truhlar, D. G.; Ko, E. J.; Savage, G. P.; Williams, C. M.; Coote, M. L.; Tsanaktsidis, J. *Journal of Organic Chemistry*, **2013**, *78*, 6677.
- (144) Inanaga, J.; Baba, Y.; Hanamoto, T. *Chemistry Letters*, **1993**, *2*, 241.
- (145) Davies, K. A.; Wulff, J. E. *Organic Letters*, **2011**, *13*, 5552.

- (146) Eaton, P. E. *Accounts of Chemical Research*, **1968**, *1*, 50.
- (147) Clark, R. D.; Untch, K. G. *Journal of Organic Chemistry*, **1979**, *44*, 248.
- (148) Miesch, M.; Wendling, F.; Franck-Neumann, M. *Tetrahedron Letters*, **1999**, *40*, 839.
- (149) Inanaga, K.; Takasu, K.; Ihara, M. *Journal of the American Chemical Society*, **2005**, *127*, 3668.
- (150) Stork, G.; Hudrlik, P. F. *Journal of the American Chemical Society*, **1968**, *90*, 4462.
- (151) Reetz, M. T.; Chatziiosifidis, I.; Huebner, F.; Heimbach, H. *Organic Synthesis*, **1984**, *62*, No pp. given.
- (152) Kerr, W. J.; Watson, A. J. B.; Hayes, D. *Chemical Communications*, **2007**, 5049.
- (153) Masamune, S.; Ellingboe, J. W.; Choy, W. *Journal of the American Chemical Society*, **1982**, *104*, 5526.
- (154) Rizzo, C. J.; Dunlap, N. K.; Smith, A. B., III *Journal of Organic Chemistry*, **1987**, *52*, 5280.
- (155) Wang, X.; Butler, S. C.; Gallucci, J. C.; Paquette, L. A. *Journal of Organic Chemistry*, **2009**, *74*, 6825.
- (156) Marciniak, B. *Hydrosilylation*, **2009**, *1*, 3.
- (157) Piers, W. E.; Marwitz, A. J. V.; Mercier, L. G. *Inorganic Chemistry*, **2011**, *50*, 12252.
- (158) Blackwell, J. M.; Morrison, D. J.; Piers, W. E. *Tetrahedron*, **2002**, *58*, 8247.
- (159) Zheng, G. Z.; Chan, T. H. *Organometallics*, **1995**, *14*, 70.
- (160) Menozzi, C.; Dalko, P. I.; Cossy, J. *Journal of Organic Chemistry*, **2005**, *70*, 10717.
- (161) Menozzi, C.; Dalko, P. I.; Cossy, J. *Synlett*, **2005**, 2449.
- (162) Magnus, P.; Stent, M. A. H. *Organic Letters*, **2005**, *7*, 3853.
- (163) Johnson, C. R.; Raheja, R. K. *Journal of Organic Chemistry*, **1994**, *59*, 2287.

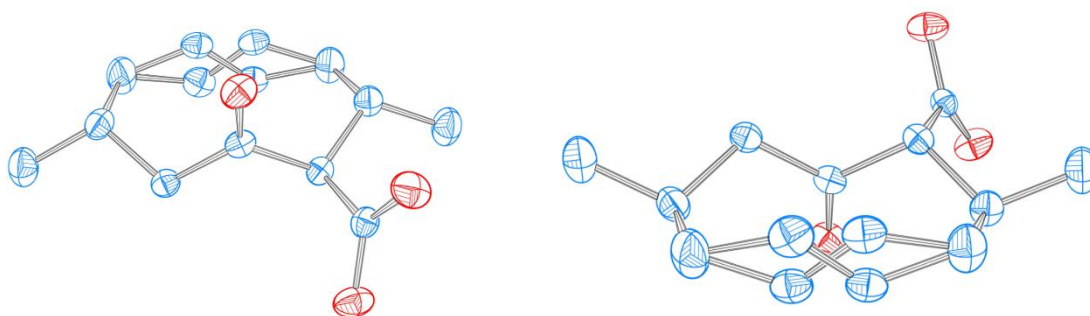
- (164) Inanaga, K.; Ogawa, Y.; Nagamoto, Y.; Daigaku, A.; Tokuyama, H.; Takemoto, Y.; Takasu, K. *Beilstein Journal of Organic Chemistry*, **2012**, *8*, 658.
- (165) Ishihara, K.; Nakamura, H.; Nakamura, S.; Yamamoto, H. *Journal of Organic Chemistry*, **1998**, *63*, 6444.
- (166) Smitha, G.; Chandrasekhar, S.; Reddy, C. S. *Synthesis*, **2008**, 829.
- (167) Paquette, L. A. *Tetrahedron*, **1997**, *53*, 13971.
- (168) Jedlinski, Z.; Stolarzewicz, A.; Grobelny, Z.; Szwarc, M. *The Journal of Physical Chemistry*, **1984**, *88*, 6094.
- (169) Lovric, M.; Cepanec, I.; Litvic, M.; Bartolincic, A.; Vinkovic, V. *Croatica. Chemica Acta*, **2007**, *80*, 109.
- (170) Poon, P. S.; Banerjee, A. K.; Laya, M. S. *Journal of Chemical Research*, **2011**, *35*, 67.
- (171) Tomooka, K.; Ezawa, T.; Inoue, H.; Uehara, K.; Igawa, K. *Journal of the American Chemical Society*, **2011**, *133*, 1754.
- (172) Warwel, S.; Kaetker, H. *Synthesis* **1987**, 935.
- (173) Ritter, T.; Hejl, A.; Wenzel, A. G.; Funk, T. W.; Grubbs, R. H. *Organometallics* **2006**, *25*, 5740.
- (174) Makowka, O. *Berichte der Deutschen Chemischen Gesellschaft*, **1908**, *41*, 943.
- (175) Criegee, R. *Angewandte Chemie*, **1938**, *51*, 519.
- (176) Jacobsen, E. N.; Marko, I.; Mungall, W. S.; Schroeder, G.; Sharpless, K. B. *Journal of the American Chemical Society*, **1988**, *110*, 1968.
- (177) Hentges, S. G.; Sharpless, K. B. *Journal of the American Chemical Society*, **1980**, *102*, 4263.
- (178) Kwong, H. L.; Sorato, C.; Ogino, Y.; Chen, H.; Sharpless, K. B. *Tetrahedron Letters*, **1990**, *31*, 2999.
- (179) Kolb, H. C.; VanNieuwenhze, M. S.; Sharpless, K. B. *Chemical Reviews*, **1994**, *94*, 2483.
- (180) Raju, B. R.; Saikia, A. K. *Molecules*, **2008**, *13*, 1942.

- (181) Deslongchamps, P.; Rowan, D. D.; Pothier, N.; Sauve, T.; Saunders, J. K. *Canadian Journal of Chemistry*, **1981**, *59*, 1105.
- (182) Becker, H.; Sharpless, K. B. *Angewandte Chemie International Edition*, **1996**, *35*, 448.
- (183) Sharpless, K. B.; Amberg, W.; Bennani, Y. L.; Crispino, G. A.; Hartung, J.; Jeong, K. S.; Kwong, H. L.; Morikawa, K.; Wang, Z. M.; et, a. *Journal of Organic Chemistry*, **1992**, *57*, 2768.
- (184) Walsh, P. J.; Sharpless, K. B. *Synlett*, **1993**, 605.
- (185) Aho, J. E.; Pihko, P. M.; Rissa, T. K. *Chemical Reviews*, **2005**, *105*, 4406.
- (186) Favre, S.; Vogel, P.; Gerber-Lemaire, S. *Molecules*, **2008**, *13*, 2570.
- (187) Kobayashi, M.; Aoki, S.; Gato, K.; Kitagawa, I. *Chemical and Pharmaceutical Bulletin*, **1996**, *44*, 2142.
- (188) Paterson, I.; Wallace, D. J.; Gibson, K. R. *Tetrahedron Letters*, **1997**, *38*, 8911.
- (189) Evans, D. A.; Trotter, B. W.; Coleman, P. J.; Cote, B.; Dias, L. C.; Rajapakse, H. A.; Tyler, A. N. *Tetrahedron*, **1999**, *55*, 8671.
- (190) Smith, A. B., III; Doughty, V. A.; Lin, Q.; Zhuang, L.; McBriar, M. D.; Boldi, A. M.; Moser, W. H.; Murase, N.; Nakayama, K.; Sobukawa, M. *Angewandte Chemie International Edition*, **2001**, *40*, 191.
- (191) Crimmins, M. T.; Katz, J. D. *Organic Letters*, **2000**, *2*, 957.
- (192) Fuwa, H.; Sasaki, M. *Organic Letters*, **2008**, *10*, 2549.
- (193) Nakamura, S.; Inagaki, J.; Sugimoto, T.; Kudo, M.; Nakajima, M.; Hashimoto, S. *Organic Letters*, **2001**, *3*, 4075.
- (194) Becker, H.; Soler, M. A.; Sharpless, K. B. *Tetrahedron*, **1995**, *51*, 1345.
- (195) Armstrong, A.; Barsanti, P. A.; Jones, L. H.; Ahmed, G. *Journal of Organic Chemistry*, **2000**, *65*, 7020.
- (196) Wai, J. S. M.; Marko, I.; Svendsen, J. S.; Finn, M. G.; Jacobsen, E. N.; Sharpless, K. B. *Journal of the American Chemical Society*, **1989**, *111*, 1123.
- (197) Hoevelmann, C. H.; Muniz, K. *Chemistry - A European Journal*, **2005**, *11*, 3951.
- (198) Seeman, J. I. *Chemical Reviews*, **1983**, *83*, 83.

- (199) Milas, N. A.; Sussman, S. *Journal of the American Chemical Society*, **1936**, *58*, 1302.
- (200) VanRheenen, V.; Kelly, R. C.; Cha, D. Y. *Tetrahedron Letters*, **1976**, *17*, 1973.
- (201) Maryanoff, B. E.; Reitz, A. B. *Chemical Reviews*, **1989**, *89*, 863.
- (202) Okude, Y.; Hirano, S.; Hiyama, T.; Nozaki, H. *Journal of the American Chemical Society*, **1977**, *99*, 3179.
- (203) Fuerstner, A. *Chemical Reviews*, **1999**, *99*, 991.
- (204) Chérest, M.; Felkin, H.; Prudent, N. *Tetrahedron Letters*, **1968**, *9*, 2199.
- (205) Nguyen, T. A.; Eisenstein, O.; Lefour, J. M.; Tran Huu Dau, M. E. *Journal of the American Chemical Society*, **1973**, *95*, 6146.
- (206) Reetz, M. T.; Jung, A. *Journal of the American Chemical Society*, **1983**, *105*, 4833.
- (207) Leitereg, T. J.; Cram, D. J. *Journal of the American Chemical Society*, **1968**, *90*, 4011.
- (208) Lattanzi, A.; Orelli, L. R.; Barone, P.; Massa, A.; Iannece, P.; Scettri, A. *Tetrahedron Letters*, **2003**, *44*, 1333.
- (209) Takamura, H.; Kikuchi, S.; Nakamura, Y.; Yamagami, Y.; Kishi, T.; Kadota, I.; Yamamoto, Y. *Organic Letters*, **2009**, *11*, 2531.
- (210) Bartoli, G.; Cipolletti, R.; Di Antonio, G.; Giovannini, R.; Lanari, S.; Marcolini, M.; Marcantoni, E. *Organic & Biomolecular Chemistry*, **2010**, *8*, 3509.
- (211) Ganic, A.; Pfaltz, A. *Chemistry - A European Journal*, **2012**, *18*, 6724.
- (212) Jin, H.; Uenishi, J.; Christ, W. J.; Kishi, Y. *Journal of the American Chemical Society*, **1986**, *108*, 5644.
- (213) Takai, K.; Tagashira, M.; Kuroda, T.; Oshima, K.; Utimoto, K.; Nozaki, H. *Journal of the American Chemical Society*, **1986**, *108*, 6048.
- (214) Wessjohann, L.; Wild, H. *Synlett* **1997**, 731.
- (215) Hiyama, T.; Okude, Y.; Kimura, K.; Nozaki, H. *Bulletin of the Chemical Society of Japan*, **1982**, *55*, 561.

- (216) Boeckman, R. K., Jr.; Hudack, R. A. *Journal of Organic Chemistry*, **1998**, *63*, 3524.
- (217) Dodge, J. A.; Nissan, J. S.; Presnell, M. *Organic Synthesis*, **1996**, *73*, 110.
- (218) Mukaiyama, T.; Shintou, T.; Fukumoto, K. *Journal of the American Chemical Society*, **2003**, *125*, 10538.
- (219) Shi, X.-X.; Shen, C.-L.; Yao, J.-Z.; Nie, L.-D.; Quan, N. *Tetrahedron Asymmetry*, **2010**, *21*, 277.
- (220) Peng, L.; Zhang, F.-M.; Yang, B.-M.; Zhang, X.-B.; Liu, W.-X.; Zhang, S.-Y.; Tu, Y.-Q. *Tetrahedron Letters*, **2013**, *54*, 6514.
- (221) Fuwa, H.; Muto, T.; Sekine, K.; Sasaki, M. *Chemistry – A European Journal*, **2014**, *20*, 1848.
- (222) Amirav, A.; Gordin, A.; Poliak, M.; Fialkov, A. B. *Journal of Mass Spectrometry*, **2008**, *43*, 141.
- (223) Mahrwald, R.; Schick, H. *Synthesis* **1990**, 592.
- (224) Xu, H.; Wolf, C. *Angewandte Chemie International Edition*, **2011**, *50*, 12249.
- (225) Crimmins, M. T.; Jung, D. K.; Gray, J. L. *Journal of the American Chemical Society*, **1993**, *115*, 3146.
- (226) Wulff, J. E.; Brant, M. G.; Mason, J. W.; Bromba, C. M.; Boulanger, M. J. *Synthesis of bicyclic compounds and method for their use as therapeutic agents*, Patent No. US20130210904A1, Department of Chemistry, University of Victoria, 2013.

Appendix 1 — X-Ray Crystallography



Crystal Summary for 338.

Crystal data for $C_{12}H_{18}O_3$; $M_r = 210.26$; Monoclinic; space group $P2_1/c$; $a = 11.4346(5)$ Å; $b = 5.0720(2)$ Å; $c = 19.8889(9)$ Å; $\alpha = 90^\circ$; $\beta = 93.249(2)^\circ$; $\gamma = 90^\circ$; $V = 1151.63(9)$ Å³; $Z = 4$; $T = 120(2)$ K; $\lambda(\text{Cu-K}\alpha) = 1.54184$ Å; $\mu(\text{Cu-K}\alpha) = 0.696$ mm⁻¹; $d_{\text{calc}} = 1.213$ g.cm⁻³; 14926 reflections collected; 2173 unique ($R_{\text{int}} = 0.0302$); giving $R_1 = 0.0377$, $wR_2 = 0.1014$ for 2071 data with $[I > 2\sigma(I)]$ and $R_1 = 0.0391$, $wR_2 = 0.1029$ for all 2173 data. Residual electron density ($e^- \cdot \text{Å}^{-3}$) max/min: 0.297/-0.162.

An arbitrary sphere of data were collected on a colorless block-like crystal, having approximate dimensions of $0.17 \times 0.15 \times 0.09$ mm, on a Bruker APEX-II diffractometer using a combination of ω - and ϕ -scans of 0.5° . Data were corrected for absorption and polarization effects and analyzed for space group determination. The structure was solved by direct methods and expanded routinely. The model was refined by full-matrix least-squares analysis of F^2 against all reflections. All non-hydrogen atoms were refined with anisotropic thermal displacement parameters. Unless otherwise noted, hydrogen atoms were included in calculated positions. Thermal parameters for the hydrogens were tied to the isotropic thermal parameter of the atom to which they are bonded ($1.5 \times$ for methyl, $1.2 \times$ for all others).

REFERENCES

Bruker AXS. (2008). *APEX-2*. Bruker-Nonius AXS, Madison, Wisconsin, USA.
G. M. Sheldrick, *Acta Cryst.*, **2008**, A64, 112.

Table 1. Crystal data and structure refinement for **338**.

Empirical formula	C ₁₂ H ₁₈ O ₃	
Formula weight	210.26	
Temperature	120(2) K	
Wavelength	1.54184 Å	
Crystal system	Monoclinic	
Space group	P2 ₁ /c	
Unit cell dimensions	$a = 11.4346(5)$ Å	$\alpha = 90^\circ$
	$b = 5.0720(2)$ Å	$\beta = 93.249(2)^\circ$
	$c = 19.8889(9)$ Å	$\gamma = 90^\circ$
Volume	1151.63(9) Å ³	
Z	4	
Density (calculated)	1.213 g.cm ⁻³	
Absorption coefficient (μ)	0.696 mm ⁻¹	
F(000)	456	
Crystal color, habit	colorless, block	
Crystal size	0.17 × 0.15 × 0.09 mm ³	
θ range for data collection	3.87 to 71.10°	
Index ranges	-13 ≤ h ≤ 14, -6 ≤ k ≤ 6, -23 ≤ l ≤ 18	
Reflections collected	14926	
Independent reflections	2173 [R _{int} = 0.0302]	
Completeness to $\theta = 71.10^\circ$	97.1 %	
Absorption correction	Semi-empirical from equivalents	
Max. and min. transmission	0.7534 and 0.6819	
Refinement method	Full-matrix least-squares on F ²	
Data / restraints / parameters	2173 / 0 / 157	
Goodness-of-fit on F ²	1.049	
Final R indices [I > 2 σ (I)]	R ₁ = 0.0377, wR ₂ = 0.1014	
R indices (all data)	R ₁ = 0.0391, wR ₂ = 0.1029	
Largest diff. peak and hole	0.297 and -0.162 e ⁻ .Å ⁻³	

Table 2. Atomic coordinates and equivalent isotropic displacement parameters (Å²) for **338**. U(eq) is defined as one third of the trace of the orthogonalized U_{ij} tensor.

	x	y	z	U(eq)
O(1)	0.03484(8)	0.72665(17)	0.44866(5)	0.032(1)
O(2)	0.13302(8)	1.09287(17)	0.47731(4)	0.033(1)
O(3)	0.20190(7)	1.17332(15)	0.33068(4)	0.027(1)
C(1)	0.12376(9)	0.8824(2)	0.44652(5)	0.021(1)
C(2)	0.21669(9)	0.7893(2)	0.40037(5)	0.021(1)
C(3)	0.18847(9)	0.9362(2)	0.33302(5)	0.021(1)
C(4)	0.13494(9)	0.7855(2)	0.27306(5)	0.022(1)
C(5)	0.18624(11)	0.8652(2)	0.20617(6)	0.028(1)
C(6)	0.31404(12)	0.7632(3)	0.20224(7)	0.043(1)

C(7A)	0.3835(2)	0.8249(7)	0.26539(15)	0.031(1)
C(8A)	0.3954(2)	0.6649(7)	0.31661(16)	0.031(1)
C(7B)	0.3657(2)	0.6646(7)	0.26804(16)	0.029(1)
C(8B)	0.4191(2)	0.8165(7)	0.31552(13)	0.024(1)
C(9)	0.43596(11)	0.7304(3)	0.38695(7)	0.036(1)
C(10)	0.34155(10)	0.8527(2)	0.43018(6)	0.026(1)
C(11)	0.11037(12)	0.7613(3)	0.14638(7)	0.037(1)
C(12)	0.35966(12)	0.7518(3)	0.50231(7)	0.039(1)
H(10)	-0.0152	0.7941	0.4728	0.048
H(2A)	0.2088	0.5949	0.3930	0.025
H(4A)	0.0493	0.8165	0.2698	0.027
H(4B)	0.1479	0.5945	0.2805	0.027
H(5A)	0.1875	1.0621	0.2036	0.033
H(6A)	0.3132	0.5701	0.1949	0.051
H(6B)	0.3507	0.8471	0.1637	0.051
H(6C)	0.3149	0.6189	0.1687	0.051
H(6D)	0.3635	0.9079	0.1863	0.051
H(7AA)	0.4218	0.9911	0.2688	0.037
H(8AA)	0.3757	0.4855	0.3080	0.037
H(7BA)	0.3604	0.4811	0.2769	0.035
H(8BA)	0.4472	0.9850	0.3032	0.028
H(9A)	0.5023	0.8553	0.3857	0.043
H(9B)	0.4658	0.5675	0.4093	0.043
H(9C)	0.5147	0.7849	0.4051	0.043
H(9D)	0.4314	0.5358	0.3893	0.043
H(10A)	0.3519	1.0485	0.4306	0.032
H(11A)	0.0305	0.8298	0.1486	0.056
H(11B)	0.1087	0.5683	0.1478	0.056
H(11C)	0.1431	0.8193	0.1044	0.056
H(12A)	0.3091	0.8504	0.5315	0.059
H(12B)	0.4418	0.7761	0.5180	0.059
H(12C)	0.3397	0.5640	0.5037	0.059

Table 3. Anisotropic displacement parameters (\AA^2) for **338**. The anisotropic displacement factor exponent takes the form: $-2\pi^2[h^2a^{*2}U_{11} + \dots + 2hka^*b^*U_{12}]$

	U_{11}	U_{22}	U_{33}	U_{23}	U_{13}	U_{12}
O(1)	0.0300(5)	0.0273(5)	0.0406(6)	-0.0066(4)	0.0148(4)	-0.0042(3)
O(2)	0.0311(4)	0.0297(5)	0.0380(5)	-0.0143(4)	0.0085(4)	-0.0019(3)
O(3)	0.0355(5)	0.0161(4)	0.0306(5)	0.0004(3)	0.0062(3)	0.0023(3)
C(1)	0.0243(5)	0.0190(5)	0.0195(5)	0.0015(4)	0.0017(4)	0.0016(4)
C(2)	0.0244(5)	0.0175(5)	0.0211(6)	-0.0003(4)	0.0036(4)	0.0020(4)
C(3)	0.0200(5)	0.0175(5)	0.0246(6)	0.0005(4)	0.0062(4)	0.0032(4)
C(4)	0.0226(5)	0.0201(5)	0.0239(6)	0.0014(4)	0.0023(4)	0.0008(4)
C(5)	0.0328(6)	0.0282(6)	0.0228(6)	0.0016(4)	0.0048(5)	-0.0009(5)

C(6)	0.0310(7)	0.0721(11)	0.0262(7)	-0.0036(6)	0.0076(5)	0.0010(6)
C(7A)	0.0228(12)	0.0343(17)	0.0356(18)	-0.0038(12)	0.0095(11)	-0.0004(11)
C(8A)	0.0232(12)	0.0315(17)	0.038(2)	-0.0045(13)	0.0084(11)	0.0043(12)
C(7B)	0.0244(12)	0.0298(16)	0.0330(18)	-0.0060(12)	0.0078(11)	0.0013(11)
C(8B)	0.0187(11)	0.0232(14)	0.0298(16)	0.0000(10)	0.0063(10)	-0.0009(10)
C(9)	0.0250(6)	0.0514(8)	0.0314(7)	-0.0009(6)	0.0026(5)	0.0095(5)
C(10)	0.0239(5)	0.0291(6)	0.0260(6)	-0.0008(4)	0.0020(4)	0.0024(5)
C(11)	0.0369(7)	0.0500(8)	0.0249(7)	-0.0014(5)	0.0002(5)	0.0050(6)
C(12)	0.0326(7)	0.0574(9)	0.0270(7)	0.0031(6)	-0.0007(5)	0.0058(6)

Table 4. Bond lengths [Å] for **338**.

atom-atom	distance	atom-atom	distance
O(1)-C(1)	1.2904(14)	O(2)-C(1)	1.2320(14)
O(3)-C(3)	1.2137(14)	C(1)-C(2)	1.5184(15)
C(2)-C(10)	1.5484(15)	C(2)-C(3)	1.5508(15)
C(3)-C(4)	1.5161(15)	C(4)-C(5)	1.5382(16)
C(5)-C(11)	1.5256(17)	C(5)-C(6)	1.5564(18)
C(6)-C(7A)	1.481(3)	C(6)-C(7B)	1.491(4)
C(7A)-C(8A)	1.304(5)	C(8A)-C(9)	1.486(4)
C(7B)-C(8B)	1.338(4)	C(8B)-C(9)	1.488(3)
C(9)-C(10)	1.5475(16)	C(10)-C(12)	1.5261(17)
O(1)-H(1O)	0.8400	C(2)-H(2A)	1.0000
C(4)-H(4A)	0.9900	C(4)-H(4B)	0.9900
C(5)-H(5A)	1.0000	C(6)-H(6A)	0.9900
C(6)-H(6B)	0.9900	C(6)-H(6C)	0.9900
C(6)-H(6D)	0.9899	C(7A)-H(7AA)	0.9500
C(8A)-H(8AA)	0.9500	C(7B)-H(7BA)	0.9500
C(8B)-H(8BA)	0.9500	C(9)-H(9A)	0.9900
C(9)-H(9B)	0.9900	C(9)-H(9C)	0.9900
C(9)-H(9D)	0.9900	C(10)-H(10A)	1.0000
C(11)-H(11A)	0.9800	C(11)-H(11B)	0.9800
C(11)-H(11C)	0.9800	C(12)-H(12A)	0.9800
C(12)-H(12B)	0.9800	C(12)-H(12C)	0.9800

Symmetry transformations used to generate equivalent atoms:

Table 5. Bond angles [°] for **338**.

atom-atom-atom	angle	atom-atom-atom	angle
O(2)-C(1)-O(1)	124.04(10)	O(2)-C(1)-C(2)	121.79(10)
O(1)-C(1)-C(2)	114.14(9)	C(1)-C(2)-C(10)	111.44(9)
C(1)-C(2)-C(3)	104.72(8)	C(10)-C(2)-C(3)	111.90(9)
O(3)-C(3)-C(4)	121.05(10)	O(3)-C(3)-C(2)	119.26(10)

C(4)-C(3)-C(2)	119.48(9)	C(3)-C(4)-C(5)	113.01(9)
C(11)-C(5)-C(4)	110.81(10)	C(11)-C(5)-C(6)	109.88(11)
C(4)-C(5)-C(6)	111.17(10)	C(7A)-C(6)-C(5)	110.32(14)
C(7B)-C(6)-C(5)	113.20(13)	C(1)-O(1)-H(10)	109.5
C(1)-C(2)-H(2A)	109.6	C(10)-C(2)-H(2A)	109.6
C(3)-C(2)-H(2A)	109.6	C(3)-C(4)-H(4A)	109.0
C(5)-C(4)-H(4A)	109.0	C(3)-C(4)-H(4B)	109.0
C(5)-C(4)-H(4B)	109.0	H(4A)-C(4)-H(4B)	107.8
C(11)-C(5)-H(5A)	108.3	C(4)-C(5)-H(5A)	108.3
C(6)-C(5)-H(5A)	108.3	C(7A)-C(6)-H(6A)	109.6
C(5)-C(6)-H(6A)	109.6	C(7A)-C(6)-H(6B)	109.6
C(7B)-C(6)-H(6B)	131.3	C(5)-C(6)-H(6B)	109.6
H(6A)-C(6)-H(6B)	108.1	C(7A)-C(6)-H(6C)	134.6
C(7B)-C(6)-H(6C)	108.9	C(5)-C(6)-H(6C)	108.9
C(7A)-C(6)-H(6D)	80.0	C(7B)-C(6)-H(6D)	108.9
C(5)-C(6)-H(6D)	108.9	H(6A)-C(6)-H(6D)	133.4
H(6C)-C(6)-H(6D)	107.8	C(8A)-C(7A)-H(7AA)	118.1
C(6)-C(7A)-H(7AA)	118.1	C(8A)-C(7A)-C(6)	123.9(4)
C(7A)-C(8A)-C(9)	127.5(4)	C(7B)-C(8B)-C(9)	122.3(3)
C(8B)-C(7B)-C(6)	124.6(3)	C(8A)-C(9)-C(10)	114.96(13)
C(8B)-C(9)-C(10)	110.86(13)	C(12)-C(10)-C(9)	109.03(10)
C(12)-C(10)-C(2)	111.30(10)	C(9)-C(10)-C(2)	111.17(9)
C(7A)-C(8A)-H(8AA)	116.2	C(9)-C(8A)-H(8AA)	116.2
C(8B)-C(7B)-H(7BA)	117.7	C(6)-C(7B)-H(7BA)	117.7
C(7B)-C(8B)-H(8BA)	118.9	C(9)-C(8B)-H(8BA)	118.9
C(8A)-C(9)-H(9A)	108.5	C(10)-C(9)-H(9A)	108.5
C(8A)-C(9)-H(9B)	108.5	C(10)-C(9)-H(9B)	108.5
H(9A)-C(9)-H(9B)	107.5	C(8A)-C(9)-H(9C)	129.5
C(8B)-C(9)-H(9C)	109.5	C(10)-C(9)-H(9C)	109.5
C(8B)-C(9)-H(9D)	109.5	C(10)-C(9)-H(9D)	109.5
H(9C)-C(9)-H(9D)	108.1	C(12)-C(10)-H(10A)	108.4
C(9)-C(10)-H(10A)	108.4	C(2)-C(10)-H(10A)	108.4
C(5)-C(11)-H(11A)	109.5	C(5)-C(11)-H(11B)	109.5
H(11A)-C(11)-H(11B)	109.5	C(5)-C(11)-H(11C)	109.5
H(11A)-C(11)-H(11C)	109.5	H(11B)-C(11)-H(11C)	109.5
C(10)-C(12)-H(12A)	109.5	C(10)-C(12)-H(12B)	109.5
H(12A)-C(12)-H(12B)	109.5	C(10)-C(12)-H(12C)	109.5
H(12A)-C(12)-H(12C)	109.5	H(12B)-C(12)-H(12C)	109.5

Table 6. Torsion angles [°] for **338**.

atom-atom-atom-atom	angle	atom-atom-atom-atom	angle
O(2)-C(1)-C(2)-C(10)	39.06(14)	O(1)-C(1)-C(2)-C(10)	-142.79(10)
O(2)-C(1)-C(2)-C(3)	-82.10(12)	O(1)-C(1)-C(2)-C(3)	96.05(11)
C(1)-C(2)-C(3)-O(3)	68.07(12)	C(10)-C(2)-C(3)-O(3)	-52.79(13)

C(1)-C(2)-C(3)-C(4)	-106.72(10)	C(10)-C(2)-C(3)-C(4)	132.42(10)
O(3)-C(3)-C(4)-C(5)	45.71(14)	C(2)-C(3)-C(4)-C(5)	-139.60(10)
C(3)-C(4)-C(5)-C(11)	-165.99(10)	C(3)-C(4)-C(5)-C(6)	71.50(13)
C(11)-C(5)-C(6)-C(7A)	-170.58(18)	C(4)-C(5)-C(6)-C(7A)	-47.5(2)
C(11)-C(5)-C(6)-C(7B)	-135.26(18)	C(4)-C(5)-C(6)-C(7B)	-12.2(2)
C(7B)-C(6)-C(7A)-C(8A)	-9.4(2)	C(5)-C(6)-C(7A)-C(8A)	92.2(3)
C(6)-C(7A)-C(8A)-C(9)	-163.0(2)	C(7A)-C(6)-C(7B)-C(8B)	6.3(2)
C(5)-C(6)-C(7B)-C(8B)	-85.5(3)	C(6)-C(7B)-C(8B)-C(9)	160.55(19)
C(7A)-C(8A)-C(9)-C(8B)	-9.1(2)	C(7A)-C(8A)-C(9)-C(10)	80.6(3)
C(7B)-C(8B)-C(9)-C(8A)	4.7(2)	C(7B)-C(8B)-C(9)-C(10)	-99.3(2)
C(8A)-C(9)-C(10)-C(12)	143.67(19)	C(8B)-C(9)-C(10)-C(12)	178.05(16)
C(8A)-C(9)-C(10)-C(2)	20.6(2)	C(8B)-C(9)-C(10)-C(2)	54.99(19)
C(1)-C(2)-C(10)-C(12)	51.98(13)	C(3)-C(2)-C(10)-C(12)	168.86(10)
C(1)-C(2)-C(10)-C(9)	173.73(10)	C(3)-C(2)-C(10)-C(9)	-69.39(12)

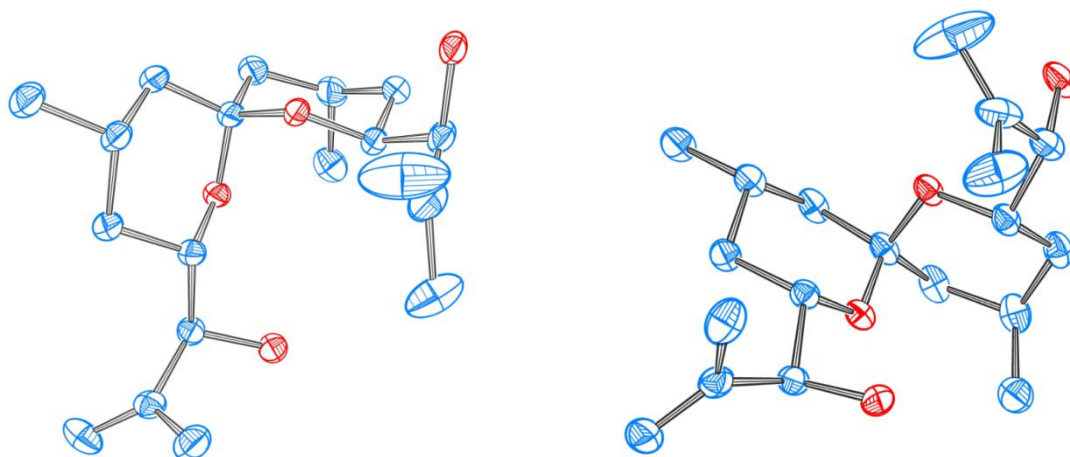
Symmetry transformations used to generate equivalent atoms:

Table 7. Hydrogen bonds for **338** [Å and °].

D-H...A	d(D-H)	d(H...A)	d(D...A)	<(DHA)
O(1)-H(10)...O(2)#1	0.84	1.81	2.6476(12)	173.6

Symmetry transformations used to generate equivalent atoms:

#1 -x,-y+2,-z+1



Crystal Summary for 382.

Crystal data for $2 \cdot (\text{C}_{19}\text{H}_{32}\text{O}_4)$; $M_r = 648.89$; Monoclinic; space group $P2_1$; $a = 10.9479(4)$ Å; $b = 16.4296(6)$ Å; $c = 10.9911(4)$ Å; $\alpha = 90^\circ$; $\beta = 103.483(2)^\circ$; $\gamma = 90^\circ$; $V = 1922.48(12)$ Å³; $Z = 2$; $T = 120(2)$ K; $\lambda(\text{Cu-K}\alpha) = 1.54184$ Å; $\mu(\text{Cu-K}\alpha) = 0.613$ mm⁻¹; $d_{\text{calc}} = 1.121$ g.cm⁻³; 33082 reflections collected; 7165 unique ($R_{\text{int}} = 0.0292$); giving $R_1 = 0.0346$, $wR_2 = 0.0935$ for 6960 data with $[I > 2\sigma(I)]$ and $R_1 = 0.0355$, $wR_2 = 0.0944$ for all 7165 data. Residual electron density ($e^- \cdot \text{Å}^{-3}$) max/min: 0.344/-0.224.

An arbitrary sphere of data were collected on a colorless rod-like crystal, having approximate dimensions of $0.24 \times 0.12 \times 0.10$ mm, on a Bruker APEX-II diffractometer using a combination of ω - and ϕ -scans of 0.5° [1]. Data were corrected for absorption and polarization effects and analyzed for space group determination. The structure was solved by dual-space methods and expanded routinely [2]. The model was refined by full-matrix least-squares analysis of F^2 against all reflections. All non-hydrogen atoms were refined with anisotropic thermal displacement parameters. Unless otherwise noted, hydrogen atoms were included in calculated positions. Thermal parameters for the hydrogens were tied to the isotropic thermal parameter of the atom to which they are bonded ($1.5 \times$ for methyl, $1.2 \times$ for all others).

The absolute stereochemistry was determined both by comparison of the known handedness of the molecule and by comparison of intensities of Friedel pairs of reflections. The Flack x parameter refined to 0.09(7) [3] and the Hooft y parameter was determined to be 0.06(4) [4]. Values of zero (0) indicate that the correct enantiomorph of the space group is present, and hence the configuration of the molecule can be reliably determined. These results agree with the known chirality from synthesis. The values also indicate that there is no racemic twinning within the sample measured.

References

- [1] Bruker AXS. (2008). *APEX-2*. Bruker-Nonius AXS, Madison, Wisconsin, USA.
 [2] G. M. Sheldrick, *Acta Cryst.*, **2008**, *A64*, 112.
 [3] H. D. Flack, *Acta Cryst.*, **1983**, *A39*, 876.
 [4] R. W. W. Hoof, L. H. Straver & A. L. Spek, *J. Appl. Cryst.*, **2008**, *41*, 96.

Table 1. Crystal data and structure refinement for **382**.

Empirical formula	C ₃₈ H ₆₄ O ₈	
Formula weight	648.89	
Temperature	120(2) K	
Wavelength	1.54184 Å	
Crystal system	Monoclinic	
Space group	P2 ₁	
Unit cell dimensions	$a = 10.9479(4)$ Å	$\alpha = 90^\circ$
	$b = 16.4296(6)$ Å	$\beta = 103.483(2)^\circ$
	$c = 10.9911(4)$ Å	$\gamma = 90^\circ$
Volume	1922.48(12) Å ³	
Z	2	
Density (calculated)	1.121 g.cm ⁻³	
Absorption coefficient (μ)	0.613 mm ⁻¹	
F(000)	712	
Crystal color, habit	colorless, rod	
Crystal size	0.24 × 0.12 × 0.10 mm ³	
θ range for data collection	4.136 to 71.569°	
Index ranges	-12 ≤ h ≤ 13, -20 ≤ k ≤ 20, -13 ≤ l ≤ 13	
Reflections collected	33082	
Independent reflections	7165 [R _{int} = 0.0292]	
Completeness to $\theta = 67.679^\circ$	99.9 %	
Absorption correction	Numerical	
Max. and min. transmission	1.0000 and 0.9244	
Refinement method	Full-matrix least-squares on F ²	
Data / restraints / parameters	7165 / 1 / 427	
Goodness-of-fit on F ²	1.028	
Final R indices [I > 2σ(I)]	R ₁ = 0.0346, wR ₂ = 0.0935	
R indices (all data)	R ₁ = 0.0355, wR ₂ = 0.0944	
Absolute structure parameter	0.09(7)	
Extinction coefficient	n/a	
Largest diff. peak and hole	0.344 and -0.224 e ⁻ .Å ⁻³	

Table 2. Atomic coordinates and equivalent isotropic displacement parameters (\AA^2) for **382**. $U(\text{eq})$ is defined as one third of the trace of the orthogonalized U_{ij} tensor.

	x	y	z	$U(\text{eq})$
O(1)	0.45586(16)	0.49397(12)	0.46047(14)	0.047(1)
O(2)	0.27654(14)	0.45441(9)	0.26056(13)	0.031(1)
O(3)	0.29226(13)	0.47891(8)	0.05497(12)	0.028(1)
O(4)	0.39609(14)	0.48913(13)	-0.14702(13)	0.045(1)
C(1)	0.3642(2)	0.62271(16)	0.4887(2)	0.041(1)
C(2)	0.3401(2)	0.53834(15)	0.43564(19)	0.035(1)
C(3)	0.2816(2)	0.53884(13)	0.29470(18)	0.030(1)
C(4)	0.1526(2)	0.57761(16)	0.2617(2)	0.039(1)
C(5)	0.0901(2)	0.56537(16)	0.1232(2)	0.041(1)
C(6)	0.0918(2)	0.47500(15)	0.0923(2)	0.038(1)
C(7)	0.22240(19)	0.43868(14)	0.13063(18)	0.030(1)
C(8)	0.2233(2)	0.34691(14)	0.1135(2)	0.041(1)
C(9)	0.3518(3)	0.30961(15)	0.1189(2)	0.046(1)
C(10)	0.4174(2)	0.35954(16)	0.0353(2)	0.042(1)
C(11)	0.41750(18)	0.44943(14)	0.06532(18)	0.032(1)
C(12)	0.4712(2)	0.50221(17)	-0.02421(18)	0.039(1)
C(13)	0.4786(2)	0.59140(17)	0.0114(2)	0.047(1)
C(14)	0.4692(3)	0.6668(2)	0.4584(3)	0.056(1)
C(15)	0.2888(3)	0.6524(2)	0.5602(3)	0.062(1)
C(16)	-0.0429(3)	0.5991(2)	0.0892(3)	0.059(1)
C(17)	0.4332(3)	0.30028(17)	0.2514(3)	0.054(1)
C(18)	0.3790(3)	0.6455(2)	-0.0510(3)	0.063(1)
C(19)	0.5782(4)	0.6180(2)	0.1018(3)	0.075(1)
O(5)	0.57192(14)	0.50577(14)	0.71781(13)	0.049(1)
O(6)	0.76977(13)	0.49969(10)	0.59915(12)	0.034(1)
O(7)	0.97863(13)	0.50941(9)	0.58502(13)	0.031(1)
O(8)	1.13661(14)	0.44185(10)	0.79225(13)	0.035(1)
C(20)	0.7180(2)	0.39488(19)	0.7983(2)	0.049(1)
C(21)	0.6966(2)	0.48524(17)	0.78370(18)	0.040(1)
C(22)	0.7921(2)	0.52903(15)	0.72572(18)	0.034(1)
C(23)	0.7775(2)	0.62100(16)	0.7269(2)	0.042(1)
C(24)	0.8671(3)	0.66319(16)	0.6594(3)	0.047(1)
C(25)	0.8516(3)	0.62481(16)	0.5296(2)	0.045(1)
C(26)	0.8528(2)	0.53199(14)	0.52925(19)	0.035(1)
C(27)	0.8105(2)	0.49545(16)	0.39924(19)	0.041(1)
C(28)	0.8347(2)	0.40386(16)	0.3965(2)	0.039(1)
C(29)	0.9720(2)	0.38626(14)	0.46225(19)	0.035(1)
C(30)	1.00110(18)	0.42331(13)	0.59278(18)	0.029(1)
C(31)	1.13656(19)	0.41647(13)	0.66783(19)	0.030(1)
C(32)	1.1911(2)	0.33158(13)	0.66818(19)	0.034(1)
C(33)	0.8322(4)	0.3662(2)	0.8864(3)	0.075(1)
C(34)	0.6403(5)	0.3407(3)	0.7297(5)	0.121(2)

C(35)	1.0020(3)	0.66399(16)	0.7366(3)	0.052(1)
C(36)	0.8012(2)	0.37137(19)	0.2627(2)	0.049(1)
C(37)	1.1340(3)	0.26705(15)	0.7322(2)	0.046(1)
C(38)	1.2877(2)	0.31810(16)	0.6172(3)	0.049(1)
H(1)	0.4473	0.4520	0.4157	0.070
H(4)	0.4393	0.4978	-0.1996	0.068
H(2)	0.2809	0.5102	0.4787	0.042
H(3)	0.3385	0.5683	0.2506	0.036
H(4A)	0.1603	0.6366	0.2805	0.047
H(4B)	0.0994	0.5532	0.3135	0.047
H(5)	0.1410	0.5949	0.0725	0.049
H(6A)	0.0354	0.4456	0.1357	0.045
H(6B)	0.0590	0.4674	0.0012	0.045
H(8A)	0.1671	0.3333	0.0317	0.049
H(8B)	0.1878	0.3213	0.1793	0.049
H(9)	0.3375	0.2538	0.0819	0.055
H(10A)	0.5051	0.3404	0.0467	0.050
H(10B)	0.3740	0.3509	-0.0534	0.050
H(11)	0.4676	0.4585	0.1527	0.039
H(12)	0.5582	0.4827	-0.0221	0.047
H(14A)	0.5481	0.6393	0.4969	0.084
H(14B)	0.4711	0.7226	0.4906	0.084
H(14C)	0.4588	0.6683	0.3674	0.084
H(15A)	0.3025	0.7056	0.5946	0.074
H(15B)	0.2221	0.6201	0.5758	0.074
H(16A)	-0.0811	0.5871	0.0012	0.089
H(16B)	-0.0405	0.6581	0.1022	0.089
H(16C)	-0.0927	0.5737	0.1423	0.089
H(17A)	0.4710	0.3529	0.2807	0.080
H(17B)	0.4997	0.2604	0.2511	0.080
H(17C)	0.3811	0.2815	0.3072	0.080
H(18A)	0.3768	0.6474	-0.1406	0.095
H(18B)	0.3945	0.7003	-0.0155	0.095
H(18C)	0.2983	0.6255	-0.0391	0.095
H(19A)	0.5840	0.6737	0.1257	0.090
H(19B)	0.6419	0.5808	0.1407	0.090
H(5A)	0.5621	0.4936	0.6419	0.074
H(8)	1.2079	0.4600	0.8271	0.052
H(21)	0.7074	0.5077	0.8701	0.048
H(22)	0.8790	0.5138	0.7719	0.041
H(23A)	0.7945	0.6403	0.8146	0.050
H(23B)	0.6899	0.6357	0.6858	0.050
H(24)	0.8394	0.7212	0.6463	0.057
H(25A)	0.7712	0.6437	0.4756	0.053
H(25B)	0.9201	0.6446	0.4923	0.053
H(27A)	0.8553	0.5231	0.3424	0.049

H(27B)	0.7195	0.5057	0.3675	0.049
H(28)	0.7796	0.3761	0.4445	0.047
H(29A)	0.9861	0.3267	0.4682	0.042
H(29B)	1.0286	0.4097	0.4131	0.042
H(30)	0.9447	0.3980	0.6419	0.035
H(31)	1.1895	0.4551	0.6320	0.036
H(33A)	0.9061	0.3827	0.8565	0.113
H(33B)	0.8300	0.3068	0.8924	0.113
H(33C)	0.8366	0.3901	0.9690	0.113
H(34A)	0.6593	0.2842	0.7381	0.145
H(34B)	0.5662	0.3586	0.6724	0.145
H(35A)	1.0065	0.6950	0.8137	0.078
H(35B)	1.0564	0.6895	0.6882	0.078
H(35C)	1.0300	0.6080	0.7577	0.078
H(36A)	0.8556	0.3968	0.2144	0.073
H(36B)	0.7133	0.3842	0.2241	0.073
H(36C)	0.8132	0.3122	0.2638	0.073
H(37A)	1.1350	0.2845	0.8177	0.069
H(37B)	1.1823	0.2166	0.7348	0.069
H(37C)	1.0471	0.2576	0.6862	0.069
H(38A)	1.3237	0.2653	0.6206	0.059
H(38B)	1.3210	0.3613	0.5773	0.059

Table 3. Anisotropic displacement parameters (\AA^2) for **382**. The anisotropic displacement factor exponent takes the form: $-2\pi^2[h^2a^2U_{11} + \dots + 2hka^*b^*U_{12}]$

	U_{11}	U_{22}	U_{33}	U_{23}	U_{13}	U_{12}
O(1)	0.0446(9)	0.0628(11)	0.0284(7)	-0.0029(7)	-0.0018(6)	0.0176(8)
O(2)	0.0335(8)	0.0374(8)	0.0233(6)	0.0031(6)	0.0081(5)	-0.0018(6)
O(3)	0.0246(7)	0.0371(7)	0.0241(6)	0.0022(5)	0.0073(5)	-0.0011(6)
O(4)	0.0307(8)	0.0840(13)	0.0221(7)	-0.0020(7)	0.0070(6)	-0.0140(8)
C(1)	0.0409(12)	0.0505(13)	0.0267(10)	-0.0031(9)	-0.0003(9)	0.0024(10)
C(2)	0.0340(11)	0.0474(12)	0.0246(9)	0.0031(8)	0.0064(8)	0.0036(9)
C(3)	0.0290(10)	0.0382(10)	0.0225(9)	0.0008(8)	0.0054(7)	-0.0007(8)
C(4)	0.0351(12)	0.0512(13)	0.0312(10)	-0.0023(10)	0.0070(9)	0.0071(10)
C(5)	0.0311(11)	0.0579(14)	0.0311(11)	-0.0008(10)	0.0036(8)	0.0098(10)
C(6)	0.0260(10)	0.0576(14)	0.0293(10)	-0.0038(9)	0.0065(8)	-0.0062(10)
C(7)	0.0282(10)	0.0400(11)	0.0238(9)	-0.0002(8)	0.0077(7)	-0.0069(8)
C(8)	0.0488(14)	0.0405(12)	0.0341(11)	-0.0013(9)	0.0116(10)	-0.0119(10)
C(9)	0.0618(16)	0.0336(12)	0.0412(13)	-0.0020(9)	0.0085(11)	0.0029(11)
C(10)	0.0407(12)	0.0496(14)	0.0350(11)	-0.0052(10)	0.0074(9)	0.0105(10)
C(11)	0.0257(10)	0.0468(12)	0.0241(9)	-0.0003(8)	0.0058(7)	0.0002(9)
C(12)	0.0248(10)	0.0696(15)	0.0233(9)	-0.0005(10)	0.0057(7)	-0.0091(10)
C(13)	0.0441(14)	0.0648(16)	0.0297(11)	0.0081(10)	0.0068(9)	-0.0246(12)
C(14)	0.0572(17)	0.0637(17)	0.0414(14)	-0.0008(12)	-0.0014(12)	-0.0182(14)

C(15)	0.0632(18)	0.0674(19)	0.0530(16)	-0.0227(14)	0.0117(13)	0.0006(14)
C(16)	0.0401(14)	0.095(2)	0.0393(13)	-0.0050(14)	0.0009(10)	0.0235(15)
C(17)	0.0686(19)	0.0424(13)	0.0468(14)	0.0073(11)	0.0076(12)	0.0103(12)
C(18)	0.0644(19)	0.0600(18)	0.0633(19)	0.0159(15)	0.0102(15)	-0.0141(15)
C(19)	0.072(2)	0.077(2)	0.0629(19)	0.0095(16)	-0.0132(16)	-0.0338(18)
O(5)	0.0246(7)	0.0999(15)	0.0226(7)	0.0005(8)	0.0052(5)	0.0052(9)
O(6)	0.0258(7)	0.0540(9)	0.0224(6)	0.0037(6)	0.0060(5)	0.0058(7)
O(7)	0.0283(7)	0.0355(7)	0.0309(7)	0.0062(6)	0.0094(5)	0.0049(6)
O(8)	0.0293(7)	0.0416(8)	0.0302(7)	-0.0064(6)	0.0011(5)	-0.0006(6)
C(20)	0.0317(12)	0.0759(18)	0.0369(12)	0.0111(12)	0.0038(9)	-0.0158(12)
C(21)	0.0256(10)	0.0733(17)	0.0209(9)	0.0029(10)	0.0032(7)	-0.0010(10)
C(22)	0.0282(10)	0.0511(13)	0.0238(9)	0.0026(9)	0.0063(7)	0.0058(9)
C(23)	0.0397(13)	0.0532(14)	0.0336(11)	0.0025(10)	0.0099(9)	0.0156(11)
C(24)	0.0568(16)	0.0392(12)	0.0500(15)	0.0083(10)	0.0196(12)	0.0151(11)
C(25)	0.0500(14)	0.0459(13)	0.0417(12)	0.0156(10)	0.0190(11)	0.0166(11)
C(26)	0.0316(11)	0.0480(13)	0.0276(10)	0.0109(9)	0.0108(8)	0.0102(9)
C(27)	0.0350(11)	0.0618(15)	0.0257(9)	0.0102(10)	0.0074(8)	0.0141(11)
C(28)	0.0316(11)	0.0602(14)	0.0243(10)	0.0025(10)	0.0037(8)	0.0048(10)
C(29)	0.0318(11)	0.0443(12)	0.0283(10)	0.0009(9)	0.0043(8)	0.0054(9)
C(30)	0.0264(10)	0.0335(10)	0.0280(10)	0.0026(7)	0.0060(8)	0.0025(8)
C(31)	0.0264(10)	0.0344(10)	0.0300(9)	-0.0001(8)	0.0067(7)	-0.0010(8)
C(32)	0.0290(10)	0.0359(11)	0.0309(10)	-0.0036(8)	-0.0035(8)	0.0013(8)
C(33)	0.080(2)	0.074(2)	0.0562(18)	0.0203(16)	-0.0160(16)	-0.0215(18)
C(34)	0.087(3)	0.074(3)	0.158(5)	-0.001(3)	-0.061(3)	-0.017(2)
C(35)	0.0529(16)	0.0404(13)	0.0655(17)	-0.0036(12)	0.0197(13)	-0.0011(12)
C(36)	0.0372(13)	0.0752(18)	0.0302(11)	-0.0013(11)	0.0022(9)	0.0037(12)
C(37)	0.0618(17)	0.0397(12)	0.0332(11)	0.0007(10)	0.0031(11)	0.0025(11)
C(38)	0.0321(12)	0.0417(13)	0.0723(18)	-0.0127(12)	0.0101(11)	0.0030(10)

Table 4. Bond lengths [Å] for **382**.

atom-atom	distance	atom-atom	distance
O(1)-C(2)	1.432(3)	O(1)-H(1)	0.8400
O(2)-C(3)	1.435(3)	O(2)-C(7)	1.436(2)
O(3)-C(7)	1.418(2)	O(3)-C(11)	1.434(2)
O(4)-C(12)	1.424(2)	O(4)-H(4)	0.8400
C(1)-C(15)	1.357(4)	C(1)-C(14)	1.462(4)
C(1)-C(2)	1.503(3)	C(2)-C(3)	1.532(3)
C(2)-H(2)	1.0000	C(3)-C(4)	1.514(3)
C(3)-H(3)	1.0000	C(4)-C(5)	1.530(3)
C(4)-H(4A)	0.9900	C(4)-H(4B)	0.9900
C(5)-C(16)	1.521(3)	C(5)-C(6)	1.524(4)
C(5)-H(5)	1.0000	C(6)-C(7)	1.516(3)
C(6)-H(6A)	0.9900	C(6)-H(6B)	0.9900
C(7)-C(8)	1.520(3)	C(8)-C(9)	1.523(4)

C(8)-H(8A)	0.9900	C(8)-H(8B)	0.9900
C(9)-C(17)	1.527(4)	C(9)-C(10)	1.530(4)
C(9)-H(9)	1.0000	C(10)-C(11)	1.513(3)
C(10)-H(10A)	0.9900	C(10)-H(10B)	0.9900
C(11)-C(12)	1.528(3)	C(11)-H(11)	1.0000
C(12)-C(13)	1.514(4)	C(12)-H(12)	1.0000
C(13)-C(19)	1.364(4)	C(13)-C(18)	1.450(4)
C(14)-H(14A)	0.9800	C(14)-H(14B)	0.9800
C(14)-H(14C)	0.9800	C(15)-H(15A)	0.9500
C(15)-H(15B)	0.9500	C(16)-H(16A)	0.9800
C(16)-H(16B)	0.9800	C(16)-H(16C)	0.9800
C(17)-H(17A)	0.9800	C(17)-H(17B)	0.9800
C(17)-H(17C)	0.9800	C(18)-H(18A)	0.9800
C(18)-H(18B)	0.9800	C(18)-H(18C)	0.9800
C(19)-H(19A)	0.9500	C(19)-H(19B)	0.9500
O(5)-C(21)	1.429(3)	O(5)-H(5A)	0.8400
O(6)-C(26)	1.423(2)	O(6)-C(22)	1.438(2)
O(7)-C(26)	1.421(3)	O(7)-C(30)	1.435(2)
O(8)-C(31)	1.430(2)	O(8)-H(8)	0.8400
C(20)-C(34)	1.336(5)	C(20)-C(33)	1.469(4)
C(20)-C(21)	1.505(4)	C(21)-C(22)	1.525(3)
C(21)-H(21)	1.0000	C(22)-C(23)	1.520(3)
C(22)-H(22)	1.0000	C(23)-C(24)	1.528(4)
C(23)-H(23A)	0.9900	C(23)-H(23B)	0.9900
C(24)-C(35)	1.522(4)	C(24)-C(25)	1.532(4)
C(24)-H(24)	1.0000	C(25)-C(26)	1.525(3)
C(25)-H(25A)	0.9900	C(25)-H(25B)	0.9900
C(26)-C(27)	1.519(3)	C(27)-C(28)	1.530(4)
C(27)-H(27A)	0.9900	C(27)-H(27B)	0.9900
C(28)-C(36)	1.526(3)	C(28)-C(29)	1.536(3)
C(28)-H(28)	1.0000	C(29)-C(30)	1.522(3)
C(29)-H(29A)	0.9900	C(29)-H(29B)	0.9900
C(30)-C(31)	1.524(3)	C(30)-H(30)	1.0000
C(31)-C(32)	1.517(3)	C(31)-H(31)	1.0000
C(32)-C(38)	1.326(3)	C(32)-C(37)	1.488(3)
C(33)-H(33A)	0.9800	C(33)-H(33B)	0.9800
C(33)-H(33C)	0.9800	C(34)-H(34A)	0.9500
C(34)-H(34B)	0.9500	C(35)-H(35A)	0.9800
C(35)-H(35B)	0.9800	C(35)-H(35C)	0.9800
C(36)-H(36A)	0.9800	C(36)-H(36B)	0.9800
C(37)-H(37B)	0.9800	C(37)-H(37C)	0.9800
C(38)-H(38A)	0.9500	C(38)-H(38B)	0.9500

Symmetry transformations used to generate equivalent atoms:

Table 5. Bond angles [°] for **382**.

atom-atom-atom	angle	atom-atom-atom	angle
C(2)-O(1)-H(1)	109.5	C(3)-O(2)-C(7)	114.57(15)
C(7)-O(3)-C(11)	115.65(15)	C(12)-O(4)-H(4)	109.5
C(15)-C(1)-C(14)	124.8(3)	C(15)-C(1)-C(2)	118.8(3)
C(14)-C(1)-C(2)	116.5(2)	O(1)-C(2)-C(1)	109.16(19)
O(1)-C(2)-C(3)	109.78(17)	C(1)-C(2)-C(3)	112.41(18)
O(1)-C(2)-H(2)	108.5	C(1)-C(2)-H(2)	108.5
C(3)-C(2)-H(2)	108.5	O(2)-C(3)-C(4)	111.56(18)
O(2)-C(3)-C(2)	103.93(16)	C(4)-C(3)-C(2)	113.05(17)
O(2)-C(3)-H(3)	109.4	C(4)-C(3)-H(3)	109.4
C(2)-C(3)-H(3)	109.4	C(3)-C(4)-C(5)	111.03(18)
C(3)-C(4)-H(4A)	109.4	C(5)-C(4)-H(4A)	109.4
C(3)-C(4)-H(4B)	109.4	C(5)-C(4)-H(4B)	109.4
H(4A)-C(4)-H(4B)	108.0	C(16)-C(5)-C(6)	111.1(2)
C(16)-C(5)-C(4)	112.13(19)	C(6)-C(5)-C(4)	108.9(2)
C(16)-C(5)-H(5)	108.2	C(6)-C(5)-H(5)	108.2
C(4)-C(5)-H(5)	108.2	C(7)-C(6)-C(5)	112.40(18)
C(7)-C(6)-H(6A)	109.1	C(5)-C(6)-H(6A)	109.1
C(7)-C(6)-H(6B)	109.1	C(5)-C(6)-H(6B)	109.1
H(6A)-C(6)-H(6B)	107.9	O(3)-C(7)-O(2)	110.20(15)
O(3)-C(7)-C(6)	104.86(17)	O(2)-C(7)-C(6)	110.46(16)
O(3)-C(7)-C(8)	111.73(17)	O(2)-C(7)-C(8)	106.76(17)
C(6)-C(7)-C(8)	112.89(18)	C(7)-C(8)-C(9)	115.3(2)
C(7)-C(8)-H(8A)	108.5	C(9)-C(8)-H(8A)	108.5
C(7)-C(8)-H(8B)	108.5	C(9)-C(8)-H(8B)	108.5
H(8A)-C(8)-H(8B)	107.5	C(8)-C(9)-C(17)	113.9(2)
C(8)-C(9)-C(10)	108.6(2)	C(17)-C(9)-C(10)	112.0(2)
C(8)-C(9)-H(9)	107.3	C(17)-C(9)-H(9)	107.3
C(10)-C(9)-H(9)	107.3	C(11)-C(10)-C(9)	111.64(18)
C(11)-C(10)-H(10A)	109.3	C(9)-C(10)-H(10A)	109.3
C(11)-C(10)-H(10B)	109.3	C(9)-C(10)-H(10B)	109.3
H(10A)-C(10)-H(10B)	108.0	O(3)-C(11)-C(10)	111.11(18)
O(3)-C(11)-C(12)	105.18(17)	C(10)-C(11)-C(12)	113.21(18)
O(3)-C(11)-H(11)	109.1	C(10)-C(11)-H(11)	109.1
C(12)-C(11)-H(11)	109.1	O(4)-C(12)-C(13)	112.1(2)
O(4)-C(12)-C(11)	107.51(18)	C(13)-C(12)-C(11)	112.83(18)
O(4)-C(12)-H(12)	108.1	C(13)-C(12)-H(12)	108.1
C(11)-C(12)-H(12)	108.1	C(19)-C(13)-C(18)	122.2(3)
C(19)-C(13)-C(12)	118.9(3)	C(18)-C(13)-C(12)	118.8(2)
C(1)-C(14)-H(14A)	109.5	C(1)-C(14)-H(14B)	109.5
H(14A)-C(14)-H(14B)	109.5	C(1)-C(14)-H(14C)	109.5
H(14A)-C(14)-H(14C)	109.5	H(14B)-C(14)-H(14C)	109.5
C(1)-C(15)-H(15A)	120.0	C(1)-C(15)-H(15B)	120.0

H(15A)-C(15)-H(15B)	120.0	C(5)-C(16)-H(16A)	109.5
C(5)-C(16)-H(16B)	109.5	H(16A)-C(16)-H(16B)	109.5
C(5)-C(16)-H(16C)	109.5	H(16A)-C(16)-H(16C)	109.5
H(16B)-C(16)-H(16C)	109.5	C(9)-C(17)-H(17A)	109.5
C(9)-C(17)-H(17B)	109.5	H(17A)-C(17)-H(17B)	109.5
C(9)-C(17)-H(17C)	109.5	H(17A)-C(17)-H(17C)	109.5
H(17B)-C(17)-H(17C)	109.5	C(13)-C(18)-H(18A)	109.5
C(13)-C(18)-H(18B)	109.5	H(18A)-C(18)-H(18B)	109.5
C(13)-C(18)-H(18C)	109.5	H(18A)-C(18)-H(18C)	109.5
H(18B)-C(18)-H(18C)	109.5	C(13)-C(19)-H(19A)	120.0
C(13)-C(19)-H(19B)	120.0	H(19A)-C(19)-H(19B)	120.0
C(21)-O(5)-H(5A)	109.5	C(26)-O(6)-C(22)	114.30(17)
C(26)-O(7)-C(30)	114.75(16)	C(31)-O(8)-H(8)	109.5
C(34)-C(20)-C(33)	119.4(3)	C(34)-C(20)-C(21)	122.3(3)
C(33)-C(20)-C(21)	118.2(2)	O(5)-C(21)-C(20)	113.2(2)
O(5)-C(21)-C(22)	110.10(18)	C(20)-C(21)-C(22)	113.9(2)
O(5)-C(21)-H(21)	106.4	C(20)-C(21)-H(21)	106.4
C(22)-C(21)-H(21)	106.4	O(6)-C(22)-C(23)	110.31(17)
O(6)-C(22)-C(21)	105.52(18)	C(23)-C(22)-C(21)	112.42(19)
O(6)-C(22)-H(22)	109.5	C(23)-C(22)-H(22)	109.5
C(21)-C(22)-H(22)	109.5	C(22)-C(23)-C(24)	111.46(19)
C(22)-C(23)-H(23A)	109.3	C(24)-C(23)-H(23A)	109.3
C(22)-C(23)-H(23B)	109.3	C(24)-C(23)-H(23B)	109.3
H(23A)-C(23)-H(23B)	108.0	C(35)-C(24)-C(23)	112.5(2)
C(35)-C(24)-C(25)	113.9(2)	C(23)-C(24)-C(25)	108.7(2)
C(35)-C(24)-H(24)	107.1	C(23)-C(24)-H(24)	107.1
C(25)-C(24)-H(24)	107.1	C(26)-C(25)-C(24)	114.53(19)
C(26)-C(25)-H(25A)	108.6	C(24)-C(25)-H(25A)	108.6
C(26)-C(25)-H(25B)	108.6	C(24)-C(25)-H(25B)	108.6
H(25A)-C(25)-H(25B)	107.6	O(7)-C(26)-O(6)	110.31(16)
O(7)-C(26)-C(27)	110.78(17)	O(6)-C(26)-C(27)	105.53(19)
O(7)-C(26)-C(25)	105.6(2)	O(6)-C(26)-C(25)	111.37(18)
C(27)-C(26)-C(25)	113.38(19)	C(26)-C(27)-C(28)	113.03(18)
C(26)-C(27)-H(27A)	109.0	C(28)-C(27)-H(27A)	109.0
C(26)-C(27)-H(27B)	109.0	C(28)-C(27)-H(27B)	109.0
H(27A)-C(27)-H(27B)	107.8	C(36)-C(28)-C(27)	111.1(2)
C(36)-C(28)-C(29)	112.13(19)	C(27)-C(28)-C(29)	109.3(2)
C(36)-C(28)-H(28)	108.1	C(27)-C(28)-H(28)	108.1
C(29)-C(28)-H(28)	108.1	C(30)-C(29)-C(28)	109.59(17)
C(30)-C(29)-H(29A)	109.8	C(28)-C(29)-H(29A)	109.8
C(30)-C(29)-H(29B)	109.8	C(28)-C(29)-H(29B)	109.8
H(29A)-C(29)-H(29B)	108.2	O(7)-C(30)-C(29)	110.05(16)
O(7)-C(30)-C(31)	103.68(16)	C(29)-C(30)-C(31)	116.37(17)
O(7)-C(30)-H(30)	108.8	C(29)-C(30)-H(30)	108.8
C(31)-C(30)-H(30)	108.8	O(8)-C(31)-C(32)	110.70(17)
O(8)-C(31)-C(30)	106.24(16)	C(32)-C(31)-C(30)	113.71(17)

O(8)-C(31)-H(31)	108.7	C(32)-C(31)-H(31)	108.7
C(30)-C(31)-H(31)	108.7	C(38)-C(32)-C(37)	123.0(2)
C(38)-C(32)-C(31)	120.3(2)	C(37)-C(32)-C(31)	116.59(19)
C(20)-C(33)-H(33A)	109.5	C(20)-C(33)-H(33B)	109.5
H(33A)-C(33)-H(33B)	109.5	C(20)-C(33)-H(33C)	109.5
H(33A)-C(33)-H(33C)	109.5	H(33B)-C(33)-H(33C)	109.5
C(20)-C(34)-H(34A)	120.0	C(20)-C(34)-H(34B)	120.0
H(34A)-C(34)-H(34B)	120.0	C(24)-C(35)-H(35A)	109.5
C(24)-C(35)-H(35B)	109.5	H(35A)-C(35)-H(35B)	109.5
C(24)-C(35)-H(35C)	109.5	H(35A)-C(35)-H(35C)	109.5
H(35B)-C(35)-H(35C)	109.5	C(28)-C(36)-H(36A)	109.5
C(28)-C(36)-H(36B)	109.5	H(36A)-C(36)-H(36B)	109.5
C(28)-C(36)-H(36C)	109.5	H(36A)-C(36)-H(36C)	109.5
H(36B)-C(36)-H(36C)	109.5	C(32)-C(37)-H(37A)	109.5
C(32)-C(37)-H(37B)	109.5	H(37A)-C(37)-H(37B)	109.5
C(32)-C(37)-H(37C)	109.5	H(37A)-C(37)-H(37C)	109.5
H(37B)-C(37)-H(37C)	109.5	C(32)-C(38)-H(38A)	120.0
C(32)-C(38)-H(38B)	120.0	H(38A)-C(38)-H(38B)	120.0

Symmetry transformations used to generate equivalent atoms:

Table 6. Torsion angles [°] for **382**.

atom-atom-atom-atom	angle	atom-atom-atom-atom	angle
C(15)-C(1)-C(2)-O(1)	-131.3(2)	C(14)-C(1)-C(2)-O(1)	48.7(3)
C(15)-C(1)-C(2)-C(3)	106.7(3)	C(14)-C(1)-C(2)-C(3)	-73.4(3)
C(7)-O(2)-C(3)-C(4)	57.0(2)	C(7)-O(2)-C(3)-C(2)	179.09(15)
O(1)-C(2)-C(3)-O(2)	53.3(2)	C(1)-C(2)-C(3)-O(2)	175.03(18)
O(1)-C(2)-C(3)-C(4)	174.45(19)	C(1)-C(2)-C(3)-C(4)	-63.8(2)
O(2)-C(3)-C(4)-C(5)	-54.8(2)	C(2)-C(3)-C(4)-C(5)	-171.5(2)
C(3)-C(4)-C(5)-C(16)	176.4(2)	C(3)-C(4)-C(5)-C(6)	53.0(3)
C(16)-C(5)-C(6)-C(7)	-177.34(19)	C(4)-C(5)-C(6)-C(7)	-53.3(2)
C(11)-O(3)-C(7)-O(2)	66.8(2)	C(11)-O(3)-C(7)-C(6)	-174.31(16)
C(11)-O(3)-C(7)-C(8)	-51.7(2)	C(3)-O(2)-C(7)-O(3)	59.4(2)
C(3)-O(2)-C(7)-C(6)	-56.0(2)	C(3)-O(2)-C(7)-C(8)	-179.03(17)
C(5)-C(6)-C(7)-O(3)	-64.5(2)	C(5)-C(6)-C(7)-O(2)	54.2(2)
C(5)-C(6)-C(7)-C(8)	173.69(18)	O(3)-C(7)-C(8)-C(9)	47.5(3)
O(2)-C(7)-C(8)-C(9)	-73.1(2)	C(6)-C(7)-C(8)-C(9)	165.40(19)
C(7)-C(8)-C(9)-C(17)	78.0(3)	C(7)-C(8)-C(9)-C(10)	-47.7(3)
C(8)-C(9)-C(10)-C(11)	51.5(3)	C(17)-C(9)-C(10)-C(11)	-75.3(3)
C(7)-O(3)-C(11)-C(10)	57.2(2)	C(7)-O(3)-C(11)-C(12)	-179.99(16)
C(9)-C(10)-C(11)-O(3)	-56.5(2)	C(9)-C(10)-C(11)-C(12)	-174.62(19)
O(3)-C(11)-C(12)-O(4)	-61.9(2)	C(10)-C(11)-C(12)-O(4)	59.6(2)
O(3)-C(11)-C(12)-C(13)	62.2(2)	C(10)-C(11)-C(12)-C(13)	-176.35(19)
O(4)-C(12)-C(13)-C(19)	-156.5(2)	C(11)-C(12)-C(13)-C(19)	82.0(3)

O(4)-C(12)-C(13)-C(18)	24.0(3)	C(11)-C(12)-C(13)-C(18)	-97.5(3)
C(34)-C(20)-C(21)-O(5)	16.3(5)	C(33)-C(20)-C(21)-O(5)	-167.1(2)
C(34)-C(20)-C(21)-C(22)	-110.4(4)	C(33)-C(20)-C(21)-C(22)	66.1(3)
C(26)-O(6)-C(22)-C(23)	60.0(2)	C(26)-O(6)-C(22)-C(21)	-178.33(18)
O(5)-C(21)-C(22)-O(6)	-61.6(2)	C(20)-C(21)-C(22)-O(6)	66.7(2)
O(5)-C(21)-C(22)-C(23)	58.6(3)	C(20)-C(21)-C(22)-C(23)	-173.03(18)
O(6)-C(22)-C(23)-C(24)	-58.1(3)	C(21)-C(22)-C(23)-C(24)	-175.57(19)
C(22)-C(23)-C(24)-C(35)	-75.4(3)	C(22)-C(23)-C(24)-C(25)	51.8(3)
C(35)-C(24)-C(25)-C(26)	78.5(3)	C(23)-C(24)-C(25)-C(26)	-47.9(3)
C(30)-O(7)-C(26)-O(6)	60.2(2)	C(30)-O(7)-C(26)-C(27)	-56.2(2)
C(30)-O(7)-C(26)-C(25)	-179.36(16)	C(22)-O(6)-C(26)-O(7)	62.0(2)
C(22)-O(6)-C(26)-C(27)	-178.33(17)	C(22)-O(6)-C(26)-C(25)	-54.9(2)
C(24)-C(25)-C(26)-O(7)	-70.5(2)	C(24)-C(25)-C(26)-O(6)	49.2(3)
C(24)-C(25)-C(26)-C(27)	168.0(2)	O(7)-C(26)-C(27)-C(28)	50.9(3)
O(6)-C(26)-C(27)-C(28)	-68.5(2)	C(25)-C(26)-C(27)-C(28)	169.40(19)
C(26)-C(27)-C(28)-C(36)	-175.13(19)	C(26)-C(27)-C(28)-C(29)	-50.9(2)
C(36)-C(28)-C(29)-C(30)	177.5(2)	C(27)-C(28)-C(29)-C(30)	53.9(2)
C(26)-O(7)-C(30)-C(29)	60.9(2)	C(26)-O(7)-C(30)-C(31)	-173.95(15)
C(28)-C(29)-C(30)-O(7)	-58.4(2)	C(28)-C(29)-C(30)-C(31)	-175.90(18)
O(7)-C(30)-C(31)-O(8)	68.96(18)	C(29)-C(30)-C(31)-O(8)	-170.08(17)
O(7)-C(30)-C(31)-C(32)	-169.04(16)	C(29)-C(30)-C(31)-C(32)	-48.1(2)
O(8)-C(31)-C(32)-C(38)	-124.0(2)	C(30)-C(31)-C(32)-C(38)	116.5(2)
O(8)-C(31)-C(32)-C(37)	53.6(2)	C(30)-C(31)-C(32)-C(37)	-65.9(2)

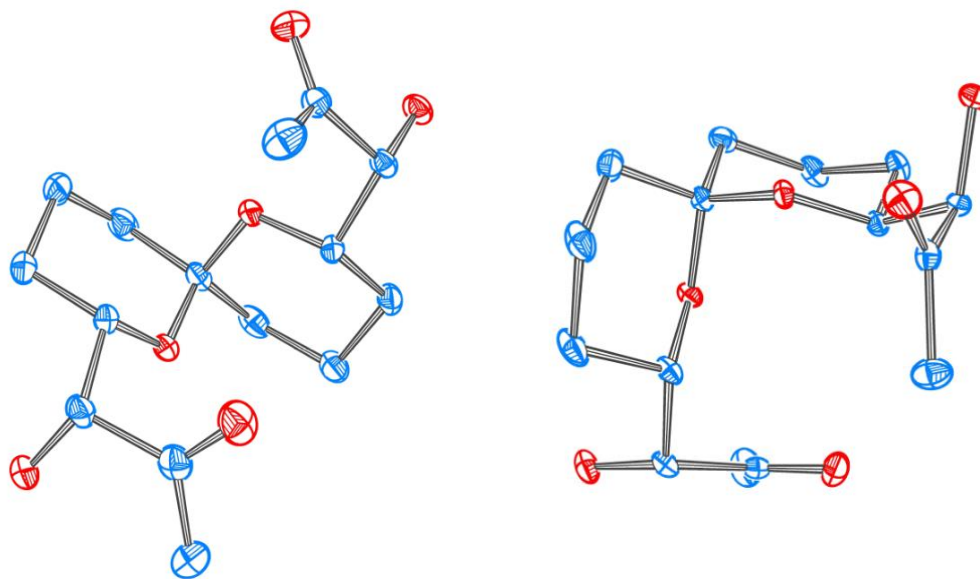
Symmetry transformations used to generate equivalent atoms:

Table 7. Hydrogen bonds for **382** [Å and °].

D-H...A	d(D-H)	d(H...A)	d(D...A)	<(DHA)
O(5)-H(5A)...O(1)	0.84	2.06	2.824(2)	150.8
O(4)-H(4)...O(5)#1	0.84	1.89	2.706(2)	164.2
O(8)-H(8)...O(3)#2	0.84	2.48	3.0525(19)	126.4
O(8)-H(8)...O(4)#2	0.84	2.07	2.870(2)	159.1

Symmetry transformations used to generate equivalent atoms:

#1 x,y,z-1 #2 x+1,y,z+1



Crystal Summary for 394

Crystal data for $C_{15}H_{24}O_6$; $M_r = 300.34$; Orthorhombic; space group $P2_12_12_1$; $a = 9.2925(3) \text{ \AA}$; $b = 9.3111(3) \text{ \AA}$; $c = 17.5745(6) \text{ \AA}$; $\alpha = 90^\circ$; $\beta = 90^\circ$; $\gamma = 90^\circ$; $V = 1520.61(9) \text{ \AA}^3$; $Z = 4$; $T = 120(2) \text{ K}$; $\lambda(\text{Cu-K}\alpha) = 1.54184 \text{ \AA}$; $\mu(\text{Cu-K}\alpha) = 0.839 \text{ mm}^{-1}$; $d_{\text{calc}} = 1.312 \text{ g.cm}^{-3}$; 17624 reflections collected; 2941 unique ($R_{\text{int}} = 0.0341$); giving $R_1 = 0.0294$, $wR_2 = 0.0765$ for 2938 data with $[I > 2\sigma(I)]$ and $R_1 = 0.0295$, $wR_2 = 0.0766$ for all 2941 data. Residual electron density ($e^- \cdot \text{\AA}^{-3}$) max/min: 0.190/-0.226.

An arbitrary sphere of data were collected on a colorless block-like crystal, having approximate dimensions of $0.250 \times 0.168 \times 0.134 \text{ mm}$, on a Bruker APEX-II diffractometer using a combination of ω - and φ -scans of 0.5° . Data were corrected for absorption and polarization effects and analyzed for space group determination. The structure was solved by Patterson methods and expanded routinely. The model was refined by full-matrix least-squares analysis of F^2 against all reflections. All non-hydrogen atoms were refined with anisotropic thermal displacement parameters. Unless otherwise noted, hydrogen atoms were included in calculated positions. Thermal parameters for the hydrogens were tied to the isotropic thermal parameter of the atom to which they are bonded ($1.5 \times$ for methyl, $1.2 \times$ for all others).

References

- Bruker AXS. (2008). *APEX-2*. Bruker-Nonius AXS, Madison, Wisconsin, USA.
 G. M. Sheldrick, *Acta Cryst.*, **2008**, *A64*, 112.
 R. W. W. Hooft, L. H. Straver & A. L. Spek, *J. Appl. Cryst.*, **2008**, *41*, 96.
 H. D. Flack, *Acta Cryst.*, **1983**, *A39*, 876.

Table 1. Crystal data and structure refinement for **394**.

Empirical formula	C ₁₅ H ₂₄ O ₆	
Formula weight	300.34	
Temperature	120(2) K	
Wavelength	1.54184 Å	
Crystal system	Orthorhombic	
Space group	P2 ₁ 2 ₁ 2 ₁	
Unit cell dimensions	$a = 9.2925(3)$ Å	$\alpha = 90^\circ$
	$b = 9.3111(3)$ Å	$\beta = 90^\circ$
	$c = 17.5745(6)$ Å	$\gamma = 90^\circ$
Volume	1520.61(9) Å ³	
Z	4	
Density (calculated)	1.312 g.cm ⁻³	
Absorption coefficient (μ)	0.839 mm ⁻¹	
F(000)	648	
Crystal color, habit	colorless, block	
Crystal size	0.250 × 0.168 × 0.134 mm ³	
θ range for data collection	5.033 to 71.346°	
Index ranges	-11 ≤ h ≤ 11, -10 ≤ k ≤ 11, -21 ≤ l ≤ 20	
Reflections collected	17624	
Independent reflections	2941 [R _{int} = 0.0341]	
Completeness to $\theta = 67.679^\circ$	99.9 %	
Absorption correction	Numerical	
Max. and min. transmission	1.0000 and 0.9311	
Refinement method	Full-matrix least-squares on F ²	
Data / restraints / parameters	2941 / 0 / 194	
Goodness-of-fit on F ²	1.058	
Final R indices [I > 2 σ (I)]	R ₁ = 0.0294, wR ₂ = 0.0765	
R indices (all data)	R ₁ = 0.0295, wR ₂ = 0.0766	
Absolute structure parameter	0.00(4)	
Extinction coefficient	n/a	
Largest diff. peak and hole	0.190 and -0.226 e ⁻ .Å ⁻³	

Table 2. Atomic coordinates and equivalent isotropic displacement parameters (Å²) for **394**. U(eq) is defined as one third of the trace of the orthogonalized U_{ij} tensor.

	x	y	z	U(eq)
O(1)	0.56442(15)	0.35445(15)	0.37648(7)	0.029(1)
O(2)	0.56094(13)	0.56846(14)	0.21142(7)	0.024(1)
O(3)	0.36704(12)	0.62021(12)	0.33790(6)	0.015(1)
O(4)	0.17524(11)	0.55628(12)	0.41802(6)	0.015(1)
O(5)	0.05694(12)	0.46183(12)	0.56105(6)	0.018(1)
O(6)	-0.02833(12)	0.29524(14)	0.45030(7)	0.025(1)

C(1)	0.7243(2)	0.5388(2)	0.33702(11)	0.033(1)
C(2)	0.59537(18)	0.44366(18)	0.32882(9)	0.021(1)
C(3)	0.49927(19)	0.46269(18)	0.25909(9)	0.019(1)
C(4)	0.34789(17)	0.50040(17)	0.28712(9)	0.017(1)
C(5)	0.24267(18)	0.5382(2)	0.22456(9)	0.027(1)
C(6)	0.09956(19)	0.5870(2)	0.25912(10)	0.030(1)
C(7)	0.12600(19)	0.7094(2)	0.31518(10)	0.025(1)
C(8)	0.23861(17)	0.66842(16)	0.37411(9)	0.017(1)
C(9)	0.2863(2)	0.79185(17)	0.42480(10)	0.022(1)
C(10)	0.3892(2)	0.73904(18)	0.48629(9)	0.023(1)
C(11)	0.31833(18)	0.61715(18)	0.53116(9)	0.019(1)
C(12)	0.26424(17)	0.49962(16)	0.47818(8)	0.014(1)
C(13)	0.16812(16)	0.39124(16)	0.51978(8)	0.014(1)
C(14)	0.10011(18)	0.28769(16)	0.46295(9)	0.017(1)
C(15)	0.1957(2)	0.17900(19)	0.42626(11)	0.026(1)
H(20)	0.5150	0.5723	0.1703	0.036
H(50)	-0.0204	0.4567	0.5365	0.027
H(1A)	0.7823	0.5065	0.3804	0.050
H(1B)	0.6928	0.6379	0.3456	0.050
H(1C)	0.7822	0.5342	0.2905	0.050
H(3)	0.4951	0.3697	0.2307	0.022
H(4)	0.3088	0.4173	0.3167	0.021
H(5A)	0.2265	0.4534	0.1917	0.032
H(5B)	0.2830	0.6161	0.1927	0.032
H(6A)	0.0340	0.6197	0.2182	0.036
H(6B)	0.0533	0.5054	0.2858	0.036
H(7A)	0.1588	0.7955	0.2870	0.030
H(7B)	0.0348	0.7338	0.3412	0.030
H(9A)	0.2009	0.8363	0.4489	0.026
H(9B)	0.3346	0.8659	0.3935	0.026
H(10A)	0.4135	0.8191	0.5211	0.027
H(10B)	0.4793	0.7043	0.4626	0.027
H(11A)	0.3889	0.5760	0.5673	0.023
H(11B)	0.2367	0.6558	0.5610	0.023
H(12)	0.3484	0.4482	0.4555	0.017
H(13)	0.2286	0.3351	0.5563	0.017
H(15A)	0.1461	0.1362	0.3826	0.039
H(15B)	0.2196	0.1037	0.4632	0.039
H(15C)	0.2844	0.2257	0.4089	0.039

Table 3. Anisotropic displacement parameters (\AA^2) for **394**. The anisotropic displacement factor exponent takes the form: $-2\pi^2[h^2a^{*2}U_{11} + \dots + 2hka^*b^*U_{12}]$

	U_{11}	U_{22}	U_{33}	U_{23}	U_{13}	U_{12}
O(1)	0.0320(7)	0.0277(6)	0.0277(6)	0.0090(5)	0.0003(6)	0.0067(6)
O(2)	0.0221(6)	0.0353(7)	0.0149(5)	0.0045(5)	0.0014(5)	-0.0023(5)
O(3)	0.0144(5)	0.0193(5)	0.0122(5)	-0.0011(4)	0.0026(4)	-0.0003(4)
O(4)	0.0140(5)	0.0188(5)	0.0124(5)	0.0036(4)	0.0002(4)	-0.0009(4)
O(5)	0.0157(5)	0.0217(5)	0.0165(5)	0.0012(4)	0.0052(4)	0.0030(4)
O(6)	0.0152(6)	0.0327(6)	0.0259(6)	-0.0002(5)	-0.0014(5)	-0.0031(5)
C(1)	0.0245(9)	0.0463(11)	0.0282(9)	0.0028(9)	-0.0056(8)	-0.0056(9)
C(2)	0.0202(8)	0.0219(7)	0.0196(8)	-0.0020(6)	0.0036(6)	0.0071(7)
C(3)	0.0198(7)	0.0217(8)	0.0146(7)	-0.0023(6)	0.0036(6)	-0.0002(6)
C(4)	0.0172(7)	0.0228(8)	0.0118(7)	-0.0021(6)	0.0006(6)	-0.0026(6)
C(5)	0.0194(8)	0.0482(11)	0.0134(7)	-0.0011(7)	-0.0008(7)	-0.0017(8)
C(6)	0.0165(8)	0.0561(12)	0.0173(8)	0.0046(8)	-0.0033(7)	0.0008(8)
C(7)	0.0196(8)	0.0345(9)	0.0220(8)	0.0105(7)	0.0035(7)	0.0069(7)
C(8)	0.0171(7)	0.0184(7)	0.0148(7)	0.0038(6)	0.0039(6)	0.0018(6)
C(9)	0.0277(8)	0.0152(7)	0.0216(8)	0.0005(6)	0.0092(7)	-0.0010(6)
C(10)	0.0283(9)	0.0221(8)	0.0173(8)	-0.0034(6)	0.0039(7)	-0.0091(7)
C(11)	0.0236(8)	0.0223(8)	0.0120(7)	-0.0002(6)	0.0000(6)	-0.0054(6)
C(12)	0.0146(7)	0.0169(7)	0.0110(6)	0.0005(5)	0.0000(6)	0.0002(6)
C(13)	0.0140(7)	0.0152(7)	0.0138(7)	0.0014(5)	0.0028(6)	0.0025(6)
C(14)	0.0180(7)	0.0168(7)	0.0160(7)	0.0040(6)	-0.0005(6)	-0.0022(6)
C(15)	0.0260(9)	0.0226(8)	0.0300(9)	-0.0089(7)	-0.0030(7)	0.0015(7)

Table 4. Bond lengths [\AA] for **394**.

atom-atom	distance	atom-atom	distance
O(1)-C(2)	1.214(2)	O(2)-C(3)	1.414(2)
O(3)-C(8)	1.4251(18)	O(3)-C(4)	1.4396(18)
O(4)-C(8)	1.4257(18)	O(4)-C(12)	1.4422(18)
O(5)-C(13)	1.4232(18)	O(6)-C(14)	1.216(2)
C(1)-C(2)	1.497(3)	C(2)-C(3)	1.527(2)
C(3)-C(4)	1.531(2)	C(4)-C(5)	1.513(2)
C(5)-C(6)	1.531(2)	C(6)-C(7)	1.527(3)
C(7)-C(8)	1.521(2)	C(8)-C(9)	1.520(2)
C(9)-C(10)	1.524(3)	C(10)-C(11)	1.531(2)
C(11)-C(12)	1.522(2)	C(12)-C(13)	1.533(2)
C(13)-C(14)	1.525(2)	C(14)-C(15)	1.493(2)
O(2)-H(2O)	0.8400	O(5)-H(5O)	0.8400
C(1)-H(1A)	0.9800	C(1)-H(1B)	0.9800
C(1)-H(1C)	0.9800	C(3)-H(3)	1.0000
C(4)-H(4)	1.0000	C(5)-H(5A)	0.9900

C(5)-H(5B)	0.9900	C(6)-H(6A)	0.9900
C(6)-H(6B)	0.9900	C(7)-H(7A)	0.9900
C(7)-H(7B)	0.9900	C(9)-H(9A)	0.9900
C(9)-H(9B)	0.9900	C(10)-H(10A)	0.9900
C(10)-H(10B)	0.9900	C(11)-H(11A)	0.9900
C(11)-H(11B)	0.9900	C(12)-H(12)	1.0000
C(13)-H(13)	1.0000	C(15)-H(15A)	0.9800
C(15)-H(15B)	0.9800	C(15)-H(15C)	0.9800

Symmetry transformations used to generate equivalent atoms:

Table 5. Bond angles [°] for **394**.

atom-atom-atom	angle	atom-atom-atom	angle
C(8)-O(3)-C(4)	114.67(12)	C(8)-O(4)-C(12)	115.33(11)
O(1)-C(2)-C(1)	121.87(16)	O(1)-C(2)-C(3)	119.64(16)
C(1)-C(2)-C(3)	118.47(15)	O(2)-C(3)-C(2)	108.62(14)
O(2)-C(3)-C(4)	113.77(14)	C(2)-C(3)-C(4)	107.80(13)
O(3)-C(4)-C(5)	110.50(14)	O(3)-C(4)-C(3)	105.28(12)
C(5)-C(4)-C(3)	114.41(13)	C(4)-C(5)-C(6)	110.00(13)
C(7)-C(6)-C(5)	109.74(15)	C(8)-C(7)-C(6)	111.27(14)
O(3)-C(8)-O(4)	110.91(12)	O(3)-C(8)-C(9)	104.82(13)
O(4)-C(8)-C(9)	110.90(12)	O(3)-C(8)-C(7)	110.56(13)
O(4)-C(8)-C(7)	105.56(13)	C(9)-C(8)-C(7)	114.20(14)
C(8)-C(9)-C(10)	110.75(13)	C(9)-C(10)-C(11)	109.54(14)
C(12)-C(11)-C(10)	111.10(13)	O(4)-C(12)-C(11)	112.01(12)
O(4)-C(12)-C(13)	104.85(12)	C(11)-C(12)-C(13)	111.96(12)
O(5)-C(13)-C(14)	108.96(12)	O(5)-C(13)-C(12)	111.22(12)
C(14)-C(13)-C(12)	110.19(12)	O(6)-C(14)-C(15)	122.97(15)
O(6)-C(14)-C(13)	119.33(15)	C(15)-C(14)-C(13)	117.69(14)
C(3)-O(2)-H(2O)	109.5	C(13)-O(5)-H(5O)	109.5
C(2)-C(1)-H(1A)	109.5	C(2)-C(1)-H(1B)	109.5
H(1A)-C(1)-H(1B)	109.5	C(2)-C(1)-H(1C)	109.5
H(1A)-C(1)-H(1C)	109.5	H(1B)-C(1)-H(1C)	109.5
O(2)-C(3)-H(3)	108.8	C(2)-C(3)-H(3)	108.8
C(4)-C(3)-H(3)	108.8	O(3)-C(4)-H(4)	108.8
C(5)-C(4)-H(4)	108.8	C(3)-C(4)-H(4)	108.8
C(4)-C(5)-H(5A)	109.7	C(6)-C(5)-H(5A)	109.7
C(4)-C(5)-H(5B)	109.7	C(6)-C(5)-H(5B)	109.7
H(5A)-C(5)-H(5B)	108.2	C(7)-C(6)-H(6A)	109.7
C(5)-C(6)-H(6A)	109.7	C(7)-C(6)-H(6B)	109.7
C(5)-C(6)-H(6B)	109.7	H(6A)-C(6)-H(6B)	108.2
C(8)-C(7)-H(7A)	109.4	C(6)-C(7)-H(7A)	109.4
C(8)-C(7)-H(7B)	109.4	C(6)-C(7)-H(7B)	109.4
H(7A)-C(7)-H(7B)	108.0	C(8)-C(9)-H(9A)	109.5

C(10)-C(9)-H(9A)	109.5	C(8)-C(9)-H(9B)	109.5
C(10)-C(9)-H(9B)	109.5	H(9A)-C(9)-H(9B)	108.1
C(9)-C(10)-H(10A)	109.8	C(11)-C(10)-H(10A)	109.8
C(9)-C(10)-H(10B)	109.8	C(11)-C(10)-H(10B)	109.8
H(10A)-C(10)-H(10B)	108.2	C(12)-C(11)-H(11A)	109.4
C(10)-C(11)-H(11A)	109.4	C(12)-C(11)-H(11B)	109.4
C(10)-C(11)-H(11B)	109.4	H(11A)-C(11)-H(11B)	108.0
O(4)-C(12)-H(12)	109.3	C(11)-C(12)-H(12)	109.3
C(13)-C(12)-H(12)	109.3	O(5)-C(13)-H(13)	108.8
C(14)-C(13)-H(13)	108.8	C(12)-C(13)-H(13)	108.8
C(14)-C(15)-H(15A)	109.5	C(14)-C(15)-H(15B)	109.5
H(15A)-C(15)-H(15B)	109.5	C(14)-C(15)-H(15C)	109.5
H(15A)-C(15)-H(15C)	109.5	H(15B)-C(15)-H(15C)	109.5

Symmetry transformations used to generate equivalent atoms:

Table 6. Torsion angles [°] for **394**.

atom-atom-atom-atom	angle	atom-atom-atom-atom	angle
O(1)-C(2)-C(3)-O(2)	-177.91(14)	C(1)-C(2)-C(3)-O(2)	3.4(2)
O(1)-C(2)-C(3)-C(4)	58.4(2)	C(1)-C(2)-C(3)-C(4)	-120.34(17)
C(8)-O(3)-C(4)-C(5)	59.18(16)	C(8)-O(3)-C(4)-C(3)	-176.80(12)
O(2)-C(3)-C(4)-O(3)	-68.14(15)	C(2)-C(3)-C(4)-O(3)	52.39(16)
O(2)-C(3)-C(4)-C(5)	53.37(19)	C(2)-C(3)-C(4)-C(5)	173.89(15)
O(3)-C(4)-C(5)-C(6)	-56.32(19)	C(3)-C(4)-C(5)-C(6)	-174.92(16)
C(4)-C(5)-C(6)-C(7)	54.4(2)	C(5)-C(6)-C(7)-C(8)	-53.28(19)
C(4)-O(3)-C(8)-O(4)	59.41(16)	C(4)-O(3)-C(8)-C(9)	179.16(12)
C(4)-O(3)-C(8)-C(7)	-57.33(17)	C(12)-O(4)-C(8)-O(3)	60.11(16)
C(12)-O(4)-C(8)-C(9)	-55.94(16)	C(12)-O(4)-C(8)-C(7)	179.88(12)
C(6)-C(7)-C(8)-O(3)	53.75(18)	C(6)-C(7)-C(8)-O(4)	-66.26(16)
C(6)-C(7)-C(8)-C(9)	171.66(14)	O(3)-C(8)-C(9)-C(10)	-63.67(15)
O(4)-C(8)-C(9)-C(10)	56.09(17)	C(7)-C(8)-C(9)-C(10)	175.19(13)
C(8)-C(9)-C(10)-C(11)	-55.23(17)	C(9)-C(10)-C(11)-C(12)	52.99(18)
C(8)-O(4)-C(12)-C(11)	54.03(16)	C(8)-O(4)-C(12)-C(13)	175.66(12)
C(10)-C(11)-C(12)-O(4)	-51.61(18)	C(10)-C(11)-C(12)-C(13)	-169.07(13)
O(4)-C(12)-C(13)-O(5)	-70.26(14)	C(11)-C(12)-C(13)-O(5)	51.41(17)
O(4)-C(12)-C(13)-C(14)	50.68(15)	C(11)-C(12)-C(13)-C(14)	172.34(13)
O(5)-C(13)-C(14)-O(6)	12.46(19)	C(12)-C(13)-C(14)-O(6)	-109.82(16)
O(5)-C(13)-C(14)-C(15)	-166.45(13)	C(12)-C(13)-C(14)-C(15)	71.27(17)

Symmetry transformations used to generate equivalent atoms:

Table 7. Hydrogen bonds for **394** [\AA and $^\circ$].

D-H...A	d(D-H)	d(H...A)	d(D...A)	$\angle(\text{DHA})$
O(2)-H(2O)...O(5)#1	0.84	2.06	2.8745(16)	163.9
O(5)-H(5O)...O(6)	0.84	2.14	2.6120(17)	115.7

Symmetry transformations used to generate equivalent atoms:

#1 $-x+1/2, -y+1, z-1/2$

Appendix 2 — List of Numbered Compounds

